INFORMATION TO USERS

This manuscript has been reproduced from the microfilm master. UMI films the text directly from the original or copy submitted. Thus, some thesis and dissertation copies are in typewriter face, while others may be from any type of computer printer.

The quality of this reproduction is dependent upon the quality of the copy submitted. Broken or indistinct print, colored or poor quality illustrations and photographs, print bleedthrough, substandard margins, and improper alignment can adversely affect reproduction.

In the unlikely event that the author did not send UMI a complete manuscript and there are missing pages, these will be noted. Also, if unauthorized copyright material had to be removed, a note will indicate the deletion.

Oversize materials (e.g., maps, drawings, charts) are reproduced by sectioning the original, beginning at the upper left-hand corner and continuing from left to right in equal sections with small overlaps.

ProQuest Information and Learning
300 North Zeeb Road, Ann Arbor, MI 48106-1346 USA
800-521-0600

HYDROGEN DEUTERIUM ISOTOPE EFFECTS IN ELECTROCHEMICAL PROTON TRANSFER

by

Mark Salomon

A thesis submitted in partial fulfillment
of the requirements for the degree of
Doctor of Philosophy
in the
Department of Chemistry
University of Ottawa
Ottawa, Canada
July 1964

B.E. Conway
Professor of Chemistry
Research Supervisor

Mark Salomon
Ph.D. Candidate

ISOTOPE EFFECTS IN METHYL RADICAL ABSTRACTION REACTIONS

MARK SALOMON

ISOTOPE EFFECTS IN METHYL RADICAL ABSTRACTION REACTIONS

MARK SALOMON
Department of Chemistry, University of Ottawa, Ottawa, Canada
Received October 18, 1963

ABSTRACT

The high k_H/k_D ratio found experimentally for methyl radical abstraction reactions is explained on the basis of classical rate theory. It is shown that if the bending frequencies in the activated complex approach zero, good agreement is found between experimental and calculated k_H/k_D values. For abstraction of H and D from hydrocarbons, both the tunneling and classical rate theories predict acceptable k_H/k_D values. Abstraction of H and D from H_2 and D_2, however, can best be explained on the basis of a classical process.

INTRODUCTION

The ratio of rate constants, k_H/k_D, for the abstraction of H and D from hydrocarbons by methyl radicals has been found to be higher than that calculated from classical rate theory when the bending frequencies of the RC—H bond is assumed to remain constant from the initial to final states (1–6). To explain these high values for k_H/k_D, several workers (1, 2) have proposed that the rates are largely determined by appreciable participation of a quantum mechanical tunneling process. The basis for the tunneling mechanism is the theory of Johnston and Rapp (3), who give the relation

$$k_H/k_D = 0.99 \exp(1580/RT). \qquad [1]$$

for methyl radical abstractions based on proton tunneling (2). This theory is attractive since it does predict the experimental values of k_H/k_D with a good degree of accuracy, but the theory does not explain the lower values of k_H/k_D found for methyl radical abstraction from H_2 and D_2. In Table I, the k_H/k_D values for various reactions are given together with the ratio of frequency factors, A_H/A_D, and the difference in activation energies, ΔE, found experimentally. It will now be shown that these observed values can be correlated with classical rate theory and that quantum mechanical tunneling need not be invoked.

CALCULATIONS

From absolute reaction rate theory (9), the ratio of rate constants is given by

$$\frac{k_H}{k_D} = \frac{\prod^{3n^{\neq}-7} \sinh \tfrac{1}{2}U_{i_D}^{\neq} \prod^{3n-6} \sinh \tfrac{1}{2}U_{i_H}}{\prod^{3n^{\neq}-7} \sinh \tfrac{1}{2}U_{i_H}^{\neq} \prod^{3n-6} \sinh \tfrac{1}{2}U_{i_D}} \qquad [2]$$

where the products and ratios of molecular mass and moments of inertia are assumed to be unity and U_i is $h\nu_i/kT$. We now examine several cases for the isotopic dependence of frequencies in the initial and activated states. If we first make the assumption that the frequencies associated with the activated complex are isotopically independent, then two limiting cases are obtained from equation 2. The first is that cleavage of a C—H bond occurs and the bending frequencies do not change from the initial to the activated state, that is, the only isotopically dependent vibration is the C—H stretch, so that equation (2) can be simplified to

$$k_H/k_D = \exp \tfrac{1}{2}(U_H - U_D). \qquad [3]$$

The second case arises when the C—H bond undergoing cleavage is stretched significantly so that the bending frequencies approach zero in the activated state. If this bending frequency is assumed to be doubly degenerate, equation 2 reduces (10) to

$$\frac{k_H}{k_D} = \tfrac{1}{2} \exp \tfrac{1}{2} \sum (U_{i_H} - U_{i_D}). \qquad [4]$$

A third case arises for the $CH_3 + H_2$ reaction when the frequencies in the activated complex are isotopically dependent. If the simple pseudo-three-atom model, the activated complex has the linear form $C \ldots H \ldots H_{(2)}$. If bending frequencies (which would be absent if the $H_{(2)}$ atom were sufficiently far away from the C atom in (CH_3) are neglected, there are two vibrations which exist (11). The first is the asymmetric one which leads to reaction and need not be considered. The second is the symmetric vibration which will result in the movement of the central H atom. Replacement of the central atom with D will then change this frequency and the symmetric vibration is therefore isotopically dependent. For abstraction from methane, the activated complex has the form C. . .H. . .C and the symmetric vibration does not involve any motion of the central H atom. For abstraction from a hydrocarbon, the activated complex has the same general form as that for methane and the symmetric vibration is assumed not to involve any motion of the central H or D atom. Hence replacement by D will have no effect and this frequency can, in principle, be neglected for this case. For $CH_3 + H_2$ and $CH_3 + D_2$ then, the ratio of rate constants is, from equation 2,

$$\frac{k_H}{k_D} = \exp \tfrac{1}{2}(U_D^{\neq} - U_H^{\neq}) \exp \tfrac{1}{2}(U_H - U_D). \qquad [5]$$

We can now calculate the isotope effect for the abstraction of H and D from hydrocarbons. When the C—H and C—D stretch vibrations in CH_4 and CD_4 are assumed to be 3020 and 2258 cm^{-1} respectively (12), then from equation 3,

$$\frac{k_H}{k_D} = \exp (1090/RT), \qquad [6]$$

which is 2.2 at 200° C. If the C—H and C—D bending frequencies of 1306 and 996 cm^{-1} (12) are doubly degenerate, then from equation 4

$$k_H/k_D = 0.5 \exp 1977/RT, \qquad [7]$$

which equals 4.1 at 200° C. Equation 7 predicts satisfactory k_H/k_D values (see Table I). There is some discrepancy, however, for the k_H/k_D values for abstraction from methane (1). This large discrepancy was explained by assuming that the potential energy barrier for abstraction from methane is higher than for ethane, propane, etc., and therefore results in a larger contribution from tunneling (1). The bond dissociation energy of methane is reported to be between 100 and 102 kcal $mole^{-1}$ (13, 14) and the corresponding value of the C—H bond energy for ethane is 98 kcal $mole^{-1}$ (14). If this difference between the C—H bond dissociation energies causes an increase in tunneling, then one would expect that proton tunneling for the reaction $CH_3 + H_2$ would be greater. This would follow from the bond dissociation energy of 103 kcal $mole^{-1}$ for H_2 (15) and also on steric grounds. The H_2 or D_2 molecule could approach the CH_3 radical more closely than a hydrocarbon molecule so that the width of the potential energy barrier would be decreased and the tunneling probability increased. The k_H/k_D ratio for abstraction from H_2 and D_2 is, however, 2.0 (7) and therefore precludes any significant tunneling.

TABLE I

Kinetic parameters for abstraction reactions

Reaction	ΔE (kcal mole^{-1})	A_H/A_D	k_H/k_D (200°)	Reference
$CH_3 + CH_4 \rightarrow CH_4 + CH_3$ $CD_3 + CD_4 \rightarrow CD_4 + CD_3$	3.5	8.91	8.1	5 1
$CD_3 + C_2H_6 \rightarrow CD_3H + C_2H_5$ $CD_3 + C_2D_6 \rightarrow CD_4 + C_2D_5$	1.5	1.0	4.95	4 4
$CD_3 + CH_3CD_3 \rightarrow CD_3H + CH_2CD_3$ $CD_3 + CH_3CD_3 \rightarrow CD_4 + CH_3CD_2$	1.9	0.72	4.95	4 4
$CD_3 + (CH_3)_3CH \rightarrow CD_3H + (CH_3)_3C$ $CD_3 + (CH_3)CD \rightarrow CD_4 + (CH_3)_3C$	1.6	0.8	4.4	2 2
$CD_3 + CH_3CH_2CH_3 \rightarrow CD_3 + CH_3CHCH_3$ $CD_3 + CH_3CD_2CH_3 \rightarrow CD_4 + CH_3CDCH_3$	1.4	1.04	4.5	2 6
$CH_3 + H_2 \rightarrow CH_4 + H$ $CH_3 + D_2 \rightarrow CH_3D + D$	1.7	0.41	2.0	7 7
$CF_3 + CHD_3 \rightarrow CF_3H + CD_3$ $CF_3 + CHD_3 \rightarrow CF_3D + CHD_2$	2.2	0.51	5.0	8 8

If the vibrations for H_2 and D_2 are taken as 4395 and 3118 cm^{-1} respectively (16), k_H/k_D is calculated to be 6.7 from equation 3. We have seen, however, that the symmetric vibration in the activated complex is isotopically dependent and equation 5 must be used to calculate k_H/k_D. In addition to this symmetric frequency, a doubly degenerate bending frequency may be generated in the activated complex if the approach of H_2 to CH_3 is close enough. These uncertainties prohibit a quantitative evaluation of the frequencies in the activated state, but their effect is clear. The "tighter" the activated complex, the smaller is the isotope effect. An activated complex which shows this behavior is that which arises during the electrochemical discharge of a proton (or a deuteron) from acid solution onto a mercury cathode. The sum of the frequencies for the activated complex Hg. . . H. . .O has been calculated by Conway and Salomon (17) and is 3550 cm^{-1}. It is also possible that the bonding in the activated state becomes tight enough to cause an inverse isotope effect, i.e. k_H/k_D is less than unity (11). Swain *et al.* (18) have found such a case for the decarboxylation of *p*-methylbenzoylacetic acid where $k_H/k_D = 0.85$.

CONCLUSION

It has been found that the k_H/k_D ratios found for methyl radical abstraction reactions can be explained on the basis of classical rate theory. There are several discrepancies noted in the literature and the main one is the k_H/k_D value obtained for abstraction from CH_4 and CD_4. There are also some minor differences in the predicted and experimental ratio of frequency factors. This can be attributed to experimental error, since an error of $\pm 2\%$ in the measurement of k_H/k_D can give large errors in A_H/A_D and in ΔE. The C—H bond has been treated as consisting of a single stretching and a doubly degenerate bending frequency. If the symmetric and asymmetric vibrations are taken into account, the effect would be to increase k_H/k_D still more. In the reactions considered, it is found that the theory of quantum mechanical tunneling need not be invoked to explain the observed isotope effects.

ACKNOWLEDGMENTS

The author wishes to thank Professors K. J. Laidler and B. E. Conway and Dr. M. Back for their interest in this work. Grateful acknowledgment is also made to the Sprague Electric Company for the award of a Fellowship.

REFERENCES

1. F. S. DAINTON, E. A. CREAK, and K. J. IVIN. Trans. Faraday Soc. **58**, 326 (1962).
2. W. JACKSON, J. R. MCNESBY, and B. DARWENT. J. Chem. Phys. **37**, 1610 (1962).
3. H. S. JOHNSTON and D. RAPP. J. Am. Chem. Soc. **83**, 1 (1961).
4. J. R. MCNESBY. J. Phys. Chem. **64**, 1671 (1960).
5. F. S. DAINTON, K. J. IVIN, and F. WILKINSON. Trans. Faraday Soc. **55**, 929 (1959).
6. W. M. JACKSON and J. R. MCNESBY. J. Am. Chem. Soc. **83**, 4891 (1961).
7. E. WHITTLE and E. W. R. STEACIE. J. Chem. Phys. **21**, 993 (1953).
8. T. E. SHARP and H. S. JOHNSTON. J. Chem. Phys. **37**, 1541 (1962).
9. S. GLASSTONE, K. J. LAIDLER, and H. EYRING. Theory of rate processes. McGraw-Hill, N.Y. 1941.
10. L. MELANDER. Isotope effects on reaction rates. Ronald Press, N.Y. 1960.
11. F. H. WESTHEIMER. Chem. Rev. **61**, 265 (1961).
12. G. HERZBERG. Infrared and raman spectra. Van Nostrand, N.Y. 1945.
13. E. W. R. STEACIE. Atomic and free radical reactions. Reinhold, N.Y. 1953.
14. T. L. COTTRELL. Strength of chemical bonds. Butterworths, London. 1958.
15. A. G. GAYDON. Dissociation energies and spectra of diatomic molecules. Chapman and Hall, London. 1953.
16. G. HERZBERG. Spectra of diatomic molecules. Van Nostrand, N.Y. 1950.
17. B. E. CONWAY and M. SALOMON. *In press* (1964).
18. C. G. SWAIN, R. F. W. BADER, R. M. ESTEVE, and R. N. GRIFFIN. J. Am. Chem. Soc. **83**, 1951 (1961).

[Reprinted from the Journal of Physical Chemistry, 68, 2009 (1964).]

Potentiostatic Determination of Electrolytic Hydrogen–Deuterium Separation Factors and the Reaction Mechanism at Mercury and Platinum

by M. Salomon and B. E. Conway

Department of Chemistry, University of Ottawa, Ottawa, Canada
(Received January 13, 1964)

The significance of the electrochemical hydrogen/deuterium separation factor has been considered in several previous papers[1,2] from this laboratory with regard to the mechanisms of the hydrogen evolution reaction (h.e.r.) at various metals and the role of proton tunneling[1]; in other papers (see below), Horiuti has considered the step of H_2^+ ion discharge as rate controlling and discussed possible isotope effects. We have previously considered the values of S in terms of the three commonly treated mechanisms of electrochemical hydrogen evolution from acid solution,[1] *viz.*

$$H_3O^+ + e + M \longrightarrow MH + H_2O \qquad (I)$$

with

$$H_3O^+ + e + MH \longrightarrow H_2 \qquad (II)$$

or

$$MH + MH \longrightarrow H_2 \qquad (III)$$

as the desorption steps and shown how the isotopic ratio R of exchange current densities[2] in pure H_2O and D_2O acid solutions is an additional criterion of reaction mechanism. In previous work, the dependence of S on potential and co-anion has been little studied and we report here *potentiostatic* determinations of S in acid solutions and some discussion of the theoretical significance of the results. At solid metals the variation of electrode potential with time at constant current is extensive,[3] so that potentiostatic control in S measurement is essential. The previous data are rather discrepant and the potential dependence of S has shown anomalous variations under controlled current conditions.[4-6] Thus, $dS/d\eta$ for mercury in H_2SO_4 solutions

(1) B. E. Conway, *Proc. Roy. Soc.* (London), **A247**, 400 (1958); *Can. J. Chem.*, **37**, 178 (1959); Transactions of the Symposium on Electrode Processes, May 4–6, 1959, Philadelphia, Pa., Yeager, Ed., John Wiley and Sons, Inc., New York, N. Y., 1961, Chapter 15, p. 267.

(2) B. E. Conway, *Proc. Roy. Soc.* (London), **A256**, 128 (1960).

(3) J. O'M. Bockris and B. E. Conway, *Trans. Faraday Soc.*, **45**, 989 (1949); J. O'M. Bockris and D. F. A. Koch, *J. Phys. Chem.*, **65**, 1941 (1961).

(4) G. P. Lewis and P. Ruetschi, *ibid.*, **66**, 1487 (1962).

has been reported variously as *ca.* 6.7 v.$^{-1}$ or 1.5 v.$^{-1}$ over the range of overpotentials η from 1.0 to 1.6 v. by the same authors in related papers.[5,6] Also, at lower potentials, S values are reported for constant current density of 0.3 ma. cm.$^{-2}$ but over a range of 300 mv.[5] This is inconsistent with the observed dependence of current on potential (Tafel line) for mercury in pure solutions. The tendency for S at mercury to reach a maximum with increasing η and then to decrease has been associated with the molecular equilibrium separation

$$H_2 + HDO \rightleftharpoons HD + H_2O \qquad (IV)$$

operating at low potentials followed by the electrochemical kinetic separation at higher potentials.[4] This view is difficult to accept since the mercury surface has no catalytic action with regard to reaction IV. Even at platinum, this equilibration is not experimentally observed[7] and in the present work the S at low potentials is dependent on the solution anion and is hence not determined by any equilibrium.

Experimental and Results

In an effort to clarify the experimental situation with regard to potential dependence of S, separation factor measurements were made under potentiostatic conditions in highly purified[8] HCl and $HClO_4$ solutions in water containing 10 vol. % of D_2O. Ultrapurification of the solutions by pre-electrolysis and distillation was carried out as developed in previous work.[8,9] Mercury was purified by multiple distillation and anodic electrolysis, followed by a final distillation. Platinum electrodes were sealed in glass bulbs as described previously. A special cell of small volume was used for the S measurements. The cell was flushed by means of purified nitrogen before a given sample of $H_2/HD/(D_2)$ was collected in an evacuated ampoule after drying. The hydrogen/deuterium content was determined by means of a mass spectrometer. Potential was controlled by a sensitive Wenking potentiostat to ±2 mv., using a hydrogen reference electrode in an isolated separate compartment of the cell. Current density–potential lines were run before and after the S measurements in order to check the Tafel parameters which agreed with accepted values allowing for time variation[3] of η at the solid metal platinum.

The separation factor at platinum is found to be a function of overpotential; the behavior observed depends on the nature of the anion of the electrolyte using HCl (aq) and $HClO_4$(aq), and may be compared (Fig. 1) with previously reported data[10] on platinum in H_2SO_4(aq) under controlled current conditions. The results of the present work are shown in Fig. 1 for platinum and Fig. 2 for mercury. At the latter metal, the S values are significantly potential dependent and $dS/d\eta = 0.6$ v.$^{-1}$ for HCl(aq) while $dS/d\eta = 1.44$ v.$^{-1}$ for $HClO_4$ solution. At platinum the $dS/d\eta$ values are much larger, and depend on the anion of the electrolyte (see Fig. 1 and 2). At mercury no evidence for

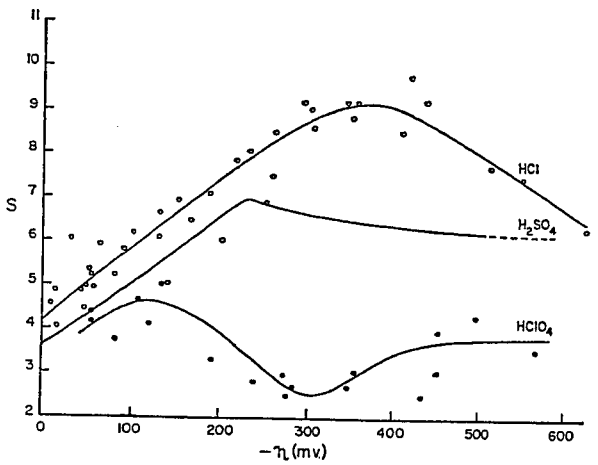

Figure 1. Electrolytic S values as a function of potential for platinum in various 1 N acid solutions (25°). Line for H_2SO_4 shown for comparison from data of Horiuti and Fukuda.[10]

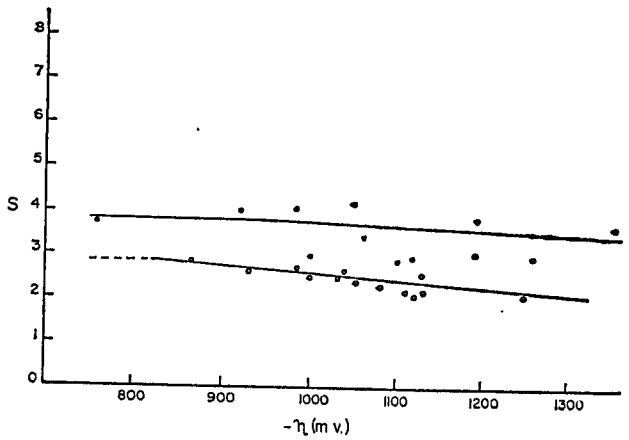

Figure 2. Electrolytic S values as a function of potential for mercury in 1 N aqueous acid solutions (25°): ●, HCl; ○, $HClO_4$.

(5) W. Vielstich, T. H. Schuchard, and M. von Stackelberg, *Ber. Bunsenges.*, **67**, 645 (1963).

(6) H. V. Buttler, W. Vielstich, and H. Barth, *ibid.*, **67**, 650 (1963).

(7) M. Enyo, M. Hoshi, and H. Kita, *J. Res. Inst. Catalysis Hokkaido Univ.*, **10**, 153 (1962).

(8) A. M. Azzam, J. O'M. Bockris, B. E. Conway, and H. Rosenberg, *Trans. Faraday Soc.*, **46**, 918 (1950).

(9) J. O'M. Bockris and B. E. Conway, *ibid.*, **48**, 724 (1952).

(10) J. Horiuti and M. Fukuda, *J. Res. Inst. Catalysis Hokkaido Univ.*, **10**, 72 (1962).

anomalous maxima[4] is obtained in highly purified solutions[11] and the S diminishes continuously with increasing η (Fig. 2). The linear dependence of S on η is in disagreement with the data of Lewis and Ruetschi[4] and differs from that of Vielstich, *et al.*,[5] where anomalous maxima were observed. In the latter work, the potentials attained at the various currents used are not, however, consistent with the accepted Tafel parameters for hydrogen evolution at mercury from acid solutions.

Discussion

For mercury, the mechanism of the h.e.r. has been discussed in terms of two widely different rate-controlling mechanisms: the H_3O^+ ion discharge step I or the H_2^+ ion neutralization (V) favored by Horiuti[12,13]

$$2H^+ + e \rightleftarrows H_2^+$$
$$H_2^+ + e \longrightarrow H_2 \qquad \text{(V)}$$

A large body of critical evidence has been adduced against the latter mechanism in publications elsewhere[14-16] but recently Keii and Kodera[13] have attempted to show that step I cannot be associated with the observed hydrogen–deuterium isotope effect of *ca.* 3.2 since their calculations using a pseudo-diatomic molecule model for $H\text{–}O^+<\begin{matrix}H\\H\end{matrix}$ and a single metal site for the Hg–H interaction lead to a claimed minimum value of S of 13 for step I, taking a doubly degenerate bending frequency involving the hydrogen atom in the M–H–O transition state. This is the only frequency in the transition state which these authors consider can be isotope dependent (on this model) since the treatment assumes hydrogen and deuterium discharge from the pseudo-diatomic ions $H^+\text{–}(H_2O)$ and $D^+\text{–}(H_2O)$ in solutions dilute enough in deuterium that most of the deuterium–oxonium species are present as H_2DO^+. The calculations of Keii and Kodera indicate a force constant f^* of 23 kcal. Å.$^{-2}$ which leads to a rather loose activated complex with bending frequency $\nu^* = 522$ cm.$^{-1}$ and hence a high S value, using data for the equilibrium constant for hydrogen–deuterium partition between liquid and vapor H_2O and HDO with the partition functions for gaseous H_2O and HOD. The problem of the high value of S which this model predicts can, however, be overcome by considering a "complex site" for proton discharge in the h.e.r. and/or the frequency of the symmetrical mode (see below). In this model, the proton is regarded as being discharged interstitially between two or three metal atoms in the metal surface. Such a picture of hydrogen chemisorption has been proposed for a number of years as a result of MH surface dipole measurements[17] and infrared studies[18] and was suggested by Conway and Bockris[19] for the situation of adsorbed hydrogen in the h.e.r. in calculations of the activation energy for step II. The significance of this model for calculations of S is that an activated complex would be involved consisting of two or three metal atoms, an oxygen atom (in "H_3O^+"*), and the transferred hydrogen or deuterium, and would exhibit five or eight vibrations instead of the two in the activated complex of Keii and Kodera.[13] This increase of the complexity of the activated complex would result in a lowering of S from the previously calculated value of 13. Quantitative calculations for the two-metal atom model and also taking into account the symmetrical stretch mode indicate[20] that S can be as low as 3.8 for mercury, using the partition function ratio for H_3O^+ and H_2DO^+ based on direct spectroscopic data for acid solutions in water and D_2O.[21] While no exact quantitative comparison with the experimental value of 3.2 (HCl aqueous solutions) would be justified, the calculations show that with a more realistic model of the activated state, values of S appreciably lower than the claimed minimum of 13 can be calculated for step I. Step I cannot hence be excluded as a rate-determining step for the h.e.r. at mercury. Furthermore, reaction order considerations[22] indicate an electrochemical reaction order in $[H^+]$ of two for step IV whereas the value observed is unity for mercury, which is consistent with step I and the frequently confirmed Tafel slope of *ca.* 2.3 ($2RT/F$).

The potential dependence of S at mercury is much smaller than at platinum and cannot be explained in terms of changing hydrogen coverage θ_H with potential[1] since $\theta_H << 1$.[23] At mercury the activated complex

(11) M. Rome and C. F. Hiskey, *J. Am. Chem. Soc.*, **76**, 5207 (1954).

(12) J. Horiuti and G. Okamoto, *Sci. Int. Phys. Chem. Res. Tokyo*, **28**, 231 (1936); see also J. Horiuti, T. Keii, and K. Hirota, *J. Res. Inst. Catalysis Hokkaido Univ.*, **3**, 1 (1951).

(13) T. Keii and T. Kodera, *ibid.*, **5**, 105 (1957); see also J. Horiuti, Transactions of the Symposium on Electrode Processes, May 4–6, 1959, Philadelphia, Pa., John Wiley and Sons, Inc., New York, N. Y., 1961.

(14) A. N. Frumkin, Transactions of the Symposium on Electrode Processes, May 4–6, 1959, Philadelphia, Pa., John Wiley and Sons, Inc., New York, N. Y., 1961, pp. 35–45.

(15) A. N. Frumkin, *Acta Physiochim.*, **18**, 23 (1943).

(16) J. O'M. Bockris, *J. Res. Inst. Catalysis Hokkaido Univ.*, **2**, 105 (1953).

(17) J. C. P. Mignolet, *Discussions Faraday Soc.*, **8**, 105 (1950).

(18) R. P. Eischens and A. Pliskin, 135th National Meeting of the American Chemical Society, Boston, Mass., April, 1959.

(19) B. E. Conway and J. O'M. Bockris, *Can. J. Chem.*, **35**, 1124 (1957).

(20) B. E. Conway and M. Salomon, *Ber. Bunsenges*, in press.

(21) G. Swain, R. F. W. Bader, and R. Thornton, *Tetrahedron*, **10**, 200 (1960).

(22) B. E. Conway and M. Salomon, *Electrochim. Acta*, in press.

(23) A. N. Frumkin, *Discussions Faraday Soc.*, **1**, 57 (1947).

has a symmetric vibrational mode (not considered by Keii and Kodera) along the direction of the reaction coordinate (the asymmetric mode becomes the motion of hydrogen leading to decomposition) and this may be potential dependent since the H_3O^+–metal interaction varies with potential across the double layer, and the O in "H_3O^+" becomes electrostatically more tightly bound with increasing cathodic potential. The increase of the differential double-layer capacity at mercury which occurs with increasing potential on the cathodic branch may be regarded as supporting evidence for this viewpoint, since if the cations tend to become more tightly bound, the time average thickness of the double layer will tend to decrease and the capacity hence increase.

The above general model can offer some explanation for the dependence of S on η and the electrolyte anion for the case of platinum. At low potentials, up to η = *ca.* −200 mv., the potential–log current density line for platinum prepared under the present conditions exhibits a change of Tafel slope from 0.03 v. toward a limiting current with increasing current densities, and a descending Tafel slope of 0.12 v. or greater. The potential region where some change of Tafel slope occurs is similar to that where the separation factor changes its dependence on potential (Fig. 1). These data suggest that the initial high dependence of S on η in, *e.g.*, HCl, is associated with the hydrogen atom recombination reaction proceeding under conditions of increasing coverage while the behavior at higher potentials is associated with the atom–ion desorption step[24] proceeding on the fully covered available surface. Anion effects may still arise at platinum at appreciable cathodic potentials since specific changes of capacity behavior are observed at such potentials from F^- to Cl^-, Br^-, and I^- solutions.[25]

Initial chemisorption may occur at a two- or three-site center,[19,26] and the resulting tight activated complex could then give a low separation factor. As coverage increases, proton discharge may then proceed at sites with smaller "multiplicity," possibly finally being adsorbed on top of a metal atom: this would give the loosest activated complex and hence a maximum separation factor. The effect of the nature of the anion now becomes clearer. As the tendency of the anion to be specifically adsorbed increases,[25] it may be suggested that the adsorbing hydrogen atoms must find sites of lower multiplicity and/or lower binding energy,[27] so that the separation factor would tend to increase. This is related to the effect of changing coverage on S and R discussed previously.[1,2] The order of decreasing effect of specific adsorption of anions is known to be $Cl^- >> SO_4^{-2} \geq ClO_4^-$.[27a] From Fig. 1, it is seen that the separation factor increases as the tendency for specific adsorption increases, and hydrogen adsorption energy decreases.[27b]

These effects, discussed qualitatively here, have also been examined more quantitatively by a statistical mechanical treatment of isotope effects in the h.e.r. and satisfactory agreement between theory and experiment is found.[20] Also the isotope ratios R of exchange currents[2] can be shown to be consistent with the S values.

Acknowledgments. The authors wish to express their gratitude to Dr. A. Tickner and Mr. R. Sander for their advice on mass spectrometric techniques and their time spent in analyzing our hydrogen–deuterium samples.

M. S. is indebted to the Sprague Electric Co. for the award of a Fellowship and for support of part of the experimental work.

(24) J. O'M. Bockris and A. M. Azzam, *Trans. Faraday Soc.*, **48**, 145 (1951).

(25) P. V. Popat and N. Hackerman, *J. Phys. Chem.*, **62**, 1198 (1958); see also A. N. Frumkin, "Advances in Electrochemistry," Vol. 3, Delahay, Ed., Interscience Publishers, Inc., 1963, Chapter 5.

(26) This may lead to an extent of coverage by hydrogen somewhat larger than that corresponding to one atom of hydrogen per platinum atom, at high potentials. This may not be inconsistent with the apparent coverages measured since real areas are usually uncertain.

(27) (a) M. Breiter, L. Kandler, B. Kennel, and H. Feigl, Tech. Rept. No. AF61(052)-305, October 31, 1960; (b) F. Boeld and M. Breiter, *Z. Elektrochem.*, **64**, 897 (1960); M. Breiter and B. Kennel, *ibid.*, **64**, 1180 (1960).

Sonderdruck aus der Zeitschrift:
Berichte der Bunsengesellschaft für physikalische Chemie (früher Zeitschrift für Elektrochemie)
Band 68, Heft 4, 1964 (Seite 331–340), Verlag Chemie, GmbH., Weinheim/Bergstr.

Isotope Effects in Electrochemical Proton Discharge

By *B. E. CONWAY* and *M. SALOMON*

Department of Chemistry, University of Ottawa
Ottawa, Canada

(Eingegangen am 9. März 1964)

Calculations of the H/D and H/T separation factors (S) and exchange current density ratios (R) for the proton discharge mechanism on mercury, nickel, and iron are presented. A vibrational analysis of the activated complexes is made by reference to both a linear three-center transition state model and a surface interstitial site model in which H is regarded as being adsorbed adjacent to two metal atoms in the surface. It is shown that the isotope effects observed experimentally, e.g. at mercury, can be accounted for in terms of a slow proton discharge mechanism. Calculations are made for discharge from H_3O^+ and H_2O molecules. The values of R are shown to be consistent with the values of S_D calculated and observed. An explanation is also given qualitatively for the potential dependence of S_D at mercury in terms of electrostriction effects in the double layer.

Die H/D- und H/T-Trennfaktoren (S) und die Quotienten der Austauschstromdichten (R) werden für den Protonenentladungsmechanismus an Quecksilber, Nickel und Eisen berechnet. Eine Analyse der Schwingungszustände des aktivierten Komplexes wird für zwei Modelle vorgenommen: für einen linearen Dreizentren-Übergangszustand und für ein Zwischengitterplatzmodell an der Metalloberfläche, bei dem angenommen wird, daß Wasserstoffatome zwischen zwei Metallatomen an der Grenzfläche adsorbiert werden. Es wird gezeigt, daß die z.B. an Quecksilber experimentell gefundenen Trennfaktoren im Einklang sind

mit den unter Annahme einer geschwindigkeitsbestimmenden Protonenentladung berechneten. Die Berechnungen werden für die Entladung aus H_3O^+ und aus H_2O-Molekeln durchgeführt. Die Werte für R erweisen sich als konsistent mit den berechneten und beobachteten Werten für S_D. – Die Potentialabhängigkeit von S_D kann qualitativ durch den Einfluß der Elektrostriktion der Doppelschicht erklärt werden.

I. Introduction

In recent years, the significance of the H/D separation factor (S_D) in relation to various possible mechanisms of the electrochemical hydrogen evolution reaction, ("h.e.r.") has been considered [1–4]. Although data on the values of S_D for various metals in acid and alkaline solutions have been available for some years [5, 6] little attention has been paid towards the dependence of S on the overpotential η. Recently Vielstich and co-workers [7, 8] have studied S_D and S_T as a function of η for several metals and Conway and Salomon [9] have studied the $S_D - \eta$ relationship as a function of the nature of the anion. H/D isotope effects based on a tunneling mechanism have been discussed theoretically by Conway and Christov [10]. Also the ratios of exchange currents, R, in pure H_2O and D_2O have been measured [11, 2] and discussed in terms of reaction mechanism [11]. In the latter work, the role of isotope effects in both the zero point energies of initial and activated states were considered semi-quantitatively and the role of isotopic differences of steady state coverage by H and D was evaluated [2].

Two principal rate limiting mechanisms of the h.e.r. have been considered for mercury in acid solution: (i) the discharge of protons from H_3O^+ ions in the double layer and (ii) the mechanism of Horiuti [3] involving the steps

$$2\,H_3O^+ + e = H_2^+ + 2\,H_2O$$

followed by rate limiting

$$H_2^+ + e \rightarrow H_2.$$

The slow discharge step (i) has been considered by Horiuti [3] to be inoperative at mercury and Keii and Kodera [4] have calculated a value of 13 for S_D at mercury which is therefore claimed [4] to disprove the applicability of the discharge mechanism because $S_D \doteq 3$ at mercury. Since various other evidence concerning the lack of significant H-adsorption pseudocapacity at mercury (see ref. [23]) and the observation of an electrochemical reaction order of unity [12, 13] indicates process (i) to be operative, it is necessary to re-examine the theory of the H/D isotope effects at mercury and other metals in order to establish if the observed value of S_D = ca. 3–4 and $R = 1.9$ at Hg can in fact, be accounted for by the slow discharge mechanism. It is therefore the purpose of the present paper to present new calculations of S_D for the proton discharge mechanism and to show that this mechanism is in fact operative at mercury and possibly at nickel and iron in acid solutions.

In the present treatment an analysis of the vibrational modes in the activated complex is made taking into account the symmetrical stretching mode which was neglected by Keii and Kodera [4]. In our previous treatment for S_D [1, 2], estimates of the maximum isotope effects were made by a thermodynamic calculation for the purpose of comparing the predictions of S_D for various mechanisms.

II. Formulation of the Rate Equations

In terms of absolute rate theory, the discharge of an H, D, or T entity from aqueous H_3O^+, H_2DO^+ and H_2TO^+ ions can be represented by

$$H_3O^+_{\text{d.l.}} + M + e_M = X_H^{\ddagger} \rightarrow MH + H_2O$$

$$H_2DO^+_{\text{d.l.}} + M + e_M = X_D^{\ddagger} \rightarrow MD + H_2O$$

$$H_2TO^+_{\text{d.l.}} + M + e_M = X_T^{\ddagger} \rightarrow MT + H_2O$$

where $X^{\ddagger}$ represents the activated complex and the subscript d. l. refers to the initial state position of the oxonium ion in the electrode double layer at some potential ψ_1 at the outer Helmholtz plane [14, 15] relative to that in the bulk solution. The rate of proton discharge can be written as

$$i_H = ZF\frac{kT}{h}(1-\Theta_H)\,C_{H_3O^+_{\text{d.l.}}}\frac{f_H^{\ddagger}}{f_M F'_{H_3O^+}} \times \exp\left[-\beta(\Phi-\psi_1)F/RT\right] \quad (1)$$

where the f's are the molecular partition functions of the indicated species and F' is the molecular partition function per unit area (F is that per unit volume), Θ_H is the fractional coverage by H, Φ is the electrode solution potential difference and all other terms have their usual significance. The concentration of H_3O^+ ions in the double layer can be related to the bulk concentration by the isotherm [15]

$$C_{H_3O^+_{\text{d.l.}}} = C_{H_3O^+_b}\frac{F'_{H_3O^+}}{F_{H_3O^+}}\exp\left(-\psi_1 F/RT\right) \quad (2)$$

and combination of equations (1) and (2) gives

$$i_H = ZF\frac{kT}{h}(1-\Theta_H)\,C_{H_3O^+_b}\frac{f_H^{\ddagger}}{f_M F_{H_3O^+}} \times \exp\left[-\psi_1 F/RT\right]\exp\left[-\beta(\Phi-\psi_1)F/RT\right]. \quad (3)$$

In equation (3) the transmission coefficient has been omitted since it is generally regarded as having a value near unity and assumed to be independent of H or D mass [16]. For discharge from H_2DO^+, H_2TO^+ and D_3O^+, the relevant rate equations are

$$i_D = ZF\frac{kT}{h}(1-\Theta_t)\,C_{H_2DO^+_b}\frac{f_D^{\ddagger}}{f_M F_{H_2DO^+}} \times \exp\left[-\beta(\Phi-\psi_1)F/RT\right]\exp\left[-\psi_1 F/RT\right] \quad (4\,a)$$

$$i_T = ZF\frac{kT}{h}(1-\Theta_t)\,C_{H_2TO^+_b}\frac{f_T^{\ddagger}}{f_M F_{H_2TO^+}} \times \exp\left[-\beta(\Phi-\psi_1)F/RT\right]\exp\left[-\psi_1 F/RT\right] \quad (4\,b)$$

$$i_D = ZF\frac{kT}{h}(1-\Theta_D)\,C_{D_3O^+_b}\frac{f_D^{\ddagger}}{f_M F_{D_3O^+}} \times \exp[-\beta(\Phi-\psi_1)F/RT]\exp[-\psi_1 F/RT] \qquad (4c)$$

respectively. Equations (4a) and (4b) refer to dilute solutions of D and T in H_2O and equation (4c) refers to discharge of a deuteron from pure D_2O acid (D_3O^+) solutions; Θ_t refers to the total coverage by H, D or T.

In equations (3) and (4), tunneling correction factors have been neglected. This is based on our recent experimental results for the low temperature behaviour of the h.e.r. at mercury and platinum [17], where no unequivocal evidence to indicate significant tunneling is found at temperatures down to $-150\,°C$ in methanolic and supercooled ethanolic HCl and DCl solutions. Thus, the apparent heat of activation [18] is found to be independent of temperature at mercury in CH_3OH and CH_3OD down to $-125\,°C$ and at platinum down to $-150\,°C$, although the Tafel slopes are greater than the classical values, at the lower temperatures. If appreciable proton tunneling occurred, the previous calculations of Conway [10] indicate that a) the H/D isotope effect should be potential dependent and b) the Tafel slope should be larger than the classical value $2.3\,RT/\beta F$. The calculations of Bell indicate correspondingly that the heat of activation should decrease with decreasing temperature [19]. Johnston and Rapp [20] have, however, shown that a temperature independent heat of activation can arise over a small temperature range and their theory has been successfully applied to gas phase H atom transfer reactions [21]. Salomon [22] has, however, shown that these atom transfer reactions can be described by the classical (activated) mechanism. Hence it appears that proton tunneling may not occur in either the electrochemical or gas phase transfer reactions to any appreciable extent.

III. Isotope Effects Arising for the Slow Proton Discharge Step

The separation factor S_D for solutions containing H and D is defined as

$$S_D = \left(\frac{C_D}{C_H}\right)_{soln}\cdot\left(\frac{C_H}{C_D}\right)_{gas} \qquad (5)$$

where C is the total concentration of the indicated species in the solution and the gas phase. For solutions sufficiently dilute in D that the only significant D containing species is H_2DO^+, the term (C_H/C_D) gas may be replaced by the ratio of rates of formation of MH and MD given by equations (3) and (4a); that is

$$S_D = \left(\frac{C_D}{C_H}\right)_{soln}\frac{C_{H_3O^+}}{C_{H_2DO^+}}\frac{f_{H_2DO^+}}{f_{H_3O^+}}\frac{f_H^{\ddagger}}{f_D^{\ddagger}}. \qquad (6)$$

Similarly, the hydrogen-tritium separation factor is given by

$$S_T = \left(\frac{C_T}{C_H}\right)_{soln}\frac{C_{H_3O^+}}{C_{H_2DO^+}}\frac{f_{H_2TO^+}}{f_{H_3O^+}}\frac{f_H^{\ddagger}}{f_T^{\ddagger}}. \qquad (7)$$

Finally, the ratio of exchange current densities, R, for H_2 and D_2 production from pure H_2O and D_2O solutions, respectively can be obtained from equations (3) and (4c) as

$$R = \frac{f_{D_3O^+}}{f_{H_3O^+}}\frac{f_H^{\ddagger}}{f_D^{\ddagger}}\exp[\beta(\Phi_D^0-\Phi_H^0)F/RT]. \qquad (8)$$

In equation (8), the ratio $(1-\Theta_H)/(1-\Theta_D)$ is taken as unity since Θ_H for mercury is less than 0.05 [23]. The difference in reversible potentials $\Phi_D^0-\Phi_H^0$ which also enters into the calculation of R was estimated by Conway [1] by reference to the cell

$$Pt\,|\,H_2\,|\,HCl_{a^{\pm}=1}\,\|\,DCl_{a^{\pm}=1}\,|\,D_2\,|\,Pt$$

studied by Lange [24] and found to be -9 mV.

IV. Calculation of Initial State Quantities

In this section we evaluate all the quantities in equations (6) to (8) except the $f^{\ddagger}$ ratios which will be calculated in the following section. The molecular partition function ratio $f_{H_2DO^+}/f_{H_3O^+}$ is obtained from the spectroscopic work of Swain et al. [25]*) who calculated an equilibrium constant of 8.2 for the reaction

$$2\,D_3O^+ + 3\,H_2O \rightleftarrows 2\,H_3O^+ + 3\,D_2O$$

in excellent agreement with the value obtained experimentally by Heinzinger and Weston [26]. Then $f_{D_3O^+}/f_{H_3O^+}$ can be evaluated, and from the rule of the geometric mean,

$$\frac{f_{H_2DO^+}}{3f_{H_3O^+}} = \frac{3f_{D_3O_+}}{f_{HD_2O^+}} = \frac{f_{HD_3O^+}}{f_{H_2DO^+}}$$

it is found that [25]

$$\frac{f_{H_2DO^+}}{f_{H_3O^+}} = 3\left(\frac{f_{D_3O^+}}{f_{H_3O^+}}\right)^{1/3} = 80.08. \qquad (9)$$

Since the above relations give the relevant partition function ratios, a material balance calculation can be made to calculate the concentrations of the various oxonium ions present in solution (cf. reference [25]).

Table 1
Concentrations of Various Oxonium Ions in 1 N Acid Solution

$C_D/C_H = 0.1111$			$C_T/C_H = 1.807\cdot10^{-7}$	
H_3O^+	0.7982	mole litre^{-1}	H_3O^+	0.99999... mole litre^{-1}
H_2DO^+	0.1865		H_2TO^+	$3.99-10^{-7}$
HD_2O^+	0.0150		HT_2O^+	10^{-10}
D_3O^+	0.0004		T_3O^+	$\ll 10^{-10}$

The results are given in Table 1 for a solution 10% in D_2O (by volume) and normal with respect to the acid. From this composition, $(C_D/C_H) = 0.1111$ and $C_{H_3O^+}/C_{H_2DO^+} = 4.28$ so that equation (6) becomes

$$S_D = 38.08\frac{f_H^{\ddagger}}{f_D^{\ddagger}}. \qquad (10)$$

*) That is, using data directly for the ions and molecules *in solution* and not by reference to equilibria involving H_2O, HOD and D_2O in the vapour phase [3–5].

In order to calculate S_T, the partition function ratios for the various H and T containing species were evaluated using the method of Bader [27]. The valency angle of H_3O^+ was taken as 107° [28] and the bond length as 1.05 Å [29, 30]. The librational frequency shifts were calculated from the inverse square roots of the average moments of inertia using the relationship given by Moelwyn-Hughes [31]. From the rule of the geometric mean, we have again

$$\frac{f_{H_2TO^+}}{3f_{H_3O^+}} = \frac{3f_{T_3O^+}}{f_{HT_2O^+}} = \frac{f_{HT_3O^+}}{f_{H_2TO^+}}$$

and it is found that

$$\frac{f_{H_2TO^+}}{f_{H_3O^+}} = 3\left(\frac{f_{T_3O^+}}{f_{H_3O^+}}\right)^{1/3} = 425.1. \qquad (11)$$

Next, we assume a "random isotope distribution" [32] for the equilibrium reaction

$$H_2O + T_2O = 2\,HTO \qquad K = 4.0$$

and calculate the following equilibrium constants:

$$H_2O + H_2TO^+ = HTO + H_3O^+ \qquad K = 0.906$$
$$H_2O + T_3O^+ = HTO + HT_2O^+ \qquad K = 8.157$$
$$2\,T_3O^+ + 3\,H_2O = 2\,H_3O^+ + 3\,T_2O \qquad K = 6.286$$

For a solution of 10^{-5} mole T_2O in 1 l H_2O and normal with respect to acid strength, a material balance calculation using the above equilibrium constants leads to the results given in Table 1. For the above concentration of T, $(C_T/C_H)_{soln} = 1.81 \cdot 10^{-7}$ and $C_{H_3O^+}/C_{H_2TO^+} = 2.51 \cdot 10^7$. Hence equation (7) becomes

$$S_T = 192.5\,\frac{f_H^{\ddagger}}{f_T^{\ddagger}}. \qquad (12)$$

Finally the ratio of exchange current densities R is obtained from equation (8) (assuming $\beta = 1/2$) as

$$R = 16.265\,\frac{f_H^{\ddagger}}{f_D^{\ddagger}}. \qquad (13)$$

V. *Calculation of the $f^{\ddagger}$ Ratios*

(i) *Partition Functions*

The H and D transition states in the proton discharge from H_3O^+ and H_2DO^+ may be regarded*) as linear "three-center" pseudo-triatomic structures of the form

$$M \overset{1}{-} H \overset{2}{-} OH_2$$
$$M - D - OH_2.$$

The partition function ratio for these activated states is

$$\frac{f_H^{\ddagger}}{f_D^{\ddagger}} = \Pi^{2}\frac{f_{t,H}^{\ddagger}}{f_{t,D}^{\ddagger}}\,\Pi^{2}\frac{f_{r,H}^{\ddagger}}{f_{r,D}^{\ddagger}}\,\Pi^{3}\frac{\sinh u_{i,D}^{\ddagger}}{\sinh u_{i,H}^{\ddagger}} \qquad (14)$$

where f_t and f_r are the translational and rotational contributions, respectively, and the vibrational contribution is put into the hyperbolic sine form [16] where $u_i = h\nu_i/2kT$. The ratio of translational partition functions for two-dimensional motion at the interface is taken as unity (this is obviously also the case for an immobile activated complex) and the ratio of rotational partition functions (describing the librational energy differences) is also taken as unity since f_r values are inversely proportional to the square roots of the moments of inertia which will be practically independent of H or D for the two activated complexes. Hence equation (14) reduces to

$$\frac{f_H^{\ddagger}}{f_D^{\ddagger}} = \Pi^{3}\frac{\sinh u_{i,D}^{\ddagger}}{\sinh u_{i,H}^{\ddagger}} \qquad (15)$$

i.e. the main isotopic effect arises from the differences of vibrational frequencies.

In order to make a vibrational analysis, we use a general quadratic function and obtain for the three-center transition state [33, 34]

$$\left.\begin{aligned}
\lambda_1 + \lambda_2 &= \frac{k_1}{m_M} + \frac{k_2}{m_{OH_2}} + \frac{k_1 + k_2 - 2k_{12}}{m_X} \\
\lambda_1\lambda_2 &= \frac{k_1k_2 - k_{12}^2}{m_M m_X + m_M m_{OH_2} + m_X m_{OH_2}} \\
\lambda_3 &= \left[\frac{1}{m_M d_1^2} + \frac{1}{m_X}\left(\frac{1}{d_1} + \frac{1}{d_2}\right)^2 + \frac{1}{m_{OH_2} d_2^2}\right] d_1 d_2 k_3
\end{aligned}\right\} \qquad (16)$$

where $\lambda = 4\pi^2\nu^2$ and λ_1, λ_2, λ_3, refer to the symmetric, asymmetric and bending modes of frequencies ν_1, ν_2 and ν_3, respectively; k_1, k_2 and k_3 are the respective force constants in md/Å; d is the bond distance in Å, and m is the mass of the indicated species (m_X is the isotopic mass of H, D, or T). Since the asymmetric mode corresponds to decomposition (i.e. to reaction), λ_2 can be taken as zero [34] which leads to the condition

$$k_1k_2 - k_{12}^2 = 0. \qquad (17)$$

The interatomic distances involved in the activated complexes for the discharge mechanism at several metals were calculated as follows: the position of the reacting H, D, or T atom is assumed to be half way between its position in the initial and final states (this corresponds approximately to taking β as 0.5); the metallic radii for the three metals Fe, Ni and Hg were taken as 1.24, 1.24 and 1.50 Å respectively [35]; the O–H distance in the initial state of H_3O^+ is taken as 1.05 Å [29, 30] and finally the thickness of the double layer is taken as 1.79 Å [36]. This gives a total distance of 0.5 Å through which the proton is transferred from the initial to the final state, cf. [36].

Calculations of $\nu_1^{\ddagger}$ and $\nu_3^{\ddagger}$ are made by taking the condition that $k_1k_2 - k_{12}^2 = 0$ as given by equation (17). Since the coupling constant k_{12} can be significant for activated complexes [34], k_1 or k_2 is not necessarily taken as zero. We shall take the condition $k_1 > k_2$ for the following reasons: the activated complex has the form M–H–O in which the initial bond between H and O is partially broken while the bond between M and H is partially formed. The condition that the system M–H–O be an activated complex is that one of its frequencies is low and becomes a translation [37].

*) The justification for this kind of assumption has been treated in several papers – see ref. [34].

This condition is met by taking the frequency for the asymmetric stretch in the dissociating bond as zero and the force constant (k_2) which opposes this condition in the symmetric stretch mode as small or zero.

(ii) *Force constants*

There are several methods which can be used to evaluate the force constants required in equation (16). The most familiar method is of course that developed by Eyring and Polanyi [38] who used the London equation [39] to obtain the total energy, E, of the activated complex. For a three atom system, E is given by

$$E = \frac{Q_1 + Q_2 + Q_3 \pm \left\{\frac{1}{2}[(\alpha_1 - \alpha_2)^2 + (\alpha_2 - \alpha_3)^2 + (\alpha_3 - \alpha_1)^2]\right\}^{1/2}}{1 + \Delta}$$

where Q and α are the Coulomb and exchange energies respectively, and Δ is the electron overlap integral. Eyring and Polanyi assumed Q/α to be a constant and set Δ equal to zero. However, since Q, α and Δ are all functions of internuclear distance, and in addition Δ will strongly depend upon the effective quantum number n, this method is to be regarded as "semi-empirical". Thus, in calculating the isotope effect S_D at a nickel cathode for the atom-atom recombination mechanism by this method, Horiuti et al. [5] obtained an activation energy of 75 kcal · mole^{-1} which exceeds the experimental value by at least one order of magnitude [37].

Sato [40] has proposed an alternative procedure in which Δ is taken as the adjustable parameter to set the activation energy equal to the observed value. According to Sato, if Δ is regarded as a constant, then Q and α can be calculated from spectroscopic data for the diatomic molecule. However, since Δ is in fact not constant, but varies strongly with internuclear distance, the method is really no improvement over the original one of Eyring and Polanyi (cf. Weston [41]).

A third method, the one used here, is that in which the geometry and force constants of the activated complex are chosen by reference to analogous situations in other molecules. Thus, if reasonable values for k_1, k_2 and k_3 can be estimated by reference to the force constants of molecules of similar structure, such values can be used to give the observed isotope effect, say S_D, and then used to calculate the remaining two isotope effects S_T and R. The values of the k's used in the present calculations are given in Table 2 and are compared with the k' values found spectroscopically for the isolated M–H and H_3O^+ molecules. It is seen that k_1 values for all three metals are taken as being nearly equal in the activated complex while they differ significantly for the corresponding isolated M–H molecules. This choice of k_1 values can be justified on the following grounds: The M–H bond in the activated complex is a stretched bond and may be considered to be only partially formed as discussed previously. Since k_1 is determined by the sum $Q + \alpha$, we can show qualitatively that the main factor determining k_1 is the exchange energy α. The exchange energy is determined by the overlap integral Δ which in turn is strongly dependent upon internuclear distance. It can be seen from the Q/α ratio that if $Q < \alpha$, then changes in Δ will have a large effect on k_1 whereas if $Q > \alpha$, then changes in Δ will have smaller effects on k_1. Since electron overlap decreases as the effective quantum number, n, increases, it follows that the fraction Q/α will vary in the order Fe < Ni < Hg. The extent of increase of Q/α with increasing effective quantum number has been estimated by Rosen and Ikehara [42]. For example, Q is 14% in the H_2 molecule [37], about 18% in the Na_2 molecule [42] and about 24% in Ni_2 [5]. Since α decreases in the order $\alpha_{Fe} > \alpha_{Ni} > \alpha_{Hg}$ it follows that by stretching the M–H bonds, the change in force constant, dk_1, will vary for the three metals in the order $dk_1(Hg) < dk_1(Ni) < dk_1(Fe)$. This is the condition we have used in the present calculations.

Table 2
Numerical Data Used for Vibrational Analysis of the Activated Complex

	Interatomic Distances (Å)		Force Constants (md Å^{-1})			Force Constants for the Isolated Molecule	
	d_1	d_2	k_1	k_2	k_3	k_1'	k_2'
Hg	1.99	1.30	1.159 1.15	0 0.1 (in H_3O^+)	0.1–0.2 0.1–0.2	1.159 (HgH)	4.9 (H_3O^+)
Ni	1.73	1.31	1.95 1.15	0.49 (in H_3O^+) 0.87 (in H_2O) 0.10 (in H_3O^+) 0.159 (in H_2O)	0.1–0.2 0.1–0.2	2.11 (NiH)	4.9 (H_3O^+) 7.8 (H_2O)
Fe	1.73	1.31	1.10	0.10 (in H_3O^+) 0.159 (in H_2O)	0.1–0.2	ca. 2.2 (FeH) (cf. ref. [2])	4.9 (H_3O^+) 7.8 (H_2O)

Therefore, although this method avoids arbitrariness in assignment of values to Q, α and Δ, it must still be considered empirical since k_1 and k_2, although chosen rationally, are still adjustable parameters. However, the method is no more empirical than the other two methods described above. The calculated isotope effects are, to a fairly good approximation, independent of slight changes which might be assumed in the geometry of the activated complex (e.g. changes of geometry equivalent to taking β as 0.4 to 0.6 do not change the calculated isotope effects noticably). Also, in the calcula-

Table 3
Calculated Isotope Effects (at 25 °C) Arising for the Proton Discharge Step from H_3O^+ or H_2O

Metal		H_3O^+ bending force constant k_3 0.1	0.15	0.2	H_2O bending force constant k_3 0.1	0.15	0.2	Stretching Force Constants
Hg	S_D	3.4	3.2	2.6	–	–	–	
	S_T	4.6	4.0	2.2	–	–	–	$k_1 = 1.159$
	R	1.9	1.8	1.5	–	–	–	$k_2 = 0$
Hg	S_D	4.5	4.3	3.5	–	–	–	$k_1 = 1.15$
	S_T	9.0	7.9	4.4	–	–	–	$k_2 = 0.1$ (for discharge from H_3O^+)
	R	2.6	2.4	2.0	–	–	–	
Ni	S_D	5.5	4.4	3.6	6.6	5.3	4.3	$k_1 = 1.15$
	S_T	11.2	8.2	6.2	12.7	9.5	6.9	$k_2 = 0.1$ (for discharge from H_3O^+)
	R	3.2	2.5	2.0	5.5	4.5	3.6	$k_2 = 0.159$ (for discharge from H_2O)
Ni	S_D	5.7	4.5	4.3	7.1	5.8	4.6	$k_1 = 1.95$
	S_T	12.9	9.4	8.3	16.3	12.2	8.9	$k_2 = 0.49$ (for discharge from H_3O^+)
	R	3.4	2.7	2.6	5.8	4.7	3.8	$k_2 = 0.78$ (for discharge from H_2O)
Fe	S_D	5.6	4.4	3.6	6.0	4.9	3.9	$k_1 = 1.10$
	S_T	11.5	8.5	6.4	12.9	9.7	7.1	$k_2 = 0.1$ (for discharge from H_3O^+
	R	3.2	2.6	2.1	5.0	4.1	3.2	$k_3 = 0.159$ (for discharge from H_2O)

tions of S_D described below, several values of the various force constants have been considered in order to explore the sensitivity of the calculated values of S_D (see Table 3) to the values of the k's used and to examine in particular to what extent values of S_D lower than 13 [4] can be justified. In no case, by any rational choice of k values, can S_D exceed about 7.5–9. This is evident from equation (15) where, if the stretching frequency for the symmetrical mode approaches zero, a contribution of a factor of $(1/2)^{1/2}$ to the $f_H^{\ddagger}/f_D^{\ddagger}$ ratio still arises.

We have therefore first considered those values of k_1 which can give the observed isotope effect S_D by arbitrarily assuming that the "O–H" force constant in H_3O^+ or H_2O is reduced by 98 to 100% of its initial value as discussed above in connection with the choice of values which satisfy equation (17). For the force constant k_3 for the doubly degenerate bending mode, a series of values has been taken about and including the value of 0.15 md Å^{-1} calculated by Keii and Kodera [4], (see below). In order to test Keii and Kodera's method of evaluating the bending force constants, Conway and Salomon [43] have calculated the bending force constant of the F–H–F$^-$ ion (using the molecular parameters for the HF molecule) as a model for the transition state in homogeneous proton transfer. A bending frequency of 1225 cm^{-1} is calculated which is in satisfactory agreement with the observed value of 1240 cm^{-1}. Hence we may accept as largely satisfactory Keii and Kodera's value of 0.15 md Å^{-1} for k_3. The main objection to their calculation is the neglect of the symmetrical stretching frequency.

VI. Calculation of Separation Factors

Evaluation of the frequencies for the activated complex from equation (16) using the data given in Table 2, enables the values of the partition function ratios of equation (15) to be calculated. For example, the results for discharge on Hg from acid solution, taking $k_1 = 1.15$, $k_2 = 0.1$, and $k_3 = 0.20$, are

$$\left(\frac{\sinh h\nu_D^{\ddagger}/2kT}{\sinh h\nu_H^{\ddagger}/2kT}\right)_{Str} = 0.4918;$$

$$\left(\frac{\sinh h\nu_T^{\ddagger}/2kT}{\sinh h\nu_H^{\ddagger}/2kT}\right)_{Str} = 0.3538;$$

$$\left(\frac{\sinh h\nu_D^{\ddagger}/2kT}{\sinh h\nu_H^{\ddagger}/2kT}\right)^2_{bend} = 0.1852;$$

$$\left(\frac{\sinh h\nu_T^{\ddagger}/2kT}{\sinh h\nu_H^{\ddagger}/2kT}\right)^2_{bend} = 0.0644.$$

From equations (10) and (12), respectively, we find $S_D = 3.5$ and $S_T = 4.4$. The results of the calculations for Hg, Ni and Fe in which k_3 is varied is given in Table 3. Table 4 gives the observed values of S_D, S_T

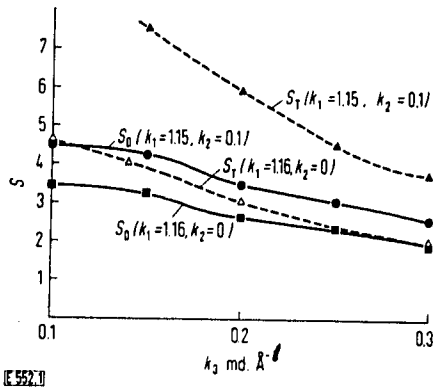

Fig. 1
Dependence of calculated S_D and S_T values on choice of force constants (case of discharge of protons from oxonium ions at mercury)

and R for comparison. The dependence of the S_D and S_T values calculated on choice of force constants is shown in Fig. 1.

VII. Calculation of the Ratio of Exchange Currents, R

In order to calculate R from equation (13), we must carry out a vibrational analysis for the complexes

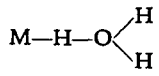

and

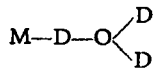

Also, if we are to treat these complexes by the three-center transition state model as above (i.e. "OH_2" and "OD_2" in the complex are regarded as single mass points), we must separate the partition function contributions associated with the two unreacting O–H and O–D bonds from the total partition function ratio $f_H^{\ddagger}/f_D^{\ddagger}$. This is done by assuming*) that these bonds remain unchanged (e.g. see Johnston and Pitzer [34]), with the exception that the particles involved in these bonds no longer possess translational motion since the activated complex may be regarded as being immobile. The partition function contribution of the two unreacting OH and OD bonds is written as $(f_{OH}/f_{OD})^2$ and by separating this term from $f_H^{\ddagger}/f_D^{\ddagger}$ in equation (13), we obtain

$$R = 16{,}265\left(\frac{f_{OH}}{f_{OD}}\right)^2 \prod^{3} \frac{\sinh h\nu_{i,D}^{\ddagger}/2kT}{\sinh h\nu_{i,H}^{\ddagger}/2kT} \qquad (18)$$

where the $\nu_i^{\ddagger}$'s are now evaluated by equation (16) using the masses m_{OH_2} or m_{OD_2} where applicable. Using the rule of the geometric mean

$$\left(\frac{f_{OH}}{f_{OD}}\right)^2 = \left(\frac{f'_{H_3O^+}}{f'_{D_3O^+}}\right)^{3/2} = \frac{1}{712}. \qquad (19)$$

The primes in f'_{H_3O}/f'_{D_3O} indicate that the translational contribution has been removed. Hence equation (18) becomes

$$R = 22 \prod^{3} \frac{\sinh h\nu_{i,D}^{\ddagger}/2kT}{\sinh h\nu_{i,H}^{\ddagger}/2kT}. \qquad (20\,a)$$

By an identical procedure, it can by shown that for discharge from the water molecules H_2O and D_2O, R is given by

$$R = 32 \prod^{3} \frac{\sinh h\nu_{i,D}^{\ddagger}/2kT}{\sinh h\nu_{i,H}^{\ddagger}/2kT}. \qquad (20\,b)$$

Values of R for various values of the force constants are given in Table 3 for mercury, nickel, and iron based on the slow discharge mechanism.

VIII. Model for Interstitially Adsorbed H and the Calculation of S_D

In previous publications [9, 44] it was suggested that proton discharge might occur to a site below the geometrical "electrode surface", i.e. interstitially between two or more metal atoms at the surface [61]. The hydrogen atom is then regarded as being bonded by two single electron bonds formally similar to those involved in the boron hydrides. There is considerable evidence to support this type of chemisorption as discussed previously [9, 44], e.g. the sign of the M–H surface dipole [45] and the infra-red spectrum for adsorbed H [59]. The purpose of this section is to show that this perhaps more realistic model of the surface situation for adsorbed H atoms can also lead to a satisfactory calculation of S_D values compatible with the observed isotope effects. The method of calculation will be exemplified with reference to the estimation of S_D for mercury. The other isotope effects S_T and R will follow the same trend as discussed previously for the three-center transition state model and hence need not be repeated.

The model used here is essentially equivalent to the planar XYZ_2 molecule discussed by Herzberg [46] and can be schematically represented by

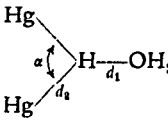

We are now employing, for convenience, the same symbols as those given by Herzberg and these should not be confused with those symbols used in the analysis of the three-center transition state model above. For this four-center model there will be six vibrational modes*) described by the six equations

$$\lambda_1+\lambda_2+\lambda_3 = k_1\left(\frac{1}{m_{OH_2}}+\frac{1}{m_x}\right)+k_2\left(\frac{1}{m_{Hg}}+\frac{2}{m_x}\cos^2\alpha\right)+\frac{2k_\delta+k_{\delta'}}{d_2^2}\left(\frac{1}{m_{Hg}}+\frac{2}{m_x}\sin^2\alpha\right) \qquad (21\,a)$$

$$\lambda_1\lambda_2+\lambda_2\lambda_3+\lambda_1\lambda_3 = k_1k_2\left(\frac{1}{m_{OH_2}m_{Hg}}+\frac{1}{m_xm_{Hg}}+\frac{2}{m_xm_{OH_2}}\cos^2\alpha\right)+k_2\frac{2k_\delta+k_{\delta'}}{d_2^2}\left(\frac{1}{m_{Hg}^2}+\frac{2}{m_xm_{Hg}}\right)+k_1\frac{2k_\delta+k_{\delta'}}{d_2^2}\left(\frac{1}{m_{OH_2}m_{Hg}}+\frac{1}{m_xm_{Hg}}+\frac{2}{m_{OH_2}m_x}\sin^2\alpha\right) \qquad (21\,b)$$

*) This assumption is made for the following reason: the activated complex is regarded as a state of the H_3O^+ system in which one proton has been stretched towards the metal surface and yet retains its full charge; this is consistent with the usual assumption that the electrical energy of the activated state for a one-electron transfer step differs from that of the initial state by the quantity $\beta F \Delta\Phi$ where $\beta =$ ca. 0.5 and $\Delta\Phi$ is the difference of potential between the metal and the outer Helmholtz layer. If charge were lost in the activation step, the unreacting OH or OD bonds would suffer an increase in frequency and force constant [2] and the significance of $\beta \doteq 0.5$ would be unclear.

*) The physical directions of displacement of atoms in each of these modes are shown in figure 24 a–f in reference [46].

$$\lambda_1\lambda_2\lambda_3 = k_1 k_2 \frac{2k_\delta + k_{\delta'}}{d_2^2} \times \left(\frac{1}{m_{OH_2} m_{Hg}^2} + \frac{1}{m_x m_{Hg}^2} + \frac{2}{m_x m_{OH_2} m_{Hg}}\right) \quad (21\,c)$$

$$\lambda_4 + \lambda_5 = k_2\left(\frac{1}{m_{Hg}} + \frac{2}{m_x}\sin^2\alpha\right) + \frac{k_{\delta'}}{d_1^2 d_2^2}\left(\frac{2d_2^2}{m_{OH_2}} + \frac{d_1^2}{m_{Hg}} + \frac{2(d_2 + d_1\cos\alpha)^2}{m_x}\right) \quad (21\,d)$$

$$\lambda_4\lambda_5 = k_2\frac{k_{\delta'}}{d_1^2 d_2^2}\left(\frac{2d_2^2}{m_{OH_2} m_{Hg}} + \frac{d_1^2}{m_{Hg}^2} + \frac{2(d_1^2 + d_2^2)}{m_x m_{Hg}} + \frac{4d_1 d_2\cos\alpha}{m_x m_{Hg}} + \frac{4d_2^2}{m_{OH_2}^2}\sin^2\alpha\right) \quad (21\,e)$$

$$\lambda_6 = \frac{k_\Delta}{d_1^2 d_2^2\cos^2\alpha}\left(\frac{d_1^2}{2m_{Hg}} + \frac{d_2^2\cos^2\alpha}{m_{OH_2}} + \frac{(d_1 + d_2\cos\alpha)^2}{m_x}\right) \quad (21\,f)$$

where the k's are the force constants; d's are the internuclear distances; m is the mass of the indicated species (m_x denotes the H or D mass); and α is the angle between the two bonds of H to two metal atoms. d_1, d_2 and α are calculated according to the geometry of the problem, using the data previously applied to the three-center model. It is found that d_1, d_2 and α are 1.33 Å, 1.89 Å and 104°50′, respectively.

Here k_1 is the O–H stretch force constant which is taken as approaching zero (see below); k_2 is the Hg–H single electron bond force constant and is taken to be slightly less than one half the force constant for the two electron bond in diatomic Hg–H (i.e. $k_2 = 0.4$–0.5 md Å^{-1}); k_δ is the Hg–H–Hg bending force constant and is taken as one half the value of the analogous bend in diborane [60] (i.e. $k = 0.1$); $k_{\delta'}$ is the force constant for the bend in H_3O^+ and is again taken as half its normal value of 0.5 md Å^{-1}; k_Δ refers to the force constant associated with a change of the angle between the H–O bond and the plane of "Hg_2–H". Since the H–O bond force constants are taken as being very low or zero, the mode λ_6 becomes a type of libration and its force constant k_Δ would also tend to become low and can be safely taken as around 0.01 md Å^{-1}. This method of taking reduced bending force constants in the activated complex follows that used by Johnston and Sharp [47].

The condition that the XYZ_2 type of configuration be an activated complex is that one of it frequencies can be considered to effectively approach zero. This is the vibrational mode λ_2 which leads to reaction: in order to make $\lambda_2 = 0$, k_1 is taken as zero in equation (21c) and equations (21a) and (21b) reduce to

$$\lambda_1 + \lambda_3 = k_2\left(\frac{1}{m_{Hg}} + \frac{2}{m_x}\cos^2\alpha\right) + \frac{2k_\delta + k_{\delta'}}{d_2^2}\left(\frac{1}{m_{Hg}} + \frac{2}{m_x}\sin^2\alpha\right) \quad (22\,a)$$

and

$$\lambda_1\lambda_3 = k_2\frac{2k_\delta + k_{\delta'}}{d_2^2}\left(\frac{1}{m_{Hg}^2} + \frac{2}{m_x m_{Hg}}\right) \quad (22\,b)$$

respectively. Neglecting translational and rotational contributions to the partition function for the activated complex (cf. the three-center model above), the partition function ratio for the activated complex becomes

$$\frac{f_H^+}{f_D^+} = \prod^5 \frac{\sinh u_{i,D}^+}{\sinh u_{i,H}^+}. \quad (23)$$

The frequencies for the activated complex are obtained from equations (21) and (22) and substituted into equation (23) from which it is found that $S_D = 2.1$ which is somewhat lower than the S_D values calculated on the basis of the three-center model. This is to be expected since there are more degrees of freedom associated with the dual site model.

This complex site model for proton discharge must be regarded as quantitatively satisfactory and a physically more preferable model. We shall not, however, expect to be able to distinguish which model is to be preferred on the basis of the quantitative degree of agreement with experiment but the importance of the above calculation lies in the fact that with a physically more realistic model for H adsorption, the same magnitudes of S_D can be calculated which are still well below those claimed as limiting maximum values by Keii and Kodera for the discharge step, and are in adequate agreement with experiment.

IX. Comparison with Experimental Data

The main purpose of the comparisons to be made in this section is not to attempt to demonstrate any exact agreement with experimental results, which would be presumptuous for calculation of isotope effects, but rather to show: a) that the value of $S_D = 13$ deduced by Keii and Kodera [4] can be brought to a value comparable with the experimental results by the appropriate inclusion of a symmetrical stretching mode in the activated complex and by choosing reasonable

Table 4
Observed Isotope Effects at Hg, Ni, and Fe Cathodes

Metal		Proton Source: H_3O^+	H_2O
Hg	S_D	2.5–4 [5–9, 48]	–
	S_T	5.8 [49]	–
	R	1.9 [11]	–
Ni	S_D	6–5 [6]	6.7 [5], 4.5–6.5 [7, 8]
	S_T	–	–
	R	3.0 [2]	–
Fe	S_D	–	7.2[53], 7 [8, 54] (max. value)
	S_T	–	12.0 [8] (max. value)
	R	3.0 [50]	–

values for the force constant of this mode; b) that hence the radical deduction from the previous calculations of S_D [4] that the slow discharge mechanism of proton transfer at mercury is inapplicable, is unnecessary.

The experimental values of S_D (Table 4) seem to be well established [6–9, 48] for mercury with $S_D = 3 - 4$,

and varying somewhat with potential. Thus v. Buttlar, Vielstich and Barth [8] find that S_D decreases by 1.33 V^{-1} over 0.6 volts in 0.2% D-containing solution in 2N H_2SO_4 and Conway and Salomon [9] have found a decrease of S_D of 0.6 V^{-1} (1 N HCl) and 1.44 V^{-1} (1 N $HClO_4$) in 10% D_2O. The values deduced in the calculation above thus agree quite well with the experimentally determined data. The calculated values of S_T on mercury are also in adequate agreement with the observed value of 5.8 [49]. The calculation of the R values are also in satisfactory agreement with the experimental values ($R = 1.9$ for Hg [11]) and 3.0 for Ni [2] and 3.0 for Fe [50]). This supports the slow discharge mechanism as also indicated from some other criteria [51, 52].

X. *Dependence of the Separation Factor on Potential*

In the recently reported experiments [7–9], it has become apparent that S_D depends significantly on electrode potential as indicated for mercury by Rome and Hiskey [47]. It is of interest now to offer an interpretation of the origin of this effect. Vielstich and co-workers [8] have regarded it as arsing on account of different values of the transfer coefficient α for electrochemical discharge of H and D from H_2O and HOD. For the slightly different case of discharge from acids in H_2O and pure D_2O, no evidence is found for an isotopic dependence of α at Ni, Pt, Au, Cu and Pd [2] and Fe [49]. However, for mercury, Post and Hiskey [11] report a difference of about 3 mV for the Tafel slopes in pure H_2O and D_2O acid solutions.

On the basis of the theoretical calculations, we may suggest that the observed diminution of S_D values with increasing overvoltage η could arise from either or both of the following possibilities:

a) Increase of potential results in a compression (electrostriction) of solvent in the double layer (as treated by MacDonald [55]), with a consequent effect on the force field in which the proton transfer occurs in the double layer. We should expect the compressional effect to increase the force constants for the lateral bending modes since the H or D or T particle would suffer more repulsion with neighboring solvent molecules in the double layer. This electrostriction effect may, in addition, enhance the possibility of discharge at adual site, i.e. initially discharge may occur at single metal sites and as the potential is made more cathodic, the discharge at multiple metal metal sites may become more significant. Also, the electric field in the double layer may affect the force constant of the symmetrical stretching mode.

b) Secondly, this field may also affect the librational behavior of neighboring solvent molecules in the double layer as suggested previously [2, 56].

Proton tunneling effects which could lead to potential dependence of S are however not indicated since the isotopic difference of Tafel slopes is small [2, 9, 10a] and the apparent energy of activation is independent of temperature [13].

XI. *Conclusion*

Using the general quadratic potential function for vibrational analysis of transition state complexes in electrochemical proton discharge, it is shown that the isotope effects at Hg, and possibly at Ni and Fe cathodes can be adequately explained on the basis of a slow proton discharge mechanism. In the previous attempts to calculate S_D and S_T by Kodera et al. [4, 57, 59], the important symmetrical stretching mode in the activated complex was neglected. The resulting supposition [4] that the H_2^+ ion discharge step is to be preferred to that slow proton discharge at mercury hence need not be maintained. A tentative explanation has also been offered of the effect of electrode potential on the values of S_D at mercury. Proton tunneling effects are probably not significant.

Acknowledgements

One of us (M.S.) wishes to acknowledge the award of a Fellowship by the Sprague Electric Company. We are also indebted to the National Research Council for support of this work.

Bibliography

[1] B. E. Conway, Proc. Roy. Soc. [London] *A 247*, 400 (1958).
[2] B. E. Conway, ibid. *A 256*, 128 (1960).
[3] J. Horiuti, T. Keii and K. Hirota, J. Res. Inst. Catalysis, Hokkaido, Univ. *2*, 1 (1951).
[4] T. Keii and T. Kodera, ibid. *5*, 105 (1957).
[5] J. Horiuti, G. Okamato and K. Hirota, Sci. Pap. Inst. physic. chem. Res. [Tokyo] *29*, 233 (1936).
[6] H. F. Walton and J. H. Wolfenden, Trans. Faraday Soc. *34*, 436 (1938).
[7] W. Vielstich, T. H. Schuchard and M. v. Stackelberg, Ber. Bunsenges. physik. Chem. *67*, 645 (1963).
[8] H. v. Buttlar, W. Vielstich and H. Barth, ibid. *67*, 650 (1963).
See also G. R. Lewis and P. Ruetschi, J. physic. Chem. *66*, 1487 (1962).
[9] B. E. Conway and M. Salomon, J. physic. Chem. in press 1964.
[10] a) B. E. Conway, Canad. J. Chem. *37*, 178 (1959).
b) St. G. Christov, Z. Elektrochem., Ber. Bunsenges. physik. Chem. *62*, 567 (1958).
[11] B. Post and C. F. Hiskey, J. Amer. chem. Soc. *73*, 161 (1951).
[12] K. Vetter, Trans. Symp. Electrode Processes, Philadelphia (1959) p. 47, The Electrochemical Society, John Wiley, 1961.
[13] B. E. Conway and M. Salomon, Electrochim. Acta, in press (1964).
[14] D. C. Grahame, Chem. Reviews *41*, 441 (1947).
[15] R. Parsons, Modern Aspects of Electrochemistry, Chapter III, Academic Press (1954).
[16] L. Melander, Isotope Effects on Reaction Rates, Ronald Press, N. Y., (1960).
[17] B. E. Conway and M. Salomon, J. chem. Physics, in press (1964).

[18] M. I. Temkin, J. physik. Chem. (russ.) *22*, 1081 (1948).
[19] R. P. Bell, Proc. Roy. Soc. [London], *A 139*, 466 (1933); *A 148*, 241 (1935).
[20] H. S. Johnston and D. Rapp, J. Amer. chem. Soc. *83*, 1 (1961).
[21] W. M. Jackson, J. R. McNesby and D. Darwent, J. chem. Physics *37*, 1610 (1962).
[22] M. Salomon, Canad. J. Chem. *42*, 610 (1964).
[23] A. N. Frumkin, Acta physicochim. URSS *13*, 23 (1943); Discuss. Faraday Soc. *1*, 64 (1947).
[24] E. Lange, Z. Elektrochem. angew. physik. Chem. *44*, 43 (1938).
[25] C. G. Swain and R. F. W. Bader, Tetrahedron [London] *10*, 182 (1960); C. G. Swain, R. F. W. Bader and E. R. Thornton, ibid, *10*, 200 (1960).
[26] K. Heinzinger and R. E. Weston, Paper presented at Vienna Meeting on Isotopes, December 1963.
[27] R. F. W. Bader, Ph. D. thesis, Massachusetts Inst. Tech. (1957).
[28] E. R. Thornton, J. Amer. chem. Soc. *84*, 2474 (1962).
[29] B. E. Conway, J. O'M. Bockris and H. Linton, J. chem. Physics *24*, 834 (1956).
[30] B. E. Conway, Modern Aspects of Electrochem., Chapter 2, Vol. III in press (1964).
[31] E. A. Moelwyn-Hughes, Physical Chemistry, Pergamon, p. 502 (1961).
[32] H. A. Smith and K. R. Fitch, J. physic. Chem. *67*, 920 (1963).
[33] E. B. Wilson, J. C. Desius and P. C. Cross, Molecular Vibrations, Chapter 8, McGraw Hill, N. Y., 1955.
[34] F. Westheimer, Chem. Reviews, *61*, 265 (1961); see also S. I. Miller, J. physic. Chem. *66*, 978 (1962) and H. S. Johnston and K. S. Pitzer, Ass. Inst. Chem. Eng. J. *5*, 277 (1959).
[35] L. Pauling. Nature of the Chemical Bond, Cornell University Press, Ithaca, N. Y. (1948).
[36] J. O'M. Bockris and R. Parsons, Trans. Faraday Soc. *47*, 914 (1951).
[37] S. Glasstone, K. J. Laidler and H. Eyring, Theory of Rate Processes, McGraw Hill 1941.
[38] H. Eyring and M. Polanyi, Z. physik. Chem. *B 12*, 279 (1931).
[39] F. London, „Problem der Modernen Physik", Sommerfeld Festschrift, p. 104, Hirzel, Leipzig 1928.
[40] S. Sato, J. chem. Physics *23*, 592, 2465 (1955).
[41] R. E. Weston, J. chem. Physics *31*, 892 (1952).
[42] N. Rosen and S. Ikehara, Physic. Rev. *43*, 5 (1933).
[43] B. E. Conway and M. Salomon, Extended Abstracts, Symposium on Electrolytes, Electrochemical Society Meeting, Toronto, May 1964.
[44] B. E. Conway and J. O'M. Bockris, Canad. J. Chem. *35*, 1124 (1957).
[45] J. C. P. Mignolet, Disc. Faraday Soc. *8*, 105 (1950).
[46] G. Herzberg, Infrared and Raman Spectra, D. Van Nostrand, N. Y. (1959).
[47] T. E. Sharp and H. S. Johnston, J. chem. Physics *37*, 1541 (1962).
[48] M. Rome and C. F. Hiskey, J. Amer. chem. Soc. *76*, 5207 (1954).
[49] J. O'M. Bockris, S. Srinivasan, and M. A. V. Devanathan, J. electroanalyt. Chem. [Amsterdam] *6*, 205 (1936).
[50] J. O'M. Bockris and D. F. A. Koch, J. physic. Chem. *65*, 1941 (1961).
[51] J. O'M. Bockris, Modern Aspects of Electrochemistry, Chap. IV, Academic Press (1954).
[52] J. O'M. Bockris and E. C. Potter, J. chem. Physics *20*, 614 (1952).
[53] H. A. Smith, C. O. Thomas and J. C. Posey, J. electrochem. Soc. *106*, 516 (1959). This work was done in 45 mole percent D_2O.
[54] B. Topley and H. Eyring, J. Amer. chem. Soc. *55*, 5058 (1933); J. chem. Physics *2*, 217 (1934).
[55] J. R. MacDonald and C. A. Barlow, J. chem. Physics *36*, 3062 (1962).
[56] B. E. Conway, Trans. Philadelphia Symposium on Electrode Processes 1959 (the Electrochemical Society), p. 267, John Wiley, N. Y. (1961).
[57] T. Kodera, J. Res. Inst. Catalysis, Hokkaido Univ. *8*, 161 (1959).
[58] T. Kodera and N. Saito, ibid. *8*, 5 (1959).
[59] W. A. Pliskin and R. P. Eischens, Z. physik. Chem. N. F. *24*, 11 (1960).
[60] N. V. Sidgwick, Chemical Elements and their Compounds, p. 343, Oxford.
[61] O. Beeck, Advances Catalysis related Subjects, *2*, 151 (1950).

PREFACE

Of all reactions on metal electrodes, that of the evolution of hydrogen has been the most studied. The hydrogen evolution reaction is unique in electrochemistry in that it has been studied for over sixty years and yet the rate-controlling step on most metals is still in dispute. Prior to the 1930's, the hydrogen evolution reaction was studied from a purely empirical viewpoint. The theory of absolute reaction rates was in its infancy and the heavy isotope of hydrogen had not yet been found. The existence of the heavy isotope of hydrogen discovered by Urey et al. (127) in 1931, precipitated an avalanche of papers dealing with kinetic and equilibrium isotope effects. Together with absolute rate theory, the kinetic isotope effect has proved to be a valuable complementary approahh for elucidation of reaction mechanism.

In 1932 Urey and Washburn (120a) reported that water which had accumulated in commercial electrolytic hydrogen cells was particularly high in deuterium content. Lewis and MacDonald (120b) showed that separation of H/D isotopes by electrolysis was very effective. It was not long after these initial discoveries that this electrolytic separation of isotopes was employed in studies of mechanism in the hydrogen evolution reaction (h.e.r.). Topley and Eyring (175) and Horiuti and

co-workers (9,68) were the first to study isotope separation at metal cathodes and their work was soon followed by that of Walton and Wolfenden (113). From this early work, it appeared that the isotope effects at high overpotential metals (Hg, Pb, and Sn) were small and at the transition metals, were large. This immediately led to the distinction of non-catalytic metals (Hg, Pb, and Sn) from the catalytic metals (the transition metals) with regard to separation factors. Prior to the use of isotopes, it was generally assumed that a proton discharge step was rate limiting at the high overpotential metals and that a recombination of adsorbed hydrogen was rate-limiting at the transition metals. However, when Horiuti and Okamoto (9) reported their initial findings on the electrolytic separation of hydrogen isotopes, it was claimed that the proton discharge step could not be operative at Hg cathodes, and in its place they proposed an atom-ion recombination mechanism to be rate-limiting, i.e. $Hg\text{-}H + H^+ \longrightarrow Hg + H_2$. In a later paper (10), Horiuti *et al.* replaced this mechanism by the molecule-ion neutralization step. In this mechanism, the rate-limiting step is regarded as the neutralization of the molecule-ion according to the reaction $H_2^+ + e \longrightarrow H_2$. The discharge step was rejected by Horiuti in 1936 on the basis that theoretical calculations of the isotope effects for a slow discharge step resulted in values much higher than those observed experimentally.

The origin of the theoretically high values of the isotope effects can be traced to Topley and Eyring's (175) original treatment of the discharge step where the activated complex was considered as consisting of a single free proton or hydrogen atom. The original treatment of the activated complex considered by Topley and Eyring (175) has been extended by Keii and Kodera (168) who claim that the discharge step cannot be rate-limiting at any metal cathodes. Despite this apparent defect in the evidence supporting the discharge mechanism, studies other than those involving isotopes (e.g. reaction order H-coverage) all support the discharge mechanism as being rate-determining at mercury and the other high over-potential metals. Hence the controversy over the rate-limiting step at Hg, Pb, and Sn began in 1936 and continues to the present time. Horiuti (12) also now regards the molecule-ion mechanism as being rate-determining at platinum electrodes in acid solution at low current densities. Again, evidence from studies other than those involving isotopes indicates an atom recombination mechanism to be rate-determining at platinum. The strong feature of Horiuti's theory has been its ability to predict the isotope effects for H/D and H/T separation. His theory has been attacked from many points of view with the exception of the isotope effect. It is the object of the work

in this thesis therefore to re-investigate the isotope effects at mercury and platinum electrodes, and the present study involves both experimental and theoretical considerations of the mechanisms operative at these cathodes.

Reproducibility of previously reported observed isotope effects has not been too satisfactory. Although qualitative agreement between various workers has been found, the agreement is far from being quantitative. In addition, recent studies on electrolytic hydrogen isotope separation indicates that the old classification in which the observed values were divided into two groups, breaks down under certain conditions, e.g. when potential dependence is considered and for certain cases low isotope effects are observed at the catalytic metals such as Pt and Ni. Hence part of the work presented in this thesis is involved with the investigation of this problem by experimental studies of the kinetic isotope effect under conditions of controlled electrode potential and the effect of anions.

During the 1930's, Bell showed that in reactions involving a proton transfer step, quantum mechanical tunneling effects must be considered. Bell and co-workers (e.g. see references 16-19, 76,217) have studied this problem for many years in non-electrochemical reactions. The problem of proton tunneling at metal electrodes has received some theoretical attention, particularly since the 1950's, but experimental studies,

particularly at low temperatures, have been lacking. Another aspect of the present work was therefore the study of the hydrogen evolution reaction at low temperatures to either confirm or disprove the existence of significant proton tunneling.

Most of the work described in this thesis is in press or in course of publication, as indicated in the following list of papers:

1). Potentiostatic Investigation of the Separation Factor S_D at Mercury and Platinum Cathodes and the Effect of Anions, M. Salomon and B.E. Conway, J. Phys. Chem., July-August, 1964.

2). Isotope Effects in Electrochemical Proton Discharge, B.E. Conway and M. Salomon, Ber. Bunsenges, August-September, 1964. [68, 331 (1964)].

3). Low Temperature Studies in Electrochemical Proton Discharge and the Role of Quantum Mechanical Tunneling, B.E. Conway and M. Salomon, J. Chem. Phys., submitted for publication.

4). Electrochemical Reaction orders in the hydrogen and Oxygen Evolution Reactions, B.E. Conway and M. Salomon, Electrochimica Acta, accepted for publication, 1964.

Other papers, related to the present work are:

5). The H/D Isotope Effect in Proton Conductance, B.E. Conway and M. Salomon, Extended abstract No. 196, Electrochemical Society Symposium, Toronto, May 2-7, 1964.

6). Isotope Effects in Methyl Radical Abstraction Reactions, M. Salomon, Can. J. Chem., 42, 610 (1964) (see attached paper).

ACKNOWLEDGMENTS

The author wishes to express his thanks to Professor B.E. Conway under whose direction this work was done. Professor Conway was always prepared to give freely of his time and advice whenever difficulties arose.

The author also wishes to thank Dr. A. Tickner and Mr. R. Sander for their advice on mass spectrometric techniques and for their time spent in analyzing the H/D samples. Thanks are also due to Dr. S. Schuldiner for making available his original results, in detail, for the h.e.r. on platinum from which some of the reaction order plots could be made. Finally the author is indebted to the Sprague Electric Company for an award of a Fellowship.

TABLE OF CONTENTS

Page No.

CHAPTER III

Page No.

CHAPTER V

LIST OF FIGURES

LIST OF TABLES

ABSTRACT

Experimental and theoretical studies of proton discharge in electrochemical reactions are presented. The separation factor S_D has been studied as a function of over-potential and the effects of anions were investigated. Low temperature studies have been carried out in alcoholic solutions of electrolytes for elucidation of the role of proton tunneling effects. No appreciable tunneling behaviour is found.

The separation factor S_D has been found to be appreciably dependent upon electrode potential and the nature of the anion in potentiostatic experiments in HCl, $HClO_4$. For mercury electrodes, S_D is found to decrease as potential increases from about 4 to 3 over a potential region of 0.5 volt in 1N HCl solutions. In 1N $HClO_4$ solutions, S_D decreases from ca. 3.5 to 2.5 over a 0.5 volt range of potential. At platinum, S_D is observed to reach a maximum value as a function of potential. Both the magnitude and the potential at which the maxima occur are dependent upon the nature of the anion. The results at mercury are interpreted on the basis of a slow proton discharge mechanism. The results at platinum electrodes are explained in terms of an atomic recombination rate-controlling step by reference to a complex site model for proton discharge. In this model, the discharge of protons at a metal

cathode is believed to occur interstitially in the surface between 2,3 or 4 metal atoms, i.e. the chemisorbed hydrogen atom is pictured as being situated "within" rather than "on" the outermost layer of surface metal atoms.

Calculations of the H/D and H/T separation factors (S) and exchange current density ratios (R) for the proton discharge mechanism on mercury, nickel, tungsten, and iron are presented. A vibrational analysis of the activated complexes is made by reference to both a linear three-center transition state model and a surface interstitial site model in which hydrogen is regarded as being adsorbed adjacent to the metal atoms. It is shown that the isotope effects observed experimentally, e.g. at mercury in acid solution and nickel in alkaline solution, can be accounted for in terms of a slow discharge mechanism. The valuesof R are shown to be consistent with the calculated and observed value of S_D. An explanation is also given qualitatively for the potential dependence of S_D at mercury in terms of electrostriction effects in the double-layer, and at platinum in terms of the complex site model for proton discharge.

Exchange current densities have been measured for mercury in CH_3OH/HCl and CH_3OD/DCl solutions down to -125°C, and for platinum in C_2H_5OH/HCl down to -150°C. The apparent

activation energies are independent of temperature for the hydrogen (and deuterium) evolution reactions at mercury and platinum, thereby indicating no appreciable contribution by proton tunneling. However, at mercury, the ratio of apparent frequency factors, A_H^*/A_D^*, is found to be about 0.5 which some workers (26,29) have claimed indicates the possibility of proton tunneling. This conclusion is incorrect and a method is presented in which the <u>true</u> difference in activation energies $\Delta E_D^{\neq} - \Delta E_H^{\neq}$, and the <u>true</u> ratio of frequency factors, A_H/A_D, can be evaluated. For the mercury electrode in methanolic solution, it is then found that $\Delta E_D^{\neq} - \Delta E_H^{\neq} \doteq 0.7$ and $A_H/A_D \doteq 1$.

CHAPTER I

INTRODUCTION

1. General Introduction and Statement of the Problem

The hydrogen evolution reaction (h.e.r.) was one of the first electrochemical problems to be studied from a kinetic and mechanistic viewpoint. Its apparent simplicity lead Tafel (1) to propose his now well known relation

$$\eta = a + b \ln i$$

where η is the so-called overpotential (see below), i is the current density and a and b are constants. Tafel found the constants a and b to be dependent upon the metal employed as a cathode for the evolution of hydrogen. The constant b was recognized by early workers (1,2,3,4,5,) to be dependent on the reaction mechanism and over the last sixty years or so, the voluminous work on the h.e.r. has led to the consideration of the following possible pathways (6,7,8);

Discharge Mechanism

acid solutions:

$$H_3O^+ + M + e_M \longrightarrow MH_{(ads)} + H_2O \qquad [1]$$

neutral or alkaline solutions:

$$H_2O + M + e_M \longrightarrow MH_{(ads)} + OH^- \qquad [1a]$$

Atom plus Ion Mechanism

acid solutions:

$$H_3O^+ + M\text{-}H + e_M \longrightarrow M + H_2O + H_2 \qquad [2]$$

neutral or alkaline solutions:

$$H_2O + M\text{-}H + e_M \longrightarrow M + OH^- + H_2 \qquad [2a]$$

Atom-Atom Recombination

$$2M\text{-}H \longrightarrow 2M + H_2 \qquad [3]$$

In the above scheme, [1] or [1a] is always a necessary primary step which is followed either by [2] or [3]. Horiuti and co-workers (9,10,11,12) have proposed an alternative scheme of reactions in which the discharge step is replaced by a "dual mechanism"; that is the electrode reaction proceeds through either the atom-atom recombination mechanism or by the molecule-ion neutralization step. Horiuti's dual theory can be represented in terms of the two alternative reactions

Molecule-Ion Neutralization

$$2H_3O^+ + e_M \rightleftharpoons H_2^+ + 2H_2O \qquad [4]$$

$$H_2^+ + e_M \longrightarrow H_2 \qquad [4a]$$

Atom-Atom Recombination

$$2MH_{(ads)} \longrightarrow 2M + H_2 \qquad [3]$$

Reaction [4] is an equilibrium reaction which precedes the

step [4a] regarded as rate-determining by Horiuti. The dual theory was originally formulated (9) as a basis for the explanation of small isotope effects which were experimentally observed for electrochemical hydrogen and deuterium separation at mercury and some other cathodes. Since the 1930's it is probably safe to estimate that the number of papers published dealing specifically with the h.e.r. is at least one thousand. There has been frequent disagreement between workers of the "discharge mechanism" school and the "dual theory" school, and despite the seemingly large amount of evidence in support of the discharge theory, there has hitherto been no theoretical justification of small isotope effects in terms of the discharge step. When the vast number of publications in the field are considered, it is quite surprising to find such an important omission. It is on account of this omission in both the experimental and theoretical justification of the discharge mechanism, that much of the work described in this thesis deals specifically with this problem. It will be shown that the observed effects can, in fact, be accounted for in terms of mechanisms [1], [2] and [3] and that the mechanism [4], [4a] cannot explain the experimental data observed for the h.e.r., particularly for the cases of mercury and platinum which have been studied the most extensively.

Another problem, the consideration of which also constitutes a major part of this thesis, is the role of

tunneling in electrochemical proton transfer. Proton tunneling in the discharge step [1] was first discussed by Bawn and Ogden (13) and Appelby and Ogden (14) following the work of Bell (15,16; see also more recent discussions by Bell 17,18,19). In the early work of Bawn and Ogden (13), too wide a potential barrier was considered and the effect of varying electrode potential was not examined (this is discussed in detail in Chapter III). The high values of the H/D separation factors S (defined below) obtained by Appelby and Ogden and claimed to support a proton transfer by tunneling have never been confirmed. The early papers of Gurney (20,21) gave a quantum mechanical description of electrode processes by an <u>electron</u> tunneling mechanism but are no longer considered valid in the original form published on account of the neglect of the role of adsorption of H at the metal, first considered by Horiuti and Polanyi [159] and Butler [160]. Bell (cf. 15-18) was the first to treat quantitatively the kinetics of proton transfer reactions in terms of quantum mechanical tunneling of protons. Since the work of Bawn and Ogden, the problem of tunneling in electrode reactions did not receive any significant attention until 1953 when theoretical interest was renewed (22,23,24,25,26). The theoretical calculations all predict significant deviations from classical Arrhenius behavior below room temperature. These calculations indicate that proton tunneling becomes particularly

important at temperatures of around -40°C and below. However, isotope effects in the h.e.r. have hitherto never been studied below 0°C and no work has been done on the kinetics of the h.e.r. at low temperatures with the purpose of investigating the role of tunneling. Hence another aspect of the present work was to extend the study of the h.e.r. and of associated isotope effects to temperatures down to -150°C in order to examine the role of quantum mechanical tunneling. As will be discussed in more detail below, the study of isotope effects in the h.e.r. offers a particularly suitable approach towards this problem since criteria additional to those normally considered in non-electrochemical reactions are available (23-26) for establishing the role of proton tunneling, viz. (a) the values of the Tafel slope b; (b) the dependence of b on the isotopic mass, and (c) the dependence of the separation factor on electrode potential.

2. Definition of Terms and the Role of the Structure of the Double Layer*

Electrochemical proton transfer reactions are by their nature heterogeneous. Hence, the rates of proton transfer will depend upon such factors as the adsorptive properties of the

---

* Detailed reviews of the problem of the structure of the double-layer have been published elsewhere (27,28,29,30) and in a previous thesis from this Department.

metal cathode, the presence of adsorbed intermediates, products, or anions on the cathode and the metal-solution potential difference. Hence proton transfer at a charged interface is unique in that it depends on several factors which are not involved in analogous homogeneous prototropic acid-base reactions. A brief review of some basic definitions and models is therefore required and will provide a basis for consideration of the apparent reaction orders to be deduced in Chapter II for several of the reactions shown above.

The model used in considering electrochemical ion discharge is shown schematically in Figure 1 and represents the adsorption of ions in the double-layer by both "electrostatic" and more conventionally "chemical" forces. The hatched plane represents the metal surface and the dotted planes represent different regions of the double-layer. Specifically adsorbed ions i.e. those which are both chemi-, and electrostatically adsorbed approach the metal surface more closely than do non-specifically adsorbed ions (27,28). The plane containing the former kind of ions constitutes the inner Helmholtz layer at some potential ψ_1 and the latter constitutes the outer Helmholtz layer at some potential ψ_1; ψ_1 is identical with the potential of the outer Helmholtz layer designated by Grahame (27) as ψ_o. In the absence of specific adsorption, ψ_1 may be taken as ψ_o in Grahame's treatment; ϕ_M is the inner potential of the metal according to the definition of Lange (31, cf. also 28); ψ_s is the inner potential of the bulk solution which is taken as zero

Figure 1

Model for adsorption and distribution of ions at a metal electrode interface.

DOUBLE LAYER

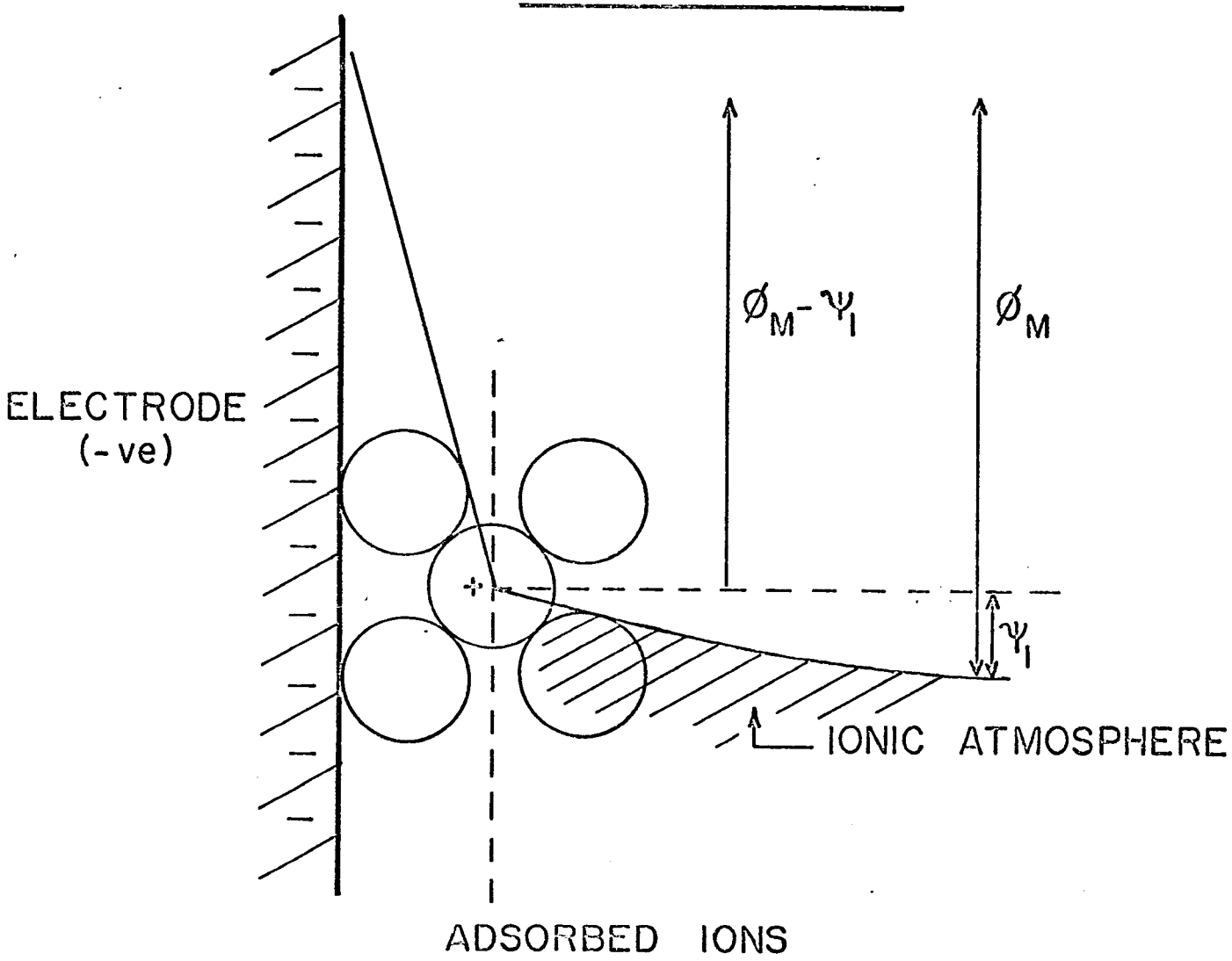

by convention to provide a reference for the scale of potentials. If we regard the electrical behaviour of the double-layer at the interface as being equivalent to that of an ideal condenser, then from simple electrostatics a differential capacity C can be defined as

$$C = -dq/d\phi \qquad [5]$$

where -q is the electronic excess charge on the metallic side of the electrical double-layer, i.e. it is equal to the total net charge of ions in the double-layer with the sign reversed; ϕ is the potential of the electrode relative to that of the electrocapillary maximum (e.c.m.) at which q = 0. Unlike ordinary electronic condensers, the charge at the metal-solution interface is not proportional to potential so that C may vary with ϕ. An integral capacity K is therefore defined as

$$K = -q/\phi \qquad [6]$$

and the charge q can be obtained from integration from

$$q = -\int_0^{\phi} C \, d\phi \qquad [7]$$

The limits are as shown because q = 0 when ϕ = 0. The integral capacity can be calculated from equations [5] and [6] by

$$C = K + \phi\left(\frac{dK}{d\phi}\right)$$

Since at the electrocapillary maximum ϕ = 0, it follows that

C = K under this special condition.

The differential capacity of the region between the metal surface and the outer Helmholtz plane is designated as C_o and is defined as

$$C_o = - dq/d(\phi^o - \psi_1) \qquad [8]$$

where ϕ^o is the rational potential difference which is defined (27) as the difference in the potential of the electrode and that ($\phi^{e.c.m.}$) at its e.c.m. when there is no specific adsorption. The corresponding integral capacity is similarly given by

$$-q = K_o^{''} (\phi^o - \psi_1) \qquad [9]$$

and q can be evaluated by equating the charge of the metallic surface to that of the diffuse double-layer (taken with opposite sign) in which only long range electrostatic ion-distribution effects are operative. It can be shown (27,32) that for a z-z electrolyte

$$q = -2 \left(\frac{\varepsilon RT \, c_{M^+}}{2\pi} \right)^{1/2} \sinh \left(\frac{zF\psi_1}{2RT} \right) \qquad [10]$$

The negative sign is chosen because q is positive when ψ_1 is negative and vice-versa; c_{M^+} is the total concentration of cations in the bulk (in g. ions litre^{-1}) and ε is the dielectric constant which is assumed to be constant in the double-layer. Then from equations [8], [9] and [10]

$$K_o\,(\phi_M - \phi^{o.c.m.} - \psi_1) = \left(\frac{2\,\varepsilon RT\,c_{M^+}}{\pi}\right)^{1/2} \sinh\left(\frac{z\,\psi_1 F}{2RT}\right) \qquad [11]$$

and

$$C_o = \frac{zF}{RT}\left(\frac{\varepsilon RT\,c_{M^+}}{2\pi}\right)\cosh\frac{z\,\psi_1 F}{2RT} \qquad [12]$$

Here, $\phi_M - \phi^{o.c.m.}$ has been substituted for ϕ^o, i.e. assuming no specific adsorption effects which can make $\phi^{o.c.m.}$ different from $\phi_o{}^{o.c.m.}$. When $\phi_M - \phi^{o.c.m.} \gg \psi_1$ (i.e. at potentials of ϕ_M sufficiently removed from the potential of zero charge, i.e. the potential for which q = 0) equation [11] reduces to the following approximate form for dilute solutions:

$$\psi_1 = \frac{RT}{F}\ln c_{M^+} + \text{const.} \qquad [13]$$

In acid solutions in the absence of added neutral salts, c_{M^+} must be written as the concentration of hydronium ions, H_3O^+, i.e.

$$\psi_1 = \frac{RT}{F}\ln c_{H^+} + \text{const.} \qquad [13a]$$

Frumkin (29) has also shown that for the case of a multivalent cation, M^{z+} and for the condition that $c_{M^{z+}} \gg c_{H^+}$, the following approximate relation is obtained

$$\psi_1 \approx \frac{RT}{zF}\ln c_{M^{z+}} + \text{const.} \qquad [13b]$$

In concentrated acid solutions, ψ_1 becomes independent of

cation concentration (34,35) and this will affect the pH dependence of the kinetics of the h.e.r. as will be discussed below.

If the hydrogen electrode is at its reversible potential ϕ_r then there is no net reaction. If the potential is adjusted cathodically to some new potential ϕ_M by an increment η, the overpotential, the electrode is said to be polarized and a net reaction occurs (production of H_2 gas). Then by this definition

$$\phi_M = \eta + \phi_r \qquad [14]$$

and from the Nernst equation* for ϕ_r

$$\phi_M = \eta + \frac{RT}{F} \ln c_{H^+} + \text{const.} \qquad [15]$$

---

* Here the formal expression for ϕ_r is given in terms of H^+ ion concentration rather than activity. In dilute solutions, the term in concentration is retained whereas for concentrated solutions the mean activity would be preferred. This simplification is also used in following equations.

CHAPTER II

GENERAL ELECTROCHEMICAL KINETIC APPROACH

1. Introduction

An important approach in the distinction and characterisation of reaction mechanisms in electrode kinetics, and the h.e.r. in particular, has been the evaluation of the Tafel slope parameter b. The conditions for which this is deduced are important to define and various cases will be examined below. The limiting results which are obtainable are complementary to the reaction orders and isotope effects with regard to elucidation of the reaction mechanism.

2. General Kinetic Equations for the H.E.R., and the Tafel Slope Parameter

A. Principles Involved in Formulation of Rate Equations

For electrochemical reactions, rates can be conveniently measured in terms of current i which is directly proportional to the actual velocity v expressed as moles of product formed per second per square centimetre of electrode surface; thus, for a process involving z Faradays per g. mole in the charge

transfer,

$$i = zF v \qquad [16]$$

Since reactants are charged and the products usually uncharged or dipolar, there can be a variation of electrochemical potential of the initial state of the reaction with the absolute metal-solution potential difference, ϕ_M, and this causes a variation of the standard electrochemical free energy of activation $\Delta\bar{G}^{o\neq}$ (see below) given by

$$\Delta\bar{G}^{o\neq} = \Delta G^{o\neq} + \beta(\phi_M - \psi_1)\, zF \qquad [17]$$

The parameter β is defined as that fraction of $\phi_M - \psi_1$ through which the reactant is transferred to reach the activated state and $\Delta G^{o\neq}$ is the value of the standard free energy of activation when $\phi_M - \psi_1 = 0$. If surface coverage of adsorbed intermediates becomes significant, $\Delta G^{o\neq}$ may also be changed by some fraction γ of the dependence of the energy of adsorption U_{ads} of the intermediates on coverage (36,37,38). If this dependence is written as $f(\theta)$, where $U_{ads,\theta} = U_{ads,0} - f(\theta)$, equation [17] becomes, for a discharge step,

$$\Delta\bar{G}^{o\neq} = \Delta G^{o\neq} + \gamma f(\theta) + \beta(\phi_M - \psi_1)F \qquad [17a]$$

It has been shown previously by Conway and Gileadi (37) that the exact form of $f(\theta)$ is not required for the derivation of Tafel slopes or pH effects but does become important when capacity

phenomena are studied (37,38). Two general forms of $f(\theta)$ are usually employed and correspond to (a) limiting Langmuir conditions for which $f(\theta) = 0$ or $\theta \rightarrow 0$ or 1 and (b) to the Temkin isotherm (39) where $f(\theta)$ is approximately linear in θ for $0.2 > \theta > 0.8$.

Finally the activity of reactant ions at the outer Helmholtz plane must be expressed in terms of bulk activity, as first considered by Frumkin (33). This is done by writing an electrostatic isotherm (33), which for hydronium ions has the form

$$(c_{H_3O^+})_s = \underline{K}\,(c_{H_3O^+})_b \exp - \psi_1 F/RT \qquad [18]$$

where the subscripts s and b refer to surface and bulk concentrations, respectively and $\underline{K}$ is a constant. The terms in equations [16], [17a] and [18] may now be combined to give the basic kinetic equation

$$i_1 = k_1(c_{H_3O^+})_b \exp - \psi_1 F/RT\,(1-\theta_H) \exp -[\gamma f(\theta) + \beta(\phi_M - \psi_1)F]/RT \qquad [19]$$

amongst other constant terms

where k_1 is a rate constant involving ΔG° and θ_H is the fractional surface coverage by H.

(i) The Discharge Reaction

Equation [19] is easily recognized as the rate equation for discharge of protons from hydronium ions onto a metal cathode.

This equation can be rewritten in terms of the overpotential (cf. equation [14]) as

$$i_1 = k_1\left(c_{H_3O^+}\right)_b \exp-(1-\beta)\,\psi_1 F/RT \cdot \exp-\beta\phi_r F/RT \cdot \exp-\beta\eta F/RT \qquad [19a]$$

In equation [19a], the term $1-\theta_H$ has been taken as unity since θ_H will generally be small if discharge is rate-determining (but except when [3] is at quasi-equilibrium and θ_H can be significant, e.g. at the highly catalytic metals). As a consequence $f(\theta)$ is zero. The Tafel slope is defined as the differential $(d\eta/d \ln i)_{c_{H^+}}$ and from [19a]

$$(d\eta/d \ln i)_{c_{H^+}} = \frac{RT}{\beta F}$$

when $\beta = 1/2$, the slope is 118 mv. at $T = 298^\circ K$ (see Table I).

(11) The Atom + Ion Mechanism

If mechanism II or III is rate-determining, then the discharge step can usually be assumed to be in quasi-equilibrium, viz.

$$H_3O^+ + M + e_M \underset{k_{-1}}{\overset{k_1}{\rightleftharpoons}} MH + H_2O$$

The rate of the reverse of reaction [1] is

$$i_{-1} = k_{-1}\,\theta_H \exp -[(1-\gamma)f(\theta) - (1-\beta)(\phi_M - \psi_1)F]/RT \qquad [20]$$

and since the reaction is assumed to be at equilibrium, $i_1 = i_{-1}$ and $k_1/k_{-1} = K_1$,

Table I

Tafel Slopes

Mechanism	Langmuir Conditions $\theta \rightarrow 0$	Langmuir Conditions $\theta \rightarrow 1$	Temkin Conditions Activated	Temkin Conditions Non-Activated
Discharge	$\frac{RT}{\beta F}$	-	-	-
Atom - Ion	$\frac{RT}{(1+\beta)F}$	$\frac{RT}{\beta F}$	$\frac{RT}{(r+\beta)F}$	$\frac{RT}{(1+\beta)F}$
Atom - Atom	$\frac{RT}{2F}$	-	$\frac{RT}{2rF}$	$\frac{RT}{2F}$
Horiuti	$\frac{RT}{(1+\beta)F}$	$\frac{RT}{\beta F}$	$\frac{RT}{(r+\beta)F}$	$\frac{RT}{(1+\beta)F}$

so that from equations [19] and [20]

$$\frac{\theta_H}{1-\theta_H} = K_1 \left(c_{H_3O^+}\right)_b \exp - \frac{f(\theta)}{RT} \cdot \exp -\phi_M F/RT \qquad [21]$$

Under Langmuir conditions $f(\theta)$ is zero and with $\theta_H \longrightarrow 0$ equation [21] becomes

$$\theta_H = K_1 \left(c_{H_3O^+}\right)_b \exp -\phi_M F/RT \qquad [22]$$

If the Langmuir isotherm is not applicable for adsorption of H as discussed in a number of previous studies at transition metals (103,155), $f(\theta) \neq 0$ and for intermediate coverages of around $\theta \doteqdot 0.5$, equation [21] may be solved for $f(\theta)$, i.e.

$$f(\theta) \doteqdot RT \ln (c_{H_3O^+})_b - \phi_M F + \ln K_1 \qquad [23]$$

The rate of the atom + ion reaction ([2], [2a]) is given by

$$i_2 = k_2 \left(c_{H_3O^+}\right)_b \theta_H \exp -(1-\beta)\, \psi_1 F/RT \exp -[\gamma f(\theta) + \beta \phi_M F]/RT \qquad [24]$$

which, in terms of the overpotential η, becomes

$$i_2 = k_2 \left(c_{H_3O^+}\right)_b \theta_H \exp -(1-\beta)\, \psi_1 f/RT \exp -\beta \phi_r F/RT \exp -[\gamma f(\theta) + \beta \eta F]/RT \qquad [24a]$$

It is necessary to consider the process of dissociative chemisorption for the H_2 molecule since in certain cases the form of

equation [24] can be changed. As an H_2 molecule approaches a surface it can become physically adsorbed without dissociation. This process usually requires little or no activation energy. The molecule may then undergo dissociative chemisorption and depending on whether the potential energy curves for $H_2 \longrightarrow MH_2$ and $2H \longrightarrow 2MH$ cross above or below the line for zero energy (referred to that of H_2 molecules at an infinite distance from the surface), activated or non-activated adsorption, respectively, will arise. The situation is schematically represented in Figures 2a and b (Figure 2c represents on intermediate case in wich adsorption is non-activated at low or zero coverage and becomes activated as the coverage is increased so that the potential energy curve for $2H \longrightarrow 2MH$ becomes more shallow). From these figures it is seen that if adsorption is non-activated, the change in $\Delta\overline{G}^{o^{\ddagger}}$ for a given increment in θ will be equal to the change in ΔG^{o}, i.e. $\gamma = 1$. For the case of activated adsorption γ is less than unity and will normally be close to one half. Hence equations [24] and [24a] apply to the case of activated adsorption. For non-activated adsorption, the rate equations are

$$i_2 = k_2 \left(c_{H_3O^+}\right)_b \theta_H \exp-(1-\beta)\, \psi_1^{P}/RT \cdot \exp-[f(\theta) + \beta \phi_M^{P}]/RT \qquad [25]$$

Figure 2

Schematic potential energy diagrams for non-activated and activated adsorption conditions.

a) Non-activated adsorption; energy of desorption = activation energy for desorption.

b) Activated adsorption; curves cross above the zero energy line.

c) Intermediate activated adsorption case; curves cross above the zero energy line only at finite coverage but not at zero coverage.

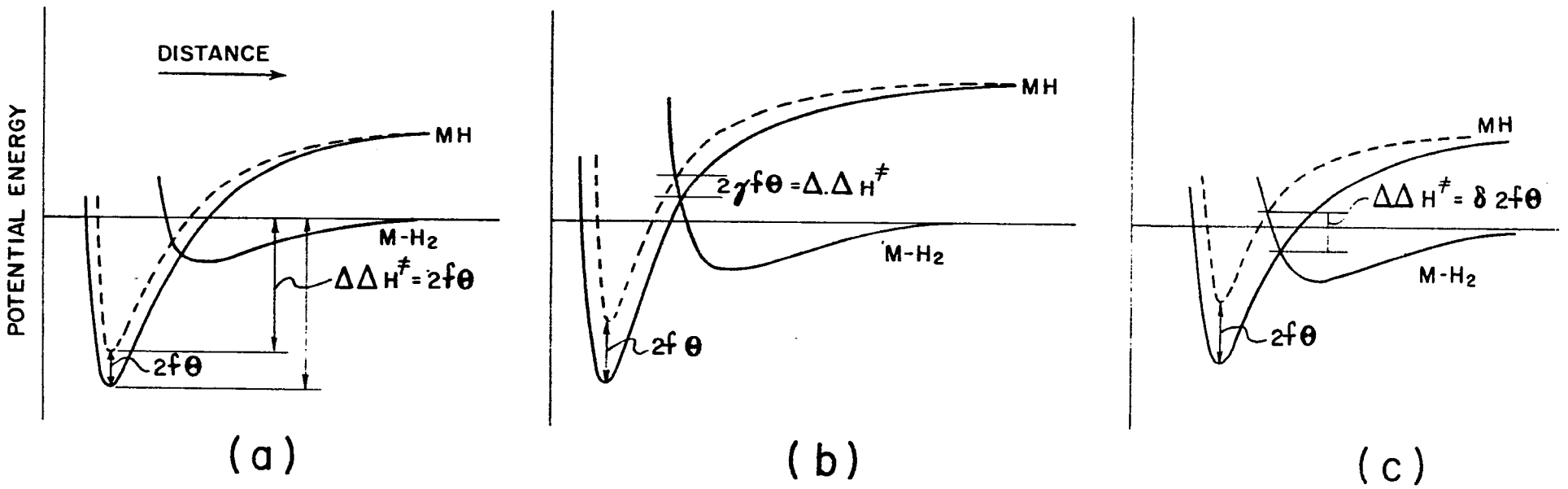
POTENTIAL ENERGY
DISTANCE
MH
M-H2
ΔΔH≠ = 2fθ
2fθ
(a)
MH
2γfθ = Δ.ΔH≠
M-H2
2fθ
(b)
MH
ΔΔH≠ = δ 2fθ
M-H2
2fθ
(c)

and

$$i_2 = k_2\left(c_{H_3O^+}\right)_b \theta_H \exp-(1-\beta)\,\psi_1 F/RT.\ \exp-\beta\phi_r F/RT.$$

$$\exp-\,[f(\theta) + \beta\eta F]/RT \qquad [25a]$$

The Tafel slopes are obtained from equations [24]-[25] and depend upon the nature of the adsorption involved and the extent of coverage.

In terms of the Langmuir isotherm ($f(\theta) = 0$), two cases arise. The first is that for low coverage when θ_H is potential dependent. From equations [22] and [24a] [$f(\theta) \longrightarrow 0$]

$$i_2 = k_2 K_1\left(c_{H_3O^+}\right)_b^2 \exp-(1-\beta)\,\psi_1 F/RT.\ \exp-(1+\beta)\phi_r F/RT.$$

$$\exp-(1+\beta)\,\eta\, F/RT \qquad [26]$$

Differentiation with respect to η at constant electrolyte composition gives the familiar Tafel slope of $RT/(1+\beta)F$ or 0.040 volt when $\beta = 1/2$ and $T = 298^{\circ}K$. The second Langmuir case is that for full surface coverage ($\theta_H = 1$ in equation [24a]) and leads to a Tafel slope of $RT/\beta F$ or 0.118 volt at $298^{\circ}K$ which is identical with that for the discharge step [1].

In order to obtain the Tafel slopes under conditions for which the Temkin isotherm is applicable, equation [23] is substituted into either [24a] or [25a]. Assuming (36, 37, 38) the variation of the pre-exponential term in θ_H is relatively

negligible in comparison with that of the exponential term in θ_H, combination of equation [23] with [24a] or [25a] yields,

$$\ln i_2 = (1+\gamma) \ln \left(c_{H_3O^+}\right)_b - \frac{(1-\beta)\psi_1 F}{RT} - \frac{(\gamma+\beta)\phi_r F}{RT} - \frac{(\gamma+\beta)\eta F}{RT} + \text{constante} \qquad [26]$$

and

$$\ln i_2 = 2\ln c_{H_3O^+ b} - \frac{(1-\beta)\psi_1 F}{RT} - \frac{(1+\beta)\phi_r F}{RT} - \frac{(1+\beta)\eta F}{RT} + \text{constants}, \qquad [26a]$$

respectively. Taking $\gamma = \beta = 1/2$, the Tafel slopes corresponding to the expressions [26] and [26a] are obtained by differentiation with respect to η at constant electrolyte composition and are $RT/(\gamma+\beta)F$ and $RT/(1+\alpha)F$, respectively (see Table I).

(iii) The Atom + Atom Recombination Mechanism

If reaction [3] is rate-determining, then using the above principles, the rate is

$$i_3 = k_3 \theta^2 \cdot \exp 2f(\theta) \qquad [27]$$

if adsorption is non-activated and

$$i_3 = k_3 \theta^2 \cdot \exp 2\gamma f(\theta) \qquad [27a]$$

for the case of activated adsorption.

For the Langmuir case $f(\theta) = 0$ and as θ_H tends to unity the Tafel slope from equation [27] tends to become infinite. For the case of low surface coverages, i.e. $\theta \ll 1$, equations [22], [27] and [14] give

$$\ln i_3 = 2 \ln \left(c_{H_3O^+}\right)_b - \frac{2\beta_r F}{RT} - \frac{2\gamma F}{RT} + \text{constants} \qquad [28]$$

at constant electrolyte composition, so that the Tafel slope is $RT/2F$ or 0.029 volt at 298°K.

For the two Temkin cases equations [23], [27], [27a] and [14] give

$$\ln i_3 = 2 \ln \left(c_{H_3O^+}\right)_b - \frac{2\beta_r F}{RT} - \frac{2\gamma F}{RT} + \text{constants} \qquad [29]$$

for non-activated adsorption and

$$\ln i_3 = 2\gamma \ln \left(c_{H_3O^+}\right)_b - \frac{2\gamma\beta_r F}{RT} - \frac{2\gamma^2 F}{RT} + \text{constants} \qquad [29a]$$

for activated adsorption. The Tafel slopes are therefore $RT/2F$ and $RT/2\gamma F$ from equations [29] and [29a], respectively.

(iv) <u>The Ion-Molecule Neutralization Step</u>

A full kinetic analysis of this mechanism has not been given previously except in so far as it has been incorrectly assumed (8) that the kinetics are the same as those for the reaction [2]; this is, however, not the case. According to

Horiuti (10,11,12), the ion-molecule neutralization step [4a] is rate-determining at mercury and at platinum at low current densities. Step [4] is a pre-rate determining equilibrium and the rates of forward and backward reactions, respectively, are

$$i_4 = k_4 (1-\theta) \left(c_{H_3O^+}\right)_b^2 \cdot \exp -2\psi_1 F/RT \exp -[\gamma f(\theta) + \beta(\phi_M - \psi_1)F]/RT$$

and

$$i_{-4} = k_{-4}\, \theta \exp -[-(1-\gamma)f(\theta) - (1-\beta)(\phi_M - \psi_1)F]/RT$$

where θ now refers to the intermediate H_2^+. Since it is supposed that $i_4 \doteq i_{-4}$, when [4a] is rate-determining, it follows that

$$\frac{\theta}{1-\theta} = k_4 \left(c_{H_3O^+}\right)_b^2 \exp -\psi_1 f/RT \cdot \exp -f(\theta)/RT \cdot \exp -\phi_M F/RT \qquad [30]$$

The Langmuir limiting condition of $\theta_{H_2^+} \longrightarrow 0$ leads to

$$\theta = K_4 \left(c_{H_3O^+}\right)_b^2 \exp -(\phi_M + \psi_1)F/RT \qquad [31]$$

In the range of coverages over which the Temkin isotherm is applicable, equation [30] reduces to

$$f(\theta) = 2RT \ln\left(c_{H_3O^+}\right)_b - (\phi_M + \psi_1)F + \text{constants} \qquad [32]$$

In equations [31] and [32], it will be noted that a term in ψ_1 remains since reaction [4] involves <u>two</u> H_3O^+ ions, and chemisorbed H_2^+ in the double-layer is assumed not to be in electrostatic equilibrium with H_2^+ ions in solution. In this respect the treatment and derived results differ from those of Parsons (8) where the reaction scheme [4]-[4a] was regarded as electrochemically equivalent to [1]-[2] (with [2] rate determining). The results of Parsons are only obtained if the H_2^+ ions are regarded as being at the ψ_1 plane and in equilibrium with H_2^+ ions in solution which seems unreasonable since H_2^+ will be formed in [4] only as an adsorbed transient intermediate. If the potential of the plane at which H_2^+ is adsorbed is denoted by ψ_i and differs from ψ_1, then equation [31] would be

$$\theta = K_4 \left(c_{H_3O^+}\right)_b^2 \exp -[\phi_M + (2-\beta)\psi_1 - (1-\beta)\psi_i]F/RT \qquad [31a]$$

which becomes identical with equation [31] when $\psi_i \equiv \psi_1$.

The rate of step [4a] when rate-determining is then

$$i_{4a} = k_{4a}\,\theta \cdot \exp-[-f(\theta) + \beta(\phi_M - \psi_1)F]/RT \qquad [33]$$

for non-activated adsorption and

$$i_{4a} = k_{4a}\,\theta \cdot \exp -[-\gamma f(\theta) + \beta(\phi_M - \psi_1)F]/RT \qquad [33a]$$

for activated adsorption. Four cases arise for the Tafel

slopes. For the Langmuir case of $\theta \rightarrow 1$, equation [33] becomes upon introduction of equation [14]

$$\ln i_{4a} = \frac{\beta \psi_1 F}{RT} - \frac{\beta \phi_r F}{RT} - \frac{\beta \eta F}{RT} + \text{constants} \qquad [34]$$

For $\theta \ll 1$, from equations [31], [33] and [14]

$$\ln i_{4a} = 2 \ln \left(c_{H_3O^+}\right)_b - \frac{(1-\beta)\psi_1 F}{RT} - \frac{(1+\beta)\phi_r F}{RT} - \frac{(1+\beta)\eta F}{RT} + \text{constants} \qquad [34a]$$

The Tafel slopes are therefore $RT/\beta F$ and $RT/(1+\beta)F$ for the two cases in [34] and [34a] respectively.

For the non-activated and activated Temkin cases ($\theta \approx 0.5$), respectively, equations [33] and [33a] and [32] and [14] lead to

$$\ln i_{4a} = 2 \ln \left(c_{H_3O^+}\right)_b - \frac{(1-\beta)\psi_1 F}{RT} - \frac{(1+\beta)\phi_r F}{RT} - \frac{(1+\beta)\eta F}{RT} + \text{constants} \qquad [35]$$

and

$$\ln i_{4a} = 2\gamma \ln \left(c_{H_3O^+}\right)_b - \frac{(\gamma+\beta)\psi_1 F}{RT} - \frac{(\gamma+\beta)\phi_r F}{RT} - \frac{(\gamma+\beta)\eta F}{RT} + \text{constants} \qquad [35a]$$

so that Tafel slopes of $RT/(1+\beta)F$ and $RT/(\gamma+\beta)F$ are respectively obtained.

3. pH and Neutral Salt Effects: The Concept of Apparent and True Reaction Orders*

A. General

The relevance of determination of reaction orders to elucidation of mechanisms of chemical reactions is well known and their evaluation forms an important part of reaction kinetics in relation to criteria of mechanisms. In the case of electrochemical reactions, reaction orders will depend on the isotherm for adsorption of the reactants at the electrode interface and the adsorption behavior of intermediates involved in the reaction. As pointed out by Vetter (48) (see comments by Parsons (41)), electrochemical reaction orders have hitherto been relatively little considered. The general dependence of reaction rate upon potential and the electrochemical isotherm for adsorption of reactant ions was first developed by Frumkin (33) in terms of the Gouy-Stern theory of the double-layer (28,42) and examined by Bockris, Conway *et al.* (6,43,44,45) and the Russian workers (46,47,48) with regard to the kinetics of the h.e.r. at Hg, Ni and Ag cathodes

---

* This section contains original material which has been accepted for publication as a paper in Electrochimica Acta under the title "Electrochemical Reaction Orders in the Hydrogen and Oxygen Evolution Reactions". It is logically best presented in this Chapter following the general kinetic treatment given above.

in a number of papers. In previous work, the adsorption of any intermediate radical species, e.g. adsorbed H in the h.e.r., has been regarded as non-activated (36,49) and the Langmuir isotherm has usually been assumed to apply to the adsorbed intermediates involved. This is now known to be not generally justified since, for example, electrochemical energies of adsorption of H are known to be dependent on coverage.

In this section, a brief review of relevant previous work is given and also several new results are presented for cases of electrode reactions involving the formation of intermediates which may be adsorbed under either Langmuir or Temkin conditions.

B. Definition and Derivation of Reaction Order Differentials

(i) Application to the discharge step [1]

The rate of the discharge step can be written, using equation [19a], in the two alternative forms

$$\ln i = \ln \left(c_{H_3O^+}\right)_b - \frac{(1-\beta)\psi_1 F}{RT} - \frac{\beta \phi_M F}{RT} + \text{constants} \qquad [19b]$$

or

$$\ln i = \ln \left(c_{H_3O^+}\right)_b - \frac{(1-\beta)\psi_1 F}{RT} - \frac{\beta \phi_r F}{RT} - \frac{\beta \eta F}{RT} + \text{constants} \qquad [19c]$$

from which the following three general derivatives may be obtained:

$$\text{(i)}\ \left[\frac{\partial \eta}{\partial \ln (c_{H_3O^+})_b}\right]_i \quad ; \quad \text{(ii)}\ \left[\frac{\partial \ln i}{\partial \ln (c_{H_3O^+})_b}\right]_\eta \quad ; \quad \text{(iii)}\ \left[\frac{\partial \ln i}{\partial \ln (c_{H_3O^+})_b}\right]_\phi \qquad [36$$

Derivative (i) simply expresses the effect of pH on the overpotential η. Derivatives (ii) and (iii) are reaction order type derivatives, and the latter must be regarded as the "chemically significant" reaction order since it gives the dependence of rate (ln i) on the reactant concentration ($\ln c_{H^+}$) when conditions are chosen such that variations of double-layer configuration are absent, i.e. for constant ionic strength or ψ_1 potential. Ideally the "constant ϕ" condition in derivative (iii) should refer to constant rational potential, ϕ^o, but this is not always experimentally possible to express, since $\phi^{o.c.m.}$ may depend on solution composition. The derivative (i) is the one which has been usually considered (8,33,44) in previous papers on double-layer and pH effects in electrochemical kinetics. The derivative (i) is obtained from equation [14c] and two cases may be distinguished. The first is that for dilute acid solutions where both ψ_1 and ϕ_r are functions of the activity of hydronium ions (cf. equations [13a] and [15]) and derivative (i) is therefore zero. The second case* is that for the addition of

* This is analogous to the case where certain ionic homogeneous reactions are studied at controlled constant ionic strength.

neutral salts where the total cation concentration is kept constant and ψ_1 therefore remains constant (cf. equation [14]). The potential ψ_1 will also tend to become constant in concentrated acid solutions, i.e. as $c_{H_3O^+} \geqslant 1N$ (34,35) and the only potential term dependent upon $\ln \left(c_{H_3O^+}\right)_b$ is then the reversible potential ϕ_r. Hence derivative (i), for the case of constant ψ_1, is $(1-\beta)RT/\beta F$.

Similarly for derivatives (ii) and (iii), there are two cases each for either a pH dependent or independent ψ_1 potential. The results of the differentiations are shown in Table II.

(ii) Application to the atom-ion mechanism [2]

Unlike the discharge mechanism where coverage effects are not considered since θ_H is usually small, the treatment for atom-ion recombination leads to 4 cases for each derivative in equation [36] corresponding to the two Langmuir conditions of $\theta \longrightarrow 0$ or $\theta \longrightarrow 1$; also four cases arise for the activated and non-activated Temkin conditions depending upon whether ψ_1 is constant or pH dependent.

(a) Langmuir Conditions

From equation [26], the rate of reaction for step [2]

Table II

Kinetic Derivatives for Rate-controlling Steps in the Hydrogen Evolution Reaction

Mechanism	$(\partial\eta/\partial \ln c_{H_3O^+})_i$ Langmuir $\theta\to 0$	Langmuir $\theta\to 1$	Temkin Act.	Temkin Non Act.	$(\partial \ln i/\partial \ln c_{H_3O^+})_\eta$ Langmuir $\theta\to 0$	Langmuir $\theta\to 1$	Temkin Act.	Temkin Non Act.	$(\partial \ln i/\partial \ln c_{H_3O^+})_\phi$ Langmuir $\theta\to 0$	Langmuir $\theta\to 1$	Temkin Act.	Temkin Non Act.
dil. soln.	0	-	-	-	0	-	-	-	β	-	-	-
Discharge												
conc. soln.	$\frac{(1-\beta)RT}{\beta F}$	-	-	-	$(1-\beta)$	-	-	-	1	-	-	-
dil. soln.	0	0	0	0	0	0	0	0	$(1+\beta)$	β	$(\beta+\gamma)$	$(1+\beta)$
Atom + Ion												
conc. soln.	$\frac{(1-\beta)RT}{(1+\beta)F}$	$\frac{(1-\beta)RT}{\beta F}$	$\frac{(1-\beta)RT}{(\gamma+\beta)F}$	$\frac{(1-\beta)RT}{(1+\beta)F}$	$(1-\beta)$	$(1-\beta)$	$(1-\beta)$	$(1-\beta)$	2	1	$(1+\gamma)$	2
dil. soln.	0	0	0	0	0	0	0	0	2	0	2γ	2
Atom + Atom												
conc. soln.	0	0	0	0	0	0	0	0	2	0	2γ	2
dil. soln.	0	0	0	0	0	0	0	0	$(1+\beta)$	β	$(\gamma+\beta)$	$(1+\beta)$
Electro-chemical (Horiuti)												
conc. soln.	$\frac{(1-\beta)RT}{(1+\beta)F}$	$-\frac{RT}{F}$	$\frac{(\gamma-\beta)RT}{(\gamma+\beta)F}$	$\frac{(1-\beta)RT}{(1+\beta)F}$	$(1-\beta)$	$-\beta$	$(\gamma-\beta)$	$(1-\beta)$	2	0	2γ	2

can be written in the forms

$$\ln i_2 = 2 \ln \left(c_{H_3O^+}\right)_b - \frac{(1-\beta)\psi_1 F}{RT} \frac{(1+\beta)\phi_M F}{RT} + \text{constants} \qquad [26b]$$

or

$$\ln i_2 = 2 \ln \left(c_{H_3O^+}\right)_b - \frac{(1-\beta)\psi_1 F}{RT} \frac{(1+\beta)\phi_r F}{RT} - \frac{(1+\beta)\gamma F}{RT} + \text{constants} \qquad [26c]$$

for the condition $\theta \ll 1$. For the limiting Langmuir condition of $\theta \longrightarrow 1$, the two working equations take the form

$$\ln i_2 = \ln c_{H_3O^+ b} - \frac{(1-\beta)\psi_1 F}{RT} - \frac{\beta\phi_M F}{RT} + \text{constants} \qquad [26d]$$

or

$$\ln i_2 = \ln \left(c_{H_3O^+}\right)_b - \frac{(1-\beta)\psi_1 F}{RT} - \frac{\beta\phi_r F}{RT} - \frac{\beta\gamma F}{RT} + \text{constants} \qquad [26e]$$

The derivatives (i), (ii) and (iii) from equations [36] can now be obtained either for ψ_1 constant or pH dependent and their values are given in Table II.

(b) Application of the Temkin Isotherm

The working equations [26] and [26a] for the Temkin conditions and the corresponding derivatives are obtained by the same method as that used above. It is to be noted that the non-activated Temkin case gives results identical with those for

the low coverage Langmuir case ($\theta \rightarrow 0$, see Table II). This follows since the working equations [26a] and [26b and c] are identical.

(iii) Application to the atom-atom recombination mechanism [3]

Here ψ_1 effects associated with the diffuse-layer do not enter into the rate equations if step [1] is sufficiently in equilibrium when step [3] is rate-controlling, so that θ_H can be expressed as a quasi-equilibrium function of ϕ_M and $\left(c_{H_3O^+}\right)_b$. Non-activated and activated conditions for adsorption of H may arise as discussed in section (ii). Under high coverage conditions, $\theta_H \rightarrow 1$ and is then not a function of ϕ_M and $\left(c_{H_3O^+}\right)_b$, i.e. the reaction order is zero. When θ_H is low and a function of ϕ_M, θ_H will be dependent on $\left(c_{H_3O^+}\right)_b$ and the reaction order will be 2. The values of the various derivative quantities for this mechanism are given in Table II.

(iv) Application to the molecule-ion neutralization step [4, 4a]

The relevant derivatives (cf. equations [36]) for the "Horiuti" mechanism are obtained from equations [34] and [35] considering again the pH dependence of ψ_1 and ϕ_r. The results are given in Table II.

4. Review of pH Effects in the Kinetics of the H.E.R. at Hg and Pt

A. Introduction

In this section, the mechanisms operative at mercury and platinum cathodes are discussed in terms of the Tafel slope parameter b and the pH effects. The only previous attempt to study the problem of electrochemical reaction order was made by Vetter (40) who correctly obtained a reaction order of unity for the h.e.r. at Hg in acid solution, but incorrectly interpreted the data for neutral and alkaline solutions (see below). The present treatment (84) is significantly different as it provides additional diagnostic criteria of reaction mechanism. This section is therefore concerned with the discussion of the mechanisms operative in the h.e.r. at Hg and Pt cathodes by reference to exporimental studies of pH effects in the kinetics. The use of isotopes in kinetic studies will be discussed in the following chapters.

B. Mercury

The experimental situation at mercury for the current-potential relation seems to be well established for acid solutions and a reaction order plot based on data obtained from previously published papers of Bagotski and Jablokova (47,48) has been given by Vetter (40) who finds a reaction order $(\partial \ln i / \partial \ln a_{H^+})_{\phi, \psi_1}$

of unity below pH 8 which is consistent with a rate-determining step [1]. The plot giving this result is shown in Figure 3 and was taken from Vetter's paper. The corresponding derivatives $(\partial \ln i / \partial \ln a_{H^+})_{\eta, \psi_1}$ and $(\partial \eta / \partial \ln a_{H^+})_{i, \psi_1}$, are 0.44 and 54 mV, and are derived from Figs. 4 and 5 (47,48). These derivatives are consistent with rate-determining step [1] with $\beta = 0.56$ (7,29,85,86), as supported by the data of Ammar and Hassanein (87), shown in Figures 6, 7 and 8 for concentrated $HClO_4$ solutions where, in comparison with HCl solutions, specific adsorption effects associated with the Cl^- anion (88) are diminished and the diffuse-layer potential ψ_1 is more or less constant. Although the reaction order is not exactly unity (probably owing to residual specific adsorption effects), it is much nearer unity than 0 or 2 which are the limiting reaction orders (see Table I and Chapter I) corresponding to the steps [4-4a] involving the H_2^+ ion discharge mechanism. For the latter process the experimentally observed Tafel slope of 120 mV. is only predicted if $\theta_{H_2^+} \rightarrow 1$ (when $\theta_{H_2^+} \ll 1$, the Tafel slope is $RT/(1+\beta)F$). Under the conditions of $\theta_{H_2^+} \rightarrow 1$, the derivatives (i) and (ii) on p. 28 are -59 mV. and -0.5, respectively, values which are not observed experimentally; in fact, the observed derivatives have the opposite sign. Hence the H_2^+ ion mechanism is not supported for mercury in acid solutions. These results are summarised in Table III. Physically $\theta_{H_2^+} \rightarrow 1$ will be unlikely and such a condition is not supported by capacity or charging data (see below). Mituya (89) has claimed that at low current densities the

Figure 3

Reaction order $(\partial \ln 1/\partial pH)_{\phi,\psi_1}$ for Hg after Vetter (40); ϕ = -1.4 volt.

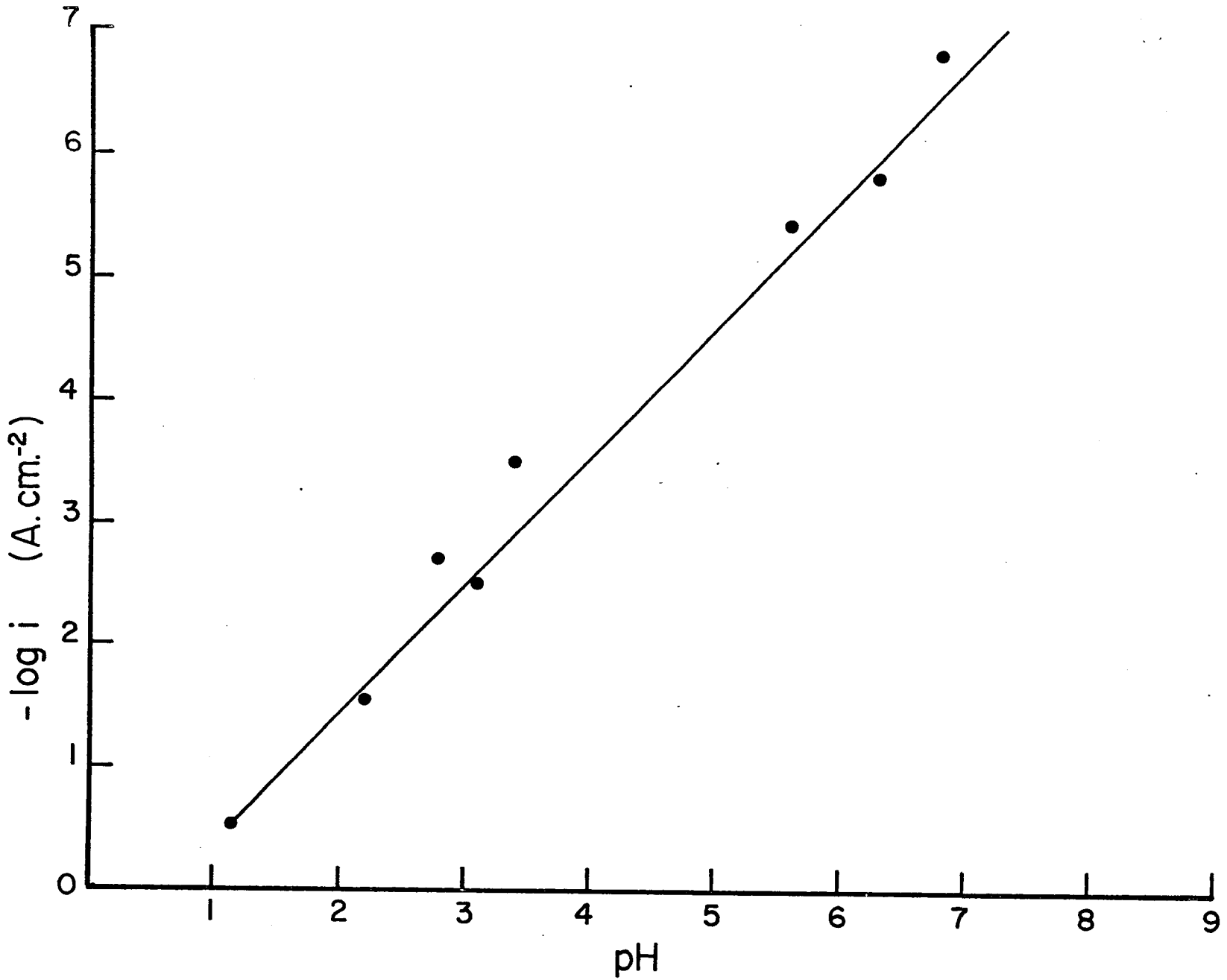
7
6
5
4
3
2
1
0
- log i (A.cm.-2)
1
2
3
4
5
6
7
8
9
pH

Figure 4

Reaction order $(\partial \ln i / \partial pH)_{\eta, \psi_1}$, for Hg after Bagotski and Yablokova (48); $\eta = -1.2$ volt.

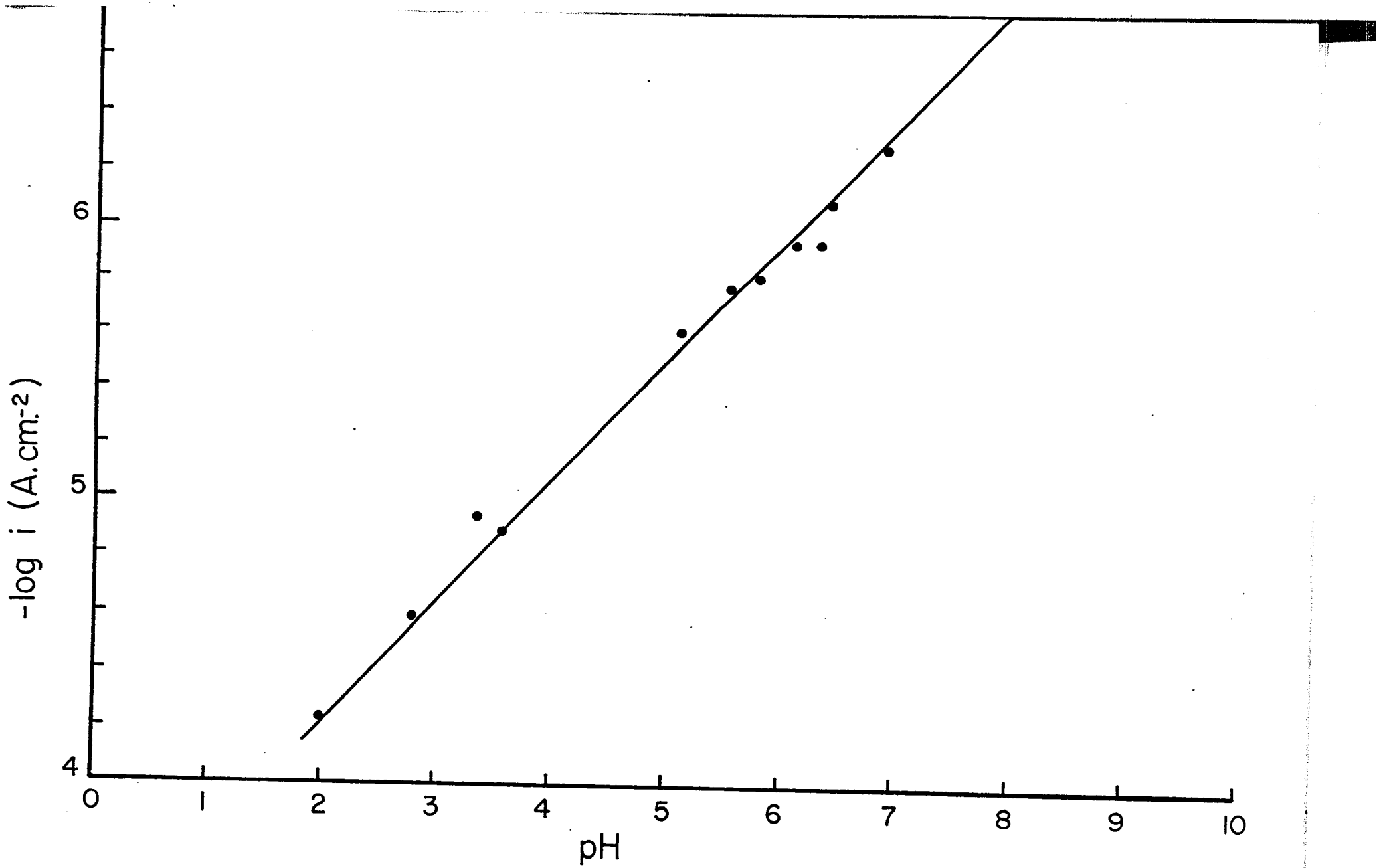
-log i (A.cm.-2)
6
5
4
0
1
2
3
4
5
6
7
8
9
10
pH

Figure 5

Derivative $(\partial\eta / \partial pH)_{i, \varphi_1}$ for Hg after Bagotski and Yablokova (48); $i = 10^{-4}$ amp/cm^2.

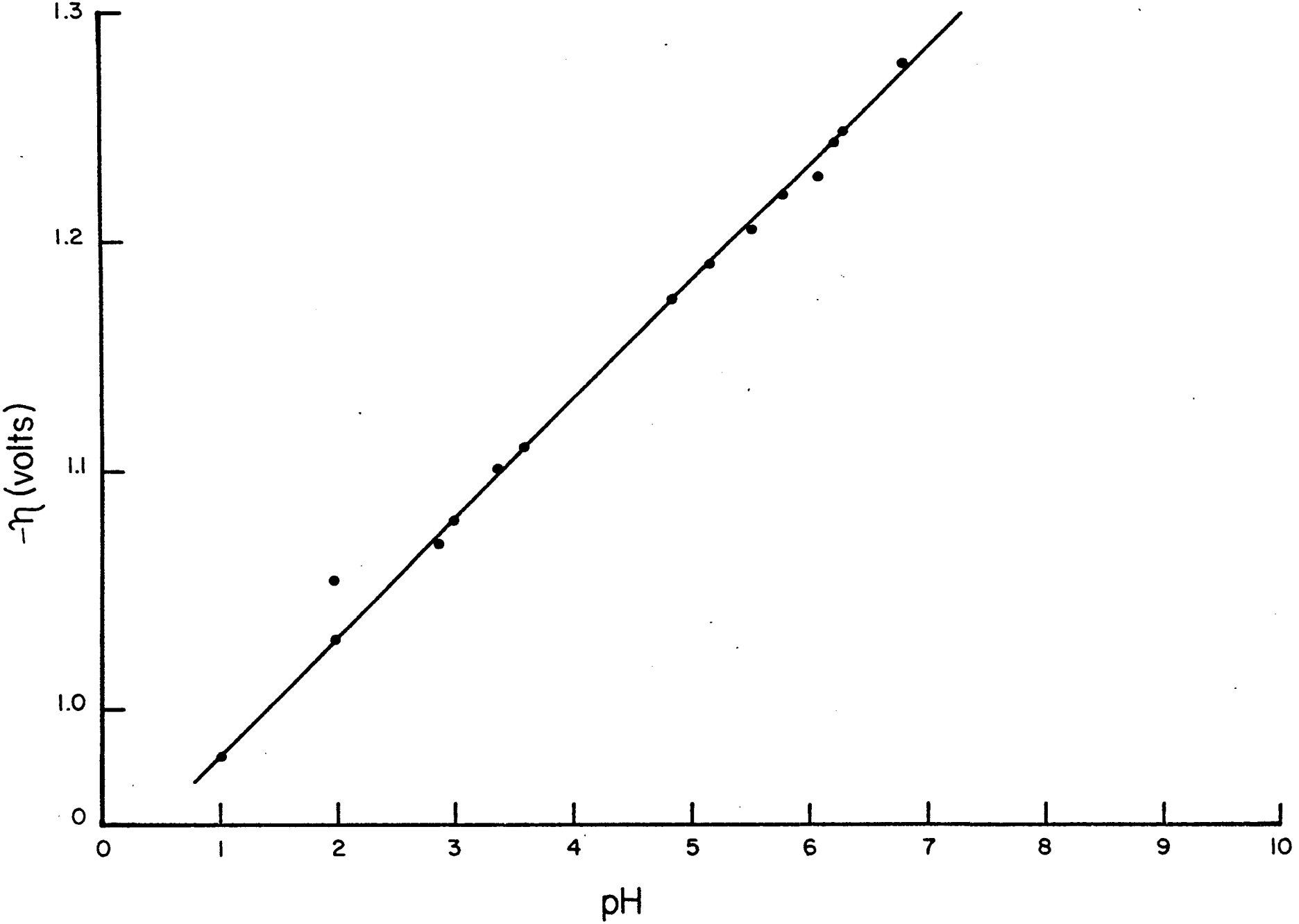
1.3
1.2
1.1
1.0
0
-η (volts)
0
1
2
3
4
5
6
7
8
9
10
pH

Figure 6

Reaction order $(\partial \ln i / \partial pH)_{\phi, \psi_1}$ for Hg in $HClO_4$ using the data of Ammar and Hassanein (87); ϕ = -0.76 volt.

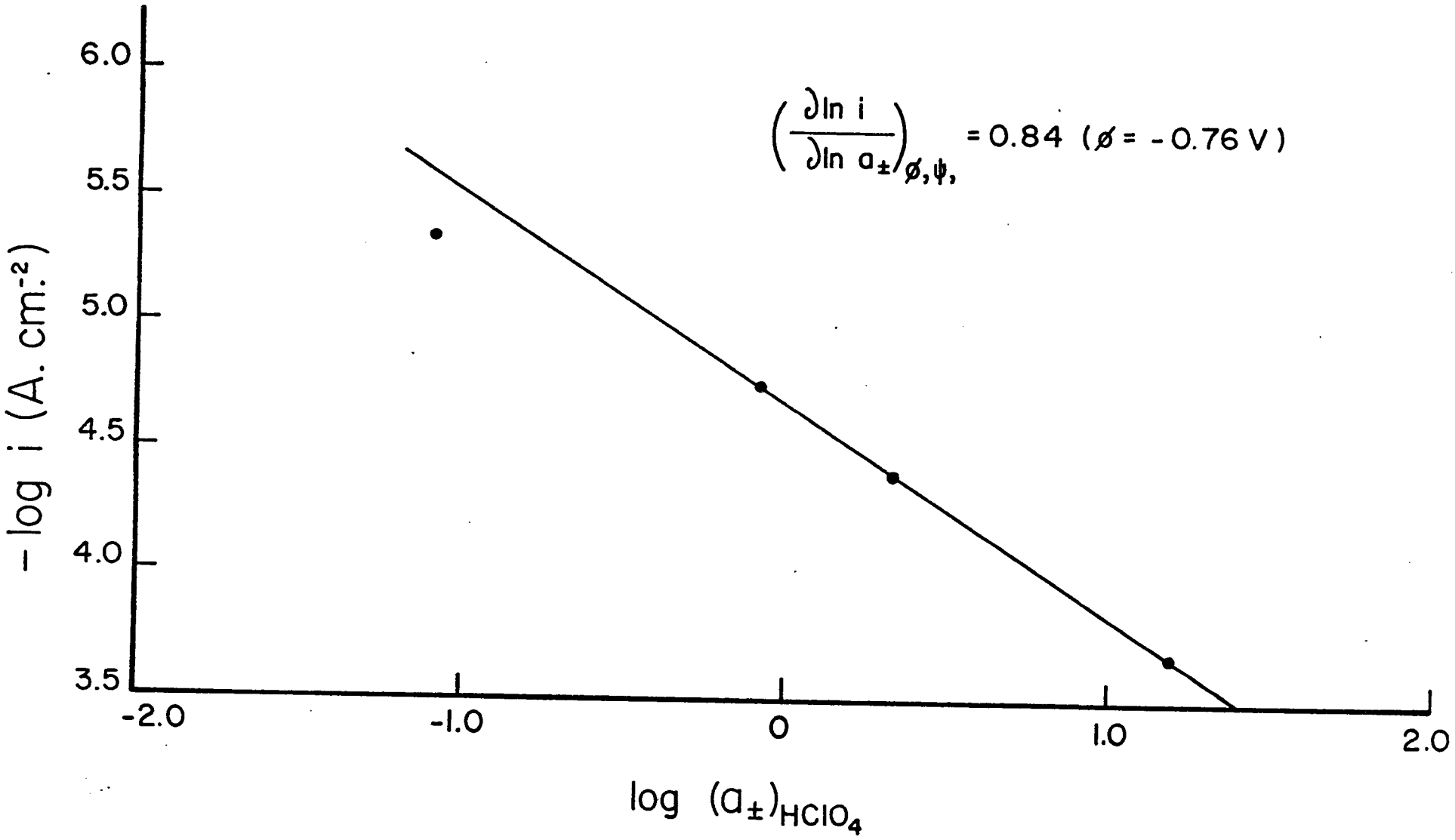
$\left(\frac{\partial \ln i}{\partial \ln a_{\pm}}\right)_{\phi,\psi,} = 0.84$ (ϕ = -0.76 V)
6.0
5.5
5.0
4.5
4.0
3.5
- log i (A. cm.$^{-2}$)
-2.0
-1.0
0
1.0
2.0
log $(a_{\pm})_{HClO_4}$

Figure 7

Reaction order $(\partial \ln i / \partial pH)_{\eta, \psi_1}$ for Hg in $HClO_4$ using the data of Ammar and Hassanein (87); η = -0.76 volt.

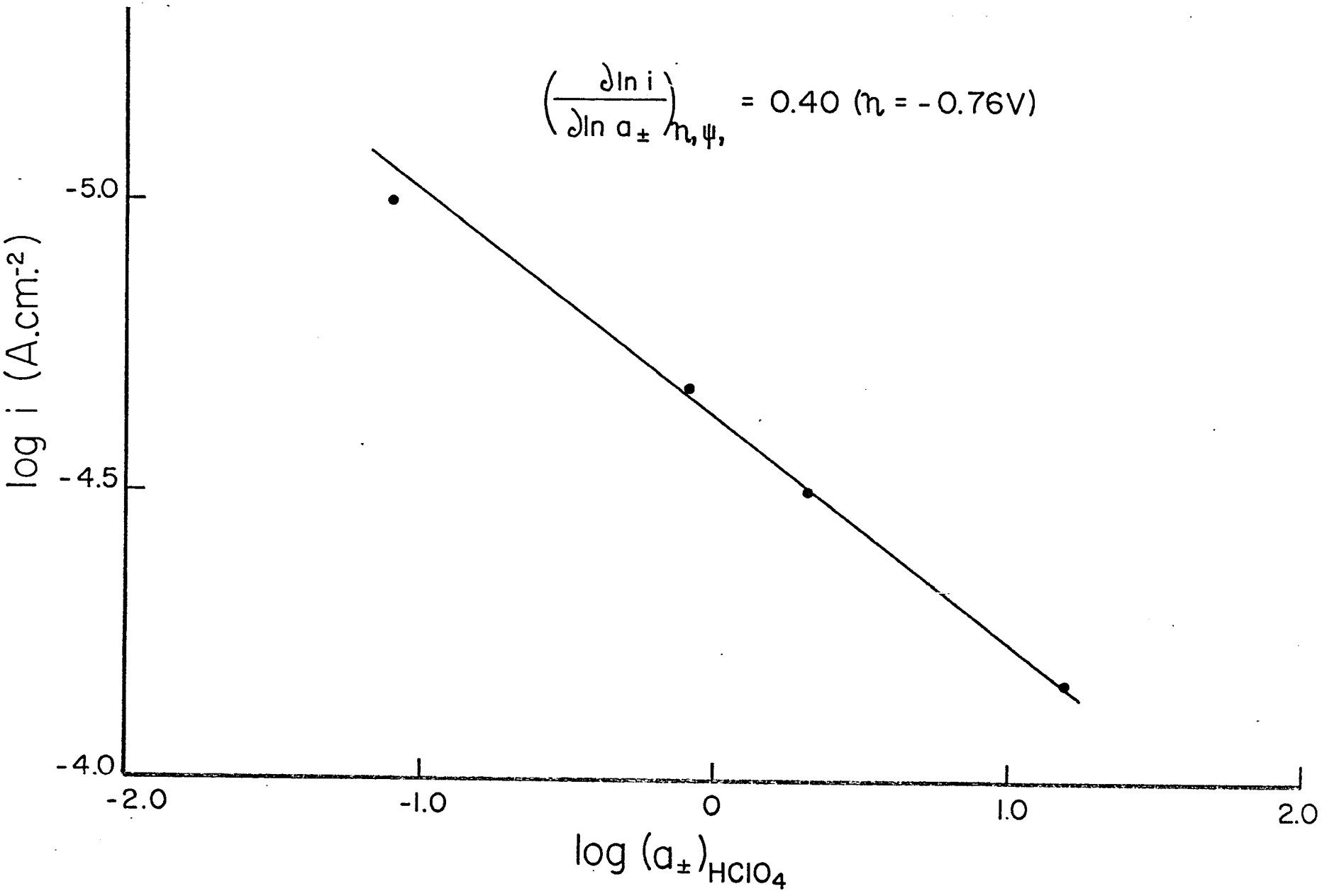
$\left(\frac{\partial \ln i}{\partial \ln a_{\pm}}\right)_{\eta,\psi,} = 0.40$ ($\eta = -0.76V$)
log i (A.cm^{-2})
-5.0
-4.5
-4.0
-2.0
-1.0
0
1.0
2.0
log $(a_{\pm})_{HClO_4}$

Figure 8

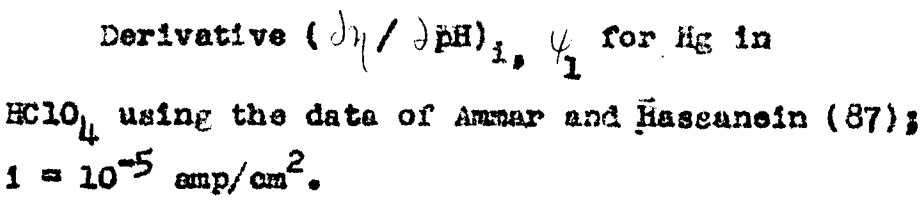

$HClO_4$ using the data of Ammar and Hasanein (87);
$i = 10^{-5}$ amp/cm^2.

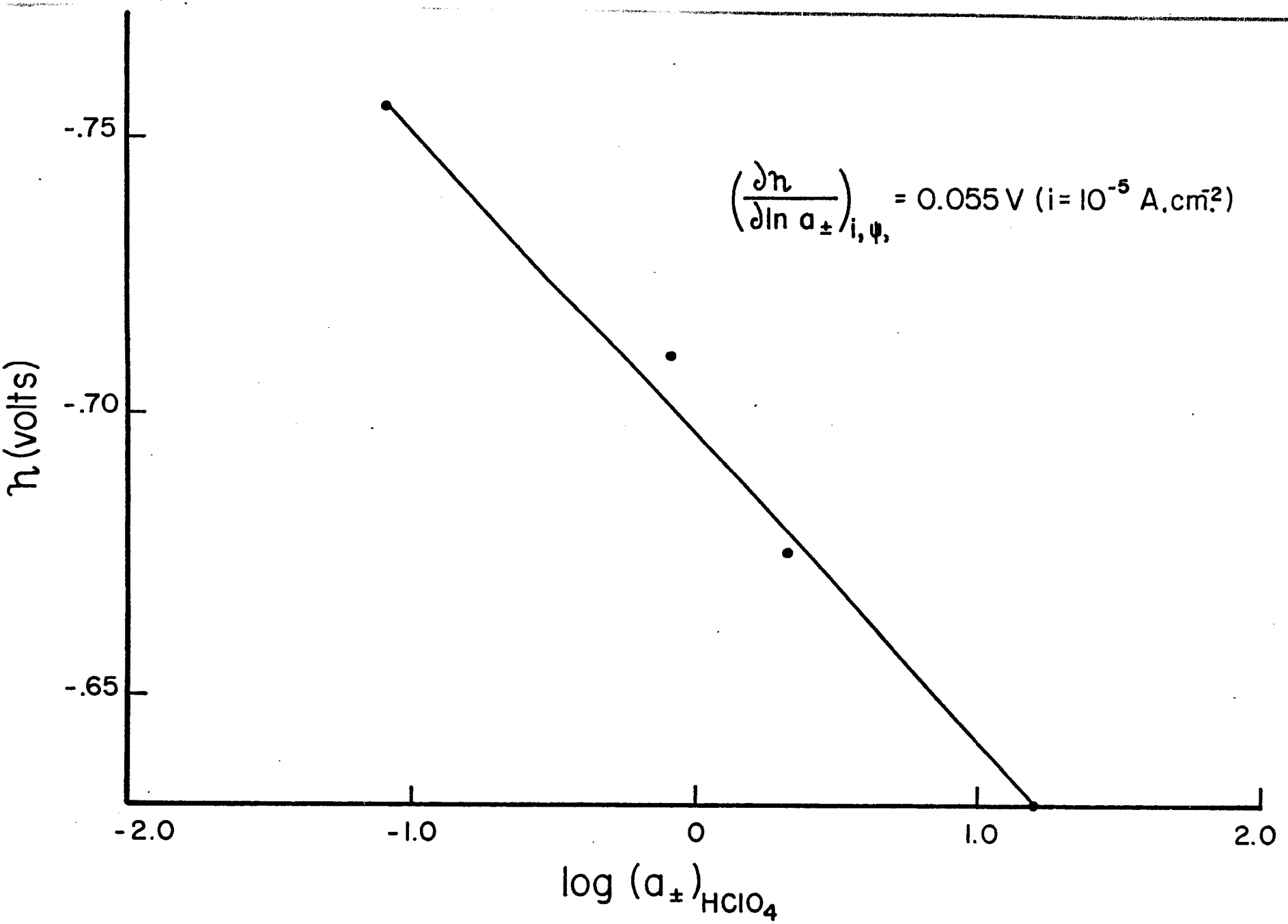
-.75
-.70
-.65
η (volts)
$\left(\frac{\partial \eta}{\partial \ln a_{\pm}}\right)_{i,\psi,}$ = 0.055 V (i = 10^{-5} A.cm^{-2})
-2.0
-1.0
0
1.0
2.0
log $(a_{\pm})_{HClO_4}$

Tafel slope changes from 2.3 RT/βF to 2.3 RT(1 + β)F as required for the H_2^+ ion discharge mechanism. However, this critical result has not been substantiated* and was not found in the similar careful high vacuum work of Bowden and Grew (90) down to 10^{-9} - 10^{10} amp. cm.$^{-2}$ at mercury, and with which the results of Mituya were not compared (89). It may be noted that the change of slope of the Tafel equation for Hg which Mituya has observed, occurs near the potential of zero charge at which a change of slope can be predicted for any cation reduction on account of changing ψ_1 potential (30,93) with electrode potential ø.

Above pH 8, a reaction order of apparently zero is found (40) for mercury and it was concluded by Vetter (40) that this corresponded to the rate-controlling proton discharge from water (step [1a]). However, it has been shown (91) that the h.e.r. at mercury in the presence of KCl and $BaCl_2$ is associated with integrally differing Tafel slopes which indicate an amalgam decomposition reaction of the kind

$$K^+_{aq.} + e + Hg \longrightarrow Hg/K; \quad Hg/K + H_2O \longrightarrow 1/2\ H_2 + OH^- + K^+$$

In the presence of excess neutral salt, the K^+ ion discharge step could also give the observed reaction order of zero in

---

* Bockris (92) has pointed out that under the conditions used by Mituya, platinum may have contaminated the mercury surface to an extent significant at the very low current densities involved.

$[H^+]$. However, with the above evidence (91), the proton discharge from water as a step relevant to alkaline solution conditions can be excluded. The alternative view that proton discharge occurs from water at a potential determined by the equilibrium

$$K/Hg \rightleftharpoons K^+ + Hg + e$$

has also been proposed (29), but this mechanism cannot be distinguished from [105] by reaction order determination alone, and some of the experimental data are still conflicting (see 29). In addition to the these objections, two other difficulties arise with the reaction sequence [4], [4a] as follows:

If [4a] were rate-determining so that [4] would then be in quasi-equilibrium (10,11,94), an equilibrium pseudo-capacitance (37,95) associated with formation and adsorption of the H_2^+ intermediate should arise as is implicit in Horiuti's equation (given in ref. 94) relating $\theta_{H_2^+}$ to ϕ. The pseudo-capacitance-potential relation will then be skewed (96) and can attain values substantially higher than the normal ionic double-layer capacity at mercury. This effect will be different from that considered by Frumkin (29,97) who suggested that the formation of H_2^+ will increase the normal ionic-double-layer capacitance at mercury by a factor of two. It must be noted that no evidence for either of these effects has been found experimentally.

Horiuti has objected (94) to Frumkin's observations (29,97) on the grounds that there will be additional electronic repulsion between H_2^+ ions in the double-layer and this will lead to a depression of the ionic double-layer capacity. However, it is difficult to see how such electron overlap repulsions will be more important than those associated with the net charges upon H_2^+ ions. Thus, the latter effects may be estimated from the theory of ionic interaction in the double-layer developed by Bockris, Devanathan and Müller (98) where image interactions were taken into account. Taking the dielectric constant as about 6* (98, 99) for the region of the double-layer in which the repulsive ionic interactions arise betwen H_2^+ ions, the repulsion energy may be calculated from the above theory as limitingly about 13 kcal. $mole^{-1}$ at hypothetical full coverage by H_2^+ ions assuming an hydration radius of about 2 Å. The coulombic repulsion effects will decrease approximately as $\theta_{H_2^+}^{3/2}$ (98), and would not be expected to be particularly greater for H_2^+ than H^+ (or H_3O^+ aq.) ions involved in the simple discharge step [1], since these ions will be similarly hydrated (68). The experimental and theoretical pH effects at mercury cathodes are compared in Table III.

C. Platinum

The best data available for the h.e.r. at smooth platinum in acid solutions from which reaction order plots may be made,

* The value of 6 rather than 36 (98) is taken since the H_2^+ radical-ion will probably be chemisorbed (11,100) close to the surface.

are those of Schuldiner*(101), as shown in Figs. 9, 10 and 11 for the high (b = 0.10 v) and low(b = 0.03 v) Tafel slope regions (see Table III). The reaction orders (Fig. 9) are 1.1 and 2.1, respectively, for these two Tafel regions. These data can be interpreted as follows. At low potentials, the Tafel slope is ca. 2.3 RT/2F indicating the recombination step [3] as rate-controlling. This is supported by the reaction order of 2(.1) observed (see Fig. 9) and by the small slope of only 11 mV. for the depencence of η on log $[c_{H^+}]$ shown in Fig. 11. This slope for step [3] should ideally be zero (see Table II) and the observed small finite slope is probably due to effects of the an(ions) adsorbed in the double-layer on the energy of adsorption and coverage by H at the platinum electrode, e.g. as found experimentally (102,103). That such anion effects are important for this mechanism is indicated by recent results obtained in the present work (see Chapters III-VI) on the H/D isotope separation factor S at Pt in various acid solutions; the S values were found to vary appreciably with the electrolyte anion and significantly with electrode potential, at overpotentials between 0 and -350 mV. This is also supported by the results of Popat and Hackerman (104) on the double-layer capacity at platinum where specific anion effects are found at appreciable cathodic potentials.

---

* The author is specially indebted to Dr. Schuldiner for providing him with the detailed original data from which the reaction order plots could be made.

Figure 9

Reaction order $(\partial \ln i / \partial \text{pH})_{\phi, \psi_1}$ for Pt,
(data of Schuldiner (101); ϕ = -0.12 volt

○ b = 0.03 volt

● b = 0.10 volt.

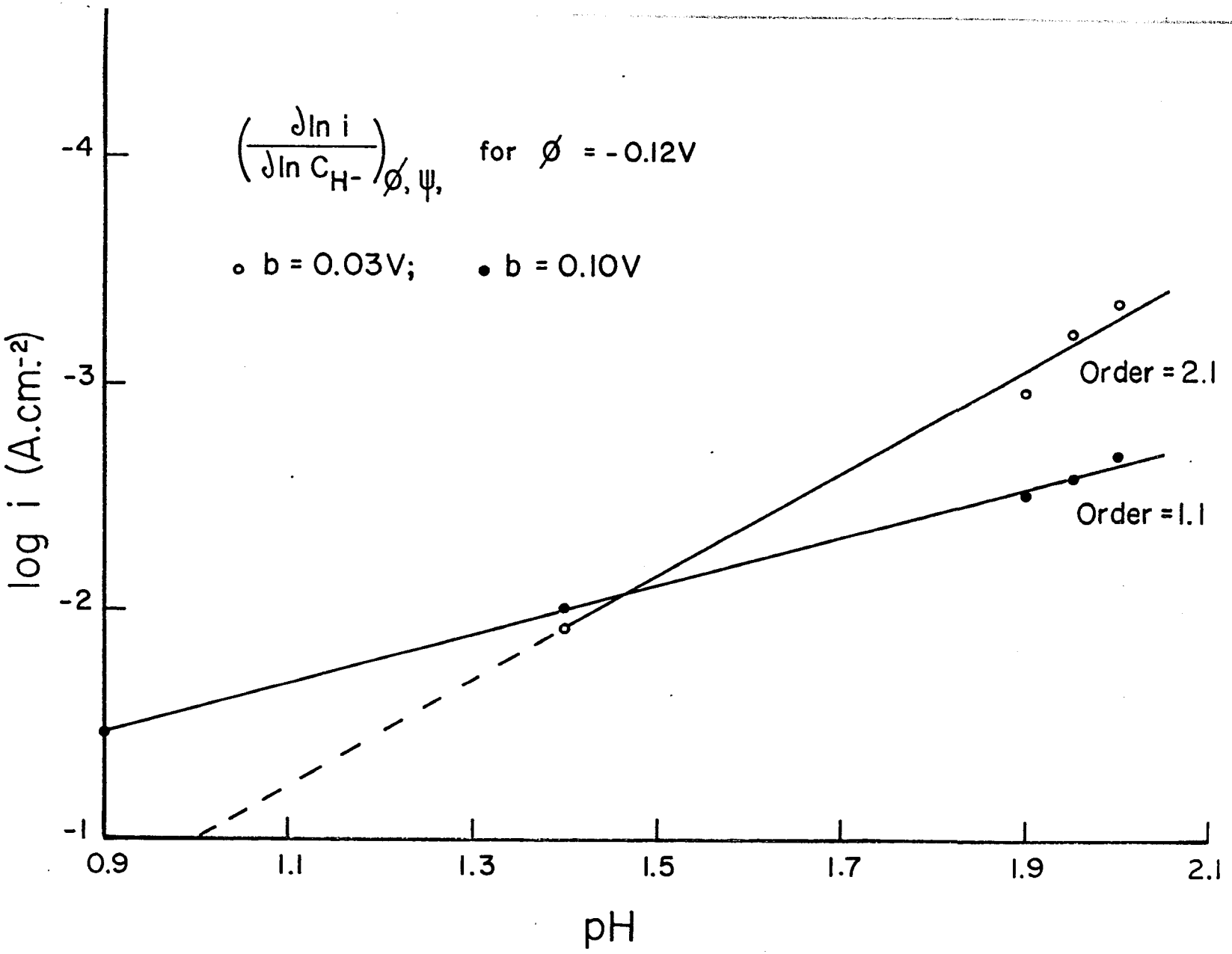
$\left(\frac{\partial \ln i}{\partial \ln C_{H^-}}\right)_{\phi,\psi,}$ for ϕ = -0.12V
o b = 0.03V; • b = 0.10V
Order = 2.1
Order = 1.1
log i (A.cm^{-2})
-4
-3
-2
-1
0.9
1.1
1.3
1.5
1.7
1.9
2.1
pH

Figure 10

Reaction order $(\partial \ln i / \partial pH)_{\eta, \psi_1}$ for Pt in the Tafel region of b = 0.10 volt (data of Schuldiner (101)).

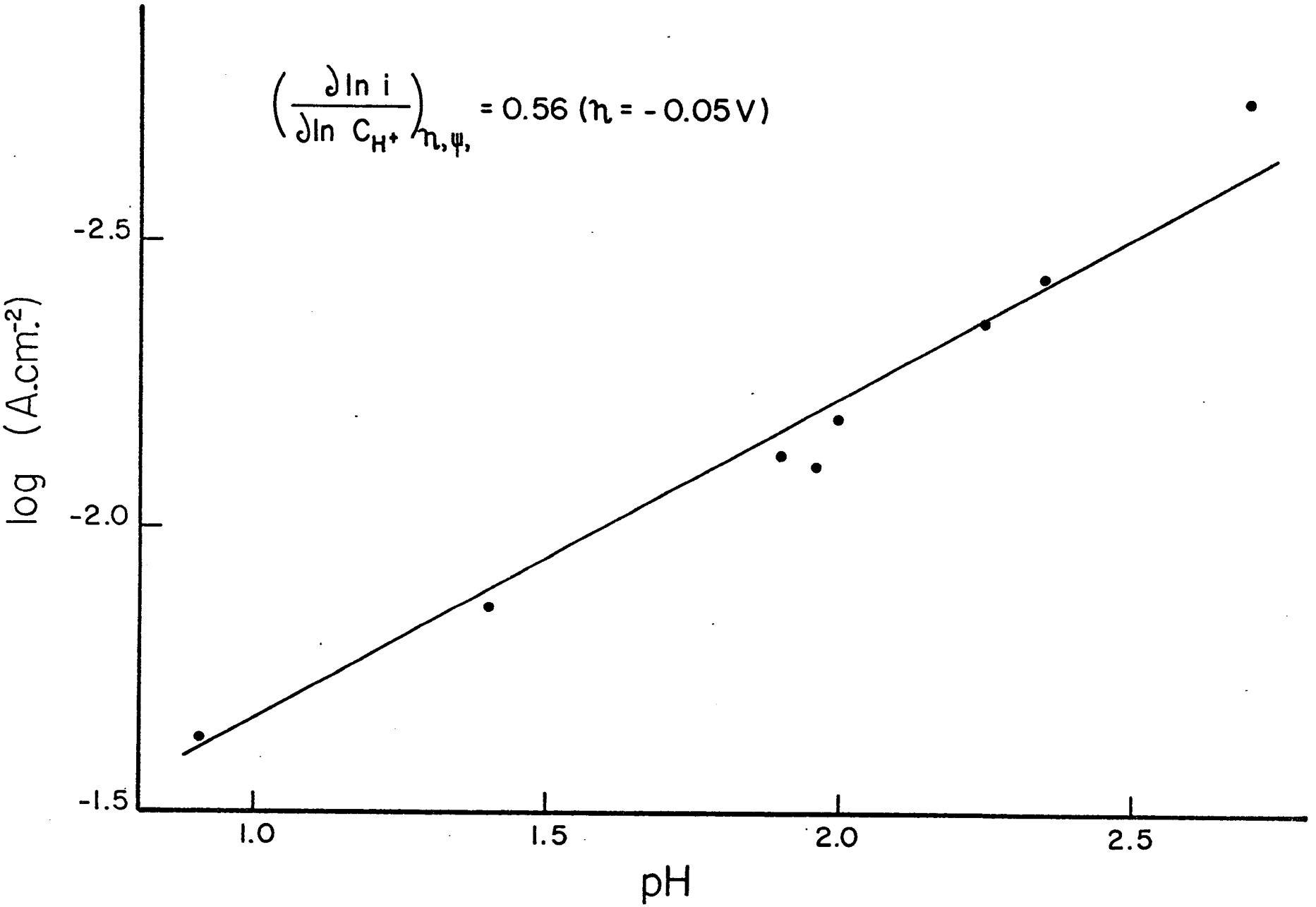
$\left(\frac{\partial \ln i}{\partial \ln C_{H^+}}\right)_{\eta,\psi,} = 0.56\ (\eta = -0.05\,V)$
log (A.cm.$^{-2}$)
-2.5
-2.0
-1.5
1.0
1.5
2.0
2.5
pH

Figure 11

Derivative $(\partial\eta / \partial \mathrm{pH})_i$, φ_1 for Pt (data of Schuldiner (101)).

b = 0.03 volt; $i = 10^{-2.2}$ A.cm^{-2}

b = 0.10 volt; $i = 10^{-2.0}$ A.cm^{-2}

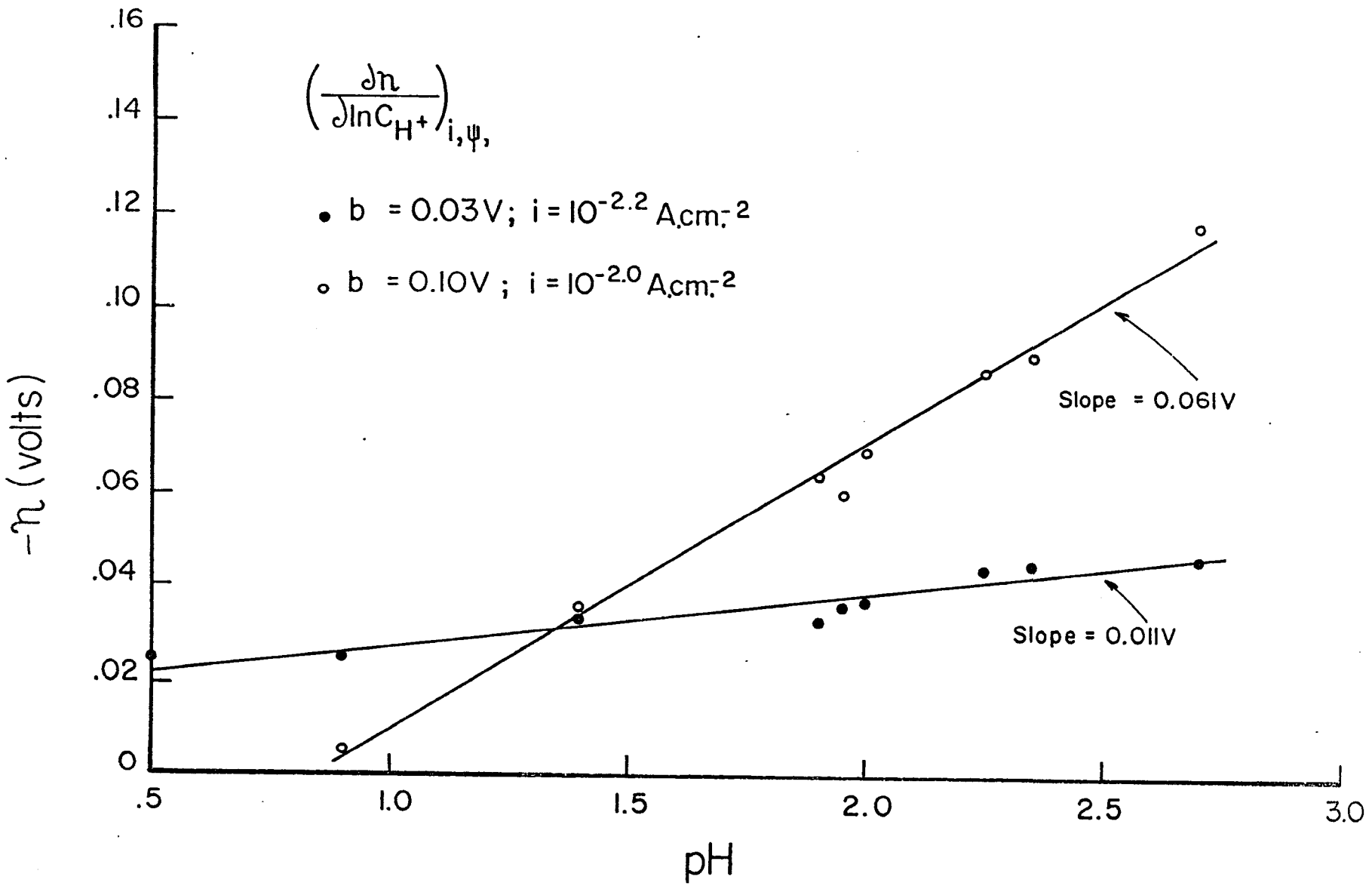
$\left(\frac{\partial \eta}{\partial \ln C_{H^+}}\right)_{i,\psi,}$
• b = 0.03V; $i = 10^{-2.2}$ A.cm^{-2}
∘ b = 0.10V ; $i = 10^{-2.0}$ A.cm^{-2}
Slope = 0.061V
Slope = 0.011V
$-\eta$ (volts)
.16
.14
.12
.10
.08
.06
.04
.02
0
.5
1.0
1.5
2.0
2.5
3.0
pH

Table III

Comparison of Experimental and Theoretical Reaction Order and other Derivatives for the h.e.r.

Derivative	Theoretical*							Observed			
	ATOM + ATOM Tomkin		ATOM + ION	ION	HORIUTI ELECTROCHEMICAL			Hg		Pt	
	θ→1	Non Act.	θ→1	Discharge	θ→1	θ→0	Tomkin Non Act.	Neutral Salt[1]	Conc. Solns[2]	30 mv Tafel Region[3]	100 mv Tafel Region[3]
$\left(\frac{\partial \eta}{\partial \ln c_{H_3O^+}}\right)_{i,\psi_1}$	0	0	59	59	-59	30	30	0.55	0.56	0(?)	58
$\left(\frac{\partial \ln i}{\partial \ln c_{H_3O^+}}\right)_{\eta,\psi_1}$	0	0	0.5	0.5	-0.5	0.5	0.5	0.44	0.41	0(?)	0.55
$\left(\frac{\partial \ln i}{d \ln c_{H_3O^+}}\right)_{\phi,\psi_1}$	2	1	1	1	0	2	2	1.0	0.83	2.1	1.1

Note: * Taking $\beta = 0.5$

1. Based on work of Bagotsky and Yablokova (47,48).
2. " " " " Amvar and Hassanein (87).
3. " " " " Schuldiner (101).

At higher current densities, however, where the Tafel slope is 0.10 V. (ca. 2.32RT/F), the derivatives (Figs. 9, 10,11) correspond (see Table II) to rate-determining step [2] under Langmuir conditions. The only other mechanism and conditions which could give a reaction order of unity would be [3] proceeding under activated adsorption conditions (see equation 29a) ($\gamma = 0.5$) but the Tafel slope would then be 2.3 RT/F (not observed) and the derivatives $(\partial \ln i/\partial \ln c_{H^+})_{\eta,\psi_1}$ and $(\partial\eta/\partial \ln c_{H^+})_{i,\psi_1}$ would both be zero. This is not observed (see Table III). Hence [2] is indicated as the rate-determining step for the high current density region. The results thus support the assignment of mechanism given by Bockris and Azzam (105) based on the observation of a coverage controlled limiting current at $\theta_H = 1$.

Horiuti has claimed that the H_2^+ ion discharge mechanism is also operative at platinum at low current densities. In Schuldiner's experiments (101), two Tafel regions are observed. A low current density region having a slope of 30-40 mV followed by one having a slope of ca. 100 mV at higher current densities. In the low current density region, it is found that $(\partial\eta/\partial \ln c_{H_3O^+})_{i,\psi_1} = 0$, $(\partial \ln i/\partial \ln c_{H_3O^+})_{\eta,\psi_1} = 0$ and $(\partial \ln i/\partial \ln c_{H_3O^+})_{\theta,\psi_1} = 2$. This corresponds to the atom-atom

recombination mechanism [3]. For a Tafel slope of 2.3 RT(1+β)F, the H_2^+ ion discharge mechanism predicts values of 30 mV, 0.5 and 2, respectively, for these quantities. At higher current densities, it is found that $(\partial\eta / \partial \ln c_{H_3O^+})_{i,\psi_1} = 64$ mV, $(\partial \ln i / \partial \ln c_{H_3O^+})_{\eta,\psi_1} = 0.5$ and $(\partial \ln i / \partial \ln c_{H_3O^+})_{\phi,\psi_1} = 1$. For these quantities, the atom-ion recombination step respectively predicts 60 mV, 0.5 and 1 while the H_2^+ ion mechanism predicts -60 mV, -0.5 and 0, and is hence inapplicable at platinum (see Table III) for the Tafel region of 120 mV slope.

There can be little doubt that, on the above experimental evidence, the Horiuti mechanism [4] is, in fact, not rate-controlling at Hg or Pt. It is possible that the H_2^+ molecule-ion may be an intermediate radical in step [2]. This intermediate is known from studies of the oxidation properties of H atoms when introduced into acid solutions from the gas phase (106,107,108). If adsorbed H_2^+ species are actually formed on an electrode, the rate of their discharge must be very fast compared with that of other any reaction in which they might take part (29).

CHAPTER III

THE KINETIC ISOTOPE EFFECT

1. Introduction

The evaluation of kinetic isotope effects is an important complementary method which can be used in the elucidation of reaction mechanisms. Since the study of the electrochemical H/D/T isotope effect applied to proton transfer mechanisms at electrodes constitutes a major portion of this thesis, it is appropriate to give a fairly detailed introductory discussion concerning the origin of primary isotope effects and a brief review of previous applications to the h.e.r.

The work constituting the present investigation may conveniently be summarised in the following three sub-divisions:

(1) Further evidence for the applicability of mechanisms [1] to [3] has been sought by investigating their major weakness, i.e. their apparent failure to predict low isotope effects. The original calculation of the H/D isotopic separation factor, S_D, by Topley and Eyring (175) gave limiting high values for the discharge step [1]. Topley and Eyring realized that their calculated value was a maximum one since zero-point energies in the activated complex were neglected, but the calculation was regarded by Horiuti et al. (9,63) as supporting the inapplicability of the slow proton discharge mechanism.

(ii) Experiments have been carried out involving the determination of the H/D isotope effect for the two metals in question, Hg and Pt, particularly with regard to measurements at controlled potentials. Horiuti et al. (9,10,11,12,68) have maintained that mechanism [4] is operative at Hg and at Pt (12) at low current densities. Their only support for this mechanism has been; (a) the apparently high theoretical values for the isotopic separation of H and D based on the original calculation of Topley and Eyring (175) and recently modified by Keii and Kodera (168), and (b) the successful explanation in 1951 (10) of the isotope effect in terms of mechanism [4]. It will be shown in this thesis, that the observed isotope effects can, in fact, be explained by mechanisms [1]-[3] and that the potential dependence and anion dependence of these isotope effects can best be explained in terms of a "complex" site model* for the proton discharge step [1].

(iii) In addition to (i) and (ii) above, the possibility of proton tunneling at metal electrodes has been studied. Low temperature isotopic studies were carried out and the indications, which are discussed in Chapters V and VI, are that tunneling contributions to the classical reaction rates are negligible.

---

* By the "complex" site model, reference is made to the possibility of interstitially adsorbed hydrogen atoms (see Chapters V and VI).

2. Classical Isotope Effects

A. Introduction

Since the electrochemical reactions considered in the present work involve a proton transfer at a metal electrode, significant changes in rates and equilibrium constants would be expected upon substitution of hydrogen by deuterium or tritium. The term "classical isotope effect" will be used to refer to those effects which can be explained by a classical mechanism, i.e. those that arise mainly on account of mass effects and hence from changes of vibrational frequencies in initial and activated states. This term is to be distinguished from that ("quantum mechanical isotope effects") which refers to the mechanism of proton tunneling, i.e. to departure from classical mechanics. Such behavior will be discussed in more detail in a following section.

B. Origin of Isotope Effects (51,53,54)

(1) General Rate Equations

There are, in general, two factors which affect the relative rates of proton, deuteron and tritium (H, D, and T) transfer reactions. These are (a) the free energy differences between the initial and activated states associated with differences in mass which affect the velocity of passage of the reacting

particle over the potential energy barrier, and (b) the possibility of quantum mechanical tunneling. The major factor which contributes to the free energy difference is the difference in zero-point energies. According to Urey's postulate (50), the potential energy of the bond in say X - H, is invariant with change of isotopic mass. Hence for two isotopically analogous molecules X - H and X - D, the electron distributions associated with these two bonds are regarded as being identical so that for a given internuclear distance, the curves relating potential energy to internuclear distance are identical. If the following two reactions are considered

$$M + H - X \rightleftharpoons X_H^{\neq} \longrightarrow MH + X \qquad [37]$$

and

$$M + D - X \rightleftharpoons X_D^{\neq} \longrightarrow MD + X \qquad [37a]$$

where $X^{\neq}$ is the activated complex (51), the potential energy curves for both the H and D species are hence identical according to the Urey postulate (50), as shown in Figure 12. The significant difference between reactions [37] and [37a] arises then from the zero-point energy differences in both initial and activated states. According to the theory of absolute reaction rates (51), the ratio of rate constants for reactions [37] and [37a] is given by

$$\frac{k_H}{k_D} = \frac{\nu_{X-D}}{\nu_{X-H}} \cdot \frac{f_H^{\neq}}{f_D^{\neq}} \cdot e^{\Delta E^{\neq}/RT} \qquad [38]$$

where f is the molecular partition function for the indicated state and species and q is that calculated per unit volume, i.e. $q = f/V$; $\Delta E^{\neq}$ is the vibrational zero-point energy difference between initial and activated states given by (see Figure 12)

$$\begin{aligned}\Delta E^{\neq} &= \Delta E^{\neq}_D - \Delta E^{\neq}_H \\ &= (E^{o}_H - E^{o}_D) - (E^{\neq}_H - E^{\neq}_D) \\ &= \tfrac{1}{2} hc(\nu^{o}_H - \nu^{o}_D - \nu^{\neq}_H + \nu^{\neq}_D) \end{aligned} \qquad [39]$$

The ratio of transmission coefficients is usually assumed to be unity (52) and hence does not appear in equation [38]. The f terms in equation [38] are to be regarded as the complete partition functions in the sense that no approximations have yet been made (see below). The molecular partition functions per unit volume in equation [38] are given by

$$q = f_{trans}\, f_{rot}\, f_{vib} \times \frac{1}{V} = \frac{(2\pi MkT)^{3/2}}{h^3} \times \frac{g_{el} g_{nuc}}{\sigma}$$

$$\times \frac{8\pi^2 (8\pi^3 ABC)^{1/2} (kT)^{3/2}}{h^3} \times \prod_{i} \left(1 - e^{-hc\nu_i/kT}\right)^{-1} \qquad [40]$$

where A, B and C are the principal moments of inertia; g_{el} and g_{nuc} account for the electronic statistical weight of the ground state and any degeneracy due to different orientations of the nuclear spins, respectively; σ is the symmetry number, M is the molecular weight and ν_i is a typical vibration frequency

Figure 12

Potential energy profile for the isotopic reactions M + HX → MH + X and M + DX → MD + X.

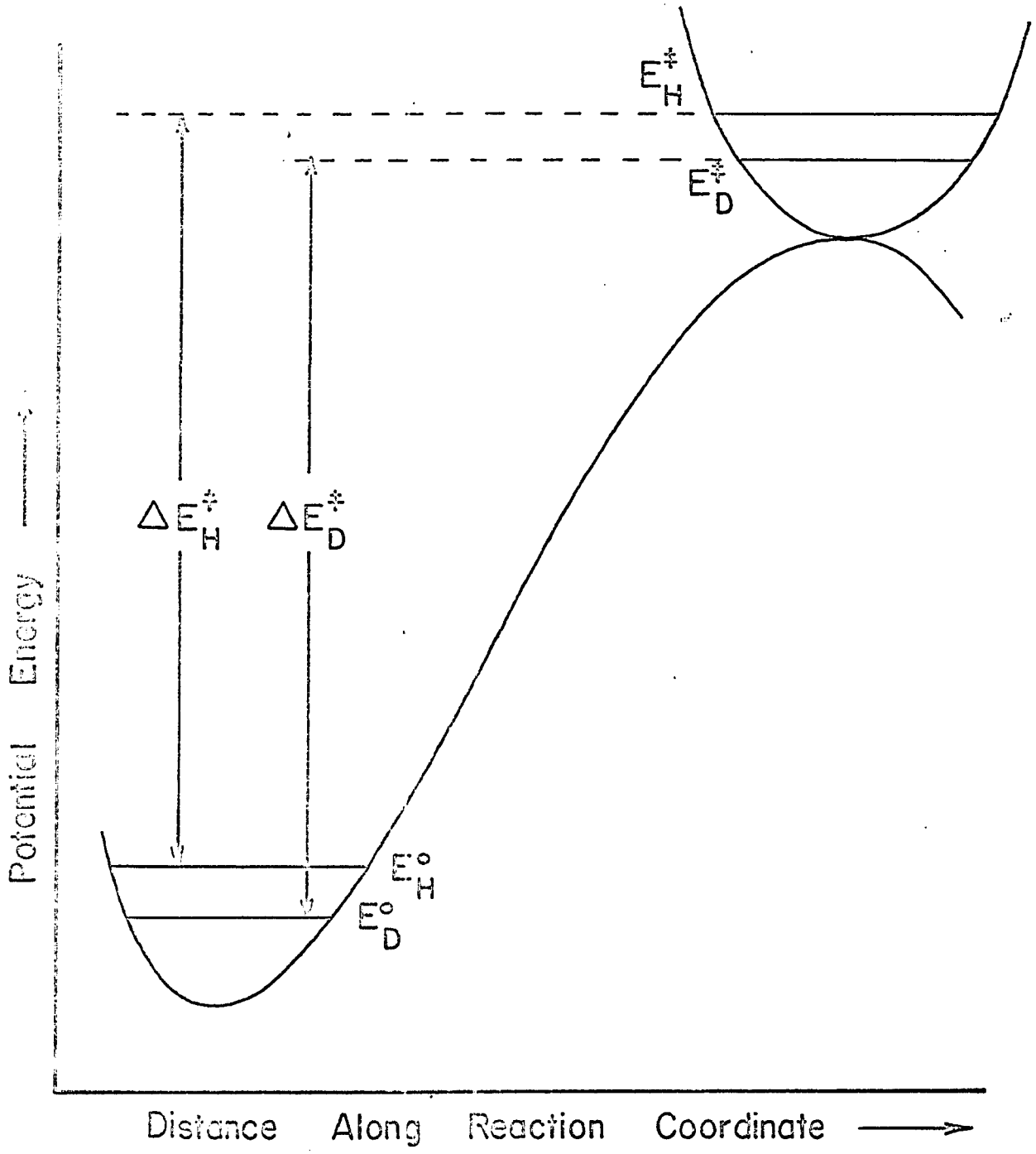
$E^{\ddagger}_H$
$E^{\ddagger}_D$
$\Delta E^{\ddagger}_H$
$\Delta E^{\ddagger}_D$
E°_H
E°_D
Potential Energy
Distance Along Reaction Coordinate

in wave numbers (cm^{-1}); all other terms have their usual significance. The complete equation [38] can be rewritten in terms of the relations [39] and [40] in the two alternative forms

$$\frac{k_H}{k_D} = \left(\frac{M_D}{M_H}\right)^{3/2} \frac{\sigma_H}{\sigma_D} \left(\frac{A_D B_D C_D}{A_H B_H C_H}\right)^{1/2} \prod_{1}^{3n-6} \left[\frac{e^{-\frac{1}{2}u_{1,D}}}{e^{-\frac{1}{2}u_{1,H}}} \cdot \frac{1-e^{-u_{1,(H)}}}{1-e^{-u_{1,(D)}}}\right] \times$$

$$\left(\frac{M_H^{\neq}}{M_D^{\neq}}\right)^{3/2} \frac{\sigma_D^{\neq}}{\sigma_H^{\neq}} \left(\frac{A_H^{\neq} B_H^{\neq} C_H^{\neq}}{A_D^{\neq} B_D^{\neq} C_D^{\neq}}\right)^{1/2} \prod_{1}^{3n^{\neq}-7} \left[\frac{e^{-\frac{1}{2}u^{\neq}_{1,H}}}{e^{-\frac{1}{2}u^{\neq}_{1,D}}} \cdot \frac{1-e^{-u^{\neq}_{1,D}}}{1-e^{-u^{\neq}_{1,H}}}\right] \qquad [41]$$

or

$$\frac{k_H}{k_D} = \left(\frac{\sigma_D^{\neq}}{\sigma_H^{\neq}} \frac{\sigma_H}{\sigma_D}\right) \left(\frac{M_H^{\neq}}{M_D^{\neq}} \cdot \frac{M_D}{M_H}\right)^{3/2} \left(\frac{A_H^{\neq} B_H^{\neq} C_H^{\neq}}{A_D^{\neq} B_D^{\neq} C_D^{\neq}} \cdot \frac{A_D B_D C_D}{A_H B_H C_H}\right)^{1/2}$$

$$\prod_{1}^{3n^{\neq}-7} \frac{\sinh \frac{1}{2} u^{\neq}_{1,D}}{\sinh \frac{1}{2} u^{\neq}_{1,H}} \prod_{1}^{3n-6} \frac{\sinh \frac{1}{2} u_{1,H}}{\sinh \frac{1}{2} u_{1,D}} \qquad [42]$$

where $u_1 = h\nu_1/kT$.

(11) Simplifications and Approximations in the Rate Equations

(a) The Teller-Redlich Product Theorem (56)

The Teller-Redlich product theorem for isotopically analogous molecules enables the vibrational product quotient for the H and D vibrations to be represented in terms of masses and

moments of inertia as follows:

$$\prod_{i}^{3n-6} \frac{\nu_{i,D}}{\nu_{i,H}} = \prod_{j}^{n} \left(\frac{m_{j,H}}{m_{j,D}}\right)^{3/2} \left(\frac{M_D}{M_H}\right)^{3/2} \left(\frac{A_D B_D C_D}{A_H B_H C_H}\right)^{1/2} \qquad [43]$$

where m denotes atomic mass of the indicated isotope. Equation [43] applies to non-linear molecules; for linear molecules the product on the l.h.s. of [43] is taken over 3n-5 vibrations and the moments of inertia decrease from three to two (which are then equal). In activated complex theory, the vibrational mode which corresponds to decomposition is $\nu_L^{\neq}$, the subscript L indicating that this frequency can be imaginary (i.e. multiplied by $\sqrt{-1}$). Applying the product theorem to the activated complex,

$$\left(\frac{M_H^{\neq}}{M_D^{\neq}}\right)^{3/2} \left(\frac{A_H^{\neq} B_H^{\neq} C_H^{\neq}}{A_D^{\neq} B_D^{\neq} C_D^{\neq}}\right)^{1/2} = \frac{\nu_{L,H}^{\neq}}{\nu_{L,D}^{\neq}} \prod_{j}^{n^{\neq}} \left(\frac{m_{j,H}^{\neq}}{m_{j,D}^{\neq}}\right)^{3/2} \prod_{1}^{3n^{\neq}-7} \frac{\nu_{i,H}^{\neq}}{\nu_{i,D}^{\neq}} \qquad [44]$$

If the product rule relations from equation [43] for initial state molecules and from [44] for the activated complex, are substituted into [42], the result is

$$\frac{k_H}{k_D} = \left(\frac{\sigma_D^{\neq} \sigma_H}{\sigma_H^{\neq} \sigma_D}\right) \frac{\nu_{L,H}^{\neq}}{\nu_{L,D}^{\neq}} \prod_{j}^{n^{\neq}} \left(\frac{m_{j,H}^{\neq}}{m_{j,D}^{\neq}}\right)^{3/2} \prod_{1}^{3n^{\neq}-7} \left(\frac{u_{i,H}^{\neq}}{u_{i,D}^{\neq}} \cdot \frac{\sinh \frac{1}{2} u_{i,D}^{\neq}}{\sinh \frac{1}{2} u_{i,D}^{\neq}}\right) \times$$

$$\prod_{j}^{n} \left(\frac{m_{i,D}}{m_{i,H}}\right)^{3/2} \prod_{1}^{3n-6} \left(\frac{u_{i,D}}{u_{i,H}} \cdot \frac{\sinh \frac{1}{2} u_{i,H}}{\sinh \frac{1}{2} u_{i,D}}\right)$$

Since the activated and initial states contain the same set of atoms, it follows that all atomic masses cancel and the above equation reduces to

$$\frac{k_H}{k_D} = \frac{\sigma_D^{\neq}\,\sigma_H}{\sigma_H^{\neq}\,\sigma_D}\;\frac{\nu_{L,H}^{\neq}}{\nu_{L,D}^{\neq}}\;\prod_{1}^{3n^{\neq}-7}\left(\frac{u_{i,H}^{\neq}}{u_{i,D}^{\neq}}\cdot\frac{\sinh\frac{1}{2}u_{i,D}^{\neq}}{\sinh\frac{1}{2}u_{i,H}^{\neq}}\right)\quad x$$

$$\prod_{1}^{3n-6}\left(\frac{u_{i,D}}{u_{i,H}}\cdot\frac{\sinh u_{i,H}}{\sinh u_{i,D}}\right) \qquad [45]$$

The factor $\nu_{L,H}^{\neq}/\nu_{L,D}^{\neq}$ has been often designated as "the temperature independent factor" (56,57).

(b) <u>Cancellation of all Bending Frequencies in Initial and Activated States</u>

One common approximation made by many workers is to assume that all but one of the vibrational contributions to the zero-point energy in initial and activated states disappear by cancellation. The vibrational mode term which does not cancel is that corresponding to the stretching modes in the initial states X - H and X - D. Equation [45] then reduces to

$$\frac{k_H}{k_D} = \left(\frac{\sigma_D^{\neq}\sigma_H}{\sigma_H^{\neq}\sigma_D}\right)\frac{\nu_{L,H}^{\neq}}{\nu_{L,D}^{\neq}}\cdot\frac{u_{str,D}}{u_{str,H}}\cdot\frac{\sinh\frac{1}{2}u_{str,H}}{\sinh\frac{1}{2}u_{str,D}} \qquad [46]$$

For the simple harmonic oscillator, the following relation holds

$$\nu = \frac{1}{2\pi}\sqrt{\frac{k}{\mu}}$$

where k is the force constant (identical for X - H and X - D bonds by the Urey postulate) and μ is the reduced mass of the particles involved. Hence for the species X - H and X - D,

$$\frac{u_H}{u_D} = \frac{\nu_H}{\nu_D} = \left(\frac{m_D}{m_H}\right)^{1/2} = \sqrt{2} \qquad [47]$$

It is seen that in equation [46]

$$\frac{\nu_{L,H}^{\neq}}{\nu_{L,D}^{\neq}} \cdot \frac{u_{str,D}}{u_{str,H}} = 1,$$

so that the general approximation has the final form

$$\frac{k_H}{k_D} = \frac{\sigma_D^{\neq}\,\sigma_H}{\sigma_H^{\neq}\,\sigma_D} \cdot \frac{\sinh \frac{1}{2} u_{str,H}}{\sinh \frac{1}{2} u_{str,D}} \qquad [48]$$

Equation [48] is probably the most general or simplest approximation and has been applied to several reactions by Eyring and Cagle (58)

(c) <u>Case for Zero Bending Frequencies in the Activated State</u>

Here reactions [37] and [37a] are taken as examples, and the activated states are assumed to be linear, i.e. M....H....X and M....D....X; then equation [45] can be written as

$$\frac{k_H}{k_D} = \frac{\sigma_D^{\neq}\sigma_H}{\sigma_H^{\neq}\sigma_D} \frac{\nu_{L,H}^{\neq}}{\nu_{L,D}^{\neq}} \prod_1^3 \left(\frac{u_{i,H}^{\neq}}{u_{i,D}^{\neq}} \frac{e^{-\frac{1}{2}u_{i,H}^{\neq}}}{e^{-\frac{1}{2}u_{i,D}^{\neq}}} \cdot \frac{1-e^{-u_{i,D}^{\neq}}}{1-e^{-u_{i,H}^{\neq}}} \right)$$

$$\prod^{3n-6} \left(\frac{u_{i,D}}{u_{i,H}} \cdot \frac{e^{-\frac{1}{2}u_{i,D}}}{e^{-\frac{1}{2}u_{i,H}}} \cdot \frac{1-e^{-u_{i,H}}}{1-e^{-u_{i,D}}} \right) \qquad [49]$$

There are 4 vibrations in the activated complex. One is the asymmetric stretch which leads to decomposition and hence is not included in the frequency terms for the activated complex. The three remaining frequencies correspond to a symmetric stretching mode and to a doubly degenerate bending mode. If the assumption is made that the symmetric stretching mode is independent of isotopic mass, then the product of frequency terms involves contributions from the doubly-degenerate mode, i.e. from

$$\left(\frac{u_{bend,H}^{\neq}}{u_{bend,D}^{\neq}} \cdot \frac{e^{-\frac{1}{2}u_{b,H}^{\neq}}}{e^{-\frac{1}{2}u_{b,D}^{\neq}}} \cdot \frac{1-e^{-u_{b,D}^{\neq}}}{1-e^{-\frac{1}{2}u_{b,H}^{\neq}}} \right)^2$$

If the additional assumption is made that these two bending frequencies approach zero* when the activated complex is formed, then $e^{-\frac{1}{2}u_{b,H}^{\neq}}/e^{-\frac{1}{2}u_{b,D}^{\neq}} = 1$ and

---

* In point of fact, this assumption is unlikely to be at all correct for proton transfer reactions (cf. 18). In the actual numerical calculations for electrochemical proton transfer presented in Chapter VIit is not made.

$$\lim_{u_b^{\neq}\to 0}\left[\frac{1-e^{-u_{b,D}^{\neq}}}{1-e^{-u_{b,H}^{\neq}}}\right]=\frac{u_{b,D}^{\neq}}{u_{b,H}^{\neq}}=\left(\frac{m_H}{m_D}\right)^{1/2} \qquad [50]$$

Since, according to this simple model, two vanishing frequencies have been assigned to the activated complex, there will be three unmatched terms in the zero point energy of the reactant and equation [49] becomes, upon introduction of equation [50],

$$\frac{k_H}{k_D}=\frac{\sigma_D^{\neq}\sigma_H}{\sigma_H^{\neq}\sigma_D}\;\frac{\nu_{L,H}^{\neq}}{\nu_{L,D}^{\neq}}\;\prod_{i}^{3}\left(\frac{u_{i,D}}{u_{i,H}}\cdot\frac{\sinh\frac{1}{2}u_{i,H}}{\sinh\frac{1}{2}u_{i,D}}\right)$$

and since

$$\frac{\nu_{L,H}^{\neq}}{\nu_{L,D}^{\neq}}\prod_{i}^{3}\frac{u_{i,D}}{u_{i,H}}=\left(\frac{2}{1}\right)^{1/2}\left(\frac{1}{2}\right)^{3/2}=\left(\frac{1}{2}\right)$$

the final approximate form for the above ratio of rate constants is

$$\frac{k_H}{k_D}=\frac{\sigma_D^{\neq}\sigma_H}{\sigma_H^{\neq}\sigma_D}\;\frac{1}{2}\prod_{i}^{3}\frac{\sinh\frac{1}{2}u_{i,H}}{\sinh\frac{1}{2}u_{i,D}} \qquad [51]$$

C. The Kineticist's Problem

(i) General Considerations

In general, the rate constant for a reaction of the type

$$A + B \rightleftharpoons X^{\neq} \longrightarrow P$$

can be written in terms of absolute rate theory by

$$\underline{k} = \gamma \frac{kT}{h} \cdot \frac{Q^{\neq}}{Q_A Q_B} e^{-\Delta E_o^{\neq}/RT} \qquad [52]$$

where Q is now the molecular partition per unit volume (if a surface reaction were considered, Q', the molecular partition function per unit area, would be employed). For convenience, kinetic data are usually reported in terms of the two parameters, A and E, in the Arrhenius equation

$$\underline{k} = A e^{-E/RT} \qquad [53]$$

The problem of computing a rate constant (or an isotopic ratio of rate constants) from equation [52] (or [42] and [45]) is that the activated complex is a rather intangible entity. Both its structure and spectra are unknown, whereas the structure, molecular mechanical properties and energy of either initial state reactants or products can usually be obtained from spectroscopic data. Similar information for the activated complex must, however, be estimated.

If the structure of the activated complex is taken as the variable parameter, the theory becomes infinitely flexible. If, however, the activated complex is treated like a normal molecule, with the exception of the single separable coordinate, then it is possible to use the results of molecular theory, structure, and spectroscopy to estimate the properties of the

activated complex. Even by reasonable assignment of force constants to the bonds in the activated complex, it is not to be expected that very reliable E values can be predicted. The A factor, often called the frequency factor, can, in some cases, be predicted to within a factor of four and more reliably than E (59). The problem, and perhaps the major difficulty of absolute rate theory, is therefore the characterization of the activated complex in a manner such that major errors are minimized.

D. Methods of Fixing Structure and Properties of Activated Complexes

(1) General Considerations

In classical mechanics, a reaction such as that given in [37] can be represented by a potential energy surface similar to that shown in Figure 13. In this surface, the energy levels, shown as contour lines, are plotted in all coordinates. The basic assumption in activated complex theory is that the highest energy state $V^{\ddagger}$ in the lowest path of potential energy locates the unique structure of the activated complex. The partition function for a linear activated complex is

$$f^{\ddagger} = f_t^3 \, f_r^2 \, f_v^{3n-6} \, f_e / \sigma^{\ddagger} \qquad [54]$$

where the f terms are as in equation [40]. From the potential energy surface $V^{\ddagger}$ is obtained as the height of the saddlepoint

Figure 13

Hypothetical potential energy surface.

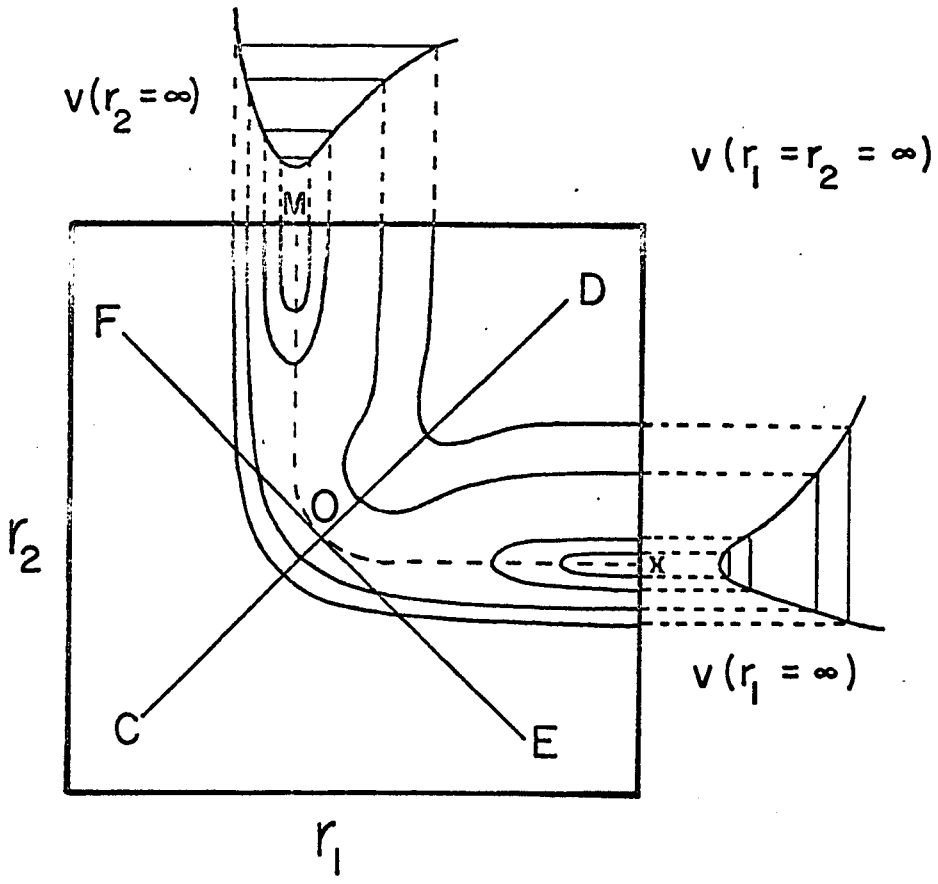
v(r2 = ∞)
v(r1 = r2 = ∞)
M
D
F
O
r2
x
v(r1 = ∞)
C
E
r1

above the zero-point potential energy level of reactants. The translational partition function can be evaluated from known molecular mass, and the structure at the saddlepoint permits one to calculate the moments of inertia for the rotational partition function and the G-matrix. The G-matrix is used to evaluate the internal kinetic energy of the complex (60,61). The curvatures of potential energy through the saddlepoint along various internal coordinates constitute the F-matrix. The vibrational frequencies, including $\nu_L^{\neq}$, are all found from solution of the secular equation (61), viz.

$$\left| FG - E\lambda \right| = 0 \qquad [55]$$

where E is the unit matrix. Thus for a given electronic state, all parameters needed for $f^{\neq}$ can, in principle, be obtained from the potential energy surface by location of the saddlepoint and evaluation of the second derivatives of energy with respect to displacement. The problem then is the evaluation of the potential energy in terms of all coordinates which will enable the calculation of the vibrational frequencies of the activated complex to be made.

(ii) Potential Energy

(a) Monatomics - In the perfect gas approximation, there is no potential energy associated with a monatomic gas.

(b) Diatomics - From band spectra, the potential energy V as a function of distance can be deduced purely on an

empirical basis. A simple theoretical treatment of the H_2 molecule has been given by Heitler and London (62), and Sugiuru (63), and its principles are reviewed here since its features have been extended to more difficult problems.

The zero-energy state is taken as two H-atoms at an infinite distance from each other. As they approach, if the two electron spins are opposed, (singlet state) a chemical bond is formed. If the spins are parallel (triplet state) repulsion arises at all distances. The energy of the system is (62)

$$W_T = \frac{Q-a}{1-A} \quad \text{and} \quad W_S = \frac{Q+a}{1+A} \qquad [56]$$

where Q, a, and A are the coulombic and exchange energies, and overlap integral, respectively. All three quantities are dependent upon internuclear distance r. Morse (64) proposed an empirical potential energy function for diatomic molecules

$$V = D_e \left[e^{-2a(r-r_e)} - 2e^{-a(r-r_e)} \right] \qquad [57]$$

where D_e is the dissociation energy, including the zero point energy, and a is the "anharmonicity constant" which can be obtained from spectroscopic data. Recently, Sato (65) proposed a Morse function for an unstable pair of atoms as

$$V^* = \frac{D_e}{2} \left[e^{-2a(r-r_e)} + 2e^{-a(r-r_e)} \right] \qquad [58]$$

For the case of a stable diatomic molecule, the Morse function may be expanded in terms of a Taylor series in r about the minimum in potential energy where $r-r_e = 0$. Denoting $r-r_e$ by R,

$$V = V_o + \frac{dV}{dR} R + \frac{1}{2} \frac{d^2V}{dR^2} R^2 + \frac{1}{6} \frac{d^3V}{dR^3} R^3 + \ldots\ldots \qquad [59]$$

The constant term is $-D_e$ and the first derivative is zero since this corresponds to the minimum value of V. The terms in the higher powers in R^3, R^4 etc. are negligible compared with that in R^2. Hence for small displacements about the minimum,

$$V = \frac{1}{2} k R^2 = \frac{1}{2} k(r-r_e)^2 \qquad [60]$$

where, the force constant, k, is given by

$$k = \frac{d^2V}{dR^2} \qquad [61]$$

At R = 0, it is found that

$$k = 2 a^2 D_e \qquad [62]$$

Eyring and Polanyi (66) proposed that Δ (equation 56) be set equal to zero and assumed that γ and α were proportional to each other at all distances r, i.e.

$$\gamma = \rho V \quad \text{and} \quad \alpha = (1 - \rho)V \qquad [63]$$

where ρ is a constant fraction of coulombic to total binding

energy, i.e. $\rho = Q/V$, and V is given by equation [57]. An alternate approximation is that of Sato who evaluated the functions D_e, Q and a from the simultaneous equations

$$D_e [e^{-2aR} - 2e^{-aR}] = Q + a/(1 + \Delta) \qquad [64]$$

$$D_e [e^{-2aR} + 2e^{-aR}] = Q - a/(1 - \Delta) \qquad [65]$$

with the assumption that Δ was constant. Solving for Q and a from [64] and [65] gives

$$Q = \frac{D_e}{4} [(3 + \Delta) e^{-2aR} - 2(1 + 3\Delta) e^{-aR}] \qquad [66]$$

$$a = [\frac{D_e}{4} (1 + 3\Delta) e^{-2aR} - 2(3 + \Delta) e^{-aR}] \qquad [67]$$

(c) <u>Linear Triatomics</u> - The potential energy for a linear triatomic molecule is changed upon bending and stretching. The energies of a three-atom system cannot be calculated rigorously by quantum mechanics and semi-empirical methods must be used. The following reaction will be considered:

$$M + H\overset{r_1}{\text{---}}X \longrightarrow M\overset{r_2}{\text{-----}}H\overset{r_1}{\text{-----}}X \longrightarrow M\overset{r_2}{\text{---}}H + X.$$

The potential energy surface for this reaction is assumed to be known and is shown in Figure 13. The path of minimum potential energy is the dotted line from H to X. A cut of the potential energy surface through O along COD gives a profile similar that obtained from a Morse function and it represents

simultaneous dissociation of M and X from H. A cut along BOP for a short distance near O is an inverted parabola and a Taylor series expansion can be made about this point. The constant term (cf. equation [59]) gives the energy difference between M and O. The first derivative is zero and for small displacements about O, the potential energy can be represented by the quadratic function

$$V - V_o = \tfrac{1}{2}(k_1 R_1^2 + k_2 R_2^2 + 2k_{12} R_1 R_2) \qquad [68]$$

where

$$k_1 = \frac{\partial^2 V}{\partial r_1^2}, \quad k_2 = \frac{\partial^2 V}{\partial r_2^2}, \quad k_{12} = \frac{\partial^2 V}{\partial r_1 r_2} \qquad [69]$$

(111) Potential Energy Surfaces

(a) The Eyring-Polanyi Method (66)

Eyring and Polanyi used the London equation (67) to calculate the total energy V of a three-atom system which is given by

$$V = \frac{Q_1 + Q_2 + Q_3 \pm \frac{1}{2}[(a_1 - a_2)^2 + (a_2 - a_3)^2 + (a_3 - a_1)^2]^{1/2}}{1 + \Delta} \qquad [70]$$

where each Q and corresponding a is that for the corresponding "diatomic" molecule (equation [56]). The parameters for the Morse potential (equation [57]), are obtained from spectroscopic data and Δ is not equal to zero. Hence the adjustable parameter becomes the constant fraction ρ defined by equation [63]. A

potential energy surface determined in this manner gives a "well" at the top of the pass. Since Q, α and Δ are all functions of internuclear distance, and Δ in addition will depend strongly on the effective quantum number, n, this method must be regarded as "semi-empirical". Thus in calculating the H/D isotope effect in the h.e.r. at a nickel cathode by this method, Horiuti et al. (68) calculated an energy of activation of 75 kcal mole^{-1} for the chemisorption of hydrogen on a nickel surface. This exceeds the experimental value by at least one order of magnitude (51)!

(b) The Sato Potential Energy Surface

Sato (65) has proposed an alternative procedure in which Δ is taken as the adjustable parameter to set the activation energy equal to the observed value. By choosing a constant value for Δ (by trial and error), Q and α can be calculated from spectroscopic data for the various diatomic combination of the atoms involved in the reaction, using equations [66] and [67]. However, since Δ is in fact not a constant, but can vary strongly with internuclear distance, this method is really no great improvement over that of Eyring and Polanyi (cf. Weston, (69)).

(c) Method of Normal Modes of Vibration (60,61,70,71,72,73)

Normal modes of vibration are defined as the vibrational degrees of freedom, i.e., the number of fundamental vibrational modes of the molecule. The normal modes of vibration of an activated complex can be determined without the knowledge of a potential energy surface by choosing force constants by reference to analogous stable molecules, e.g. as treated in references 59,60,80,81. If the vibrational properties of the activated complex can be satisfactorily fixed by considerations external to kinetics, then another method is available which is probably no worse, and possibly as acceptable as the conventional method of potential energy surfaces. The adjustable parameters in this method are the force constants of the various bonds involved. There are, however, several restrictions to the choice of force constants, as discussed below, so that the method is not "infinitely" flexible. It must, however, be regarded as empirical since the results will depend significantly on the choice of force constants, and to a much lesser degree, on the assumed geometry of the complex (59,60,81).

3. Non-Classical Barrier Penetration

A. Introduction

In classical mechanics a particle of total energy E approaching a potential energy barrier of height V will pass over the barrier with unit probability if $E > V$ and will be

reflected with unity probability if $E < V$. In quantum mechanics, a particle with energy $E > V$ may be reflected and a particle with energy $E < V$ may penetrate or "tunnel" through the barrier.

According to the de Broglie hypothesis (75), all fundamental entities of physics exhibit both wave and particle properties. Hence photons, electrons, protons, atoms and molecules would all be associated with a wavelength λ depending upon their "effective" masses, m_c, and velocities, v. The de Broglie relation is

$$\lambda = \frac{h}{m_c v} = \frac{h}{[2m_c(E-V)]^{1/2}} \qquad [71]$$

The probability of tunneling is dependent, in part, upon the height and width of the barrier. If the wavelength λ is comparable with the barrier width, then the tunneling probability is markedly increased and departure from classical behavior must be considered. From equation [71], it is expected that the largest deviations from classical behavior will arise with particles of low mass. This is quite evident for electrons which cannot, even approximately, be treated by classical mechanics. For heavier particles, tunneling contributions would be expected to fall off rapidly with increasing mass. For the proton, equation [71] can be solved for $E-V = kT$ and it is found that $\lambda = 10^{-8}$ to 10^{-9} cm. which is comparable with the width

expected for energy barriers in proton transfer reaction (17,18).

B. Bell's Treatment of Barrier Penetration (15,16,19,76)

(i) The Symmetric Eckart Barrier (15)

Assuming a statistical Boltzmann distribution of particles with respect to energy W,

$$\frac{dN}{N_o} = \frac{1}{KT} e^{-W/kT} \cdot dW \qquad [72]$$

In classical mechanics, the fraction of particles N of a total number N_o which can pass over the energy barrier of height E is

$$\frac{N}{N_o} = e^{-E/kT} \qquad [73]$$

The probability of barrier penetration can be obtained, for a suitable barrier, by solving the one-dimensional Schrödinger equation

$$\frac{\partial^2\psi}{\partial x^2} + \frac{8\pi^2 m_o}{h^2}[W - V(x)]\psi = 0 \qquad [74]$$

where V(x) is the potential energy as a function of distance. Using a symmetrical Eckart barrier (77), an exact solution (15) of equation [74] can be obtained. The general equation is

$$V(x) = \frac{Ae^{2\pi x/l}}{1+e^{2\pi x/l}} + \frac{De^{2\pi x/l}}{(1+e^{2\pi x/l})^2} \qquad [75]$$

where 2l is the width of the barrier i.e. it is the distance

between the initial and final positions of the particle. The coordinates of the maximum value of V(x) (i.e. at V_m) are

$$x_m = \frac{1}{2\pi} \log \frac{B + A}{B - A} \qquad [76]$$

$$V_m = B = \frac{(A + B)^2}{4B} \qquad [77]$$

and the curve becomes horizontal at $x = -1$, $V(x) = 0$ and at $x = +1$, $V(x) = A$. Hence A can be identified with the energy change in the reaction. For the case of $B > h^2/8\pi m_c l^2$, the solution to the Schrödinger equation giving the permeability, G_w, is

$$G_w = \frac{\cosh [2\pi(\alpha + \beta)] - \cosh [2\pi(\alpha - \beta)]}{\cosh [2\pi(\alpha + \beta)] + \cosh (2\pi\delta)} \qquad [78]$$

where

$$\alpha = \frac{1}{h} 2 m_c W , \quad \beta = \frac{1}{h} 2 m_c (W - A)$$

$$C = \frac{h^2}{8 m_c l^2} , \quad \delta = \frac{1}{2} \left(\frac{B - C}{C}\right)^{1/2} \qquad [79]$$

For the special case where the energy change in the reaction is zero (e.g. in ortho-para hydrogen conversion), equation [130] becomes

$$V(x) = \frac{Be^{2\pi x/l}}{(1 + e^{2\pi x/l})^2} \qquad [80]$$

which has a maximum value at

$$V_m = E = \frac{B}{4}$$

and the permeability is

$$G_W = \frac{\cosh(4\pi a) - 1}{\cosh(4\pi a) + \cosh(2\pi\delta)} \qquad [81]$$

The quantity G_W can be calculated for various values of W in equations [78] or [81] for a given value of E (and A). Using the energy distribution function given by equation [72], the total number of particles penetrating the barrier is

$$\frac{N}{N_o} = \frac{1}{kT} \int_0^\infty G_W e^{-W/kT} \, dW \qquad [82]$$

and the integral may be evaluated graphically as the area under the curve for $G_W e^{-W/kT}$ as a function of W. When this is done (15), a significant difference is obtained for N/N_o calculated from equations [73] and [82]. The actual energy of activation E is found to be appreciably higher than the value that would be derived by calculating rates of permeation by equations [81] and [82] as a function of temperature.

(ii) The Parabolic Barrier (16)

Bell extended the above treatment by using an approximation method to solve equation [74] in order to investigate the effect of varying E, $\underline{l}$, and a_c. This is done

first by replacing the Eckart function, equation [75], by a discontinuous segment of a parabolic curve. Secondly, instead of using the function for an exact solution of the Schrödinger equation, G is put equal to unity for $W > E$ and the permeability is given by the approximate expression

$$G' = \exp - \frac{4\pi\sqrt{2m_e}}{h} \int_{x_1}^{x_2} [V(x) - W]^{1/2}\, dx \qquad [83]$$

when $W < E$; x_1 and x_2 are the distance coordinates of the two points for which $V(x) = 0$. If the width of the base of the parabolic barrier is 2 l, the equation to the function is

$$E - V(x) = \frac{Ex^2}{l^2} \qquad [84]$$

and the solution to equation [83] is

$$G' = - \frac{2\pi^2 l \sqrt{2m_e}\,(E - W)}{h\sqrt{E}} \qquad [85]$$

Bell found no significant differences in G values from equations [81] and [85]. A factor q is defined as that quantity which when multiplied by H_o (cf. equation [72]) gives the number of particles passing over the barrier in unit time. The classical expression for q (neglecting zero-point energies) is, (cf. equation [72]),

$$q_{class} = \frac{1}{kT} \int_0^\infty e^{-W/kT}\, dW = e^{-E/kT} \qquad [86]$$

The corresponding quantum mechanical expression is

$$q = \frac{1}{kT} \int_0^\infty G_W e^{-W/kT} \, dW \qquad [87]$$

or, using the approximate treatment,

$$q = e^{-E/kT} + \frac{1}{kT} \int_0^E G' e^{-W/kT} \, dW \qquad [88]$$

From equations [85] and [88]

$$q = \frac{1}{\sigma - \gamma} (\sigma e^{-\gamma} - \gamma e^{-\sigma}) \qquad [89]$$

where

$$\gamma = \frac{E}{kT} ; \quad \sigma = \frac{2\pi^2 l \sqrt{2 m_c E}}{h} \qquad [90]$$

From the definition of q, another term, the apparent energy of activation E^*, can be defined as

$$\frac{E^*}{2.3 R} = - \frac{d \log q}{d(1/T)} \qquad [91]$$

and from equation [89]

$$\frac{E^*}{E} = - \frac{d \log q}{d\gamma} = \frac{\sigma}{\sigma - \gamma} \frac{(\sigma - \gamma - 1)e^{-\gamma} + e^{-\sigma}}{\sigma e^{-\gamma} - \gamma e^{-\sigma}} \qquad [92]$$

Limiting cases in equation [92] can arise. Thus for $e^{-\gamma} \gg e^{-\sigma}$ (e.g. at low temperatures)

$$q = \frac{\sigma e^{-\gamma}}{\sigma - \gamma} ; \quad \frac{E^*}{E} = 1 - \frac{1}{\sigma - \gamma} \qquad [93]$$

For $e^{-\gamma} \ll e^{-\sigma}$

$$q = \frac{\gamma e^{-\sigma}}{\gamma - \sigma} ; \quad \frac{E^*}{E} = \frac{\sigma}{\gamma(\gamma - \sigma)} \qquad [94]$$

and for $\gamma = \sigma$,

$$q = (1+\sigma)\, e^{-\sigma} \; ; \; \frac{E^*}{E} = \frac{\sigma}{2(\sigma+1)} \qquad [95]$$

Taking arbitrary values for $\underline{l}$ and E, and taking m_o as the mass of the proton, a plot of log q vs 1/T can be made and shows significant differences from a corresponding plot of log $q_{class.}$ versus 1/T. In addition, q is found to deviate from linearity starting at about -20^oC and approaches a constant value at about -50 to -70^oC (16), giving a low apparent energy of activation E^*.

(iii) Corrections for Parabolic Barriers (19)

Recently Bell has discussed the possibility that proton tunneling may occur at the top of the potential barrier (18,19). The theory used is based on the general treatment of Wigner (78). The treatment given in section (ii) above is valid for $W < E$ and is satisfactory when the degree of tunneling is large (cf. equations [87] - [89]). However, for a small degree of tunneling i.e. when energies are in the neighborhood of $W = E$, equation [85] is a bad approximation. The treatment (19) discussed here is therefore a refinement of the earlier ones (15,16,76).

The curvature at the top of the barrier is defined in terms of the frequency $\nu_L^{\neq}$ by

$$\nu_L^{\neq} = E^{1/2}/\pi\, l(2m_o)^{1/2} \qquad [96]$$

The permeability is given (19) by

$$G_W = \left\{1 + \exp\left[2\pi(E - W)/h\nu_L^{\neq}\right]\right\}^{-1} \qquad [97]$$

Using the simple Boltzmann distribution for the energy, the tunnel effect correction to the rate of reaction is

$$q = \exp\frac{E}{RT} \int_0^{\infty} G_W \frac{1}{RT} \exp(-W/kT).\, dW \qquad [98]$$

Provided that

$$\exp\left(\frac{E}{RT} - \frac{2\pi E.}{h\nu_L^{\neq}}\right) \ll 1,$$

the evaluation of equation [98] using [97] gives

$$q = \tfrac{1}{2}\, u_L^{\neq} / \sinh \tfrac{1}{2}\, u_L^{\neq} \qquad [99]$$

Equation [99] closely resembles the quantum correction for a real harmonic frequency in the transition state (cf. equation [45]). It can be derived from the relation $q = \frac{1}{2} u$ by replacing ν by $\nu_L^{\neq}$. Expanding equation [99] in powers of $u_L^{\neq}$ gives

$$q = 1 + \frac{(u_L^{\neq})^2}{24} + \frac{7(u_L^{\neq})^4}{5760} + \ldots\ldots \quad (u_L^{\neq} < 2\pi) \qquad [100]$$

$$\ln q = \frac{u_L^{\neq}}{24} + \frac{(u_L^{\neq})^2}{2880} + \ldots\ldots\ldots \quad (u_L^{\neq} < 2\pi) \qquad [101]$$

The first term of the expansion is identical with Wigner's result (78) based on a small tunnel effect. Equation [99] leads to expressions for the apparent activation energy $E^{\neq}$ and the

apparent frequency factor A^* which are defined in terms of the observed rate constant $\underline{k}$ by

$$E^* = RT^2 \, d \ln \underline{k}/dT; \quad \ln A^* = \ln \underline{k} + E^*/RT \qquad [102]$$

In terms of the corresponding classical quantities E and A, from equations [99] and [102] we have

$$E^* - E = RT \left[\tfrac{1}{2} u_L^{\neq} \cot \tfrac{1}{2} u_L^{\neq} - 1\right] \qquad [103]$$

$$\frac{A^*}{A} = \frac{\frac{1}{2} u_L^{\neq}}{\sin \frac{1}{2} u_L^{\neq}} \exp \left[\tfrac{1}{2} u_L^{\neq} \cot \tfrac{1}{2} u_L^{\neq} - 1\right] \qquad [104]$$

Equations [99], [103] and [104] lead to the following predictions (18)

(a) E^* should decrease with decreasing temperature approaching zero.

(b) $E^* < E$. Owing to the uncertainties involved in constructing potential energy surfaces, this prediction is not, in practice, demonstrable.

(c) A^* should be less than A and temperature dependent. However, knowledge of A also requires a knowledge of the potential energy surface and a test of whether $A^*/A < 1$ is therefore impractical.

Factors (b) - (c), although theoretically correct, are in practice not usually accessible with sufficient accuracy. Factor (a) can provide evidence for the role of significant tunneling if low enough temperatures can be obtained (18).

A further method of detecting tunneling is based on the H/D isotope effect. This is evident from equation [96] where the effective mass of the particle enters into the expression for $u_L^{\neq}$. Hence for the H/D isotope effect, the following predictions can be made (18):

1) $E_D^* - E_H^* > E_D - E_H$. This criterion again demands a detailed knowledge of the potential energy surface. However, if tunneling were appreciable, / the above inequality would be a useful criterion.

2) $A_H^* < A_D^*$. It was seen previously that the values of A_H^*/A_D^* predicted from classical theory are from 0.5 to 1.0. The value of 0.5 corresponds to the special case where bending frequencies disappear in the activated state. This is not very likely for proton transfers but is a possibility for hydrogen atom abstraction reactions (79). Hence this is probably the most useful criterion for detection of tunneling.

Although the above treatment of tunneling corrections to the classical rate is that of Bell (15-19), there are other approaches reported in the literature which treat this problem for specific reactions (80,81,82,83). In these treatments , special cases for the Eckart and parabolic potential functions have been considered.

4. Classical Electrochemical Isotope Effects

A. Definitions

(1) The Separation Factor, S

The separation factor for electrode reactions in an H/D or an H/T isotopically mixed electrolyte is defined as

$$S_D = \left(\frac{c_D}{c_H}\right)_{soln} \left(\frac{c_H}{c_D}\right)_{gas}; \quad S_T = \left(\frac{c_T}{c_H}\right)_{soln} \left(\frac{c_H}{c_T}\right)_{gas} \qquad [105]$$

where the c's are the atom concentrations of the indicated species (hydrogen, deuterium and tritium). Since the relative rate of production of H_{gas} to that of D_{gas} is dependent upon the relative values of the cathodic currents i_H and i_D, equation [105] can be rewritten in terms of the current densities as

$$S_D = \left(\frac{c_D}{c_H}\right)_{soln}^{n} \left(\frac{i_H}{i_D}\right); \quad S_T = \left(\frac{c_T}{c_D}\right)_{soln}^{n} \left(\frac{i_H}{i_T}\right) \qquad [106]$$

where n is the number of hydrogen nuclei converted into constituents of the hydrogen molecule from its ions for every act of the rate-determining step. Hence for the discharge mechanism [1], n = 1, and for the recombination mechanism [2] or [3], n = 2. These assignments of values to n apply to dilute solutions of D or T in the H-containing solvent from which the principle products of electrolysis are H_2 and HD or H_2 and HT and not the D_2 or T_2 entities. Equation [105] defines the experimentally determinable quantity and equation [106], which

is applicable strictly to solutions dilute in D or T, can be put in terms of absolute rate theory which allows S to be calculated from first principles.

(ii) The Ratio of Exchange Current Densities, R

The ratio of exchange current densities is defined as the ratio of rates of production of H_2 to D_2, respectively, from pure H and D - containing solutions, measured at the corresponding reversible potentials ϕ_r. The current passing at the reversible potential, i_o, is measured by extrapolation of the linear portion of the Tafel curve to $\eta = 0$. Hence for H_2 evolution from pure H_2O solutions and D_2 evolution from pure D_2O solutions,

$$R = \frac{i_{o,H_2}}{i_{o,D_2}} \qquad [107]$$

As mentioned above, the currents i or i_o can be replaced by their rates calculated from absolute rate theory.

B. Classical Reaction Rates

(i) The Discharge Mechanism

In this section, the derivation of absolute reaction rate equations (51) is presented for reactions [1], [2] and [3]. The rate of discharge from acid solutions can be formulated in terms of absolute rate theory (51) as

$$H_3O^+_{(s)} + H + e_M \rightleftharpoons X^{\neq}_H \longrightarrow M\text{-}H_{(ads)} + H_2O \qquad [108]$$

Similarly for discharge from a water molecule

$$H_2O_{(s)} + M + e_M \rightleftharpoons X_H^{\neq} \longrightarrow M\text{-}H_{(ads)} + OH^- \qquad [109]$$

The subscript s refers to reactant species adsorbed at the surface and e_M refers to the electron in the metal M; $X^{\neq}$ is the activated complex which is regarded in the theory (51) as being in equilibrium with the initial state reactants. The condition for equilibrium between initial and activated states is

$$\mu_M + \bar{\mu}_{H_3O^+} + \bar{\mu}_{e_M} = \bar{\mu}^{\neq} \qquad [110]$$

where μ is the chemical potential and $\bar{\mu}$ terms are the electrochemical potentials (28) of the indicated species defined in the general case by

$$\bar{\mu}_i = \mu_i + zF\phi \qquad [111]$$

where ϕ is the inner potential of the phase under consideration (28,31), z is the charge ($\pm$) and F is the Faraday. From elementary statistical mechanics it can be shown (109) that the chemical potential can be written in terms of the molecular partition function (q_i) per molecule / of substance i, i.e.,

$$\mu_i = -RT \ln q_i \qquad [112]$$

where

$$q_i = f_i/n_i \qquad [113]$$

and f_i is the molecular partition function of substance i, and n_i the number of molecules of species i. From equations [111] and [112] we have

$$\bar{\mu}_i = - RT \ln q_i + z\mathcal{F}\phi_i \qquad [114]$$

In equation [110], the activated complex has been treated as a charged species. This assumption is made for the following reason: the activated complex is regarded as a state of the H_3O^+ molecule in which one proton has been stretched towards the metal surface and yet <u>retains</u> its full charge. The electron, in terms of this model, is considered to still be in the metal electrode. Once the activated complex is formed by some change of the molecular configuration of the reactant ion or molecule, electron tunneling can then proceed to produce the final state species $M\text{-}H_{ads}$. This is consistent with the assumption that the electrical energy of the activated state for a one-electron transfer step differs from that of the initial state by the quantity $\beta\mathcal{F}\phi$ where β = <u>ca.</u> 0.5. If charge were lost in the activation step, the unreacting O-H bonds would suffer an increase in frequency (and force constants) and the significance of $\beta \doteq 0.5$ would be unclear. Hence, in the activated state, the complex is considered to be at some potential $\phi^{\ddagger}$ (see Figure 14) and the electron, which is still considered to be in the metal is at some potential ϕ_M. In the initial state, the electron is in the metal also at some potential

Figure 14

Model for the discharge of a proton at a metal cathode.

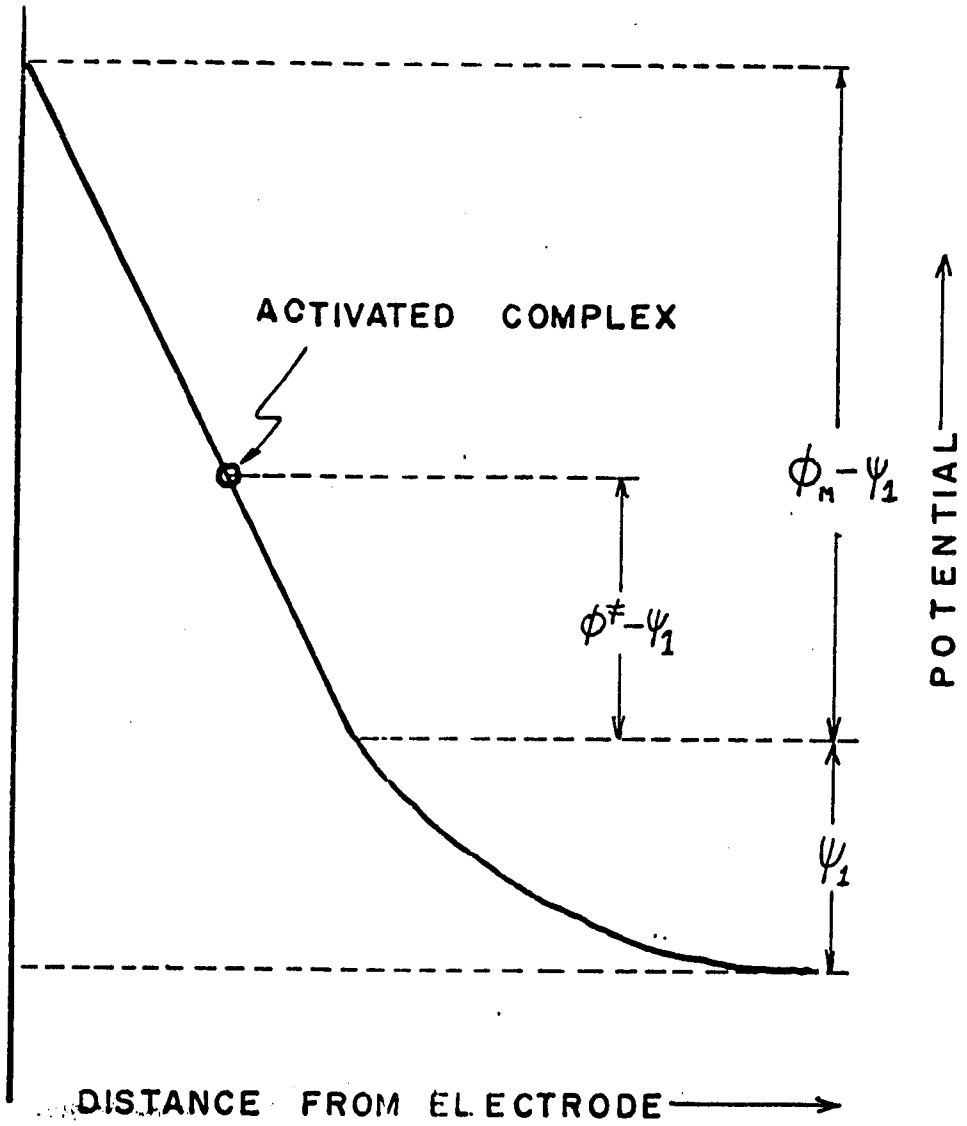
ACTIVATED COMPLEX
$\phi_M - \psi_1$
$\phi^{\neq} - \psi_1$
ψ_1
POTENTIAL
DISTANCE FROM ELECTRODE

ϕ_M and the H_3O^+ ion is adsorbed in the outer Helmholtz plane at some potential ψ_1 (see Figure 14). From equations [110] [112] and [114], it then follows that

$$q_{H_3O^+} q_M q_{e_M} e^{(\phi_M - \psi_1)F/RT} = q_H^{\neq} e^{(\phi_M - \phi^{\neq})F/RT}$$

or

$$q_{H_3O^+} q_M q_{e_M} = q_H^{\neq} e^{-(\phi^{\neq} - \psi_1)F/RT} \qquad [115]$$

From Figure 14, it is seen that the potential differences $\phi^{\neq} - \psi_1$ is some fraction of the total potential difference $\phi_M - \psi_1$. Calling this fraction β, it follows that

$$\phi^{\neq} - \psi_1 = \beta (\phi_M - \psi_1)$$

which defines β; then substituting this result into equation [115] yields

$$q_{H_3O^+} q_M q_{e_M} = q_H^{\neq} e^{-\beta(\phi_M - \psi_1)F/RT} \qquad [116]$$

Neglecting the term q_e (i.e. this term is taken as unity), equations [113] and [116] give upon rearrangement

$$n_X^{\neq} = n_M n_{H_3O^+(s)} \frac{f_H^{\neq}}{f_M f_{H_3O^+(s)}} \exp -\beta(\phi_M - \psi_1)F/RT$$

Dividing each term by the surface area to obtain the relation in terms of concentrations

$$[X_H^{\neq}] = [M][H_3O^+]_{(s)} \frac{f_H^{\neq}}{f_M Q'_{H_3O^+}} \exp -\beta(\phi_M - \psi_1)F/RT \qquad [117]$$

where the bracketed terms are now concentrations and Q' is the molecular partition function per unit area (Q is that per unit volume). The molecular partition function $f^{\neq}$ for the activated complex is unique in absolute rate theory in that one of its frequencies is zero or imaginary. This is the frequency $\nu_L^{\neq}$ which corresponds to decomposition and absolute rate theory (51) requires that

$$\lim_{\nu_L^{\neq} \to 0} f^{\neq} = \frac{kT}{h\nu_L^{\neq}} f_{\neq} \qquad [118]$$

Combining equations [117] and [118] and noting that the product $[X^{\neq}]\nu_L^{\neq}$ is the rate of reaction, we have

$$\text{RATE} = \frac{kT}{h}[M][H_3O^+]_{(s)} \frac{f_{\neq H}}{f_M Q'_{H_3O^+}} \exp -\beta(\phi_M - \psi_1)F/RT$$

In terms of a current density i (amperes $cm.^{-2}$), which is defined as the number of coulombs passing per unit time per unit area ($i = zF(\text{RATE})$), the above equation becomes

$$i = \tau z F \frac{kT}{h} [M][H_3O^+]_{(s)} \frac{f^{\neq}_{e,H}}{f^{0}_{H_3O^+}} \exp -\beta(\phi_M - \psi_1)F/RT \qquad [119]$$

where the transmission coefficient τ has been included in equation [119]. It is usually considered that all pre-rate determining steps may be assumed to be in a state of quasi-equilibrium. Hence for the equilibrium of hydronium ions between the bulk b and an adsorbed state in the double-layer

$$H_3O^+_{(s)} \rightleftharpoons H_3O^+_{(b)}$$

the condition for equilibrium is (see Chapter II, equation 18)

$$q_{H_3O^+(s)} \exp \psi_1 F/RT = q_{H_3O^+(b)}$$

Using equation [113], the above relation becomes

$$[H_3O^+]_{(s)} = [H_3O^+]_{(b)} \frac{q'_{H_3O^+}}{q^{0}_{H_3O^+}} \exp -\psi_1 F/RT \qquad [120]$$

Hence, from equations [119] and [120], the final form of the rate equation for a rate-determining proton discharge step is

$$i_H = \tau z F \frac{kT}{h} [M][H_3O^+]_b \frac{f^{\neq}_{e,H}}{f^{0}_{H_3O^+}} \exp -\psi_1 F/RT . \exp -\beta(\phi_M - \psi_1)F/RT \qquad [121]$$

The rate of reaction i_o corresponding to the special case of an electrode reaction at equilibrium and referred to as the

exchange current density, may then be defined as

$$i_o = \gamma z F \frac{kT}{h}[M][H_3O^+]_b \frac{f^{\neq}_{,H}}{f^{Q}_{M\,H_3O^+}} \exp-(1-\beta)\psi_1 F/RT \exp-\beta\phi_r F/RT \qquad [122]$$

In the course of the present work, the discharge reaction was studied in acidified isotopic solutions of H_2O and D_2O and their mixtures; it follows that discharge can occur from any of the lyonium species H_3O^+, H_2DO^+, HD_2O^+ and D_3O^+. For D discharge from H_2DO^+ we have, by analogy with [121],

$$i_{D(H)} = \gamma z F \frac{kT}{h}[M][H_2DO^+]_b \cdot \frac{f^{\neq}_{D(H)}}{f^{Q}_{M\,H_2DO^+}} \exp-(1-\beta)\psi_1 F/RT \exp-\beta\phi_M F/RT \qquad [123]$$

For discharge from the lyonium ion species D_3O^+ in pure D_2O/D^+ solution,

$$i_D = \gamma z F \frac{kT}{h}[M][D_3O^+]_b \frac{f^{\neq}_{,D}}{f^{Q}_{M\,D_3O^+}} \exp-(1-\beta)\psi_{1,D} F/RT \exp-\beta\phi_{M,D} F/RT \qquad [124]$$

For solutions dilute in the tritium isotope so that only the species H_2TO^+ need be considered, the rate of HT evolution in terms of a rate-determining discharge step is

$$i_{T(H)} = \gamma z F \frac{kT}{h}[M][H_2TO^+]_b \frac{f^{\neq}_{T(H)}}{f^{Q}_{M\,H_2TO^+}} \exp-(1-\beta)\psi_1 F/RT \cdot \exp-\beta\phi_M F/RT \qquad [125]$$

For discharge from a water molecule, i.e. under alkaline solution conditions, the above principles lead to similar results. For discharge from H_2O, HDO and D_2O, respectively, we have

$$i_H = \tau zF \frac{kT}{h}[M][H_2O]_{(b)} \frac{f^{\neq}_{,H}}{f_M{}^{Q}_{H_2O}} \exp \beta\psi_1 F/RT \exp -\beta\phi_M F/RT \qquad [126]$$

$$i_{D(H)} = \tau zF \frac{kT}{h}[M][HDO]_b \frac{f^{\neq}_{D(H)}}{f_M{}^{Q}_{HDO}} \exp \beta\psi_1 F/RT \exp -\beta\phi_M F/RT \qquad [127]$$

and

$$i_D = \tau zF \frac{kT}{h}[M][D_2O]_b \frac{f^{\neq}_{,D}}{f_M{}^{Q}_{D_2O}} \exp \beta\psi_{1,D} F/RT \exp -\beta\phi_{M,D} F/RT \qquad [128]$$

(11) The Atom + Ion Recombination Mechanism

In terms of absolute rate theory, the atom + ion recombination mechanism is

$$MH_{(ads)} + H_3O^+_{(s)} + e_M \rightleftharpoons X^{\neq}_H \longrightarrow M + H_2O + H_2$$

and the rate of reaction is given by

$$i_H = \tau zF \frac{kT}{h}[MH][H_3O^+]_b \frac{f^{\neq}_{,H}}{f_{MH}{}^{Q}_{H_3O^+}} \exp -(1-\beta)\psi_1 F/RT \cdot \exp -\beta\phi_M F/RT \qquad [129]$$

Since the primary reaction is now a pre-rate determining step, it is assumed to be in quasi-equilibrium according to

$$H_3O^+_{(s)} + M + e_M \rightleftharpoons MH + H_2O_{(s)} \qquad [130]$$

in acid solutions and

$$H_2O_{(s)} + M + e_M \rightleftharpoons MH + OH^-_{(s)} \qquad [130a]$$

in neutral or alkaline solutions. For the equilibrium in [130]

it follows that

$$[MH] = \frac{[M][H_3O^+]_b}{[H_2O]_b} \cdot \frac{f_{H_2O}}{f_{H_3O^+}{}^{Q'}{}_M} \exp - \phi_M F/RT \qquad [131]$$

and for the equilibrium in [130a]

$$[MH] = \frac{[M][H_2O]_b}{[OH^-]_b} \frac{f_{OH^-}}{f_{H_2O}{}^{Q'}{}_M} \exp - \phi_M F/RT \qquad [131a]$$

Substituting for [MH] in equation [129], the following relations are obtained for acid or neutral solutions, respectively,

$$i_H = \tau z F \frac{kT}{h} \frac{[H_3O^+]_b^2}{[H_2O]_b} \frac{f_{H_2O} f_{\neq,H}}{f_{H_3O^+}{}^{Q}{}_{H_3O^+} f_M} \exp - (1-\beta)\psi_1 F/RT \cdot$$

$$\exp - (1+\beta)\phi_M F/RT \qquad [132]$$

$$i_H = \tau z F \frac{kT}{h} \frac{[H_2O]_b^2}{[OH^-]_b} \frac{f_{OH^-} f_{\neq,H}}{f_{H_2O}{}^{Q}{}_{H_2O} f_M} \exp \beta \psi_1 F/RT \cdot$$

$$\exp - (1+\beta)\phi_M F/RT \qquad [133]$$

In a mixed H/D solution which is sufficiently low in D-content that the only significant D-containing species is H_2DO^+, production of $HD_{(gas)}$ can occur by either of the two processes

$$MH + H_2DO^+_{(s)} + e_M \rightleftharpoons X^{\neq}_{HD} \longrightarrow M + H_2O + HD$$

or

$$MD + H_3O^+_{(s)} + e_M \rightleftharpoons X^{\neq}_{DH} \longrightarrow M + H_2O + DH$$

where $X^{\neq}_{HD}$ is to be distinguished from $X^{\neq}_{DH}$ since either the H or the D species is attached to the metal. The surface coverage [MH] is determined by the discharge equilibrium [130] whereas the surface coverage [MD] is determined by the equilibrium

$$M + H_2DO^+ + e_M \rightleftharpoons MD + H_2O \qquad [134]$$

in acid solutions or

$$M + HDO + e_M \rightleftharpoons MD + OH^- \qquad [134a]$$

in neutral or alkaline solutions. The surface concentration [MD] can therefore be obtained from [134] or [134a], respectively, as

$$[MD] = \frac{[M][H_2DO^+]_b}{[H_2O]_b} \frac{f_{H_2O}}{f_{H_2DO^+} Q'_M} \exp -\phi_M F/RT \qquad [135]$$

and

$$[MD] = \frac{[M][HDO]_b}{[OH^-]_b} \frac{f_{OH^-}}{f_{HDO} Q'_M} \exp -\phi_M F/RT \qquad [135a]$$

The rate of atom + ion recombination in acid solutions dilute in D is therefore

$$i_{HD} = \tau z F \frac{kT}{h} \frac{[H_3O^+]_b [H_2DO^+]_b [M]}{[H_2O]_b} \frac{f_{H_2O}\, f^{\neq}_{,HD}}{f_{H\,DO^+} Q_{H_3O^+} f_M} \exp -(1-\beta)\psi_1 F/RT$$

$$\exp -(1+\beta)\phi_M F/RT \qquad [136]$$

$$i_{DH} = \gamma zF \frac{kT}{h} \frac{[H_3O^+]_b[H_2DO^+]_b[M]}{[H_2O]_b} \cdot \frac{f_{H_2O} f_{\neq,DH}}{f_{H_2DO^+} Q_{H_3O^+} f_M} \exp - (1-\beta)\psi_1 F/RT.$$

$$\exp -(1+\beta)\, \phi_M F/RT \qquad [137]$$

For atom + ion recombination from neutral or alkaline solutions, the rate is

$$i = \gamma zF \frac{kT}{h} \frac{[H_2O]_b[HDO]_b[M]}{[OH^-]_b} \frac{f_{OH^-} f_{\neq}}{f_{HDO} Q_{H_2O} f_M} \exp \beta \psi_1 F/RT.$$

$$\exp -(1+\beta)\phi_M F/RT \qquad [138]$$

where $f_{\neq} = f_{\neq,HD}$ if $i = i_{HD}$ or $f_{\neq,DH}$ if $i = i_{DH}$. Similarly in pure D_2O, the rate of atom + ion recombination is

$$i_D = \gamma zF \frac{kT}{h} \frac{[D_3O^+]_b^2 [M]}{[D_2O]_b} \frac{f_{D_2O} f_{\neq D}}{f_{D_3O^+} Q_{D_3O^+} f_M} \exp -(1-\beta)\psi_{1,D} F/RT \cdot$$

$$\exp -(1+\beta)\phi_{M,D} F/RT \qquad [139]$$

in acid-D solutions and

$$i_D = \gamma zF \frac{kT}{h} \frac{[D_2O]_b^2[M]}{[OD^-]_b} \frac{f_{OD^-} f_{\neq,D}}{f_{D_2O} Q_{D_2O} f_M} \exp \beta\psi_{1,D} F/RT. \exp -(1+\beta)\phi_{M,D} F/RT \qquad [140]$$

in neutral or alkaline solutions.

(iii) <u>The Atom - Atom Recombination Mechanism</u>

There are three possible types of atom-atom recombinations

corresponding to

$$\begin{aligned} MH + MH &\rightleftharpoons X_H^{\neq} \longrightarrow H_2 \\ MH + MD &\rightleftharpoons X_{HD}^{\neq} \longrightarrow HD \\ MD + MD &\rightleftharpoons X_D^{\neq} \longrightarrow D_2 \end{aligned} \qquad [141]$$

By analogy with the above treatment, it follows that in acid solutions, the corresponding rates are

$$i_H = \tau zF \frac{kT}{h} \frac{[H_3O^+]_b^2[M]^2}{[H_2O]_b^2} \frac{f_{H_2O}^2}{f_{H_3O^+}^2} \frac{f_{\neq,H}}{f_M^2} \exp -2\phi_M F/RT \qquad [142]$$

$$i_{HD} = \tau zF \frac{[H_3O^+]_b[H_2DO^+]_b[M]^2}{[H_2O]_b^2} \frac{f_{H_2O}^2 f_{\neq,HD}}{f_{H_3O^+} f_{H_2DO^+} f_M^2} \exp -2\phi_M F/RT \qquad [143]$$

$$i_D = \tau zF \frac{kT}{h} \frac{[D_3O^+]_b[M]^2}{[D_2O]_b^2} \frac{f_{D_2O}^2 f_{\neq,D}}{f_{D_3O^+}^2 f_M^2} \exp - 2\phi_{M,D} F/RT \qquad [144]$$

For recombination originating from discharge in neutral or alkaline solutions, the corresponding rate equations are

$$i_H = \tau zF \frac{kT}{h} \frac{[H_2O]_b^2[M]^2}{[OH^-]_b^2} \frac{f_{OH^-}^2 f_{\neq,H}}{f_{H_2O}^2 f_M^2} \exp -2\phi_M F/RT \qquad [145]$$

$$i_{HD} = \tau zF \frac{kT}{h} \frac{[H_2O]_b[HDO]_b[M]^2}{[OH^-]_b^2} \frac{f_{OH^-}^2 f_{\neq,HD}}{f_{H_2O} f_{HDO} f_M^2} \cdot \exp -2\phi_M F/RT \qquad [146]$$

$$i_D = \gamma z F \frac{kT}{h} \frac{[D_2O]_b^2[M]^2}{[OD^-]_b^2} \frac{f_{OD}^2 - f_{\neq,D}}{f_{D_2O}^2 f_M^2} \exp -2\phi_{M,D}F/RT \qquad [147]$$

C. S and R in Terms of Partition Functions

(i) The Discharge Mechanism

In the following treatment for the calculation of S for H/D or H/T solutions, it is assumed that the only significant D- or T-containing species are, respectively, H_2DO^+, H_2TO^+ in acid solutions and HDO and HTO in neutral or alkaline solutions. This assumption will be shown in Chapter VI to be valid under the present experimental conditions.

(a) The Separation Factors S_D and S_T

The separation factor S_D for acid solutions is obtained by combination of equations [106], [121] and [123], i.e.*

$$S_D = \left(\frac{c_D}{c_H}\right)_{soln} \frac{[H_3O^+]}{[H_2DO^+]} \frac{f_{H_2DO^+}}{f_{H_3O^+}} \frac{f_{\neq,H}}{f_{\neq,HD}} \qquad [148]$$

where n in equation [106] is unity. The ratios involving [M], ψ_1, ϕ_M, and f_M all cancel since these terms apply to the same electrode. Similarly S_D in neutral or alkaline solutions is given by

$$S_D = \left(\frac{c_D}{c_H}\right)_{soln} \frac{[H_2O]}{[HDO]} \frac{f_{HDO}}{f_{H_2O}} \frac{f_{\neq,H}}{f_{\neq,HD}} \qquad [149]$$

* The concentration terms all refer to bulk species. The subscript b will hence be omitted in the following discussion.

(cf. equations [106], [126], [127]). The separation factor S_T will be given by equations similar to [148] and [149] where D is replaced by T, i.e.

$$S_T = \left(\frac{c_T}{c_H}\right)_{soln} \frac{[H_3O^+]}{[H_2TO^+]} \frac{f_{H_2TO^+}}{f_{H_3O^+}} \frac{f_{\neq,H}}{f_{\neq,T}} \qquad [150]$$

and

$$S_T = \left(\frac{c_T}{c_H}\right)_{soln} \frac{[H_2O]}{[HTO]} \frac{f_{HTO}}{f_{H_2O}} \frac{f_{\neq,H}}{f_{\neq,T}} \qquad [151]$$

(b) The Ratio of Exchange Current Densities

For acid solutions, from equations [107,] [121] and [124]

$$R = \frac{[H_3O^+][M]_H}{[D_3O^+][M]_D} \frac{f_{D_3O^+} f_M}{f_{H_3O^+} f_M} \frac{f'_{\neq,H}}{f'_{\neq,D}} \exp(1-\beta)(\psi_{1,D}-\psi_{1,H})F/RT \cdot \exp \beta(\phi_{r,D}-\phi_{r,H})F/RT$$

The partition function ratio for the activated complex, $f'_{\neq,H}/f'_{\neq,D}$, now includes contributions from two unreacting O-H bonds and two unreacting O-D bonds. The term $f_{\neq,H}/f_{\neq,D}$ in equation [148] for the separation factor is not complicated by this problem since the unreacting groups are O-H in both the H and D complexes and contributions to the $f_{\neq}$ ratio therefore cancel. The above equation can be simplified as follows: first $[H_3O^+]/[D_3O^+]$ is

an experimental quantity which can be adjusted to unity or otherwise known exactly. The terms in [M] can be written in terms of coverage θ as $1-\theta_H/1-\theta_D$ and for rate-controlling discharge θ is small (e.g. $\theta_H \ll 0.05$ for mercury (29)) and $1-\theta_H/1-\theta_D = 1$. The terms in f_M obviously cancel because they refer to the same metal surface. ψ_1, the potential at the outer Helmholtz layer is a function of charge and $\psi_{1,D} - \psi_{1,H}$ can be safely taken as zero for a given electrode potential ϕ_M. For $[H_3O^+] = [D_3O^+]$, the term $\phi_{r,D} - \phi_{r,H}$ is the absolute difference in reversible potentials between a hydrogen electrode in pure H-containing solutions and a deuterium electrode in pure D-containing solutions. Hence the working equation for R is

$$R = \frac{f_{D_3O^+}}{f_{H_3O^+}} \frac{f'_{\neq,H}}{f'_{\neq,D}} \exp \beta(\phi_{r,D} - \phi_{r,H})F/RT \qquad [152]$$

Equation [152] neglects any isotopic dependence there might be in β. As will be seen later, this is supported experimentally. Similarly, the ratio of exchange current densities for discharge from a water molecule is given by

$$R = \frac{f_{D_2O}}{f_{H_2O}} \frac{f'_{\neq,H}}{f'_{\neq,D}} \exp (\phi_{r,D} - \phi_{r,H})F/RT \qquad [152a]$$

The terms in $\phi_{r,D} - \phi_{r,H}$ in equations [152] and [152a] will be

different in acid and alkaline solutions since the ionic products of H_2O and D_2O are not identical as discussed in Chapter VI.

(ii) The Atom + Ion Mechanism

(a) The Separation Factors

For the atom + ion recombination mechanism, there are two ways in which a deuterium atom can be evolved as HD. The total production of HD is therefore given by the sum of the currents i_{HD} and i_{DH} in equations [136] and [137], respectively. From equation [106], taking n = 2, the separation factor, S_D, is given by

$$S_D = \left(\frac{c_D}{c_H}\right)_{soln} \frac{2i_{H_2}}{i_{HD} + i_{DH}} \qquad [153]$$

Substituting for i from equations [132], [136] and [137] yields

$$S_D = \left(\frac{c_D}{c_H}\right)_{soln} 2 \frac{[H_3O^+]}{[H_2DO^+]} \frac{f_{H_2DO^+}}{f_{H_3O^+}} \frac{f_{\neq,H_2}}{f_{\neq,HD} + f_{\neq,DH}} \qquad [154]$$

or

$$S_D = \left(\frac{c_D}{c_H}\right)_{soln} \frac{[H_3O^+]}{[H_2DO^+]} \frac{f_{H_2DO^+}}{f_{H_3O^+}} \left[\frac{f_{\neq,HD}}{f_{\neq,H_2}} + \frac{f_{\neq,DH}}{f_{\neq,H_2}}\right]^{-1} \qquad [154a]$$

Similarly, for the case of discharge from a water molecule (e.g. in neutral or alkaline solution), the separation factor S_D

is obtained from equations [153], [133], and [138] as

$$S_D = \left(\frac{c_D}{c_H}\right)_{soln} 2\frac{[H_2O]}{[HDO]} \frac{f_{HDO}}{f_{H_2O}} \left[\frac{f_{\neq,HDO}}{f_{H_2O}} + \frac{f_{\neq,DH}}{f_{\neq,H_2}}\right]^{-1} \qquad [155]$$

By an identical procedure, the relations for S_T in acid and alkaline solutions are, respectively,

$$S_T = \left(\frac{c_T}{c_H}\right)_{soln} 2\frac{[H_3O^+]}{[H_2TO^+]} \left[\frac{f_{\neq,HT}}{f_{\neq,H_2}} + \frac{f_{\neq,TH}}{f_{\neq,H_2}}\right]^{-1} \qquad [156]$$

$$S_T = \left(\frac{c_T}{c_H}\right)_{soln} 2\frac{[H_2O]}{[HTO]} \frac{f_{HTO}}{f_{H_2O}} \left[\frac{f_{\neq,HT}}{f_{\neq,H_2}} + \frac{f_{\neq,TH}}{f_{\neq,H_2}}\right]^{-1} \qquad [157]$$

(b) The Ratio of Exchange Current Densities, R

The ratio of exchange current densities for the atom + ion mechanism in acid solution is obtained from equations [132] and [140], i.e.

$$R = \frac{(1-\theta_H)}{(1-\theta_D)} \left(\frac{f_{D_3O^+}}{f_{H_3O^+}}\right)^2 \frac{f_{H_2O}}{f_{D_2O}} \frac{f'_{\neq,H}}{f'_{\neq,D}} \cdot \exp\,(1+\beta)(\phi_{r,D}-\phi_{r,H})F/RT \qquad [158]$$

Similarly, in neutral or alkaline solution, from equations [133] and [140], R is given by

$$R = \frac{(1-\theta_H)}{(1-\theta_D)} \left(\frac{f_{D_2O}}{f_{H_2O}}\right)^2 \frac{f_{OH^-}}{f_{OD^-}} \frac{f'_{\neq,H}}{f'_{\neq,D}} \exp\,(1+\beta)(\phi_{r,D}-\phi_{r,H})F/RT \qquad [159]$$

(iii) The Atom + Atom Mechanism

(a) Separation Factors

In acid solution, S_D is obtained from equations [106] (taking n = 2), [142] and [143], i.e.

$$S_D = \left(\frac{c_D}{c_H}\right)_{soln} 2 \frac{[H_3O^+]}{[H_2DO^+]} \frac{f_{H_2DO^+}}{f_{H_3O^+}} \frac{f_{\neq,H}}{f_{\neq,HD}} \qquad [160]$$

From equations [106], [145] and [146], S_D in neutral or alkaline solutions is given by

$$S_D = \left(\frac{c_D}{c_H}\right)_{soln} 2 \frac{[H_2O]}{[HDO]} \frac{f_{HDO}}{f_{H_2O}} \frac{f_{\neq,H}}{f_{\neq,HD}} \qquad [161]$$

Similarly, the separation factors S_T are

$$S_T = \left(\frac{c_T}{c_H}\right)_{soln} 2 \frac{[H_3O^+]}{[H_2TO^+]} \frac{f_{H_2TO^+}}{f_{H_3O^+}} \frac{f_{\neq,H}}{f_{\neq,HT}} \qquad [162]$$

and

$$S_T = \left(\frac{c_T}{c_H}\right)_{soln} 2 \frac{[H_2O]}{[HTO]} \frac{f_{HTO}}{f_{H_2O}} \frac{f_{\neq,H}}{f_{\neq,HT}} \qquad [163]$$

(b) The Ratio R

From equations [142] and [144], the ratio of exchange current densities for atom-atom recombination in acid solution is

$$R = \frac{(1-\theta_H)^2}{(1-\theta_D)^2} \left(\frac{f_{D_3O^+}}{f_{H_3O^+}}\right)^2 \left(\frac{f_{H_2O}}{f_{D_2O}}\right)^2 \frac{f_{\neq,H}}{f_{\neq,D}} \exp 2(\phi_{r,D}-\phi_{r,H})F/RT \qquad [164]$$

Similarly, in neutral or alkaline solution, equations [145] and [147] lead to

$$R = \frac{(1-\theta_H)^2}{(1-\theta_D)^2}\left(\frac{f_{D_2O}}{f_{H_2O}}\right)\frac{f_{\hbar\parallel}^2}{f_{\hbar D}}\left(\frac{f_{OH^-}}{f_{OD^-}}\right)^2 \exp 2(\phi_{r,D}-\phi_{r,H})F/RT \quad [165]$$

5. Proton Tunneling in Electrochemical Proton Discharge Mechanisms

In the previous section, S and R relations were derived in terms of classical partition functions and the possibility of quantum mechanical tunneling was neglected. Experimentally (see below) we find no evidence to support appreciable tunneling and the above relations are therefore valid without further alterations or corrections. There have been several applications of Bell's treatment (cf. ChapterIII, section 3) and all predict significant tunneling contributions. The methods used will be reviewed here.

Bawn and Ogden (13) were the first to apply a proton tunneling calculation to the evaluation of S_D. Using a symmetrical Eckart barrier of width $2l = 2\text{-}3\text{Å}$ and a height $E = 15$ kcal mole^{-1}, S_D values of 30-100 were calculated. Two years later Appelby and Ogden (14) reported experimental values of S_D of this order of magnitude, but such results have never been reconfirmed (S_D values for Hg vary from 4 to 2 as discussed in Chapters IV-VI). In the original treatment (13), too large a barrier width was assumed and no allowance was made for the important effect on the activation energy by the applied electrode

potential. Conway (24) used a symmetrical Eckart barrier to calculate S_D for an electrode at the potential of zero charge (p.z.c) and calculated the effect of electrode potential on the tunneling rate. The calculation was made with respect to the p.z.c. since the factor A in equation [79] can be estimated as 2.5 kcal mole^{-1} (110) and E^* is experimentally about 18 kcal mole^{-1} (110) at the p.z.c. Hence for an applied potential ϕ^o, E^* is changed by $\beta\phi^o F$; the height of the barrier, E^*, as a function of rational potential ϕ^o is then

$$E^* = E_o^* + \beta\phi^o F \qquad [166]$$

Similarly A becomes

$$A = A_o + \phi^o F \qquad [167]$$

The values of W in equations [79] and [82] are changed to W' where

$$W' = W + \phi^o F \qquad [168]$$

Conway (24) showed that when log G_W, the tunneling probability, is plotted against ϕ^o, a linear relation is found for both H^+ and D^+ over a certain range of log G_W. However, the apparent Tafel slope $d\phi^o/d \ln i$, for proton discharge is 0.25 and 0.17 for deuteron discharge.

The treatment of Christov (23,25,26) is also based on Bell's methods. The assumption made by Christov is that tunneling contributes to S_D significantly so that the main difference in E_D^* and E_H^* (equations [91] and [92]) is due to

tunneling. Christov made his calculations for $\eta = 0$ and his results are therefore involved with the difference in reversible potentials for H_2 and D_2 electrodes which he did not consider. Using the above conditions, Christov then considered the result of variation of the width and shape of the barrier using the experimental values of E_D^* and E_H^* from the data of Post and Hiskey (113, 112) and found good agreement between theory and experiment for a parabolic barrier of width $2\,l = 1.65$ Å. As an indication of large tunneling contributions, he offers the value of the apparent frequency factor ratio A_H^*/A_D^* found experimentally by Post an Hiskey (111,112) as 0.5. It is unfortunate that he offers this as experimental proof of tunneling since it will be shown later in this thesis, that when proper allowance is made for the difference in reversible potentials of a hydrogen and deuterium electrode, the true frequency factor ratio $A_H/A_D \doteq 1$ as required by classical theory.

6. Previous Experimental Work on S and R

Early work on evaluation of S_D (9,113,213) has erroneously tended to establish the view that the values of S_D fall into two classes, viz. $S_D \doteq 3$ for the high overpotential metals (Hg, Pb, Sn) and $S_D \doteq 6$-7 for the transition and related metals. On this basis, many authors [e.g. (10 and 114)] have claimed that S_D (and S_T) is a valuable diagnostic test with

regard to the class in which it falls. This erroneous separation of the S_D values into two groups originates from experimental conditions rather than any experimental error. The values of S_D in the early work were studied at high current densities so that enough gas could be collected in a short time to permit accurate analysis for the H/D ratio. In the present (119) and other recent work (117) on S_D measured as a function of the overpotential, it is found that considerable dependence of S_D on η arises. In these latter experimental investigations, it has become apparent that values of S_D much lower than 6-7 can occur on the transition metals. In this thesis it is shown that values of S_D of 3-4 can be explained on the basis of either recombination mechanisms [2] or [3] and therefore low values of S_D do not necessarily correspond to the discharge mechanism [1]; thus, it will be shown (Chapters V and VI) that the criterion of mechanism based on the two groups of values of S_D breaks down under certain conditions.

Since the present work was commenced and during the course of its publication, Vielstich et al. (116,117) have measured S_D on Ni, Ag, Zn, and Hg electrodes as a function of η in KOH or H_2SO_4 electrolytes and S_D on Fe, Ni, Pt, Ag, and Hg electrodes is a function of η in KOH or H_2SO_4 solutions. For all metals except Hg, S_D was found to increase from about 3.8 at $\eta = 0$ to a maximum around 5-7 and then to decrease again.

This is consistent with the findings of Horiuti (12) and our own (see Chapter IV on experimental results). However, Lewis and Ruetschi (118) report several maxima and minima for Pt, Ni, Ag and Hg/which is not confirmed by either Vielstich, Horiuti or in the present work. Upon examining Lewis and Ruetschi's graphs of S_D vs. η, it is easily seen that the lines drawn through the experimental points are quite unreasonable and that straight or gently curved lines would provide a better approximate fit to the scattered points. This work is therefore considered to be of little practical value and will not be discussed further. For every series of measurement made by Vielstich et al., the ratio $\ln S_T / \ln S_D$ was independent of overpotential and the nature of the surface. S_T has been found to decrease from about 9 to 3 in H_2SO_4 (120). In general, values of S in acid are found to be lower than in alkaline solution. For example, at Pt S_T = 9.6 and 15.3 in acid and alkaline solution (114), respectively (values of η are not given). However, for Ni cathodes the reverse is true viz., S_T = 18 and 4 in acid an alkaline solutions, respectively, thereby indicating a change in mechanism.

Although there is qualitative agreement between various authors for the S_D- η relation, there is little quantitative agreement. This is attributed to differences in various experimental conditions such as the nature of the anion employed (119). Detailed discussion of the potential dependence of S has been avoided by other workers, and has usually been simply referred

indicating
to as/a change in mechanism. For example Horiuti and Fukuda (12) claim that the $S-\eta$ relation which rises to a maximum at $S \doteq 6.5$ from an initial value of 3.5, and then decreases slightly again (see Figure 30), corresponds to a rate-limiting H_2^+ neutralization (low S_D) followed by a rate-limiting $2H \rightarrow H_2$ (high S_D).

Other authors (116,117,118) have attributed the initial low S_D value of 3.5-3.8 to a separation arising from the thermodynamic equilibrium

$$HD_{(gas)} + H_2O_{(liq)} \rightleftharpoons HDO_{(liq)} + H_{2(gas)} \qquad [169]$$

which is catalysed by the metal electrode. The separation factor for reaction [169] is theoretically 3.62 at 25°C (121,122) and has been found experimentally (122) to be 3.88. This view is difficult to accept for Hg, Pt and Ni electrodes. It is well known that mercury has little or no catalytic action for hydrogen exchange reactions. It might be expected that this reaction could occur at equilibrium on Pt electrodes but experimentally this is not observed (123). This equilibrium was also not observed in the case of Ni electrodes (124) and there is no reason to suspect that other metals can significantly catalyze this reaction if Pt and Ni do not.

Values of R for the h.e.r. have been reported for several metals in acid solutions but apparently similar studies have not been made in neutral or alkaline solution. R values of 2 have

been reported for Hg (111,112) and smooth Pt (125) and Pd (125), and values of 3 for Ni (125), Fe (45) and W (45) are found. Values from 4-10 have been found on Ag and Cu (125)

7. Previous Theoretical Considerations of R and S

A. The Method of Conway (125,158)

(i) The Separation Factor S_D (158)

In this paper, Conway deduced maximum isotope effects by using thermodynamic cycles as a basis for the estimation of zero-point energy differences in H and D-initial states and calculated S_D and R for various mechanisms taking into account the appropriate partition function ratios. For proton discharge (reaction [1]), the total heat content of reactants and of products are referred to that of $\frac{1}{2} H_2 + H_2O + M$ through the Born-Haber cycles

$$H + H_2O + M \xrightarrow{I_H} H^+ + e + H_2O + M$$

$$\uparrow \tfrac{1}{2}D_{H_2} \qquad\qquad \downarrow \Delta H_s - I_M$$

$$\tfrac{1}{2} H_2 + H_2O + M \xrightarrow{\Delta H_1} H_3O^+ + e_M + M$$

(reference state) (initial state)

and

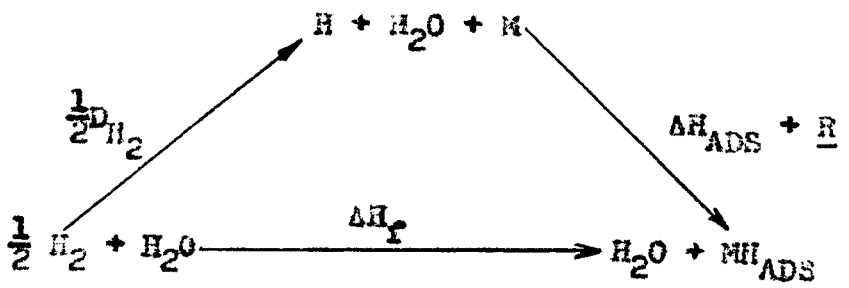

Here D_{H_2} is the dissociation energy of molecular hydrogen, I_H is the ionization potential of atomic hydrogen, ΔH_S is the heat of solvation of a proton in water, Φ_M is the metallic work function, $\Delta H_{ads.}$ is the heat of adsorption for atomic hydrogen, $\underline{R}$ is the repulsive energy between a hydrogen atom and a water molecule, and ΔH_1 and ΔH_f are the heat content changes in the formation of the initial and final states, respectively, from the reference state. An identical cycle exists for D discharge from H_2DO^+ where the reference state chosen is $\frac{1}{2} D_2 + H_2O + M$. ΔH_1 and ΔH_f are obtained from the two cycles as

$$\Delta H_1 = \tfrac{1}{2} D_{H_2} + I_H + \Delta H_S - \Phi_M \qquad [170]$$

and

$$\Delta H_f = \tfrac{1}{2} D_{H_2} + \Delta H_{ads} + \underline{R} \qquad [171]$$

Taking D_{H_2} = 103.1 kcal mole^{-1}, I_H = 313.0 kcal mole^{-1}, and

for mercury $\Phi = 104$ kcal mole^{-1}, the above equations become

$$\Delta H_i = 260.1 + \Delta H_S \qquad [170a]$$

$$\Delta H_f = 51.6 + \Delta H_{ads.} + R \qquad [171a]$$

Thus if ΔH_i and ΔH_f can be obtained as a function of distance from, say the center of the water molecule, two curves can be drawn and the activation energy is obtained from the intersection of ΔH_i *vs* distance and ΔH_f *vs* distance curves. This method was originated by Horiuti and Polanyi (159) and refined by Butler (160) and by Bockris and Parsons (110). In equations [170] and [171] the only terms which are dependent upon distance are ΔH_S, $\Delta H_{ads.}$, and R. ΔH_S and ΔH_{ads} were given in terms of Morse functions by

$$\Delta H_S = \Delta H_S^o \left[2e^{-a(r-r_e)} - e^{-2a(r-r_e)}\right] \qquad [172]$$

and

$$\Delta H_{ads} = \Delta H_{ads}^o \left[2e^{-a(r-r_e)} - e^{-2a(r-r_e)}\right] \qquad [173]$$

where ΔH_S^o is the total heat of solvation of the proton and ΔH_{ads}^o is similarly, the heat of adsorption of the hydrogen atom which is related to the M-H bond dissociation energy. For the repulsive energy function R, Butler (160) assumed the H---O repulsion to be of the same magnitude as that for repulsion between a helium and a hydrogen atom. The Butler repulsive energy function is

$$R = e^{2.3\ (3.96-1.6r)}\ \text{kcal mole}^{-1} \qquad [174]$$

Parsons and Bockris used the repulsive energy function

$$\underline{R} = [0.567\ e^{-24 \cdot r^2} + 0.215\ r\ e^{-2.4r^2}] \times 10^{-10} \text{ erg molecule}^{-1} \quad [174a]$$

which is that for the $H---H_2$ system obtained experimentally from scattering studies (161). Butler used a value of -180 kcal mole^{-1} for ΔH_S^o which corresponds to the proton affinity. Bockris and Parsons used a value of -260 kcal mole^{-1} for ΔH_S^o which seems to be more appropriate since this value corresponds to the total solvation energy of a proton in liquid water. The values of S_D calculated by Conway do not depend sensitively on the choice of the absolute magnitudes of ΔH_S^o and $\underline{R}$ since only isotopic differences in these quantities are involved.

(11) The Ratio of Exchange Currents, $\underline{R}$ (125)

In a recent paper Conway (125) estimated R values by reference to the thermodynamic cycles for pure H and pure D containing systems and reported experimental values of R for Cu, Ni, Pt and Au cathodes. For the discharge step, the difference in energies of activation was calculated from equations [170a] and [168a] and their D-analogues. The role of isotope effects in both the zero-point energies of initial and activated states were also considered and the role of isotopic differences of steady-state coverage by H and D was evaluated. The estimated isotope effects R at various metals calculated for mechanisms [1], [2] and [3], although qualitative in some respects, must be

regarded as supporting the discharge mechanism at mercury and the two recombination mechanisms at platinum, i.e. when comparisons with the experimental values of R are made.

B. The Method of Horiuti et al. (9,10,94,68,164)

(1) The Atom-Atom Recombination Mechanism (9, 10)

The separation factor S_D for atom + atom recombination is given by equation [160]. If the solution is dilute in D, then the ratio $(c_D/c_H)_{soln}$ can be written in terms of the concentrations of H_2O and HOD as

$$\left(\frac{c_D}{c_H}\right)_{soln} = \frac{[HOD]_b}{2[H_2O]_b}$$

where the subscript b refers to the bulk (aqueous) phase. Substituting into equation [160] yields

$$S_D = \frac{[HOD]_b}{[H_2O]_b} \frac{[H_3O^+]_b}{[H_2DO^+]_b} \frac{f_{H_2DO^+}}{f_{H_3O^+}} \frac{f_{\neq,H}}{f_{\neq,D}} \qquad [175]$$

Both H_3O^+ and H_2DO^+ were considered for the purposes of the calculation to be in equilibrium with gaseous water molecules according to

$$H_3O^+_b + H_2O_g \rightleftharpoons H_2O_g + H_3O^+_b \qquad [176]$$

and

$$H_2DO^+_b + H_2O_g \rightleftharpoons HOD_g + H_3O^+_b \qquad [177]$$

In terms of partition functions and equilibrium constants, the

above relations may be expressed as

$$[H_3O^+]_b = [H_3O^+]_b K_{176} = [H_3O^+]_b$$

since K_{176} is unity and

$$[H_2DO^+]_b = \frac{[HOD]_g[H_3O^+]_b}{[H_2O]_g} K_{177} = \frac{[HOD]_g[H_3O^+]_b}{[H_2O]_g} \frac{f_{H_2DO^+} f_{H_2O,g}}{f_{H_3O^+} f_{HDO,g}}$$

The ratio $[H_3O^+]_b/[H_2DO^+]_b$ is therefore

$$\frac{[H_3O^+]_b}{[H_2DO^+]_b} = \frac{[H_2O]_g}{[HOD]_g} \frac{f_{H_3O^+}}{f_{H_2DO^+}} \frac{f_{HDO,g}}{f_{H_2O,g}} \qquad [178]$$

Combination of equations [175] and [178] yields

$$S_D = \frac{[HDO]_b}{[H_2O]_b} \cdot \frac{[H_2O]_g}{[HDO]_g} \cdot \frac{f_{HDO,g}}{f_{H_2O,g}} \cdot \frac{f_{\neq,H}}{f_{\neq,D}} \qquad [179]$$

By an identical procedure, the tritium separation factor for atom-atom recombination is

$$S_T = \frac{[HTO]_b}{[H_2O]_b} \cdot \frac{[H_2O]_g}{[HTO]_g} \cdot \frac{f_{HTO,g}}{f_{H_2O,g}} \cdot \frac{f_{\neq,H}}{f_{\neq,T}} \qquad [180]$$

The ratios of water molecule concentrations in equations [177] and [178] are seen to be equal to the equilibrium constants for the reactions

$$H_2O_b + HDO_g = H_2O_g + HDO_b \quad K_{181} \qquad [181]$$

$$H_2O_b + HTO_{(g)} = H_2O_{(g)} + HTO_b \quad K_{182} \qquad [182]$$

K_{181} is 1.076 at 18°C (165) and K_{182} is 1.093 at 25°C (166). The partition function ratios for gaseous species, f_{HDO}/f_{H_2O} and f_{HTO}/f_{H_2O} were obtained numerically from spectroscopic data, and the two separation factors become

$$S_D = 68 \frac{f_{\neq,H}}{f_{\neq,T}} \qquad [183]$$

and

$$S_T = 308 \frac{f_{\neq,H}}{f_{\neq,T}} \qquad [184]$$

The ratios $f_{\neq,H}/f_{\neq,D}$ and $f_{\neq,T}$ were calculated from a Heitler-London-Eyring-Polanyi surface (66). For Ni, S_D and S_T were calculated as 6.8 and 15.1, respectively, and for Pt, S_D and S_T values of 7.2 and 16.1, respectively, were obtained. This is in satisfactory agreement with the observed values of S_D = 6.7 (9) and S_T = 18.0 (114) for Ni and for Pt, S_D = 7 (113) and S_T = 9.6 (114) in acid solutions. These values of S correspond to average values in that they were measured at high current densities without any regard to potential dependence. From the potential energy surface for the Ni - H_2 reaction, Horiuti (124) calculated an activation energy for the dissociative hydrogen chemisorption as 75 kcal $mole^{-1}$ which exceeds the experimental value by at least one power of ten (51).

(ii) The Slow Discharge Mechanism

(a) The Extension of Horiuti's Calculations by Kodera et al. (168,169,170)

From equations [148], [178] and [181], the separation

factor S_D is obtained as

$$S_D = \frac{K_{181}}{2} \frac{f_{HDO,E}}{f_{H_2O,E}} \cdot \frac{f_{\neq,H}}{f_{\neq,D}} = 34 \frac{f_{\neq,H}}{f_{\neq,D}} \qquad [185]$$

Similarly

$$S_T = \frac{K_{162}}{2} \cdot \frac{f_{HTO,E}}{f_{H_2O,E}} \cdot \frac{f_{\neq,H}}{f_{\neq,D}} = 154 \frac{f_{\neq,H}}{f_{\neq,T}} \qquad [186]$$

The method treats the activated complex as a linear pseudo-three-atom complex in which the end atoms (Hg and O) are considered as having infinite mass so that there are only two real vibrations in the activated state. They are the doubly degenerate bending vibrations and hence $f_{\neq,H}/f_{\neq,D}$ is given by

$$\frac{f_{\neq,H}}{f_{\neq,D}} = \frac{\sigma_D^{\neq}}{\sigma_H^{\neq}} \left(\frac{\sinh u_D^{\neq}/2}{\sinh u_H^{\neq}/2} \right)^2 \qquad [187]$$

The bending frequency is obtained from the familiar relation

$$\nu_{b,H} = \frac{1}{2\pi} \sqrt{\frac{k_\phi}{M_H}} = \nu_{b,D} \sqrt{2} = \nu_{b,T} \sqrt{3} \qquad [188]$$

The functions ΔH_1 and ΔH_f are obtained from equations [170 a] and [171 a] by considering the distance r between the centers of the water molecule and the metal atom to be fixed, and varying the distance above the symmetry axis x. For the three metals Hg, Ni, and Ag, the force constant k_ϕ in equation [188] is found to be around 21-31 kcal mole^{-1} $\mathring{A}^{-2}$ (i.e. about 1.0 to 1.5 md. $\mathring{A}^{-1}$). The calculation of k_ϕ for the bending modes is thus based on the

potential energy curve functions for the O-H and M-H stretch behaviour. Carrying out the remaining simple calculations, it was found that $S_D \doteq 13$ and $S_T \doteq 35$ for the slow discharge step [1] and is fairly independent of the metal. Since the observed S_D values fall into the range of 3-7, Keii and Kodera (168) have argued that the discharge mechanism cannot be operative at any metal cathode including mercury. The seriousness of this conclusion is obvious: if it is valid than we must discard the discharge step as a rate-controlling mechanism as Horiuti has done 30 years ago; if it is not valid, we must show where this conclusion is invalid and provide a model based on the slow discharge mechanism which can predict reasonable S_D and S_T values.

The error in this calculation may be attributed to the assumption that the proton is free to move about a potential energy surface with only three degrees of freedom. Hence in this model, the only contributions to the zero-point energy in the activated complex arise from the doubly-degenerate bending mode. The assumption that the metal atom is of infinite mass (i.e. it is not free to vibrate) is fictitious. Similarly, the assumption that the water molecule is fixed and does not vibrate is also unsatisfactory, although there may be large reductions in internal frequencies of an O-H bond due to increased hydrogen bonding, the reductions are not nearly so large as Keii and Kodera assume (actually they assume a complete loss of the

internal frequencies since the M and O groups were assumed to be of infinite mass). The decrease in the O-H stretching frequency due to hydrogen bonding which occurs upon taking a gaseous H_2O molecule and placing it into solution is about 100-200 cm^{-1} (171,172). If this activated complex for the discharge step at a mercury cathode is linear, i.e. of the form $Hg...H....OH_2$, there is no valid reason for assuming that a symmetric vibration does not exist. In the present treatment (see Chapters V and VI) this symmetric vibration is taken into account for calculation of S and R values. In addition, a more complex model is proposed as a possible structure for the transition state. In this model, the proton is considered to be discharged between 2-4 metal atoms.

(iii) The H_2^+ (molecule-ion) Neutralization Mechanism [4]

Horiuti (10,164) has applied to above methods to calculate S_D and S_T for the case when mechanism [4,4a] is rate-determining. Without presenting details of the calculation, it is to be noted that values of $S_D = 3.3$ to 3.8 and $S_T = 5.8$ are obtained for mercury. However, Horiuti (10) did not consider this result in relation to the other electrode kinetic criteria which do not support the H_2^+ ion neutralisation mechanism (see Chapter II).

CHAPTER IV

EXPERIMENTAL AND RESULTS

1. Experimental

A. Separation Factors in Aqueous Acid Solutions

(1) The Apparatus

The electrolysis cell and associated equipment is shown in Figure 15. The cell was designed to have minimum dead space and took a total volume of electrolyte of 70 ml. Both the anode and reference electrode compartments were separated from the cathode compartment by closed stopcocks. The top of the cathode compartment was fitted with capillary pyrex tubing which was connected to a gas burette. Gas samples of average volume of 2-5 cc. were collected in the gas burette and passed through two liquid nitrogen traps and finally to a flame-dried sample ampoule by means of a Toepler pump. The gases were analyzed for H_2 and HD (mass 2 to mass 3) by means of a 90° magnetic sector Nier type mass spectrometer (see reference 122). Potentials were kept constant to within 2-3 millivolts by means of a Wonking 61-R potentiostat. The potential of the experimental electrode was measured with respect to that of a reversible hydrogen electrode in the same electrolyte solution using a Radiometer vacuum tube high impedance potentiometer.

Figure 15

Schematic diagram of cell and associated apparatus used in the separation factor experiments

A. Counter electrode compartment

B. Study electrode compartment

C. Reference electrode compartment

D. Constant boiling point HCl

E. H_2O-D_2O mixture

F. To mercury leveling bulb

G. Liquid nitrogen traps

H. Sample ampoule

I. Toepler pump.

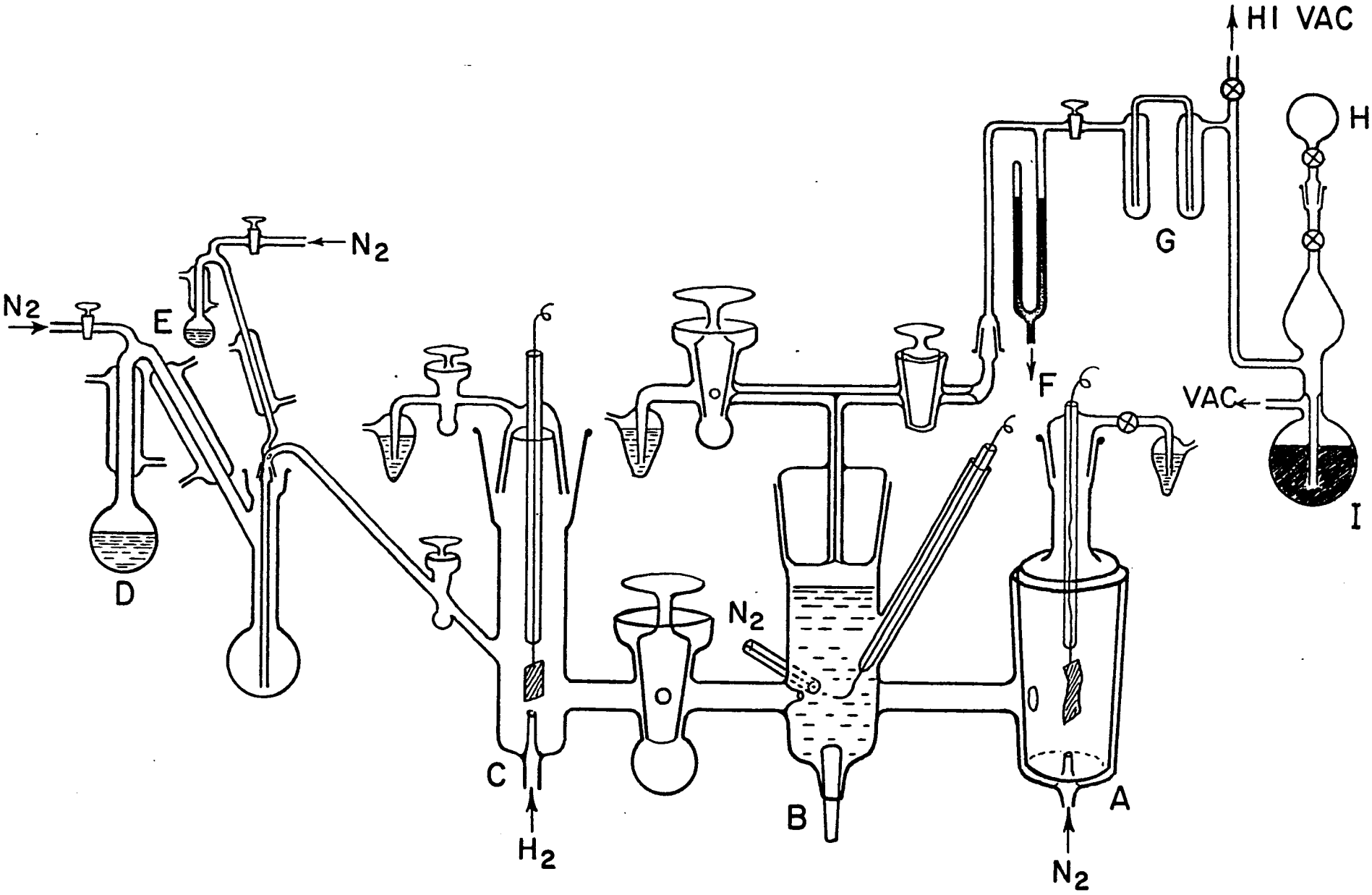
HI VAC
H
G
F
VAC
I
N2
E
N2
D
N2
C
H2
B
A
N2

The Wenking potentiostat serves to maintain a chosen constant potential at the working electrode with respect to a reference electrode. The operating principle is briefly presented below.

The experimental circuit diagram is shown schematically in Figure 16. The assigned potential $\Delta\phi_s$ is compared in the comparator D with the potential difference $\Delta\phi_1$ between the working electrode (W) and the reference electrode (R). Any difference $d\Delta\phi = \Delta\phi_s - \Delta\phi_1$ momentarily existing is amplified to $\Delta\Delta\phi$ in the voltage amplifier $S\phi$. The amplified potential difference controls the power amplifier L and the latter furnishes a correcting current which flows from the counter electrode (c) to the working electrode and re-establishes the potential $\Delta\phi_1$ equal to the assigned potential $\Delta\phi_s$. The feedback response time is several μ sec.

(11) Purification of gases

Hydrogen gas for the reference electrode was purified by passage through a $CaCl_2$ column followed by a palladium asbestos oven at 450°C and finally through two liquid nitrogen traps, the first of which contained activated charcoal. Deuterium gas (see below) was purified similarly. Nitrogen gas used for bubbling in the cathode and anode compartments was treated similarly except that the Pd-asbestos oven was replaced by an oven of Cu at 350°C for removal of oxygen and three liquid nitrogen traps were used.

Figure 16

Electronic circuit for constant potential (potentiostatic) control.

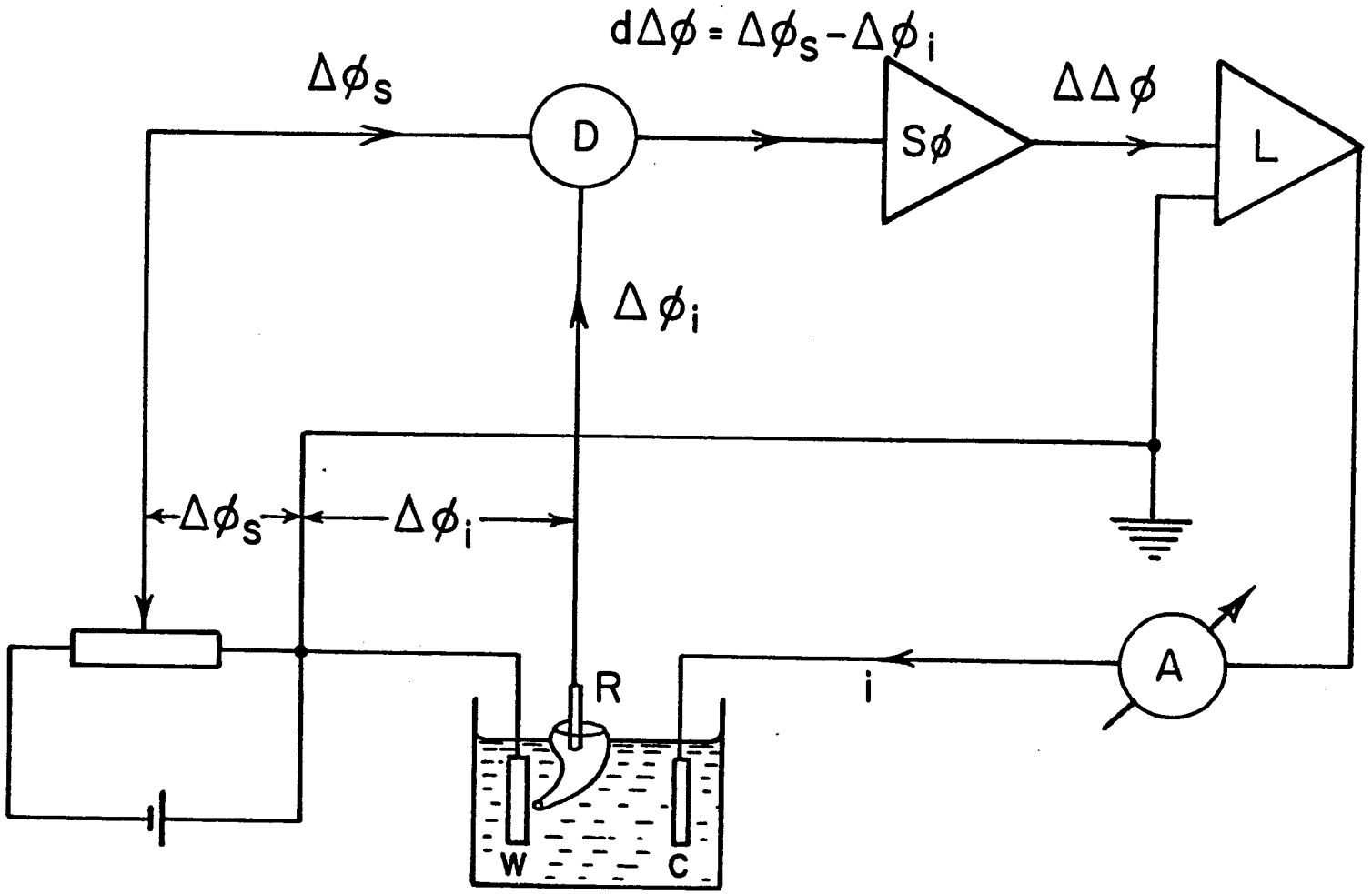
$d\Delta\phi = \Delta\phi_s - \Delta\phi_i$
$\Delta\phi_s$
D
$S\phi$
$\Delta\Delta\phi$
L
$\Delta\phi_i$
$\Delta\phi_s$
$\Delta\phi_i$
A
i
R
W
C

(iii) Preparation of Cell and Solutions

The cell and its components were immersed in cleaning solution (chromic-sulphuric acid mixture) for 24 hours before each run. The cell and other parts were then washed many times with distilled and conductance water and finally immersed in conductance water for 24 hours.

Aqueous hydrochloric acid solutions were prepared as follows (see Figure 15): Redistilled constant boiling point aqueous HCl and a 12% D_2O in H_2O mixture were refluxed in streams of purified nitrogen in separate flasks for 2-3 hours. The solutions were then distilled into a common receiving flask such that the resulting solution was 10% D_2O by volume and normal with respect to the acid. The electrolyte was mixed by bubbling the purified N_2 through it and finally passed through the all-glass connecting tubing to the cell by application of pressure of nitrogen.

Perchloric acid solutions were prepared by quantitative addition of reagent grade $HClO_4$ to conductivity water containing sufficient D_2O to give a solution 1N in acid concentration and 10% D_2O by volume. The electrolyte was then passed directly into the cell and outgassed by bubbling nitrogen.

(iv) Preparation of Electrodes

(a) Platinum. In the initial runs, the electrodes were heated in a stream of pure H_2 gas and sealed in small glass bulbs

in a hydrogen atmosphere (126). The electrode bulb, attached to a 10/30 ground glass joint was then seated in its conjugate 10/30 ground glass joint at the bottom of the cell (see Figure 15). The bulbs were broken *in situ* in the cell by a probe and the run made immediately. It was found that Pt electrodes heated in a quartz tube under H_2, and manually transferred quickly to the cell through the air by insertion into a side arm, gave identical results. This was particularly useful for obtaining S_D values at low overpotentials, i.e. at low current densities where electrodes of 4-8 cm^2 must be employed to obtain reasonable total rates of gas evolution.

(b) Mercury. Mercury electrodes were prepared initially by amalgamation of Cu foil or wire by immersion into a $Hg_2(NO_3)_2$ solution (105). Before amalgamation the electrodes were refluxed in benzene for 24-48 hours. After amalgamation the electrodes were washed many times with conductivity water and inserted into the cell within 10 minutes of their preparation. In previous work (105) it has been shown that amalgamated copper electrodes give identical electrochemical kinetic parameters for the h.e.r. (Tafel slope and exchange current) as those for the free pure mercury surface. Silver and gold foil electrodes were amalgamated by immersion into purified mercury but gave high values for S_D and high Tafel slopes. It was concluded that these latter two types of electrodes do not give a pure Hg surface due to the

great solubility of Ag and Au in mercury.

(v) Procedure. After charging the cell with electrolyte, purification of the solution by pre-electrolysis was carried out on an auxiliary Pt electrode in the cathode compartment at about 1 ma cm^{-2} for a minimum of 20 hours (128). Pre-electrolysis was terminated by removal of the Pt-electrode and insertion of a study electrode in its place. This was done while maintaining a rapid flow of N_2 gas through the cathode compartment to prevent air from entering the cell. Tafel relations were measured before and after the determinations of S_D as a function of overpotential η.

In the determination of S_D as a function of η, values of S_D were obtained at low values of η first. When a particular value of η was set by proper regulation of the potentiostat, purified N_2 was bubbled through the compartment for 3 minutes. The first 1-2 cc's collected in the gas burette were removed by evacuation and final collection of 2-5 cc's was then begun. In this way there was no possibility of H/D gases from a previous run interfering with a new determination of S_D.

B. Ratio of Exchange Current Densities, and Experiments at Low Temperatures

(i) The Apparatus

The electrolysis cells are shown schematically in Figures 17 and 18 for the solid electrodes (Pt, Hg/Cu) and the liquid

Figure 17

Schematic diagram of the low temperature cell used for platinum electrodes.

A. Counter electrode compartment

B. Study electrode compartment

C. Reference electrode compartment

W. Study electrode

L. Luggin capillary

S. Side-arm through which the solution is pumped into the cell.

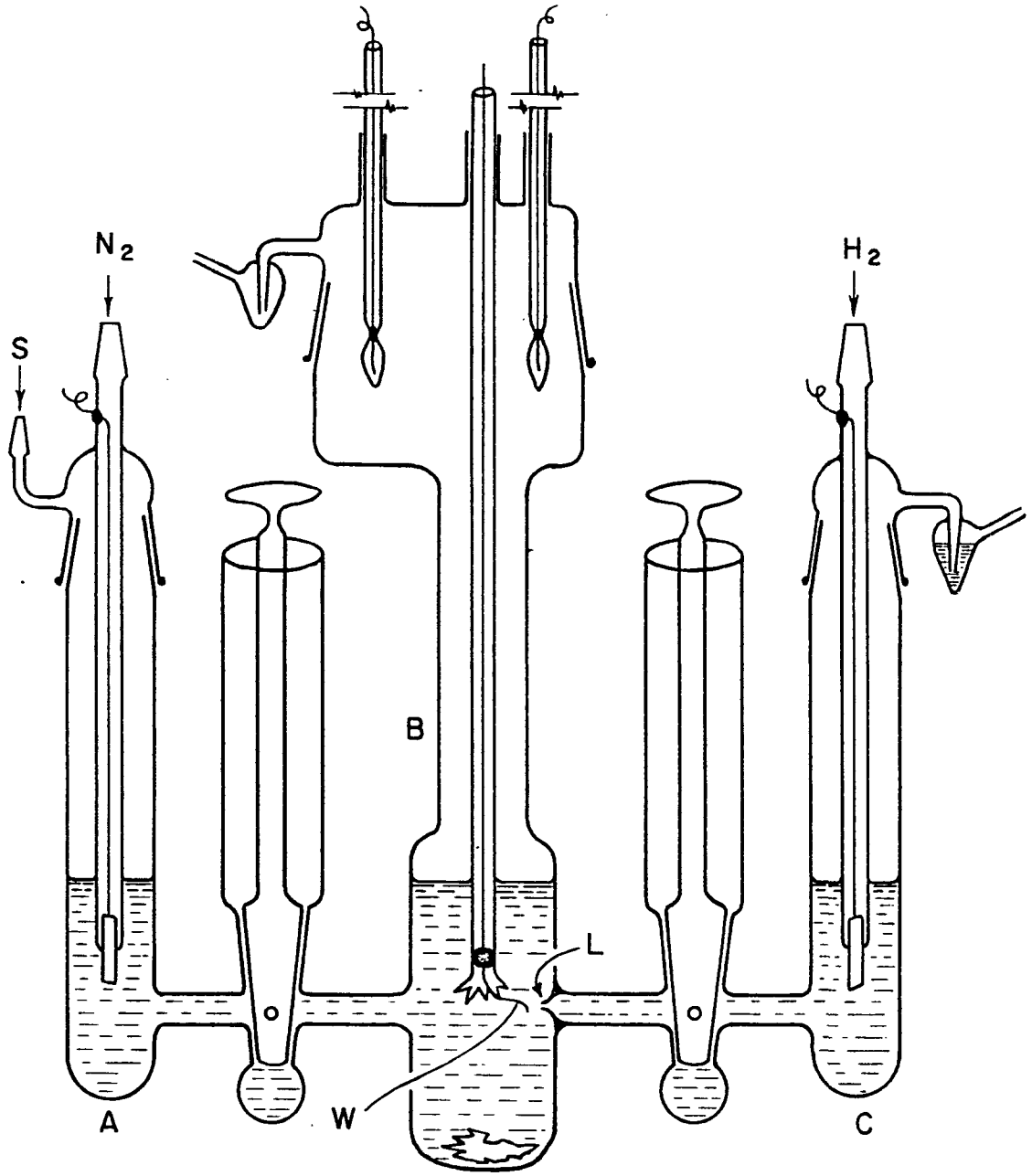
N2
S
H2
B
L
W
A
C

Figure 18

Schematic diagram of the low temperature cell used for mercury electrodes.

A. Counter electrode compartment.

B. Study electrode compartment.

C. Reference electrode

W. Study electrode

L. Luggin capillary

P. Mercury pool used for pre-electrolysis

S. Side-arm through which the solution is pumped into the cell.

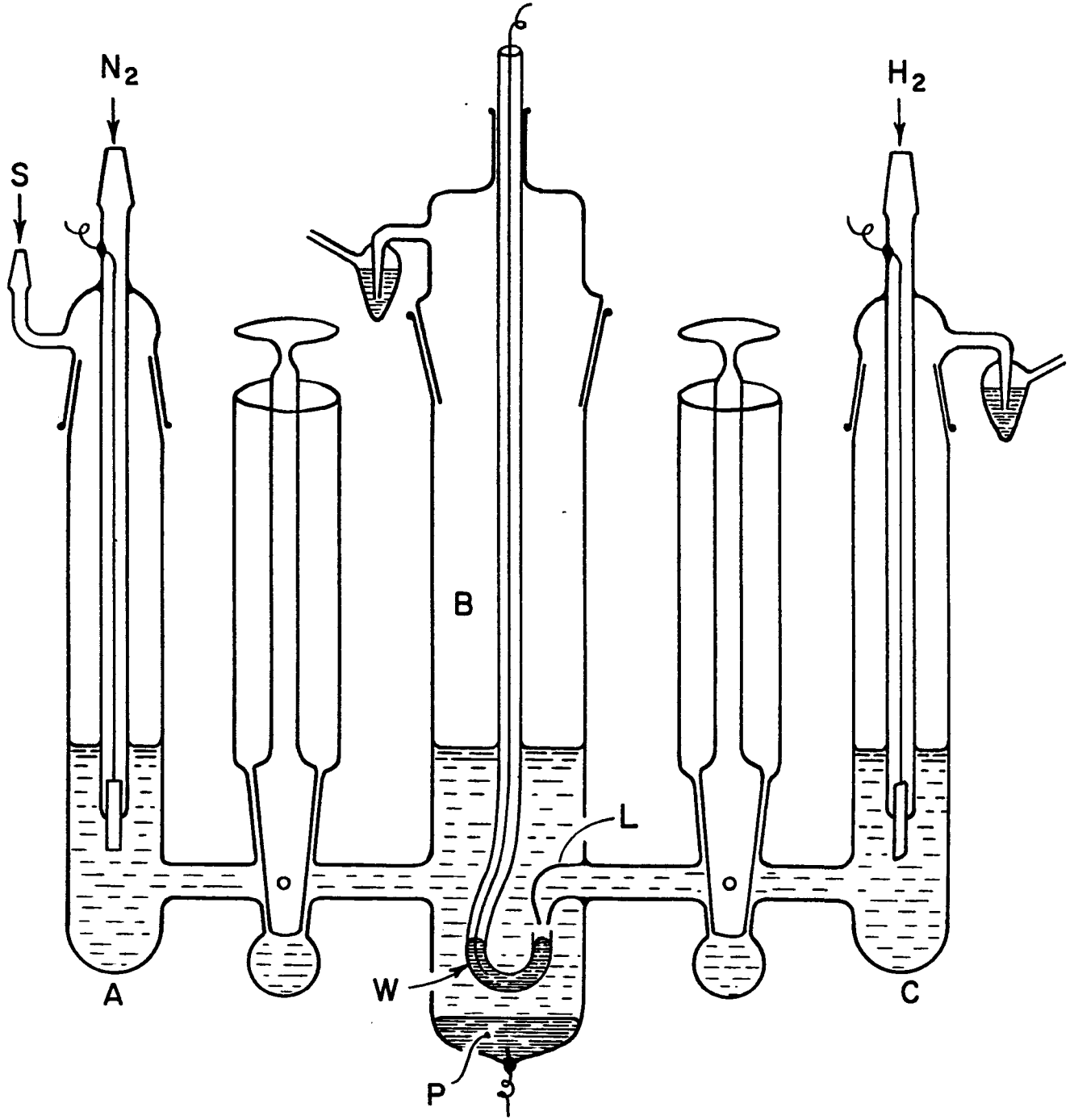
N2
S
H2
B
L
W
A
C
P

mercury electrodes, respectively. Figures 19 and 20 show the cell for Pt and its associated apparatus. Figures 21 and 22 show the mercury cell and its associated apparatus. In both cells the compartments were separated by tall solution-sealed stopcocks. This arrangement permitted the immersion of the cell into a cooling bath without contamination of the solution through the stopcocks which of course were ungreased. The cells were cooled by immersion in a Dewar flask containing either acetone/dry ice or petroleum ether/liquid nitrogen. The temperature was measured by means of a pentane thermometer.

(ii) Purification of Gases

N_2, H_2 and D_2 gases were prepared as described above. HCl gas required for the preparation of aqueous HCl solutions was produced by the action of concentrated sulphuric acid on KCl previously dried in vacuum at 150°C for 48 hours (129).

(iii) Preparation of Cell and Solutions

The procedure for cleaning the cell and associated apparatus was identical with that described above with the exception that after the final immersion in conductivity for 24 hours, the cell and its component parts were dried in an oven at 130° for 24 hours, since runs were to be conducted in CH_3OD solutions with minimum contamination by H_2O.

Methanol solutions (CH_3OH) were prepared by double distillation of spectroscopic grade methanol in a nitrogen

Figure 19

Photograph of low temperature platinum cell and associated apparatus.

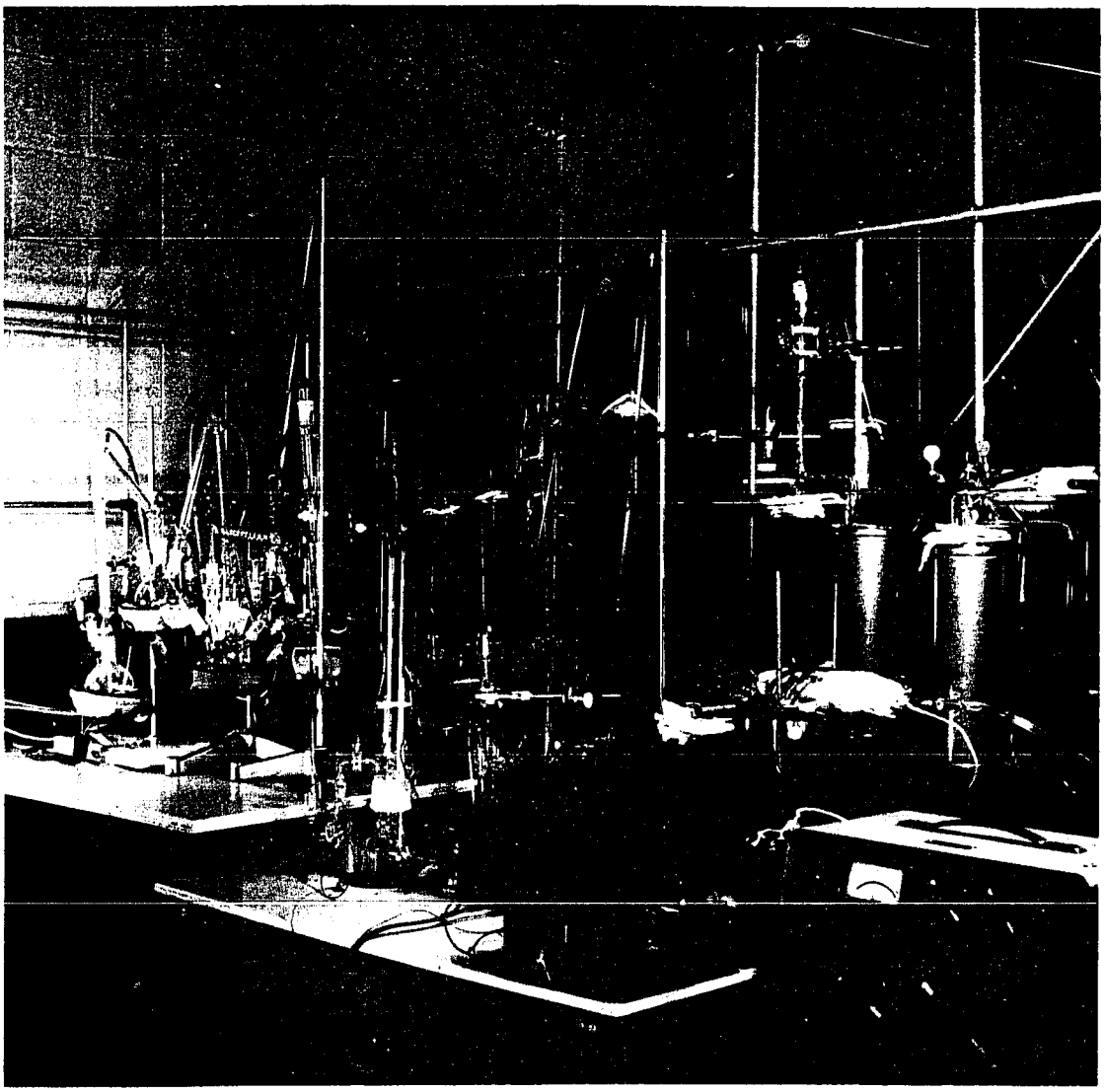

Figure 20

Detail of Figure 19.

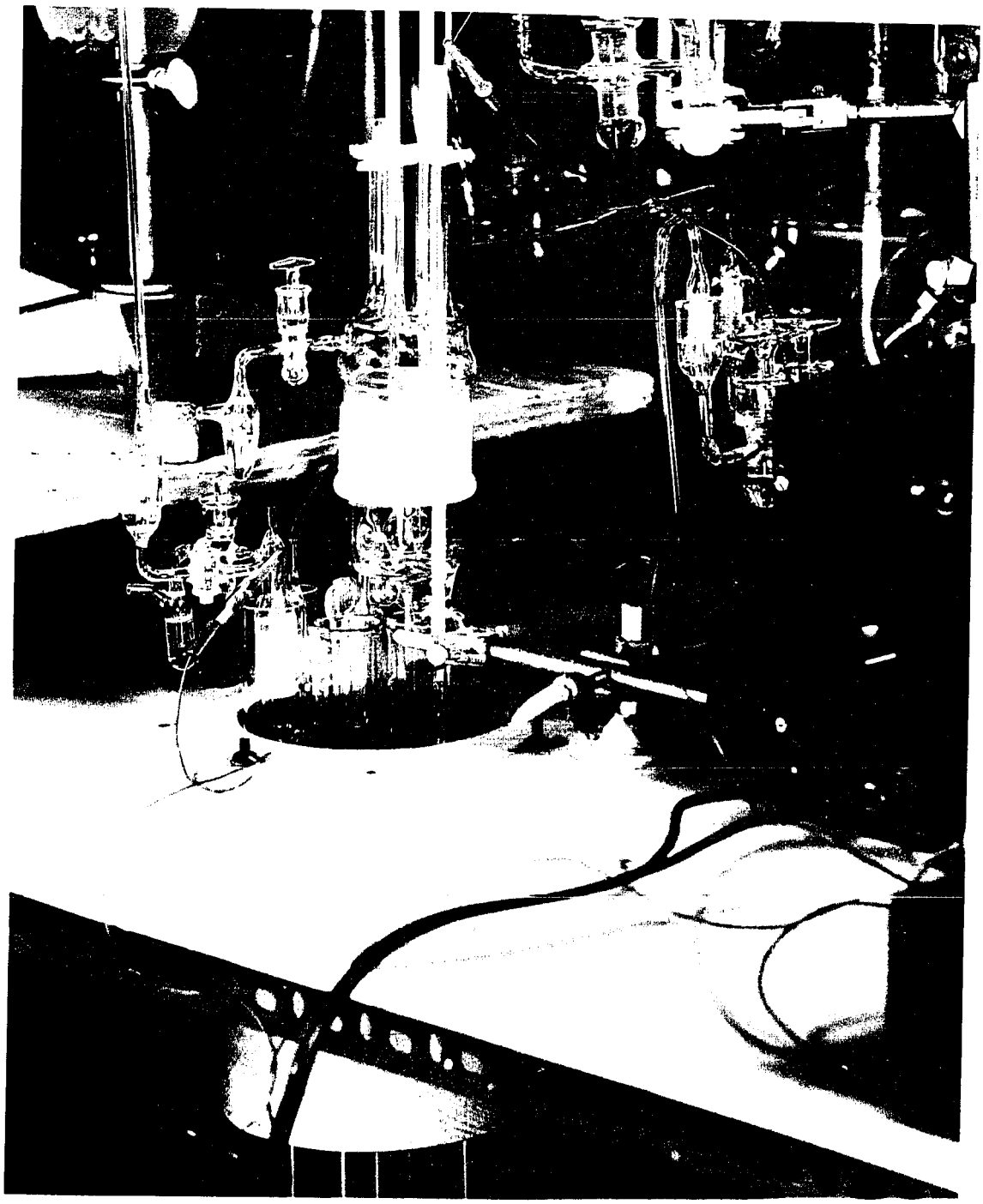

Figure 21

Photograph of low temperature mercury cell and associated apparatus.

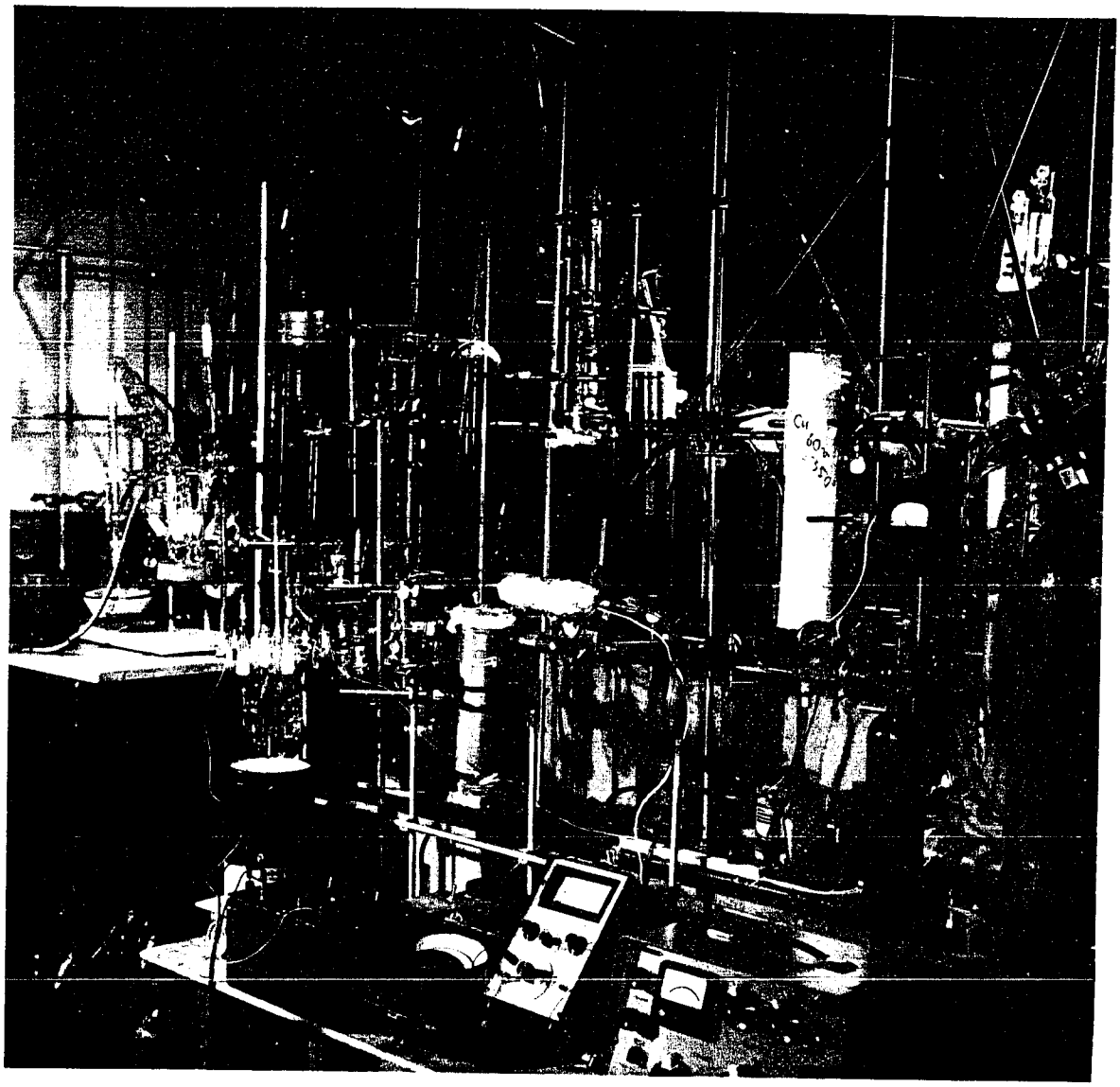

Figure 22

Detail of Figure 21.

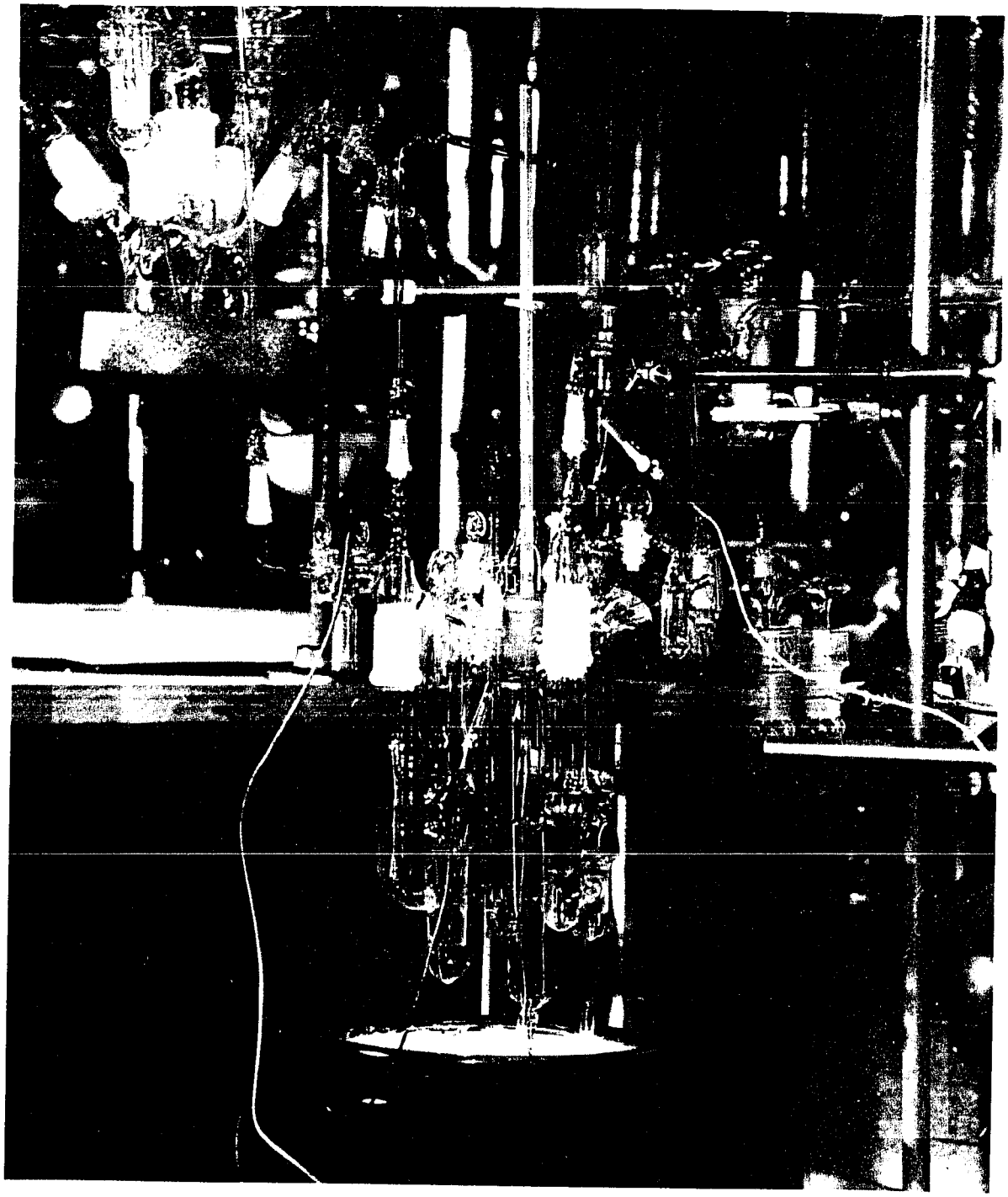

atmosphere first over a small quantity of Mg turnings and sodium borohydride to remove traces of water and any possible aldehyde impurities, and secondly into another flask into which could be bubbled dry, purified HCl gas until the concentration was approximately 1N in HCl. The methanolic HCl solution was then transferred to the cell under nitrogen pressure. The strengths of the HCl solutions were determined by titration on separate samples.

Methanol-d (CH_3OD) was prepared from magnesium methoxide and heavy water (130). Magnesium methoxide was first prepared by the action of spectroscopic grade methanol on Mg turnings and dried under vacuum for 20 hours at 60°C. Heavy water (99.7% minimum D_2O content)was then added to excess dry $Mg(OCH_3)_2$ and the product CH_3OD distilled off under reduced pressure into a dry flask into which dry DCl gas was bubbled until the concentration of DCl was about 1N. The DCl was prepared by the action of D_2SO_4 on dry KCl; the heavy sulphuric acid was prepared by the distillation of SO_3 onto D_2O in a cooled vessel.

Ethanol (C_2H_5OH) was prepared from the unde-natured material by refluxing with and distilling from CaO using a procedure similar to that described above for methanol solutions.

(iv) Preparation of Electrodes

Platinum electrodes were sealed in glass bulbs in a purified hydrogen atmosphere as described above. The bulbs were

broken in the cell while immersed in the electrolyte CH_3CH_2OH which was either 1 or 2N in HCl (no runs on Pt were made in CH_3CH_2OD).

Mercury was prepared by double distillation of the best reagent grade material followed by anodic treatment in $Hg_2(NO_3)_2$-HNO_3 solution, with stirring, and a final "vacuum" distillation in a Hulett still (133) with an air leak.

The reference electrodes were platinized hydrogen or deuterium electrodes contained in separated compartments in the usual way. Reversibility of the hydrogen reference electrode at the low temperatures was checked as follows: (a) by anodic and cathodic polarization of pairs of electrodes and examination of the recovery of the potentials to the same initial open-circuit value. The potentials recovered to within a millivolt in less than 5 minutes ; (b) by variation of the partial pressure of hydrogen by dilution with nitrogen at one of the electrodes. Satisfactory reversible behaviour was observed with respect to gas pressure.

(v) Procedure

a) Mercury. The electrolyte, anhydrous CH_3OH or CH_3OD 1N in either HCl or DCl respectively, was prepared as described above and transferred to the cell under N_2 pressure. Pre-electrolysis was set up at an auxillary mercury electrode at the bottom of the cell for a minimum of 10 hours. The study

electrode was then immersed in the solution and its current-potential behavior recorded. A Radiometer vacuum tube potentiometer was used to measure potential differences and both a calibrated Sensitive Research Corporation and a Keithly ammeter were used to record current. These readings were repeated for various temperatures down to -125°C.

b) Platinum electrodes were studied in 1 and 2N HCl in C_2H_5OH solutions down to -150°C. The method used is practically identical to that described for mercury above, except that a sacrificial Pt electrode was used for pre-electrolysis. In both these low temperature experiments, the lowest temperatures obtained were realized by supercooling the alcoholic solutions.

C. The Separation Factor S_D at Mercury in Methanol-Acid Solutions

Several experiments were carried out at mercury cathodes to determine the separation factor S_D in methanol-acid solutions. The cell employed for this purpose was that used in the low temperature runs for mercury (Figure 18) and preparation of the mercury, cell and associated apparatus was similar to that described in section B above. Methanol (CH_3OH) was distilled from Mg metal turnings into a dry flask into which DCl gas could be bubbled. The D/H ratio was then obtained by titration of a small aliquot of the resulting methanol-DCl solution with

standard base.

2. RESULTS

A. Separation Factors in Aqueous Solution

(1) Mercury

Tafel relations for amalgamated Cu electrodes are shown in Figure 23 and 24 for 1N HCl and $HClO_4$ solutions, respectively. The respective Tafel slopes are -118 mV and -110 mV and are within less than ± 5 mV of the accepted values for mercury (29,47,48,129) which have an uncertainty of ± 10 mV. Tafel slopes for Ag and Au amalgam electrodes were of the order of 140-160 mV and showed limiting currents at the high current densities which are not in accord with the accepted behavior for free pure mercury cathodes. In addition, these latter two electrodes gave high values of S_D ca. 5-8 and hence these results were rejected and will not be discussed further. The separation factor potentiostatically determined as a function of potential is shown in Figure 25. The S_D values are significantly potential dependent and $dS/d\eta = 0.6V^{-1}$ in HCl and $1.44\ V^{-1}$ in $HClO_4$ over the range of overpotentials from -0.850 to -1.350 volts. Previous work is discrepant; thus Vielstich et al. (117) find that $dS/d\eta = 1.33\ V^{-1}$ over a 0.6 volt region for 0.2% D content solution in 2N H_2SO_4. In another paper (116) Vielstich reports $dS/d\eta$ to be $6.7\ V^{-1}$ which is inconsistent with our results and also his own results published in a related paper (117). Also at lower potentials, S_D values were reported by these authors

Figure 23

Tafel relation for the h.e.r. on amalgamated copper electrodes in 1N HCl (aqueous).

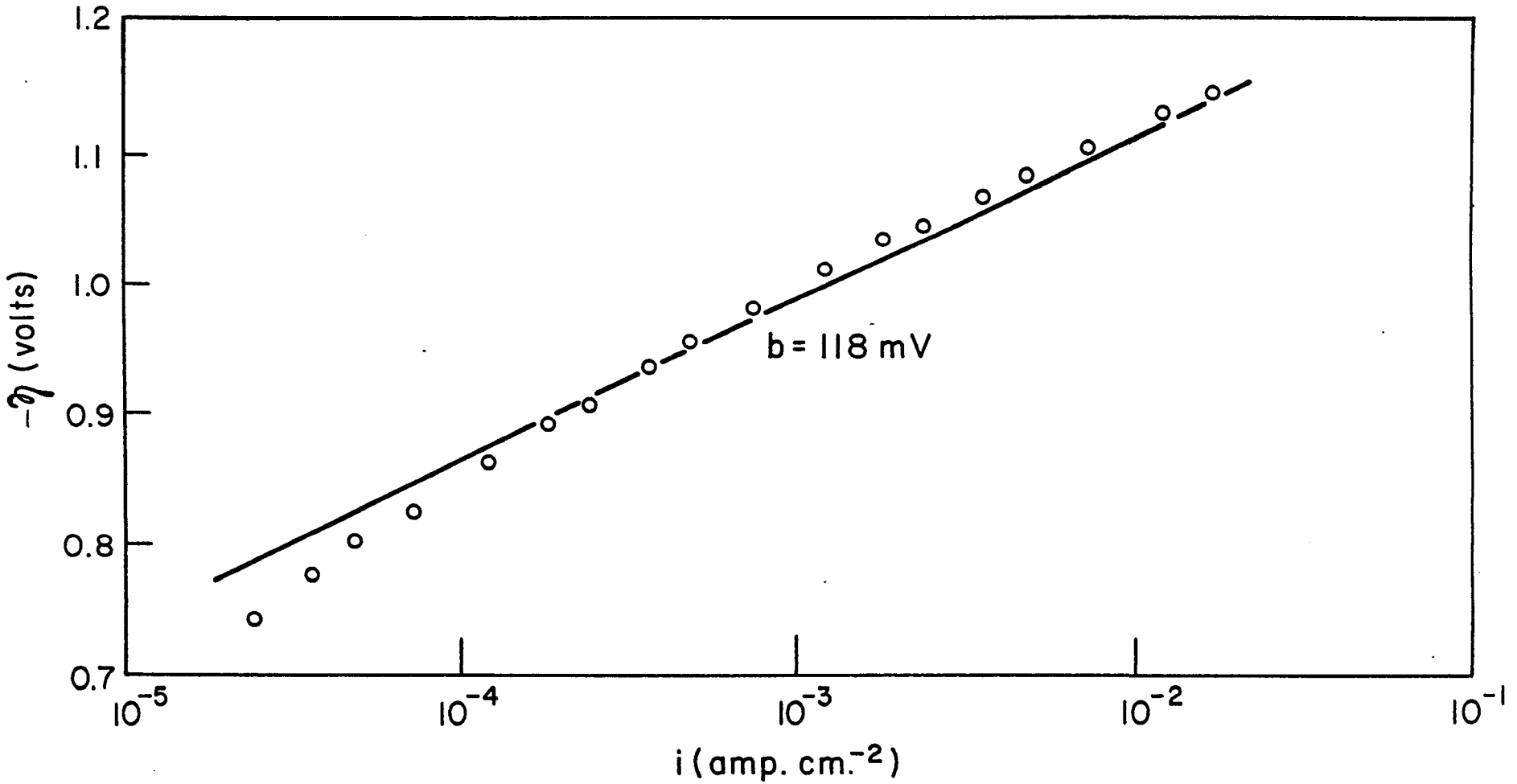
1.2
1.1
1.0
0.9
0.8
0.7
$-\eta$ (volts)
b = 118 mV
10^{-5}
10^{-4}
10^{-3}
10^{-2}
10^{-1}
i (amp. cm.$^{-2}$)

Figure 24

Tafel relation for the h.e.r. on amalgamated copper electrodes in 1N $HClO_4$ (aqueous).

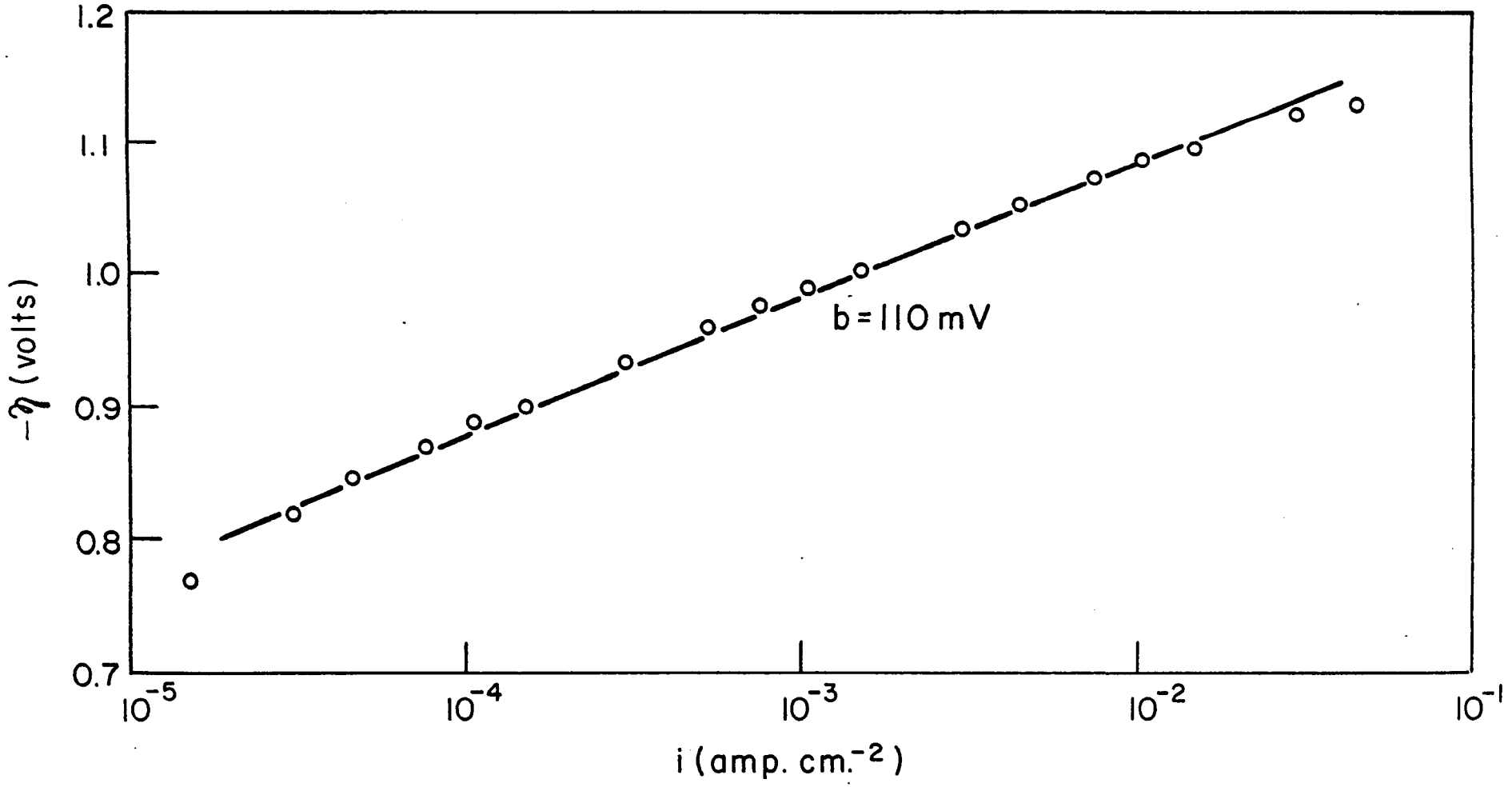
1.2
1.1
1.0
0.9
0.8
0.7
$-\eta$ (volts)
b = 110 mV
10^{-5}
10^{-4}
10^{-3}
10^{-2}
10^{-1}
i (amp. cm.$^{-2}$)

Figure 25

S_D at mercury cathodes as a function of over-potential in aqueous HCl (solid circles) and $HClO_4$ (open circles).

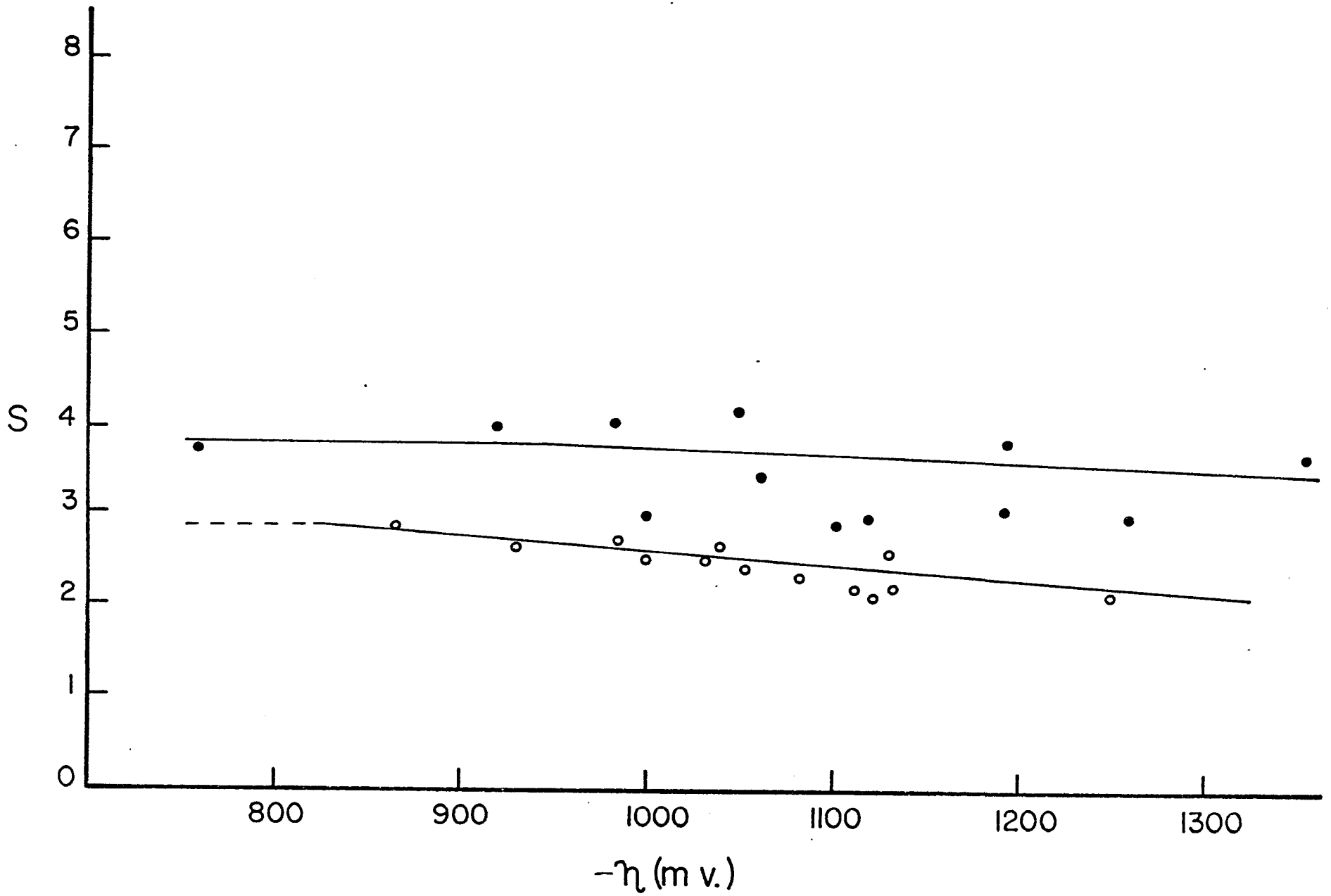
8
7
6
5
S 4
3
2
1
0
800
900
1000
1100
1200
1300
−η (m v.)

for constant current density of 0.3 mA cm^{-2} but over a range of 300 mV (116) which is quite inconsistent with the observed dependence of current density on potential (Tafel line). Our results agree quite reasonably with those of Rome and Hiskey (115). These latter authors, however, studied S_D at constant current rather than constant controlled potential and a variation of S_D from a value of 4 at low current densities to a value of 2.5 at high current densities was found.

(11) Platinum

The Tafel relations for smooth platinum are shown Figures 26 and 27 for 1N HCl and $HClO_4$ solutions, respectively. Current-potential curves were run before each experiment (circles) and after completion of the experiment (triangles). The observed kinetic behaviour is in agreement with accepted data and the time variation of η at solid metals is a common phenomenon (12,45, 114,132). The S_D- η relations are shown in Figures 28 and 29 for HCl and $HClO_4$ solutions, respectively. The S_D-η relation obtained in H_2SO_4 by Horiuti and Fukuda (12) together with that in the present work are shown in Figure 30. Although the data corresponding to the Tafel curve exhibited large time variations, the separation factor S_D was not particularly sensitive to time effects.

B. Results at Low Temperatures

(1) Mercury

Tafel relations were obtained as a function of temperature

Figure 26

Tafel relations for platinum in 1N HCl (aqueous)

O; Before $S_D - \eta$ experiments

Δ; After $S_D - \eta$ experiments.

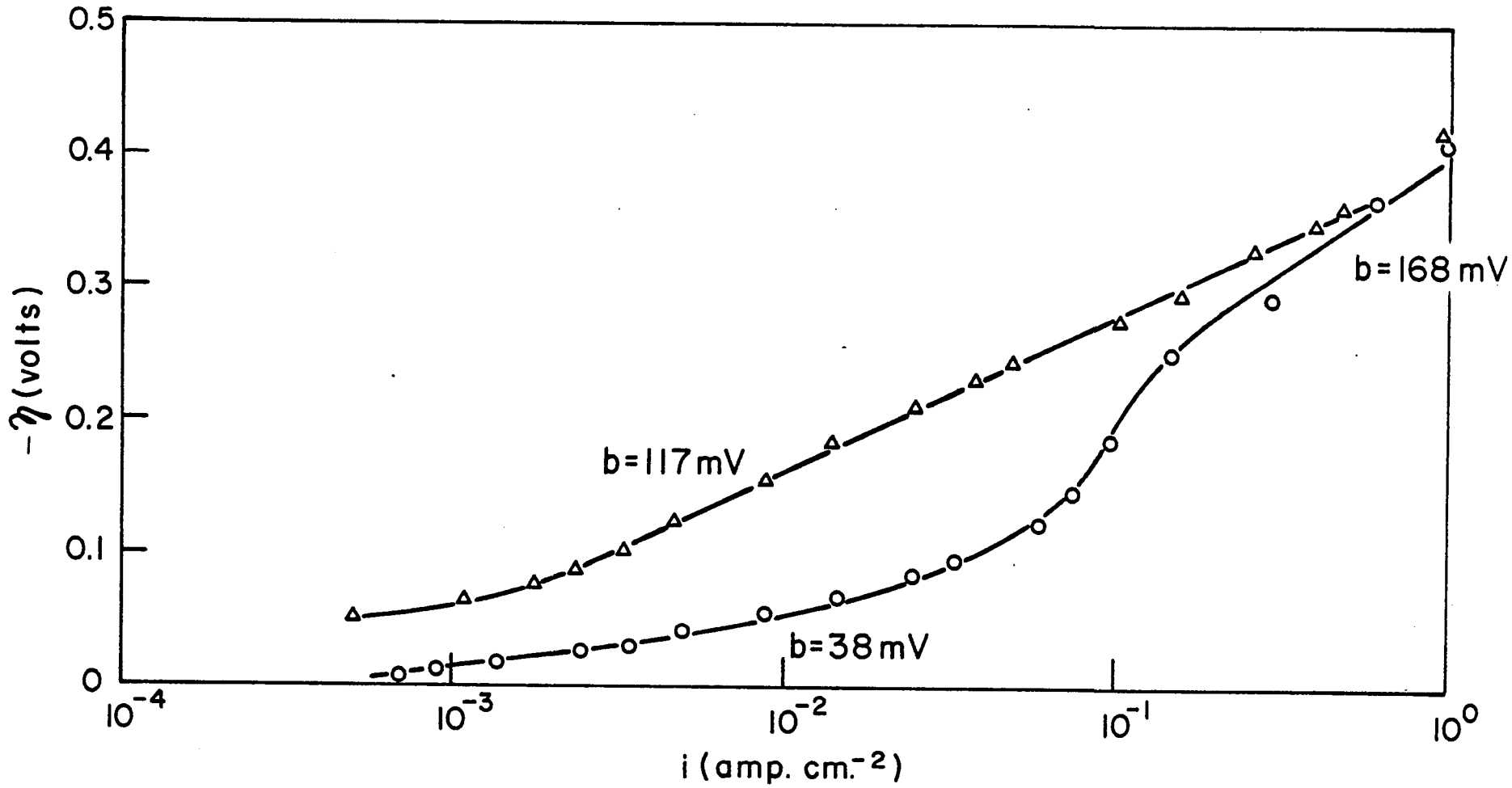
0.5
0.4
0.3
0.2
0.1
0
$-\eta$ (volts)
b=117 mV
b=168 mV
b=38 mV
10^{-4}
10^{-3}
10^{-2}
10^{-1}
10^{0}
i (amp. cm.$^{-2}$)

Figure 27

Tafel relations for platinum in 1N $HClO_4$ (aqueous)

O; Before S_D- η experiments

Δ; After S_D- η experiments.

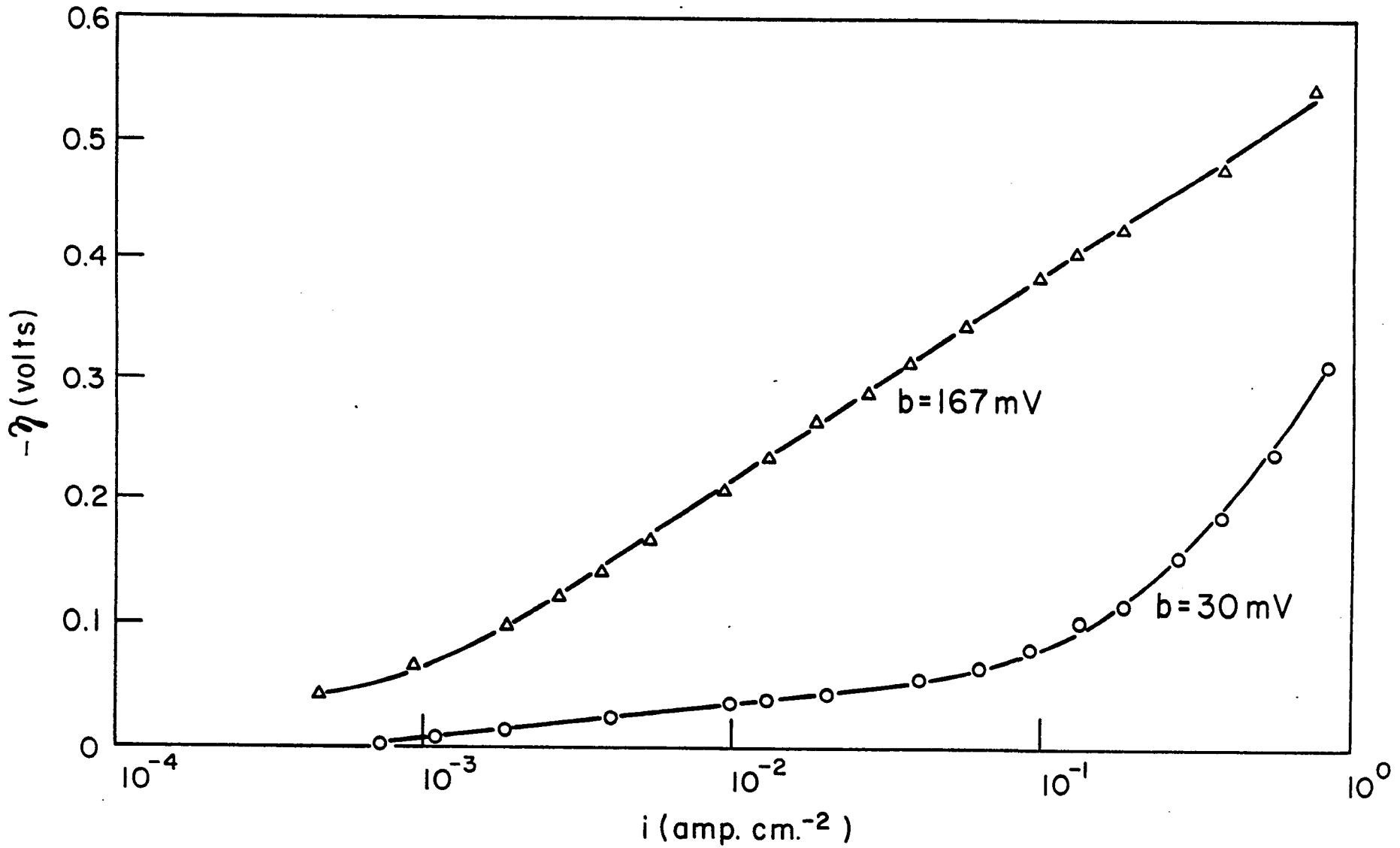
0.6
0.5
0.4
0.3
0.2
0.1
0
-η (volts)
b=167 mV
b=30 mV
10^-4
10^-3
10^-2
10^-1
10^0
i (amp. cm.^-2)

Figure 28

S_D at platinum as a function of overpotential in aqueous 1N HCl.

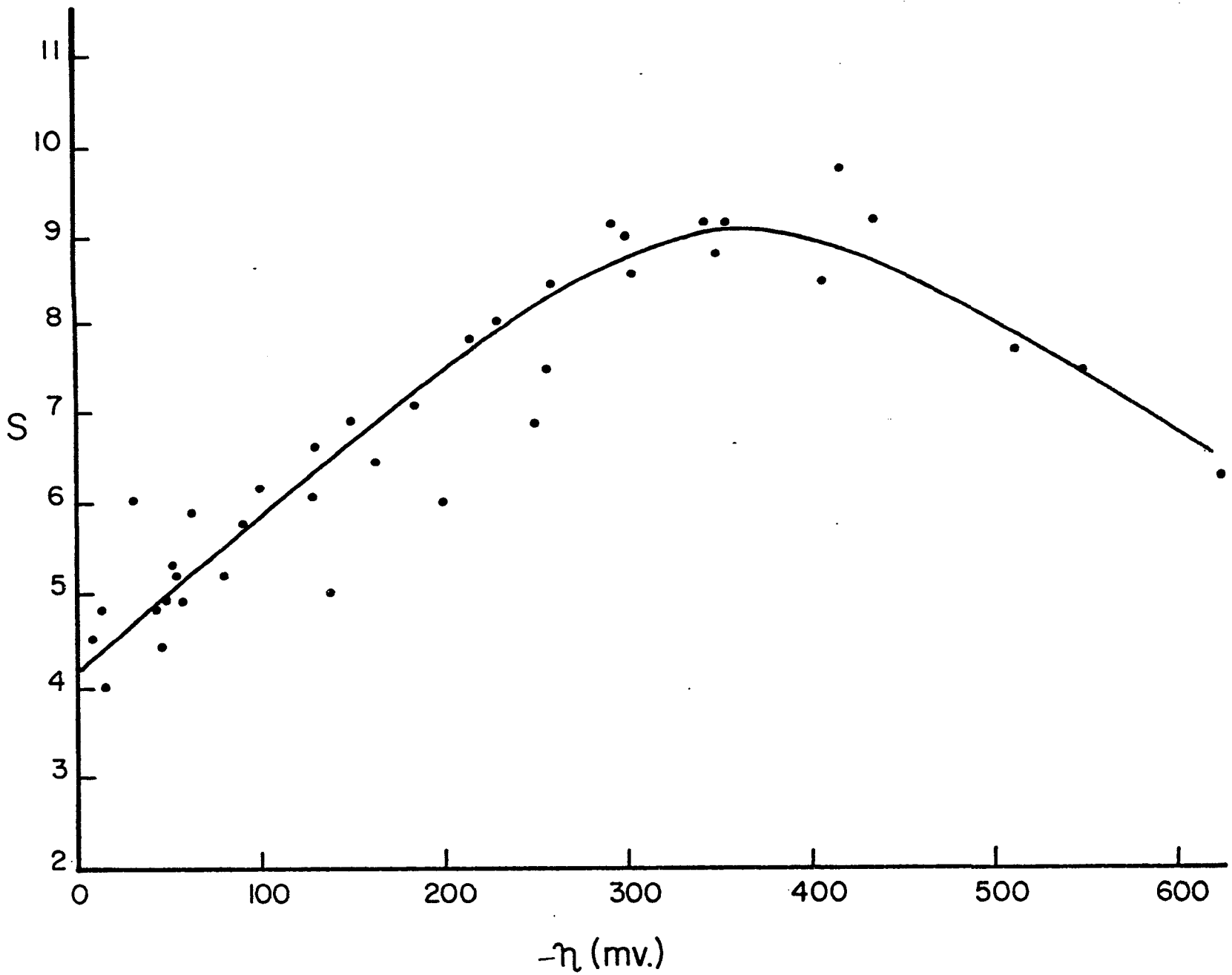
11
10
9
8
7
6
5
4
3
2
S
0
100
200
300
400
500
600
-η (mv.)

Figure 29

S_D at platinum as a function of overpotential in aqueous 1N $HClO_4$.

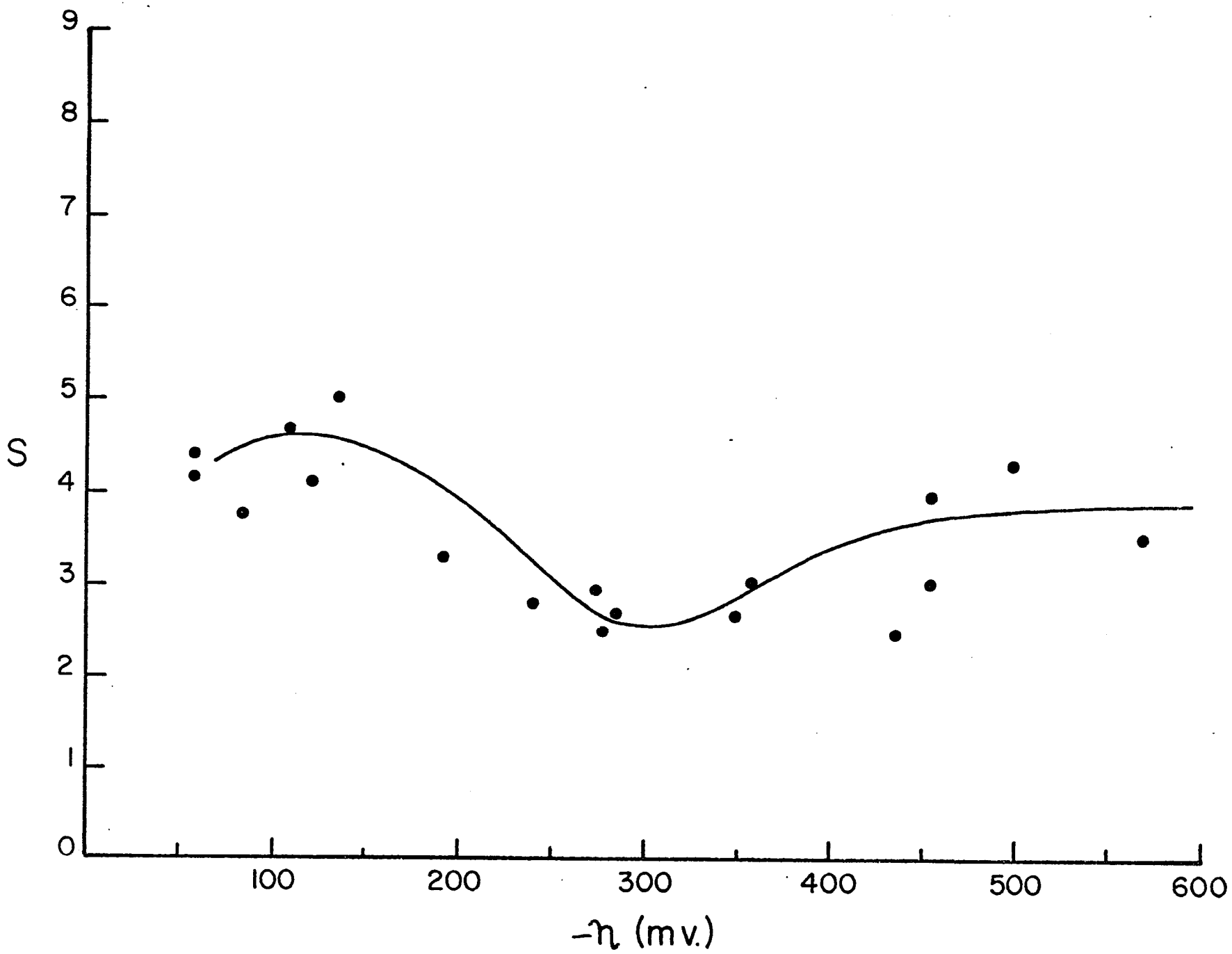
9
8
7
6
5
4
3
2
1
0
S
100
200
300
400
500
600
-η (mv.)

Figure 30

S_D at platinum as a function of overpotential in aqueous HCl, H_2SO_4, and $HClO_4$.

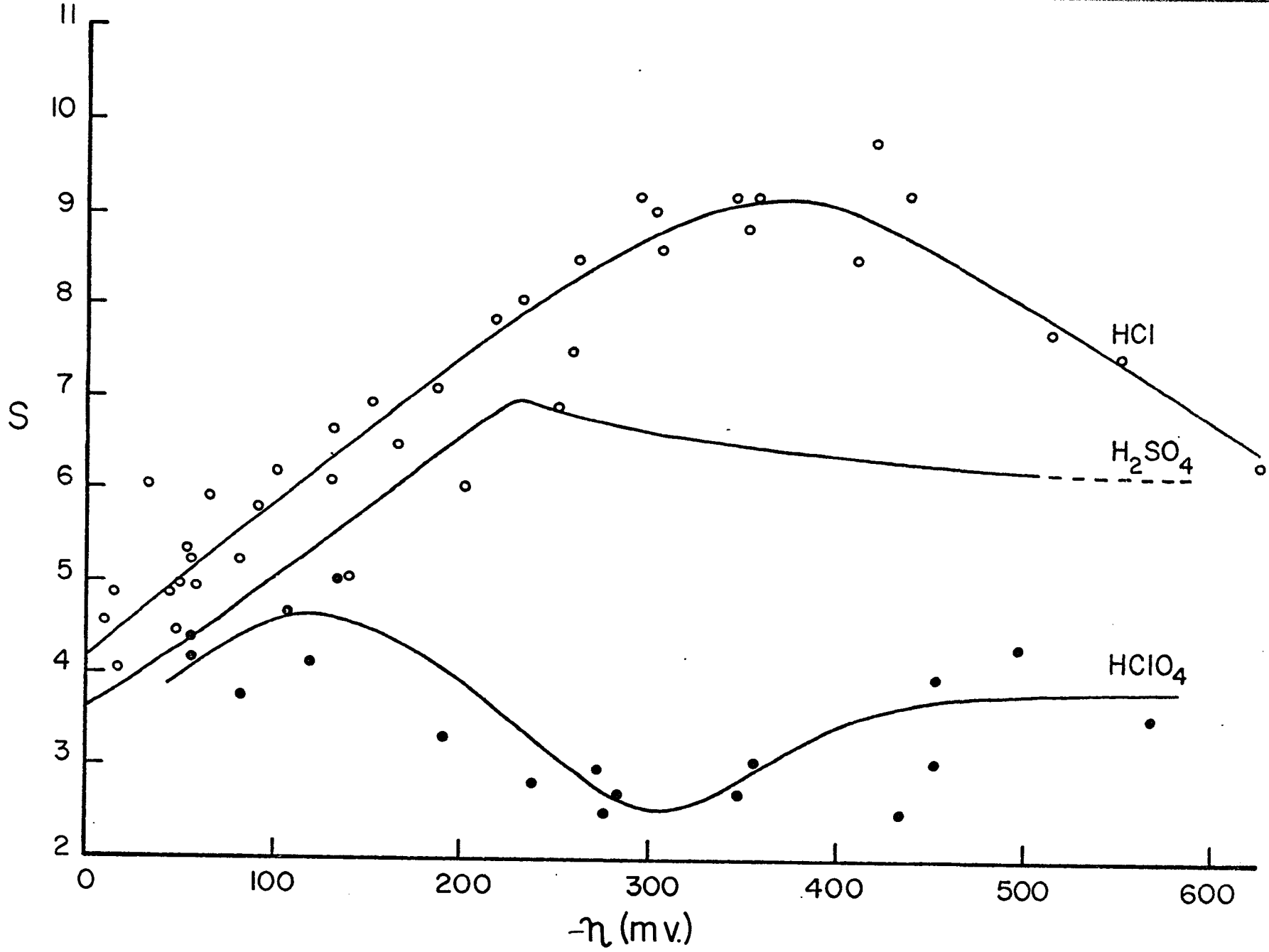
S
11
10
9
8
7
6
5
4
3
2
0
100
200
300
400
500
600
-η (mv.)
HCl
H_2SO_4
$HClO_4$

in five separate runs in anhydrous CH_3OH/1N HCl. Although the technique for high purity measurements at very low temperatures proved to be difficult and several modifications to the apparatus had to be made, a number of successful runs down to -125°C (at Hg) and -150°C (at Pt) were eventually made. The resulting Tafel relations obtained for various temperatures are shown in Figure 31 and are linear over a current density range of up to two decades and are based on 7 to 9 experimental points per decades. In previous work in methanol (133) at higher temperatures, Tafel lines were based on only 2-3 points per decade over 2-3 decades of current. The potential, η, is plotted versus the current density calculated in terms of the area for the liquid mercury pool electrode. From the slope of a log i_o *vs.* 1/T plot (Figure 32), the apparent activation energy for the h.e.r. on mercury in methanol may be calculated as 11.2 kcal mole^{-1}. Similar results were obtained for a mercury electrode in CH_3OD/DCl solutions. The Tafel relations are shown in Figure 33. The apparent activation energy, found by a least squares fit to the log i_o *vs* 1/T points (Figure 32), is 12.3 kcal mole^{-1}. Runs in CH_3OH were made down to -100°C while runs in CH_3OD were made down to -125°C.

The Tafel slope, b, defined by $b = -\frac{2.3\,RT}{\beta F}$ for the discharge step (see Chapter II,) is -125 mV at room temperature. This corresponds to a value of $\beta = 0.47$. Figure 34 shows the experimental Tafel slopes as a function of temperature. The classical slope for $\beta = 0.5$ is shown by the dashed line. It is seen that there is a significant difference between the

Figure 31

Tafel relations at mercury in CH_3OH/HCl as a function of temperature.

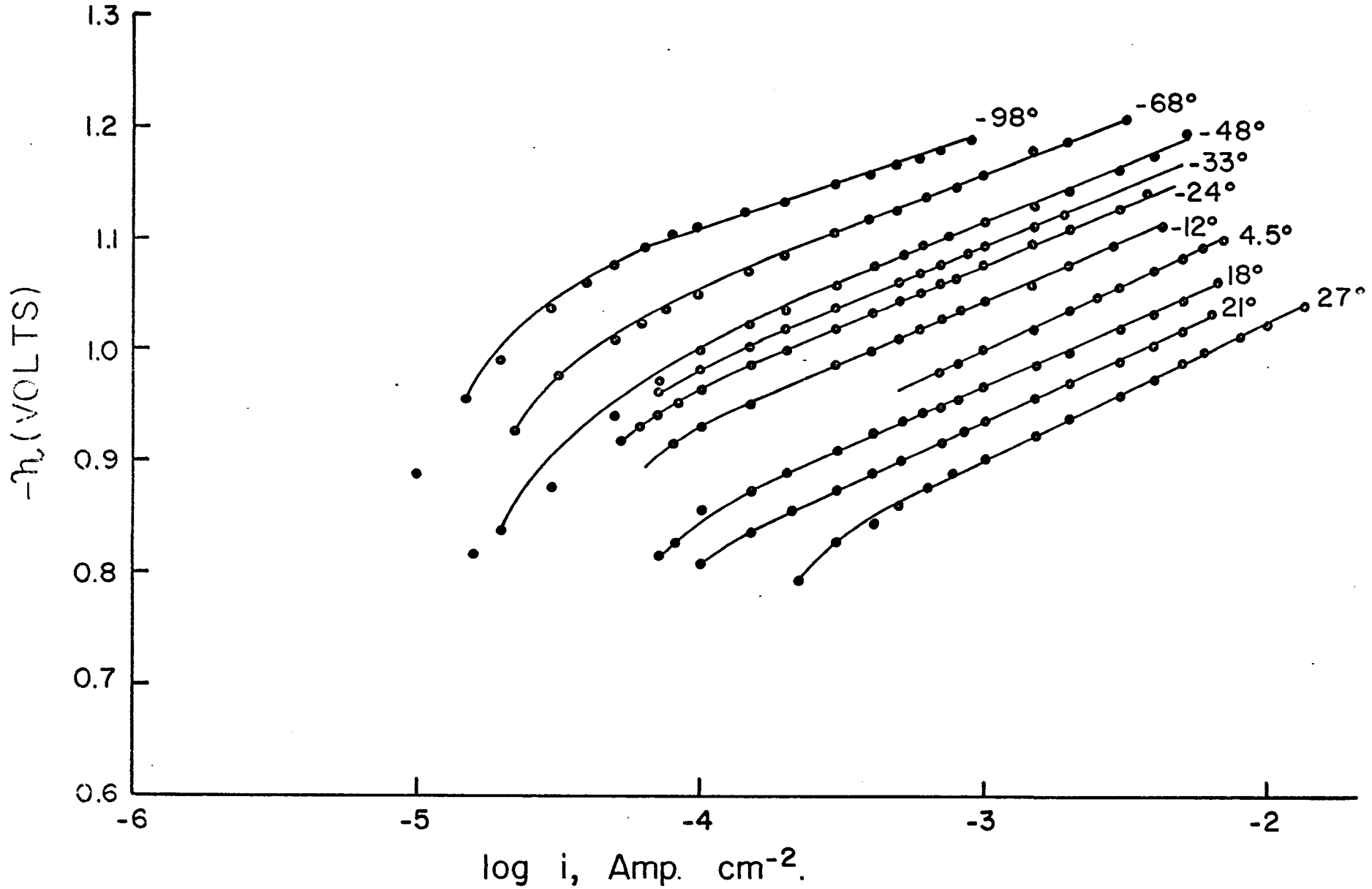
1.3
1.2
1.1
1.0
0.9
0.8
0.7
0.6
-η (VOLTS)
-6
-5
-4
-3
-2
log i, Amp. cm⁻².
-98°
-68°
-48°
-33°
-24°
-12°
4.5°
18°
21°
27°

Figure 32

Arrhenius type plots for the h.e.r. (solid circles) and the d.e.r. (open circles) at mercury cathodes in anhydrous methanol solutions.

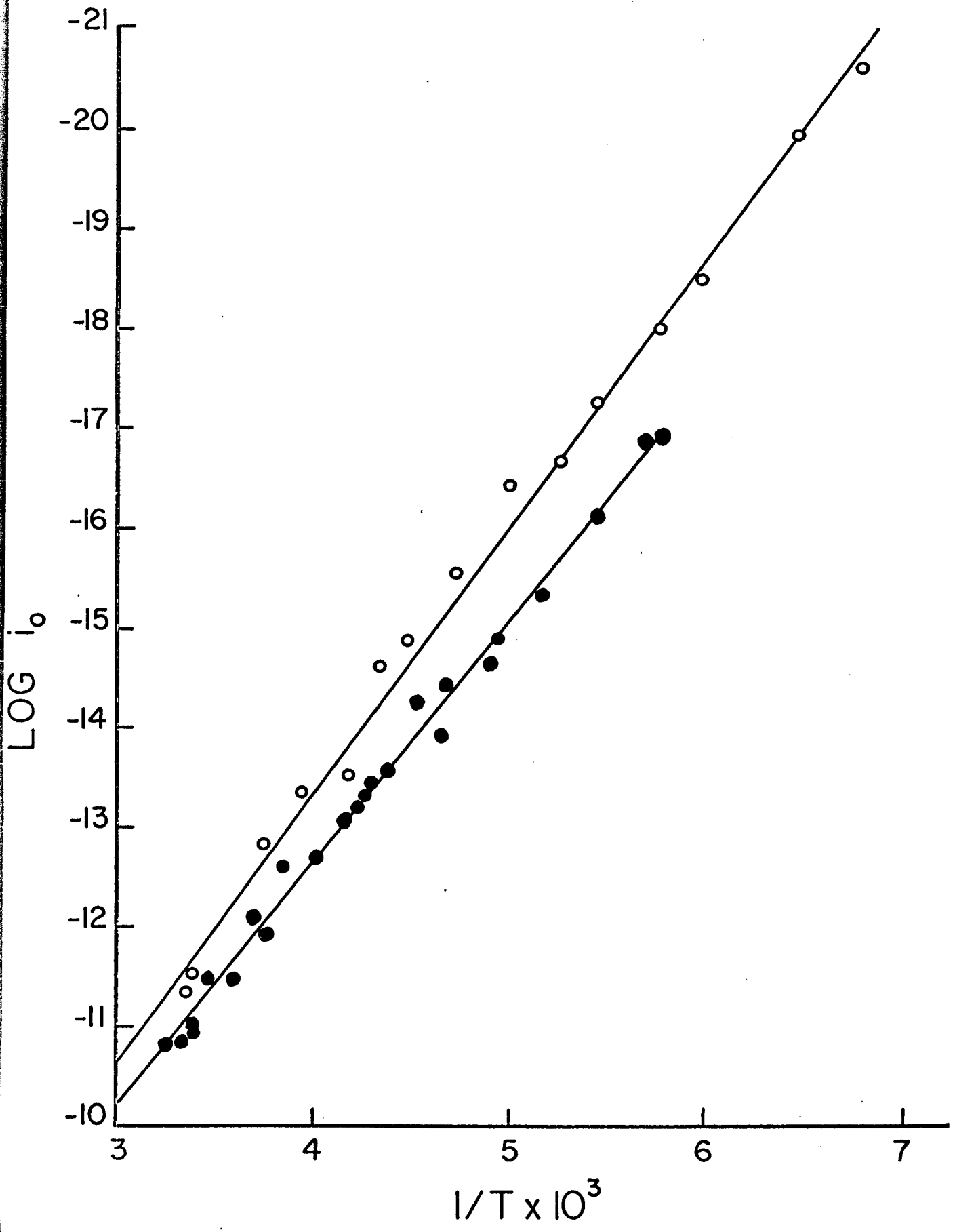
-21
-20
-19
-18
-17
-16
-15
-14
-13
-12
-11
-10
LOG i_o
3
4
5
6
7
1/T x 10^3

Figure 33

Tafel relations at mercury in CH_3OD/DCl as a function of temperature.

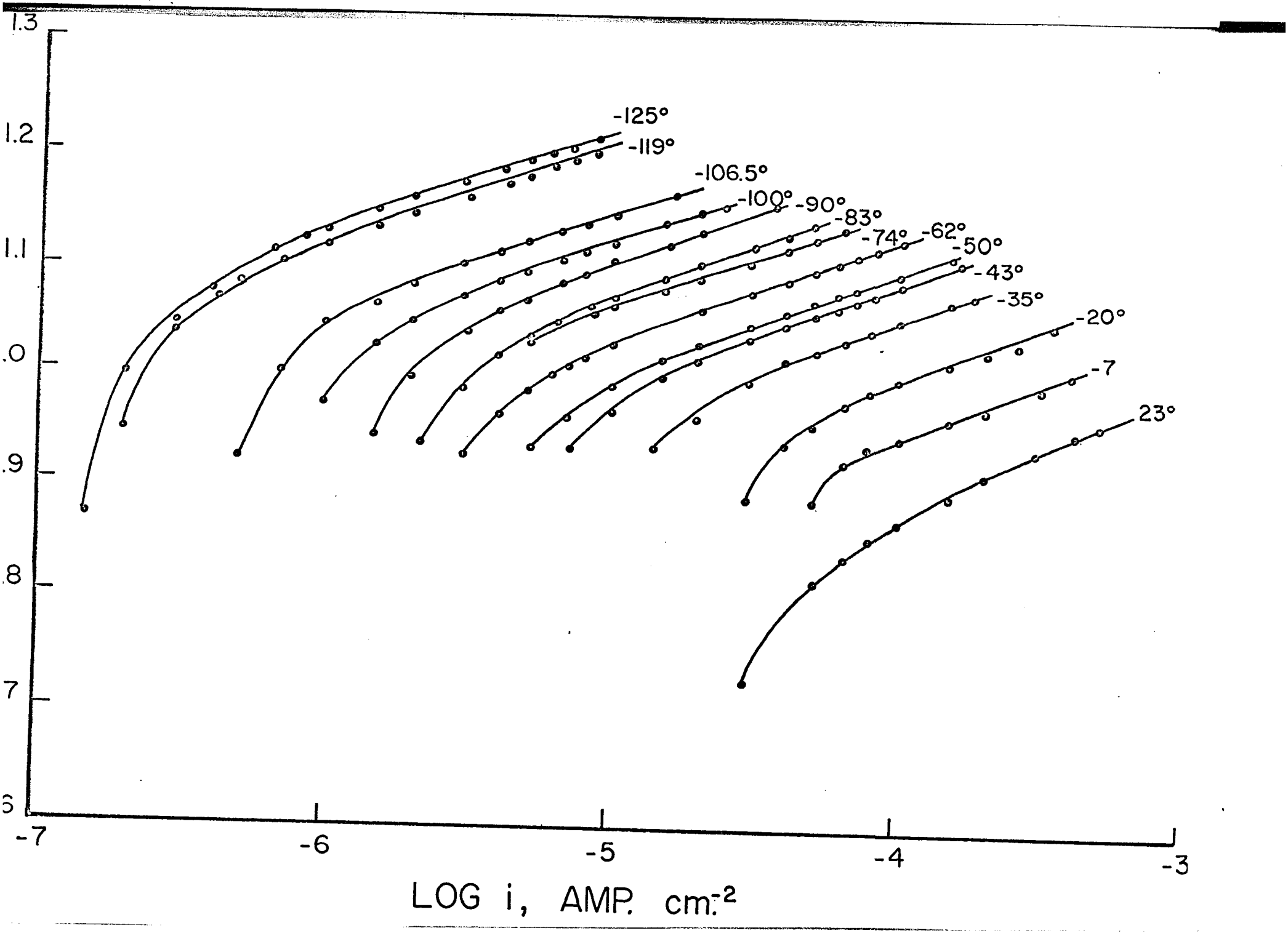
1.3
1.2
1.1
.0
.9
.8
7
6
-125°
-119°
-106.5°
-100°
-90°
-83°
-74°
-62°
-50°
-43°
-35°
-20°
-7
23°
-7
-6
-5
-4
-3
LOG i, AMP. cm.-2

Figure 34

Tafel slopes, b, as a function of temperature:

● - h.e.r. on mercury in CH_3OH/HCl

O - d.e.r. on mercury in CH_3OD/DCl

□,Δ - h.e.r. on platinum in C_2H_5OH/HCl.

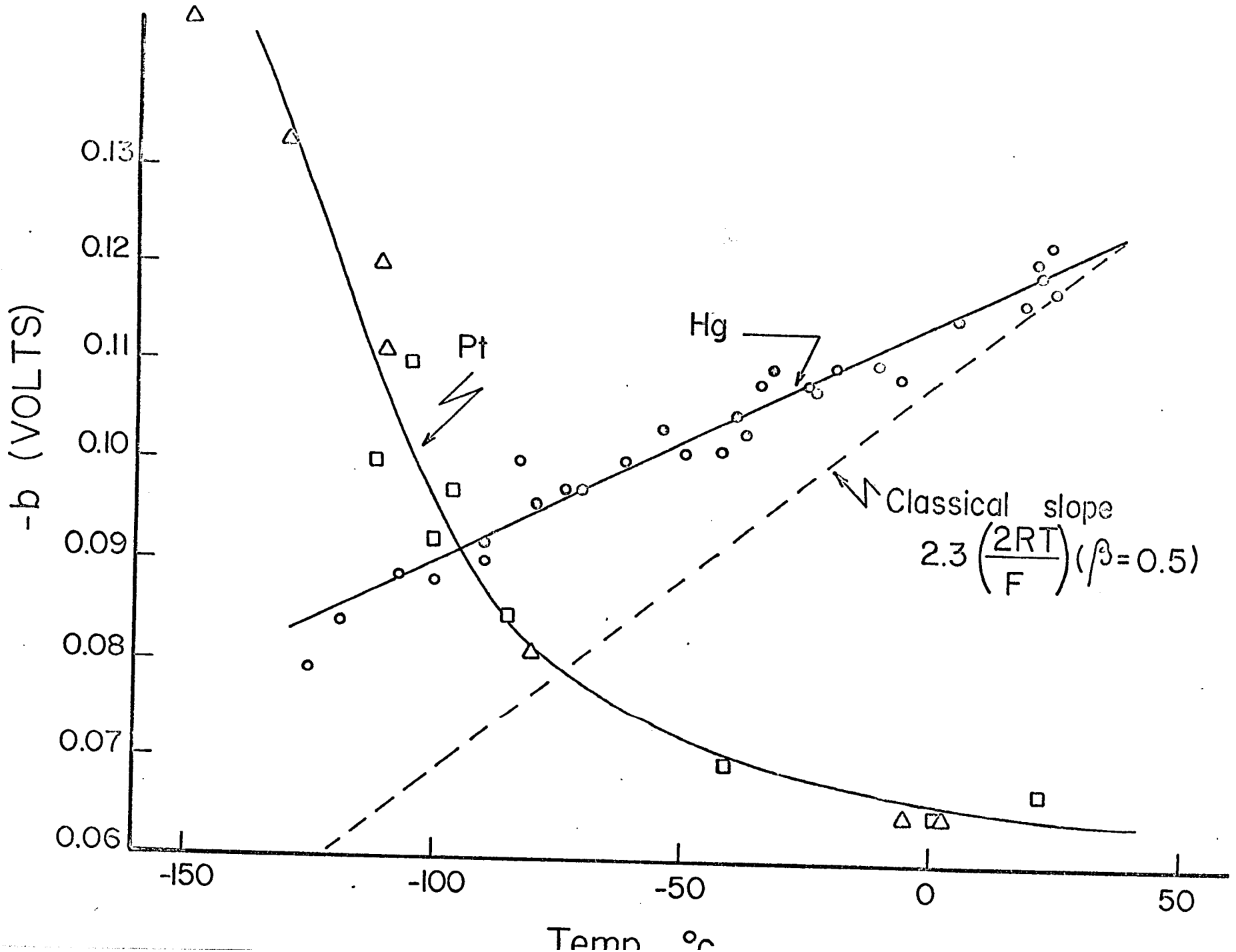
0.13
0.12
0.11
0.10
0.09
0.08
0.07
0.06
-b (VOLTS)
-150
-100
-50
0
50
Temp °c
Pt
Hg
Classical slope
2.3 (2RT/F) (β = 0.5)

experimental and classical theoretical values for $\beta = 0.5$. In addition, there is no significant difference between b values for the d.e.r. and h.e.r. at mercury. The major points of interest with regard to these results are therefore:

(1) The log i_o vs 1/T plots show no deviations from linearity.

(2) No discontinuity is found in the log i_o vs 1/T plot at the m.p. of mercury.

(3) The observed Tafel slopes are significantly higher than the values predicted by taking $\beta = 1/2$. It is in fact found that b is a linear function of temperature, but is independent of isotopic mass.

(ii) Platinum

Tafel relations for Pt were studied in ethanol solutions 1N in HCl down to -150°C and in ethanol solutions 2N in HCl down to -100°C. The Tafel curves for the 1N HCl runs are shown in Figure 35. Corresponding log i_o vs 1/T plots give identical apparent energies of activation of 5.5 Kcals $mole^{-1}$ for both the 1N and 2N acid concentrations. This is shown in Figure 36. The Tafel slope at room temperature in anhydrous ethanol was found to be -65 mV. Upon addition of water, the slope increased (b = -90 mV for 50-50 H_2O/C_2H_5OH mixtures) until in 100% H_2O the slope in this region is -120 mV. The -30-40 mV slope is not observed in ethanolic solutions as it is in aqueous solutions. The Tafel slopes for anhydrous C_2H_5OH solutions were observed to

Figure 35

Tafel relations for platinum cathodes in C_2H_5OH/HCl as a function of temperature.

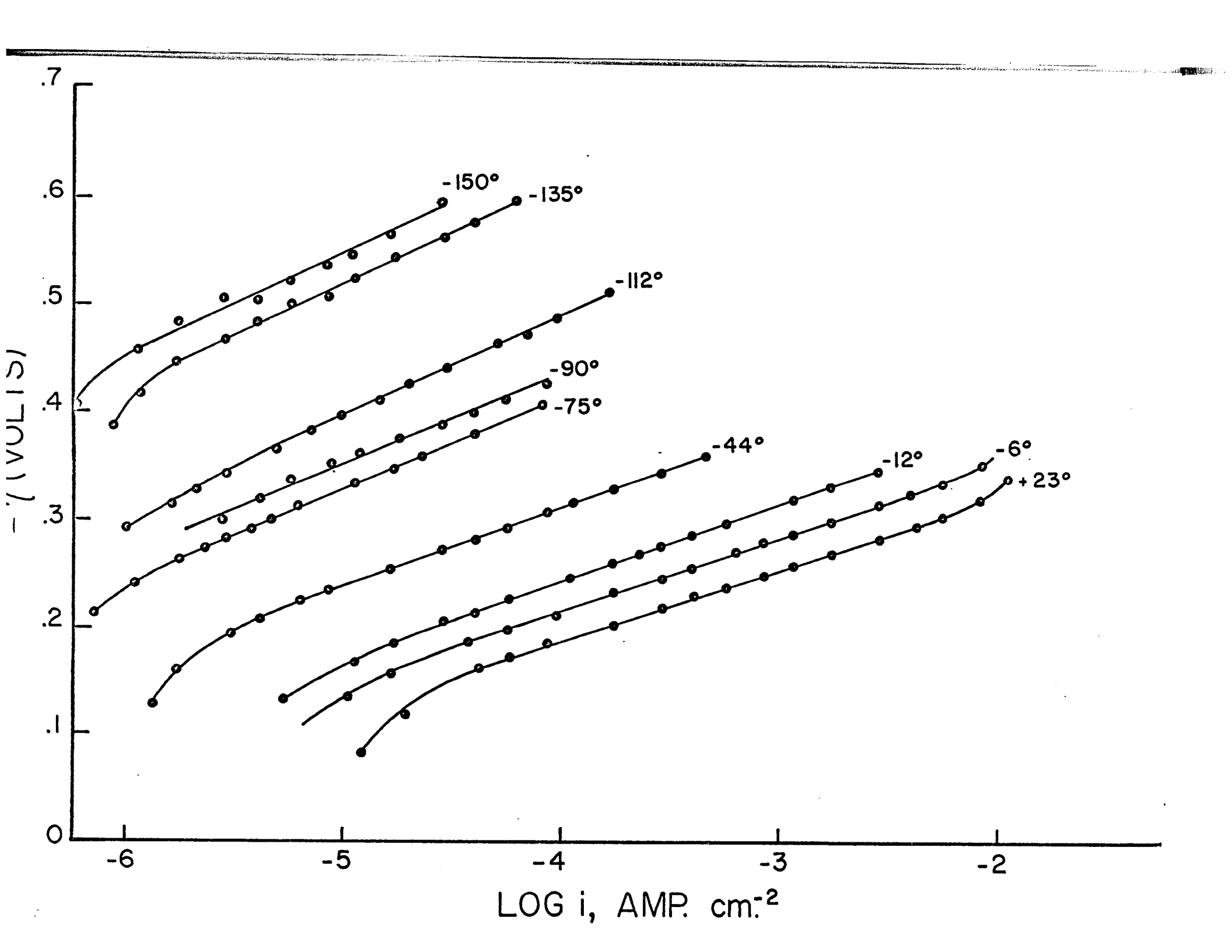
.7
.6
.5
.4
.3
.2
.1
0
-6
-5
-4
-3
-2
-150°
-135°
-112°
-90°
-75°
-44°
-12°
-6°
+23°
LOG i, AMP. cm.-2

Figure 36

Arrhenius type plot for the h.e.r. at platinum cathodes in C_2H_5OH/HCl.

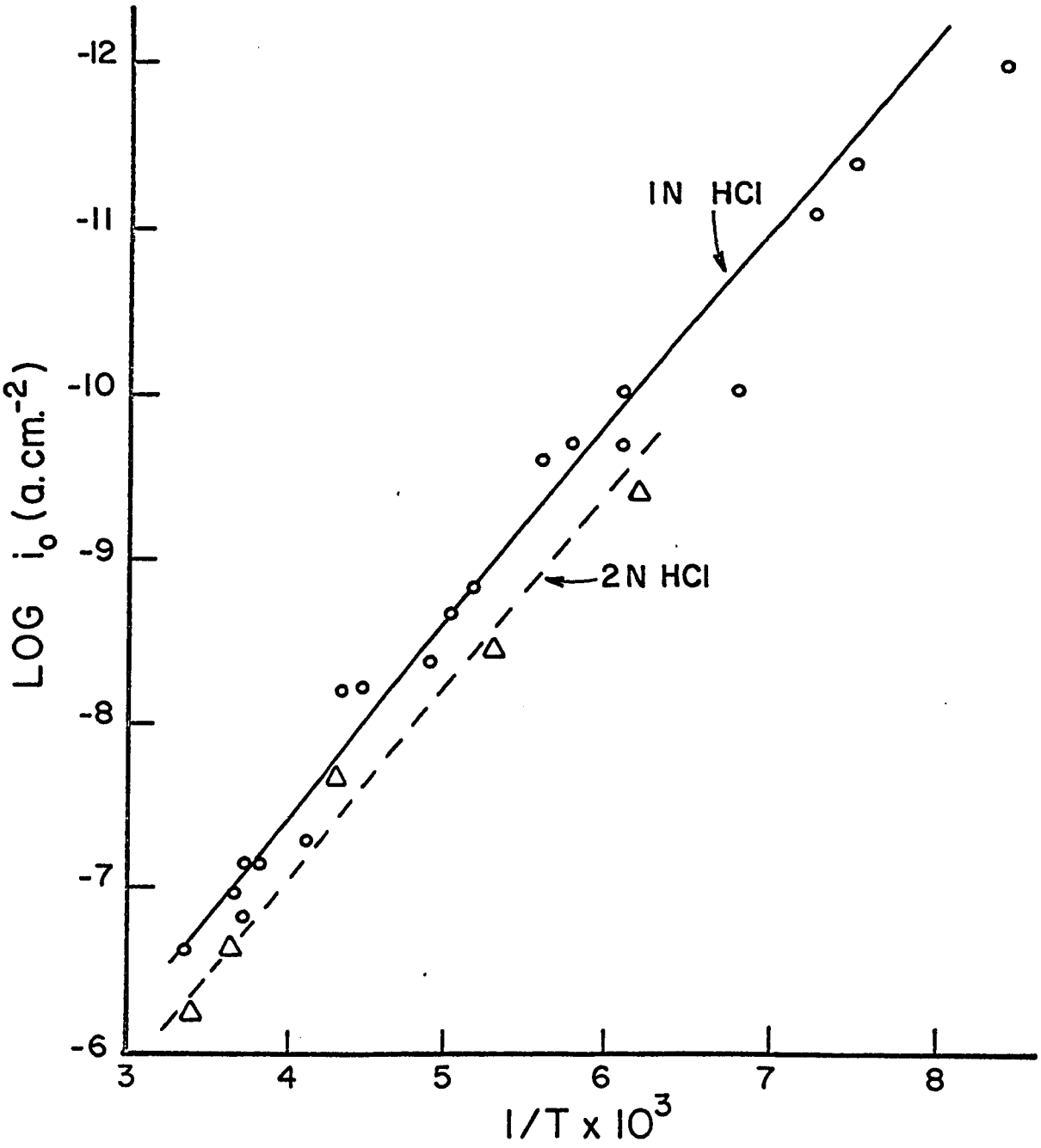
-12
-11
-10
-9
-8
-7
-6
LOG i_o (a.cm.$^{-2}$)
1N HCl
2N HCl
3
4
5
6
7
8
1/T x 10^3

remain constant down to 0°C at which point they began to increase as temperature decreased (see Figure 34). The major points of interest with regard to the platinum results are:

(1) The linearity of the log i_o vs 1/T plot down to -150°C in C_2H_5OH/HCl.

(2) The significance of the -65 mV slope with regard to mechanism.

(3) The increasing Tafel slope as temperature decreases.

C. S_D at Mercury in Acidic Methanol Solutions

Several values of S_D at room temperature at $\eta \doteq 1.1$ volt were obtained. It was found that $S_D \doteq 4.0$. Since the dependence of S_D on η was not studied in this system, the result serves only as a basis for comparison with the results in aqueous solution. The value of 4.0 for S_D is probably a minimum value since it corresponds to a high value of η (see Figure 31). This result is not inconsistent with the R values found in section B above, i.e. the R value at room temperature is 3.3 and is higher than the corresponding value of 1.9 in aqueous solution (111,112).

3. Discussion of Errors

A. Separation Factors

(1) Potential Control

A Wenking type 61-R potentiostat was used which kept the potential constant within ± 2 mV. Values of overpotentials

(η) were measured by means of a Radiometer vacuum tube potentiometer which could be read to within 0.5 mV. Experimental scatter (see Figures 28 and 29) cannot be attributed to errors in potential control or potential measurement.

(ii) H/D Analysis

Ions produced in the mass spectrometer range in mass from 1 to 6. In gas of low deuterium content, the H_2 to HD ratio is obtained from masses 2 and 3. In this case the D^+ contribution to mass 2 is negligible and the contribution of H_3^+ to mass 3 can be eliminated by an ion-pressure plot (122). The H_3^+ ion formation presumably takes place through an ion collision with a neutral molecule. Therefore the HD^+ contribution can easily be determined since the concentration of H_3^+ ions is proportional to the square of the pressure whereas the HD^+ ion concentration is proportional to the pressure itself. The electrolyte solvent (10% D_2O in H_2O by volume) could be prepared with a maximum error of 2%. The error in the mass spectrometer analysis is a maximum of 2-3%. For a 10% D_2O in H_2O solution, the $(D/H)_{soln}$ ratio is 0.111. A typical mass spectrometer analysis for $(H/D)_{gas}$ gave, for example, 8.1% HD and 91.9% H_2. The separation factor is then, using equation [105]

$$S_D = (0.111) \cdot \frac{2(91.9) + 8.1}{8.1} = 2.6 \pm 0.25$$

The maximum error in the separation factors is therefore estimated around ± 10%.

B. Results at Low Temperatures

(i) Tafel Slopes and log i_o Values

(a) Mercury

Slopes of the lines drawn through the log [current density]-potential data can be estimated to ± 2 mV. For mercury, extrapolation of the linear portion of these lines to obtain log i_o can lead to appreciable error since the extrapolation is made over 5-6 decades of current density. However, the method used to obtain the log i_o values was to draw the best line through the experimental η - log i points and calculate log i_o from the equation

$$\eta = a + b \log i$$

which gives, when $\eta = 0$,

$$\log i_o = -a/b \qquad [189]$$

where a is the value (negative for the cathodic process) of η when i is unity; also b is negative. This method is rather more precise than the graphical procedure when a long extrapolation is required.

(b) Platinum

Since for this case only a small extrapolation of the linear Tafel region to $\eta = 0$ is required, log i_o values were obtained by a direct graphical extrapolation.

(ii) Temperature Measurements

The cell was immersed in a coolant liquid in a Dewar flask provided with a mechanical stirrer. Temperature measurements were made with an (iso)-pentane thermometer. At low temperatures (around -100°C) the temperature was constant to within 2°. For example, a Tafel relation could be obtained in 5-10 minutes during which time the temperature rose about 2°C. The average temperature during this time was recorded.

(iii) Apparent Heats of Activation and Apparent Frequency Factors

(a) Mercury

The log i_o vs 1/T plots were fitted by least squares. The Arrhenius equation

$$\log k = \log A^* - \frac{E^*}{RT}$$

can be rewritten in the form

$$y = a + mx$$

The standard deviation of the slope m is given (157) by

$$(n-2)s^2 = \Sigma y^2 - \frac{(\Sigma y)^2}{n} \cdot \frac{(\Sigma xy - \frac{\Sigma x \Sigma y}{n})^2}{\Sigma x^2 - \frac{(\Sigma x)^2}{n}} \qquad [190]$$

where s^2 is the estimate of the variance of a single y measurement and the variance for m is

$$\frac{s^2}{\Sigma x^2 - n \bar{x}^2} \qquad [191]$$

Finally the standard deviation s_a of the intercept $\underline{a}$ is

$$s_a = s\left[\frac{\sum x^2}{n\sum x^2 - (\sum x)^2}\right]^{1/2} \qquad [192]$$

A least squares fit to the log i_o vs 1/T plot gives an apparent activation energy, E_H^*, of 11.21 kcals mole^{-1} and from equation [191] the error is ± 0.14 kcals mole^{-1}. Similarly, E_D^* = 12.28 ± 0.14 kcals mole^{-1}. The apparent frequency factor, A_H^*, is found to be 1.47 x 10^{-3} Amp. cm^{-2} and from equation [192] the standard deviation is ± 5%. Hence,

$$A_H^* = 1.47 \pm 0.074 \times 10^{-3} \text{ amp. cm.}^{-2} \text{ l. mole}^{-1}.$$

$$A_D^* = 2.50 \pm 0.13 \times 10^{-3} \text{ amp. cm.}^{-2} \text{ l. mole}^{-1}. \qquad [193]$$

$$E_D^* - E_H^* = 1.1 \pm 0.2 \text{ kcals. mole}^{-1}$$

$$A_H^*/A_D^* = 0.59 \pm 0.06.$$

(b) Platinum

For platinum there is significant scatter in the points on which the log i_o vs 1/T plot is based. In order to test the significance of the straight-ness of the line in Figure 36, a statistical analysis of variance of the regression coefficient of log i_o on 1/T was made for the first 9 points and last 10 points with decreasing temperature. The analysis shows that there is no significant difference of the slopes of the electrochemical Arrhenius plots (and hence E^* values) over the higher and lower ranges of temperatures. This matter is of some importance,

since it is with regard to constancy or otherwise of the heat of activation that one of the criteria for the role of significant tunnelling is based.

The procedure for the analysis of variance is briefly as follows: the data are set in two tables of $\frac{1}{T}$ (x) and -log i_c (y) for the two groups of data. The quantities y^2, $2xy$, x^2, Σy and Σx are obtained and the correlation coefficients r_1 and r_2 for the two sets of experimental results are calculated from

$$r = \frac{\Sigma(xy) - \frac{\Sigma x \Sigma y}{n}}{[(\Sigma x^2 - (\frac{\Sigma x}{n})^2)(\Sigma y^2 - (\frac{\Sigma y}{n})^2)]^{1/2}} \qquad [194]$$

for n pairs of log i and 1/T data. The corresponding regression coefficients R are then obtained from

$$R = \frac{\Sigma(xy) - \frac{\Sigma x \Sigma y}{n}}{\Sigma x^2 - (\frac{\Sigma x}{n})^2} \qquad [195]$$

The standard deviations σ_1 and σ_2 of the two groups of points about the regression lines with R values R_1 and R_2 are then calculated as

$$\sigma = \sqrt{(1-r^2)} \cdot \left(\frac{\Sigma y^2 - (\frac{\Sigma y}{n})^2}{n-2} \right)^{1/2} \qquad [196]$$

for the two groups of data. The weighted residual variance $\sigma_{1,2}^2$ is then calculated as

$$\sigma_{1,2}^2 = \frac{(n_1 - 2)\sigma_1^2 + (n_2 - 2)\sigma_2^2}{n_1 + n_2 - 4} \qquad [197]$$

The variance of R values is given by

$$\sigma_{R_1} = \sigma_{1,2}^2 \Big/ \left[\Sigma_1 x^2 - \left(\frac{\Sigma_1 x}{n}\right)^2\right] \qquad [198]$$

and similarly for σ_{R_2}. The variance of their difference σ_Δ^2 is given by

$$\sigma_\Delta^2 = \sigma_{R_1}^2 + \sigma_{R_2}^2$$

This is compared with the difference of R_1 and R_2 by obtaining the statistical parameter t as

$$t = \frac{R_1 - R_2}{\sigma_\Delta} \qquad [199]$$

and comparing the calculated value with that tabulated for $n_1 + n_2 - 4$ degrees of freedom. The values obtained are

$r_1 = 0.966$; $\sigma_1 = 0.20765$; $R_1 = 1.2388$

$r_2 = 0.975$; $\sigma_2 = 0.2424$; $R_2 = 0.9647$

$$\sigma_{1,2}^2 = 0.050413$$

$$\sigma_\Delta^2 = 0.21985$$

Then $t = \dfrac{1.2388 - 0.9647}{(0.21985)^{1/2}}$

$= 0.5844.$

With $n_1 + n_2 - 4$ (= 15) the value of t obtained is less than

that required for the 10% significance level i.e. the results over the range of temperatures studied form an indistinguishable population with a probability of better than 10:1 (the 10% level) so that there is no statistically significant trend of the apparent heat of activation with decreasing temperature. For the results at mercury, similar conclusionsapply and the deviations of individual points from a linear Arrhenius plot are less than at platinum.

(iv) Presence of H in the Pure D Solutions

The heavy water used to prepare CH_3OD and D_2SO_4 was obtained from Atomic Energy of Canada, Ltd., and contained 99.76% D_2O. In evaluating the ratio $i_{o,H}/i_{o,D}$, it is assumed, as indicated in previous work (125), that any apparent contribution to $i_{o,D}$ from the minute amounts of H present is negligible. An analysis of this problem has been published previously by Conway (125).

CHAPTER V

QUALITATIVE DISCUSSION OF RESULTS

For convenience, the discussion of experimental results has been divided into two chapters. The present Chapter contains a qualitative discussion of the experimental results. Several new concepts with regard to the h.e.r. are proposed and references to the literature, in support of these concepts, are given. Chapter VI contains a more quantitative discussion in which the conclusions of the present chapter are supported by theoretical but somewhat empirical calculations.

1. Mercury

A. Separation Factor

(1) General

In the previous discussion (Chapter II) it was shown that the pH, Tafel and capacitance behavior at mercury electrodes could only be explained in terms of the slow discharge mechanism [1]. In the separation factor experiments, no evidence for anomalous maxima, which were indicated in some of the previous work (116,118), is found and this is in agreement with aspects of other work (115,117). One of the difficulties in some of the previous work (118) was that H/D analyses were based on collection of 0.1 cc. of liquid water (i.e. H_2 and HD were oxidized to H_2O and HDO) which was analyzed by an infra-red method. Much more

gas (ca. 130 cc.) must be collected for such a procedure than that required for mass-spectrometric analysis and problems of time variation of the kinetics at low overpotentials, where longer times of electrolysis (3-12 hours) are required, become limiting. Also, in this work (118), the galvanostatic or constant current method rather than the constant potential method was used. As the authors state (118), only "average potentials" could be recorded.

The separation factors are found to decrease as η increases and it is of interest at this point to offer a qualitative explanation of this fact. Vielstich et al. (117) have regarded it as arising on account of different values of the symmetry coefficient β (cf. equation [152]) for electrochemical discharge of H and D, respectively, from H_3O^+ and H_2DO^+. For the slightly different case of discharge from acids in pure H_2O and D_2O solutions, no evidence is found for a significant isotopic dependence of β at Ni, Pt, Au, Cu, and Pd (125) and Fe (45). However, for mercury, Post and Hiskey (112) have reported a difference of about 3 mV in the Tafel slopes for pure H_2O and D_2O solutions. This difference is of the order of the usual error involved in Tafel slope measurements (i.e. $\pm$ 2 mV). On the basis of the present work in methanolic solutions, no significant difference in Tafel slopes for runs in pure H and D solutions is found.

(ii) Potential Dependence of S_D

On the basis of theoretical calculations to be presented in Chapter VI, it may be suggested that the observed diminution of S_D values with increasing overpotential could arise from either one, two or all of the following possibilities:

(1) Increase of potential results in a compression (electrostriction) of solvent in the double-layer [as treated by MacDonald (135)], with a consequent effect on the force field in which the proton transfer occurs in the double-layer. The field in the latter is ca 10^7 v. cm^{-1} so that electrostriction analogous to that at ions in solution may arise. This compressional effect could effectively increase either the force constants for lateral bending, since the H,D, or T complex could suffer more repulsion with neighboring solvent molecules in the double-layer, or change the force constants for the symmetric stretch, or both. This latter point is of importance since it is reasonable to expect that the metal-oxygen interaction (e.g. in the $Hg-H-OH_2$ complex) could very likely vary as a function of potential and that the distance of the O from the Hg surface may depend on potential. Qualitatively, it can be shown that the metal-H_3O^+ interaction is considerable and increases as potential increases. The model is that of an H_3O^+ ion adsorbed in the double-layer at the metal surface and at some potential Ψ_1. Beyond the Ψ_1 plane, the energy varies as $e\phi_x$ across the double-layer with a repulsive energy associated with electron overlap and with dehydration. As a repulsive

energy function for Hg----O, the function given by Vanderslice (173) for the O-O interaction is chosen. The Vanderslice repulsive function is

$$R_{O-O} = 1.87 \times 10^4 e^{-3.57\ r} \text{ kcals. mole}^{-1}$$

For the Hg-O repulsion, the above equation is modified by changing the scale units of the distance r to be reasonable for the Hg-O system. The modified Vanderslice potential energy repulsive function is then

$$R_{Hg-O} = 1.87 \times 10^4 e^{-3.57\ (r-0.15)} \text{ kcals mole}^{-1} \qquad [200]$$

The correction term r-0.15 in equation [200] is derived empirically as follows: for the O-O system, R equals 1 kcal $mole^{-1}$ at $r = 2.75$ Å, i.e. R is taken arbitrarily as 1 kcal $mole^{-1}$ when r is the sum of the van der Waals radii for the two atoms involved. The van der Waals radius for the O atom is 1.4 Å (194) and 1.5 Å for the Hg atom. R is therefore adjusted to equal say 1 kcal $mole^{-1}$ when r equals the sum of the van der Waals radii of O and Hg. Taking the potential drop $\phi + \psi_1$ through which the H_3O^+ ion must cross as, for example, 1 volt (23 kcal $mole^{-1}$), a Morse type curve can be drawn for the $Hg-OH_3^+$ system and is shown in Figure 37. From the change in energy as a function of distance about the minimum of this Morse type curve, a force constant of 0.2 m.d.$Å^{-1}$ is estimated, which is not by any means insignificant. The energy of interaction is found to be

Figure 37

Morse type curve for the electrostatic interaction between a charged metal surface and a hydronium ion ($\phi \rightarrow \psi_1 = 1$ volt).

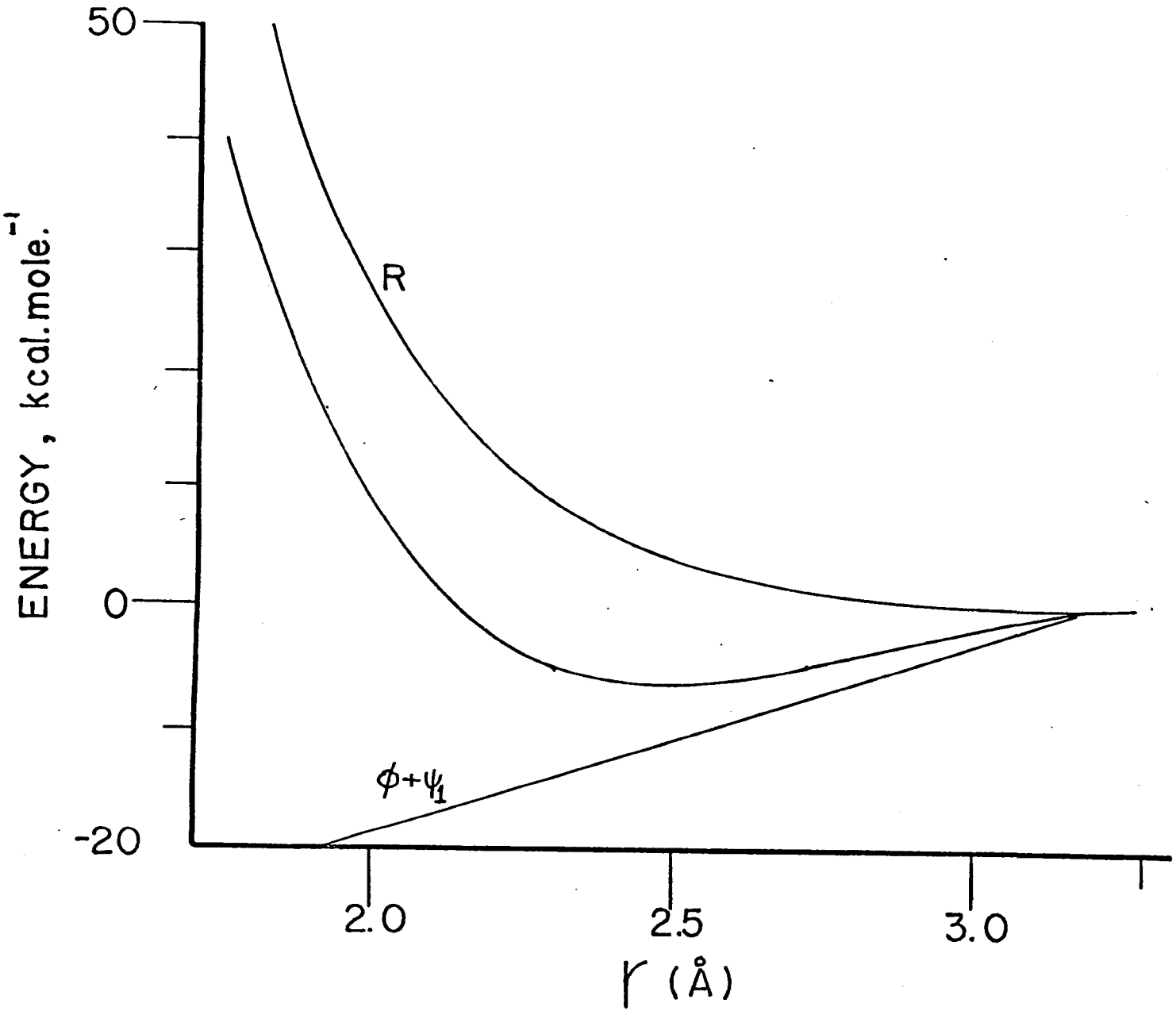
50
0
-20
ENERGY, kcal.mole.$^{-1}$
R
$\phi+\psi_1$
2.0
2.5
3.0
r (Å)

approximately -5 kcals. mole^{-1}. This interaction energy is analogous to that associated with the ψ_1 potential in the electrostatic theory of the double-layer. However, the method of calculation is quite different (see Chapter I). For Hg electrodes, the Tafel region in S measurements is between 0.9-1.4 volt, and we may expect this electrostatic attraction effect to be significant at these potentials. This calculation serves only to illustrate the fact that the Hg-O interaction can be important in the discharge step. Its effect on the symmetrical stretching frequency in the activated complex may therefore also be significant and potential-dependent.

(2) Field effects can change the potential energy-distance relation (cf. the Morse function for diatomics) and hence result in the variation of zero-point energy differences (220). This effect would be expected to be significant for transfer of charged species such as H^+OH_2 and play a minor role for uncharged species such as Hg-H. If the field effect were significant, a linear Tafel relation would not be found. Frumkin makes just this point in observing the extreme linearity of the Tafel relation at mercury over 7-9 decades of rate (29).

(3) Finally the effect of field may enhance the possibility of discharge at a dual site, i.e., initially discharge may occur at single metal sites and at high cathodic potentials

the discharge at dual sites may become more significant. Of all these explanations, (2) is the least probable one. In the next chapter, calculations are presented which support the possibilities (1) and (3).

B. Low Temperature Behaviour

(1) Tafel Slopes

(a) Temperature Dependence

In the low temperature experiments on mercury, the slopes 2.3 RT/βF are found to decrease but are always appreciably larger at each temperature than the values calculated by taking β as its usual value of 0.5. This could be explained in terms of a tunneling mechanism on the basis of which higher Tafel slopes can be predicted (cf. Chapter III), if it were not for the fact that the slopes for the d.e.r. are indistinguishable from those for the h.e.r. (figure 34) and also that the apparent heat of activation $E^{\#}$ is constant (Figure 32) and shows no sign of reaching a limiting lower value. If the tunneling mechanism were insignificant, then this Tafel slope behaviour can only be explained by taking β to be a linear function of temperature. Post and Hiskey find β to be constant in 0.1 HCl and DCl aqueous solutions of H_2O and D_2O, respectively, over the temperature range of 4° to 75°C (111,112). However Parsons et al. (129,133), who studied the h.e.r. on mercury in CH_3OH/0.1N HCl solutions

below room temperature, but not with the purpose of examining the tunnel effect, found β to be a linear function of temperature above the melting point of mercury.

The temperature dependence of β can be explained by one or several of the following possibilities:

(1) A distribution of configurations of the dipolar H_3O^+ ion with respect to the electrode surface [model (i)] is involved corresponding to a distribution of initial states in the proton transfer step. Generally more oriented states at the surface will tend to prevail at the lower temperatures. This could be consistent with relatively lower slopes of the initial state curve at lower temperatures for a more favorably oriented initial state configuration of H_3O^+. However, such a model would also be expected to lead to a temperature dependent H^* which is not observed within the experimental error.

(2) Higher temperatures favor greater population of states in vibrational levels above the ground state levels of H_3O^+ [model (ii)]. With respect to the OH bond of H_3O^+ undergoing reaction (proton transfer) towards the surface, the H^+ entity in the initial state will be slightly nearer on the average to the surface in the first vibrational state than in the ground state (anharmonicity effect). The potential drop across which such a proton would have to fall to reach the transition state would

hence be less than from the ground state, i.e. β would tend to be smaller [model (ii)]. This is in the opposite direction from that required to explain the observed trend.

(3) Surface potentials determine the effective value of β [model (iii)]. Here it would be supposed that the total metal-solution p.d. $\Delta\phi$ is made up in the usual way of $\Delta\phi_x$ due to oriented surface dipoles (solvent orientation and asymmetry potential at the metal interface) and a coulomb potential $\Delta\phi_q$ due to excess charge. Using a recent model of the double-layer (98) in which adsorbed reactant ions are outside a layer of oriented solvent molecules adsorbed at the interface, it is seen that the transition state $\neq$ could arise within a distance over which the p.d. $\Delta\phi_q$ operates, i.e. $\gamma = \Delta\phi^{\neq}/\Delta\phi_q$ (see model iii) where γ may be ca. 0.5. However, $\Delta\phi_q$ is itself some fraction α of $\Delta\phi$. The overall symmetry factor referring to effect of metal-solution p.d. on the rate i will be denoted in the usual way by β, i.e.

$$i = i_o \exp[-\beta\Delta\phi F/RT]$$

for a simple ion discharge step for constant diffuse double-layer configuration. From the above definitions, $\beta\Delta\phi F$ may be written as $\alpha\gamma\Delta\phi/RT$ with $\alpha = \Delta\phi_q/\Delta\phi$. It may be assumed that solvent dipole orientation is temperature dependent and stronger orientation tends to arise at lower temperature, so that $\Delta\phi_x$ increases. At a given $\Delta\phi$, $\Delta\phi_q$ will hence decrease, i.e. α diminishes with decreasing temperature. Since $\beta = \alpha\gamma$, then $\alpha\gamma$

will more or less remain constant (since it is the true symmetry factor determined by the potential energy profile), and β will decrease with temperature as required. This type of model was also used previously (136) to explain anomalously high slopes in the Kolbe reaction at Pt. While the above conclusions follow satisfactorily on the basis of the recent model of the double-layer, it must be admitted that such a representation of the double layer by Bockris et al. (98) offers difficulties for the mechanism of H^+ discharge since the H_3O^+ ion in its initial state in the Helmholtz layer is relatively far removed from the electrode surface and needs two steps of proton transfer to reach it.

(4) It could be argued that anion (Cl^-) adsorption increases at lower temperatures and causes an increased Tafel slope (smaller β). This appears unlikely as an explanation of β as f(T) since similar effects are also observed in aqueous solutions in the temperature range 0-40°C where the double-layer capacity information indicates that no Cl^- adsorption arises at the high negative potentials involved.

(5) The last, and perhaps the most reasonable possibility, is that proposed by Bockris and Parsons (11) for the Tafel slope behaviour in the temperature range 0-40°C. Using the simple parallel plate model for the double-layer at mercury, they assume the (local) dielectric constant does not vary with temperature and from the equation

$$C = \frac{\varepsilon}{4\pi\delta}$$

they calculate a rate of change of β approximately equal to 2.5×10^{-3} deg^{-1}. C is the differential capacity, the measured temperature dependence of which is 5×10^{-2} μF cm^{2} deg^{-1}. With the assumption that ε (dielectric constant) is constant, the observed change of C with T requires a change in double-layer thickness (δ) of 5×10^{-3} Å deg.$^{-1}$ The rate of change of β is associated with the rate of change of δ through the relation

$$\beta \doteq \frac{\text{distance from initial to activated state}}{\text{distance from initial state to final state}} \qquad [201]$$

The value $d\beta/dT = 2.5 \times 10^{-3}$ deg.$^{-1}$ is obtained by constructing the potential energy profiles for the h.e.r. at several temperatures and obtaining β as a function of temperature from equation [201]. The value of $d\beta/dT$ obtained in the present work (cf. Fig. 34) is 0.7×10^{-3} deg.$^{-1}$

(b) Depolarization Effects in the η-log i Curve

The curvature of the Tafel relation at low current densities may be attributed to specific adsorption of the anion (29). In aqueous solutions, the pH dependence of η in concentrated solutions is found to be dependent on the nature of the anion (88). The results of Jofa et al. (137) in aqueous solutions containing I^- and Br^- anions show very similar decreases of polarization (lowering of η) at low current densities. The effect of anions, which certainly influences S_D for Pt (see below) may also have an effect at Hg. This is especially true in concentrated

solutions ($\geq$ 1N) as seen in Figure 25 for S_D vs η for mercury. The curvature is not due to depolarization effects associated with oxidizing impurities since the same behavior persists in the most carefully prepared and purified solutions which have been pre-electrolyzed for appreciable periods of time.

(ii) Heats of Activation and Frequency Factors

(a) Heats of Activation

At mercury, the Arrhenius type plot of log i_o vs 1/T does not show any curvature (Figure 32). Thus the critical region (from -20°C and below) is linear and the apparent heat of activation is constant over the entire temperature range studied. We do not find, as did Parsons et al. (133), a sharp break in the Arrhenius plot (but without change of slope), towards lower i_o values at the melting point of mercury ($1/T = 4.2 \times 10^{-3} {}^{o}K^{-1}$ The present results, if anything, indicate an increase in the apparent i_o values due to a slight contraction of the mercury surface. This contraction upon solidification of the mercury surface (i.e. the decrease in apparent surface area) is estimated to be about 15% and is counterbalanced by an increase in the real surface area by at least 10%. The increase in real surface area upon solidification of a mercury surface is reported to be around 10% (137) while for gallium the increase in real surface area is around 170% (192). Hence the i_o values found experimentally can vary at the most by a factor of two and since the logarithms of those

values are plotted, the difference is quite small. Below the freezing point of mercury, it is estimated that the error involved in i_o due to a surface area change is $\pm$ 5%.

From Figure 32 we can obtain the apparent heats of activation, E^*, for the h.e.r. and d.e.r. It is found that $E_H^* = 11.2$ kcal mole^{-1} and $E_D^* = 12.3$ kcal mole^{-1} (cf. equation [193]). The value of 11.2 kcal mole^{-1} for E_H^* obtained in the present work differs from the value $E_H^* = 18$-20 kcal mole^{-1} reported by others (129,133,138) in methanol HCl solutions. In order to clarify this discrepancy, we have taken the log i_o values reported by Parsons and Bockris (129) and plotted them against 1/T and find $E_H^* \doteq 8$ kcal mole^{-1} whereas they report a value of $E^* \doteq 20$ kcal mole^{-1}. Similar results are obtained using the data of Hine and Sobkowski (138). The values of E_H^* (for $\eta = 0$) were apparently calculated (133) from the relation

$$E^* = E_H^* - \beta\eta F \qquad [202]$$

where E^* is the apparent activation energy for a given value of η (obtained by plotting log i at constant η versus 1/T). E_H^*, the value at $\eta = 0$ was then calculated from equation [202] assuming a constant value of β which is experimentally incorrect. The significant quantity to be used in E_H^* determinations is rather the exchange current density, i_o. In aqueous solution, a plot of log i_o versus 1/T indeed gives a value of 21 kcal mole^{-1} (111) which is consistent with the treatment of several other

investigators (29,88,137). The difference in apparent energies activation, for the h.e.r. and d.e.r. in methanolic solutions, $E^* = E_D^* - E_H^*$, is 1.1 kcal. mole^{-1} and is constant over a temperature range of 125°. The corresponding quantity in aqueous solution over a temperature range of 66° (+ 4° to +70°C) is 1.1 kcal. mole^{-1} (111,112).

(b) Frequency Factors

The ratio of apparent frequency factors, A_H^*/A_D^*, found in the present work is 0.59. Post and Hiskey's data for the h.e.r. in aqueous solution (111,112) lead to $A_H^*/A_D^* = 0.5$. In view of this value, several authors have concluded that proton tunneling is significant in the discharge reaction (26,29). For electrochemical reactions, however, it is necessary to define isotopic ratios of frequency factors with some care since two important factors enter into their determination which have not been previously discussed and are not involved in the case of ordinary chemical reactions. These factors will be examined quantitatively in Chapter VI where it is shown that the true frequency factor ratio, A_H/A_D, is close to unity. Hence the conclusion that tunneling is significant, based on an apparent frequency factor ratio of 0.5 (26,29), can no longer be maintained.

2. Platinum

A. Separation Factors

(1) General

The pH dependence of η and i was seen to be consistent

with a rate-limiting atom recombination step [3] at low current densities and atom-ion recombination [2] at high current densities. The observed Tafel slope of 30-40 mV at low current densities can be interpreted in terms of the limiting Langmuir assumption for $\theta_H \rightarrow 0$ or the non-activated Temkin case (see Table I) for the atom recombination mechanism [3]. The slope of ca. 120 mV observed at high current densities is described by the limiting Langmuir condition of $\theta_H \rightarrow 1$ for the atom-ion desorption process [2]. In discussing the basis for the shape of the S_D-η curves on Pt and the effect of anions (see Figure 30), the above mechanisms must not be contradictory. Horiuti (11,12) and Bockris (114) have attributed the initially increasing slope of the S_D-η relation to a change in mechanism (e.g. from [3] to [2]). That this cannot be the explanation of the shape of the S_D-η curve is arrived at by the following considerations:

(a) If this increasing value of S_D with potential is attributed to an increasing participation of the rate-determining mechanism [2] in parallel with mechanism [3], the origin of the maximum in S_D is not well explained. If the initial rate-determining step is atom-atom recombination which predominates in the low overpotential Tafel region (see Figures 26 and 27), then the increasing contribution to the rate by the atom-ion desorption mechanism, which is regarded as predominating in the high over-potential Tafel region, should lead to a constant maximum value of S_D characteristic of step [2] operating at high cathodic

potentials. The eventual decrease of S_D at high overpotentials cannot be satisfactorily explained on this basis. In addition, if it is conceded that the atomic recombination step is in fact rate-determining at low overpotentials as implied by the above assignment of mechanism based on Tafel slopes (cf. Bockris (114)), then values of S_D equal to 3-4 must be explained in terms of the atom recombination mechanism. However, Bockris (114) has maintained that S_D based on a rate-determining atom-atom recombination gives rise to values of 6-8. Horiuti (12), in an effort to avoid this apparent anomaly, proposed that H_2^+ molecule-ion neutralization step [4] is rate-determining at low overpotentials and the increase in S_D is due to a change in rate-controlling mechanism from step [4] to [3]. In Chapter II, it was shown that at platinum, both the pH behaviour and values of the Tafel slopes lead unambiguously to indication of a slow atom-atom recombination step followed by slow atom-ion desorption at higher overpotentials. If then it can be shown that values of S_D of 3-4 can arise as a lower limit for the atomic recombination mechanism, the shape of the S_D-η curve (Figure 30) can be satisfactorily explained as discussed below (see also Chapter VI).

(b) The increase in S_D which is supposed to arise on account of the parallel participation of reactions [2] and [3] as discussed above offers no explanation of the effects of anions which have been found in the present work. It is proposed here

that the initial rise in S_D is due solely to effects (e.g. changing coverage) associated with the recombination step [3] and that at the maximum, reaction [2] begins to take over as the rate-determining step. The reason for the rise in S_D may be attributed to hydrogen adsorption effects and to specific adsorption of anions. It has been established that coverage by hydrogen at smooth platinum is appreciable (142) even at the reversible potential (143). Since surface coverage by hydrogen is significant, the effect of surface interactions between adsorbed hydrogen atoms with each other, and/or with adsorbed anions must be considered as a basis for discussion of the variation of S_D with potential and anion of the electrolyte.

Hydrogen atom chemisorption cannot be considered as a simple case of covalent bond formation between a single metal atom and a hydrogen atom. Thus, in addition to the above effects, the possibility of multiple bonding between a hydrogen atom and several metal atoms must be considered. The evidence for a complex model of hydrogen atom chemisorption and anion adsorption at platinum electrodes is now presented.

(11) Nature of H-Atom Chemisorption at Metal Surfaces

Indications have existed for some time that there is a strong and weak type of hydrogen chemisorption referred to, respectively, as type A and type C (144). At sufficiently low temperatures only type C exists (145). At higher temperatures

type A is thought to predominate and the rate of adsorption is given by the Elovitch equation, rate α exp (-bx), where x is the amount of gas adsorbed in the slow process (146).

Recent approaches to the nature of bonding of hydrogen at "active" metals have been based on the d-band theory (147). In this theory, cohesion is ascribed to resonance between all possible structures in which the electrons form definite one or two electron bonds between atoms. In the case of the transition metals, Pauling concluded that there are three types of d-orbitals which are: bonding d orbitals involved in dsp hybrids; atomic d-orbitals associated with individual atoms, but not involving bonding; and metallic d orbitals, participating in electronic conduction. If hydrogen atom chemisorption proceeds through this type of bonding (i.e. its electron becomes associated with empty d-orbitals of the metal forming a covalent bond), then it would be expected that the resulting M-H species would be dipolar with the hydrogen atom constituting the positive end of of the dipole. However, Mignolet (148) has found that the "surface potential"*, for example, of nickel, covered with adsorbed hydrogen, is negative; this indicates that the negative end of the dipole is directed outwards from the surface (149). This situation is still compatible with the d-band theory if it is

---

* I.e the change of surface potential from that at the metal-vacuum interface.

assumed that the H-atoms constitute the positive part of the dipole and at the same time penetrate deep enough into the surface to be situated below the uppermost layer of metal atoms (148,150). On this basis, the model that H atom chemisorption can occur at multiple sites, i.e. interstitially in the surface (151,152) is entirely reasonable.

Eischens and Pliskin (153) have found experimental support for this model by studying the I.R. spectrum of hydrogen adsorbed at silica-supported platinum. Two bands were observed in the spectrum of hydrogen chemisorbed on platinum. The first band at 2058 cm^{-1} was attributed to a strongly bound hydrogen species and the second band at 2109 $cm.^{-1}$ was attributed to a weakly bound species. The force constant of the strongly bound species is calculated to be 2.52 md $\overset{o}{A}^{-1}$ for which Eischens and Pliskin proposed the structure Pt.H.Pt. If the two platinum atoms are rigid, (153) i.e. if they do not vibrate with respect to one another, the force constant of 2.52 md $\overset{o}{A}^{-1}$ may be regarded as twice the force constant of the single electron bond species Pt. H (because one bond is compressed while the other is stretched). The force constant for the Pt.H species would then be 1.20 md $\overset{o}{A}^{-1}$. This is similar to the force constant of 1.4 md $\overset{o}{A}^{-1}$ for the single electron bond in diborane (154). The

authors propose the two possible structures

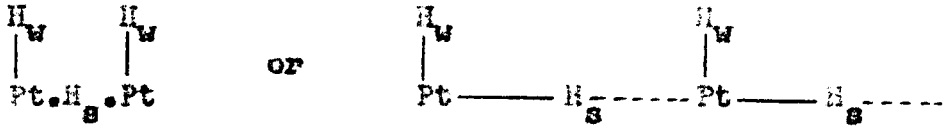

where the H_s and H_w refer, respectively, to the strongly and weakly bound species.

Mignolet (179) in his surface potential studies also found evidence for two types of H-atom adsorption. One increased the work function and the other decreased it. The former type appeared at low coverage at -190°C while the latter predominated at higher coverages at -190°C and at all coverages at 20°C.

Suhrmann et al. (180) found evidence for two types of H adsorption on platinum films from the observations of changes of electric resistance and photoelectric emission as a function of coverage. In one type of adsorption, the H decreased both the work function and the resistance and predominated at all coverages and temperatures above -183° C. A second type of adsorption was detected at low coverage below -183°C which increased both the work function and the resistance.

Sachtler and Dorgelo (181) observed that upon adsorption of hydrogen the resistance, (a) decreases at 0°C by 0.7%, (b) either increased or decreased at -196°C depending on factors such as film thickness etc., and (c) increased at -210°C

by 2.5%. These workers concluded that two types of adsorption occurred which, in this thesis, is thought to correspond to single and multiple site adsorption.

Will (167) has studied the electrochemical adsorption of hydrogen on the 100, 110 and 111 faces of platinum single crystal electrodes. The triangular sweep method (103,155) was used to estimate surface coverage on the various crystal faces as a function of temperature. In this method, a voltage varying linearly with time is applied to the electrode and the corresponding current is recorded as a function of time and hence potential. The current-time plot is equivalent to a capacity-time, or capacity-potential plot. A typical triangular sweep plot of current vs time for platinum single crystals is shown in Figure 38. Two to three maxima are observed and correspond, respectively, to two to three types of chemisorbed hydrogen. The coverage relating to these species is obtained by graphical integration of the area under each peak by reference to the following relation

$$q = \int_0^t i \, dt$$

The integral over the time interval 0-t is equivalent to one over a corresponding potential interval $\Delta\emptyset$ since $d\emptyset/dt$ is constant.

Figure 38

Triangular sweep plot of current versus time (schematic) at platinum single crystal electrodes (167).

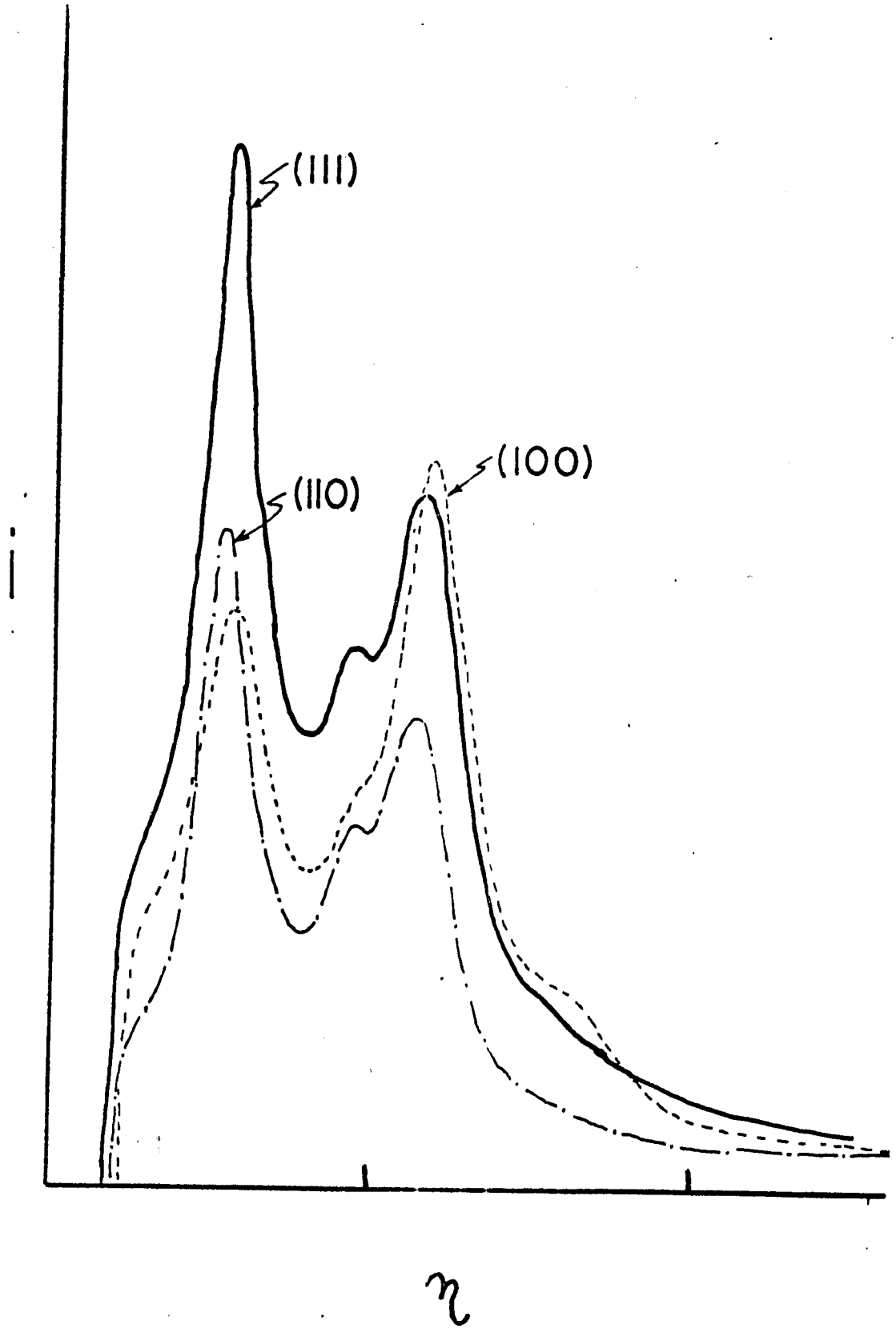
(111)
(110)
(100)
i
η

Here q is the charge which is directly proportional to the surface coverage θ_H (33) attained up to potential ϕ. The three crystal faces show distinctively different adsorption behavior. The relative heights of the first to the second adsorption maxima were found to vary on the various crystal faces in the order 110 > 111 > 100. The heats of adsorption for a given coverage were found to decrease in the order 100 > 111 > 110 and were associated with decreasing bond strength in the same order. A 2:1 ratio of total hydrogen to surface platinum atoms was found. The results were interpreted in terms of at least two different types of chemisorption involving an interstitially bound species (i.e. in the surface layer) and a species bound on the surface similar to that proposed by Bischons and Fliskin (see above).

(iii) Evidence for Effects of Anion Adsorption at Platinum Electrodes

Here we may cite, amongst other indications, the present work as evidence of effects of anion adsorption at platinum during hydrogen evolution (Figure 30). The work of Breiter et al. (103,155) on Pt, Ir, and Rh shows that as the tendency for specific adsorption of anions increases, the electrochemical H-adsorption energy decreases. Thus, it was found (103,155) that the tendency for specific adsorption of anions on platinum

decreases in the series

$$OH^- < ClO_4^- < SO_4^{-2} < Cl^- < Br^-$$

There is then a definite correlation between the negative dipole moment of Pt-H being directed towards the solution and the decrease in the hydrogen adsorption energy in the presence of adsorbed anions. Popat and Hackerman (104) have similarly found definite evidence for anion adsorption at potentials corresponding to hydrogen evolution. Their studies of double-layer capacity at appreciable negative potentials, where hydrogen evolution is occurring, show strong effects by anions in the order

$$I^- > Br^- > Cl^- > F^-$$

From these experimental facts, there can be little doubt concerning the effects of adsorbed anions at platinum electrodes during hydrogen evolution and their effects on the hydrogen chemisorption energy.

(iv) Effects of H/D Coverage and of Anions on S_D for Pt

In Chapter III, we have seen that the isotopic ratio of rate constants depends largely on the contribution of the zero-point energy differences in the initial state and the activated complex. The latter contribution is, from equation [42],

$$\prod_{1}^{3n^{\neq}-6} \frac{\sinh u^{\neq}_{1,D}/2}{\sinh u^{\neq}_{1,H}/2} \qquad [203]$$

where the product is taken over $3n^{\neq}-6$ degrees of freedom for a linear complex. If a non-linear complex is involved, as is the case for proton discharge at a dual adsorption site and for atom-atom recombination, the product is taken over $3n^{\neq}-7$ degrees of freedom. In Chapter III, it was shown that the zero-point energy differences in the initial state are independent of surface coverage and effects arising therefrom. This situation arises from the assumption that the pre-rate-determining steps are in quasi-equilibrium and therefore, terms involving coverage (e.g. θ_H and f_{MH}) are replaced by terms involving the bulk hydronium ion (e.g. $[H_3O^+]$ and $f_{H_3O^+}$). Hence the initial state is invariant with respect to the nature of the surface whereas the activated state is not. The increasing values of S_D as a function of increasing overpotential must therefore be explained by reference to equation [203] in terms of either or both of the following factors:

(a) Initial discharge may be regarded as occurring at a dual site so that if atom + atom recombination is rate-determining, the minimum number of atoms involved in the activated complex is 5 or 6. This corresponds to a minimum of 8 or 11 vibrations which will make the product in equation [203] quite small and hence tend to lead to smaller isotope effects.

Anion adsorption causes either surface interactions which weaken the M-H bond (i.e. it decreases the heat of adsorption (131,135)) or alternatively preferential adsorption of anions may arise at the available multiple sites. This effect is in a direction which increases the product in equation [203] (this follows since the M-H frequency decreases) and hence increases the isotope effect (see Chapter VI). As the tendency for the anion to be adsorbed increases, it would be expected on the above grounds, that larger isotope effects would tend to arise. This effect is precisely that which is found for S_D at platinum (see Figure 30).

(b) As the overpotential is increased at Pt, the surface coverage also tends to increase if mechanisms [2] or [3] are involved which results in increased surface interactions and a possible switch over from initially preferred multiple site adsorption to single site adsorption. Increased surface interactions result in a decrease in the heat of adsorption which gives rise to increasing k_H/k_D ratios. The switch over from multiple to single site adsorption leads to increasing k_H/k_D values because there are now $3n^{\neq}-7 = 5$ vibrations in the activated complex (this corresponds to the non-linear four atom system M-(H-H-M) compared with the 8 or 11 possible vibrations which arise when multiple site adsorption is considered.

B. Low Temperature Behaviour at Pt

(1) Tafel Slopes

(a) Assignment of Mechanism

The Tafel slope at room temperature is -65 mV and corresponds to the activated Temkin cases for either steps [2] or [3] where $\gamma \doteq 0.45$ (see Table I). Upon addition of water to the ethanol/HCl electrolyte, the Tafel slope increased to 120 mV thereby indicating rate-limiting atom-ion desorption [2] under Langmuir conditions when $\theta_H \rightarrow 1$. The rate-controlling mechanism of the h.e.r. at platinum in anhydrous ethanol is therefore believed to be the atom-ion recombination step. This situation is similar to the case for Pt in alkaline solution where the rate-determining step has also been indicated as the atom-ion recombination step (114) while in acid solution, atom-ion recombination is preceded, with respect to increasing potential, by atom-atom recombination (93).

(b) The Effect of Temperature on Tafel Slopes

As in the case of mercury, the Tafel slopes are not consistent with expected classical behaviour. They are found actually to increase as temperature decreases (see Figure 34). The increasing slopes could be associated with effects of increasing H coverage for the atom-ion mechanism proceeding under activated conditions (36) at intermediate coverage changing to conditions of fuller coverage at the lower temperatures.

(c) Depolarization Effects in the η-log i Curve

The low current density regions in the η-ln i curves, shown in Figure 35, all display a significant falling off (depolarization) of overpotential with decreasing current density similar to that observed for mercury. The effect is attributed to the specific adsorption of anions as discussed above for the case of mercury.

(ii) Heat of Activation

The runs in anhydrous ethanolic-HCl solutions at Pt were carried out down to -150°C and the extrapolated log i_o values were plotted against the reciprocal of the absolute temperature as has been shown in Figure 36. The apparent energy of activation is 5.5 kcal mole^{-1} and this may be compared with the value of 5.2 kcal mole^{-1} obtained by Parsons for the h.e.r. in 0.1N$_{aq.}$/HCl over a temperature range of 0 to 45°C (56). The Arrhenius relation is found to be linear over the entire temperature range (see discussion of errors) and therefore indicates the absence of significant proton tunneling. Since the rate-limiting step is regarded as the atom-ion recombination, it can be regarded as a type of proton discharge as in the case of mercury considered above. Owing to this similarity, it is sufficient to cite the linearity of the Arrhenius plot over the extended temperature range as conclusive evidence for a classical proton transfer mechanism. Thus, as in the case for simple proton

discharge at mercury cathodes, the contribution to the rate of reaction by quantum mechanical tunneling is hence negligible.

CHAPTER VI

QUANTITATIVE DISCUSSION OF EXPERIMENTAL RESULTS

1. General Introduction

The observed isotope effects have been qualitatively discussed in Chapter V and the object of the present chapter is to give a more quantitative basis on the conclusions previously arrived at in regard to reaction mechanism. In particular the major aims of the present chapter are:

(1) to show that the separation factors S_D and S_T at mercury electrodes can be correlated with the slow discharge mechanism and hence to eliminate existing inconsistencies with regard to other criteria for this mechanism, e.g. reaction order.

(2) to demonstrate that chemisorption of H atoms at multiple sites can lead to reasonable values of S_D, S_T, and R for the discharge step.

(3) to justify the observed isotope effects at platinum in terms of a rate determining atom-atom recombination [3] followed by atom-ion desorption [2];

(4) to demonstrate that proton tunneling in the discharge mechanism is negligible for temperatures down to -150°C and provide a proper basis for consideration of electrochemical frequency factors and activation energies.

2. New Contributions to the Calculation of Classical Isotope Effects in Electrochemical Reactions

A. Introduction

In this section, the properties of the activated complex are evaluated by considering the normal modes of vibration for an assumed geometrical structure. The method involves choosing a logical geometrical configuration for the activated complex and the variable parameter is the assignment of force constants to the various bonds involved, as discussed in Chapter III. This method has been considered (80,81) to be an improvement over the method of Eyring and Polanyi (66). Thus no assumptions need be made about the assignment of values to Φ, ΔH^{o}_{ads}, R, and ΔH^{o}_{s} needed in the Born-Haber treatment for formulation of the potential energy diagram e.g. by Butler (160). No approximate values need be given to the various parameters q, a and A to evaluate the London equation [70]. The potential dependence of the isotope effects can be explained by reference to a changing interaction force constant (see Chapter V) or by considering changes of the values of the force constants for H-H bonds which may arise from either a change in the type of adsorption site with degree of coverage or by induced heterogeneity associated with surface dipoles (174).

Previously, on the basis of a calculation of $S_p = 13$ (168), it has been considered that the discharge step could not be

operative at Hg. However, all other evidence of an electrochemical kinetic kind (e.g. see reaction order discussion, ChapterIII) supported the discharge mechanism. Hence, in the present calculations to be described below, the main purpose will be to demonstrate that satisfactory theoretical values of S_D, S_T, and R can be reasonably predicted, albeit on a somewhat empirical basis, for the slow discharge step which hence need not be rejected on the basis of the isotope effects observed experimentally.

B. Evaluation of Concentrations and Partition Function Ratios for Initial State Entities

(1) Partition Function Ratios for H and D Isotopic Species

From the equations for the separation factors S and the exchange current density ratios R, it is seen that the initial state quantities needed for the calculations are the concentrations $[H_3O^+]$, $[H_2DO^+]$ and the partition function ratios $f_{H_2DO^+}/f_{H_3O^+}$, $f_{D_3O^+}/f_{H_3O^+}$. Similar quantities are needed for the tritiated species. If the quantities $f_{D_3O^+}/f_{H_3O^+}$ and $f_{T_3O^+}/f_{H_3O^+}$ can be obtained for the aqueous species, then all other ratios and concentrations can be obtained if the rule of the geometric mean (175) is assumed (see below). The rule of the geometric mean

applied to lyonium ion species results in the following relations:

$$\left(\frac{f_{D_3O^+}}{f_{H_3O^+}}\right)^{\frac{1}{3}} = \frac{f_{H_2DO^+}}{3f_{H_3O^+}} = \frac{3f_{D_3O^+}}{f_{HD_2O^+}} = \frac{f_{HD_2O^+}}{f_{H_2DO^+}} \qquad [204]$$

and similarly

$$\left(\frac{f_{T_3O^+}}{f_{H_3O^+}}\right)^{\frac{1}{3}} = \frac{f_{H_2TO^+}}{3f_{H_3O^+}} = \frac{3f_{T_3O^+}}{f_{HT_2O^+}} = \frac{f_{HT_2O^+}}{f_{H_2TO^+}} \qquad [205]$$

The application of the rule of the geometric mean is equivalent to assuming that progressive substitution of D for H in H_3O^+ brings about equal stepwise increments in thermodynamic properties . Thus the O-H bond in H_2DO^+ is considered to have the same fundamental frequencies as an O-H bond in H_3O^+. That the rule of the geometric mean is obeyed for the system H_2O - HDO - D_2O is experimentally supported (176) and is therefore probably quite valid for solutions of H_3O^+ and corresponding isotopically substituted ions.

The method used to obtain the required quantities is essentially that of Swain and Bader (177) and will be briefly reviewed. The ratio $f_{D_3O^+}/f_{H_3O^+}$ can be obtained from the equilibrium constant (conventionally written as L) for the reaction

$$2D_3O^+ + 3H_2O \rightleftharpoons 3D_2O + 2H_3O^+ \qquad [206]$$

In terms of molecular partition functions

$$\frac{f_{D_3O^+}}{f_{H_3O^+}} = \left(\frac{f_{D_2O}}{f_{H_2O}}\right)^{3/2} \frac{1}{L^{1/2}} , \qquad [207]$$

and f_{D_2O}/f_{H_2O} is an experimentally accessible quantity (177,191). Hence an accurate value for L is requir d. This is calculated using the standard free energy difference for the reaction

$$H_{2(g)} + 2D_3O^+(D_2O) + 2Cl^-(D_2O) + 2H_2O_{(b)} \rightleftharpoons 2H_3O^+(H_2O) + 2Cl^-(H_2O) + D_2O_{(b)} \qquad [208]$$

of $\Delta G^\circ_{209} = 0.206$ kcal mole^{-1} as discussed by Purlee (178) with regard to the e.m.f. of the H_2/HCl, D_2/DCl cell examined by Noonan and LaMer (221). Combining the value for ΔG°_{208} with that for each of the following equilibria

$$D_{2(g)} + H_2O_{(b)} = H_{2(g)} + D_2O_{(b)} \qquad [209]$$

and

$$2Cl^-(H_2O) = 2Cl^-(D_2O) , \qquad [210]$$

it is found that ΔG°_{206} (hereafter referred to as ΔG°_L) equals -1.250 kcal mole^{-1} which corresponds to a value of L equal to 8.2 at 25°. The free energy ΔG°_{209} is -1.510 kcal mole^{-1} (182) and $\Delta G^\circ_{210} = 0.460$ kcal mole^{-1} (177). The quantity ΔG°_{210}, the

standard free energy change for transfer of a chloride ion from light to heavy water, is calculated on the assumption that practically all of the thermodynamic differences for solutions of ions in light and heavy water arise only from differences in librational frequencies. Swain and Bader (177) therefore give the relation

$$\Delta G^{o}_{S} = 4\,RT \ln \left(\frac{f_{lib,H}}{f_{lib,D}}\right)_{i} \left(\frac{f_{lib,D}}{f_{lib,H}}\right)_{w} \qquad [211]$$

for the standard free energy change for the process of changing the coordination about an ion from that by light to that by heavy water. The factor 4 arises from the assumption that four water molecules are supposed(117) to be coordinated. The partition function f_{lib} is that part of the molecular partition function associated with / librational of the water molecules. The subscripts i and w refer to librational motions of the solvent molecules in the presence of an ion or in pure water, respectively. The assumption is made that the behaviour of a hindered rotator can be described by the harmonic oscillator approximation, so that for the water molecule

$$f_{lib} = \prod^{3} e^{-u/2}/1-e^{-u}$$

The product is taken over three identical frequencies since the observed librational frequency for liquid water (667 cm^{-1}) is an average one. In order to calculate the librational frequency for D_2O (or T_2O as shown below), the mean of the ratios of the

moments of inertia raised to the one half power is taken. Hence, the ratio of mean librational frequencies for H_2O and D_2O is, (177),

$$\frac{\nu_{lib,H}}{\nu_{lib,D}} = 1.3815^{*} \qquad [212]$$

The total partition function ratio for light and heavy liquid waters and aqueous solutions may therefore be written generally as

$$\frac{f_D}{f_H} = \left(\frac{M_D}{M_H}\right)^{3/2} \frac{f_{lib,D}}{f_{lib,H}} \frac{f_{vib,D}}{f_{vib,H}} \qquad [213]$$

Heinzinger and Weston (183) have also reported values of the equilibrium constant L by reference to the equilibrium

$$H_3O^+ + HDO \rightleftharpoons H_2DO^+ + H_2O \qquad [214]$$

The equilibrium constant K_{214} is equal to 1.04 at 13°C (the experimental temperature, 183). From the rule of the geometric mean, it can be shown (178) that the relation between L and K_{214} is given by

$$K_{214} = \frac{3}{2} L^{-1/6} \qquad [215]$$

In order to obtain L or K_{214} as a function of temperature, the

---

* Five significant figures were given in the original publication (177).

ΔH° (standard enthalpies) terms for the equilibria [208], [210]* and [214] are used to calculate $\Delta H_L = -1.10$ kcal mole^{-1}; then L values as a function of temperature are calculated as shown in Table IV.

Table IV

L Values as a Function of Temperature

Temperature, °C.	L
0	9.6
15	8.8
25	8.2
35	7.8
50	7.2
80	6.2

The agreement between Heinzinger and Weston's value of L at 25° with that of Swain and Bader is excellent. Taking L = 8.2 at 25°C, equations [207] and [204] give:

$$f_{D_2O}/f_{H_2O} = 1437 \quad (a)$$

$$f_{HDO}/f_{H_2O} = 75.82 \quad (b) \qquad [216]$$

$$f_{D_2O}/f_{HDO} = 18.96 \quad (c)$$

* The ΔH° quantity for the equilibrium [210] is obtained on the basis that the librational frequency changes from HCl/H_2O to DCl/D_2O solutions are due only to the anion (177,172).

$$f_{D_3O^+}/f_{H_3O^+} = 19023 \quad (a)$$

$$f_{HD_2O^+}/f_{H_2DO^+} = 25.70 \quad (b)$$

$$f_{H_2DO^+}/f_{H_3O^+} = 80.08 \quad (c) \qquad [217]$$

$$f_{D_3O^+}/f_{HD_2O^+} = 8.898 \quad (d)$$

where all f ratios refer to the species in the liquid phase. Finally for the equilibrium

$$2\,OD^- + H_2O \rightleftharpoons 2OH^- + D_2O \qquad [218]$$

Swain and Bader (177) report a value of 3.21 for K_{219} at 25°C. Hence

$$\frac{f_{OD^-}}{f_{OH^-}} = (2.31)^{1/2}\left(\frac{f_{D_2O}}{f_{H_2O}}\right)^{1/2} = 21.16 \qquad [219]$$

(11) Partition Function Ratios for the H and T Isotopic Species

Partition function ratios similar to those given in equations [216] and [217] can be calculated for H and T isotopic species. The ratio $f_{T_3O^+}/f_{H_3O^+}$ is calculated by the method of Swain and Bader (177,184) using their frequencies for H_2O and H_3O^+ (cf. Thornton (185)).* The frequencies of the T_2O and T_3O^+

* Swain and Bader have used their own measured frequencies for H_2O but for H_3O^+, they use the frequencies reported by Ferriso and Hornig (188) for $H_3O^+ClO_4^-$, the solid hydroxonium perchlorate.

species were calculated from the H_2O and H_3O^+ frequencies using the formula given by Herzberg (186). The force constants for H_2O were taken from Herzberg's book (186) while those for H_3O^+ were obtained from solution of the secular equation (187) using the observed frequencies of Ferriso and Hornig (188). The force constants for the various modes of vibration in H_3O^+ are (187): $k_s = 4.915$, $k_\phi = 0.5$, $k_w = 0.06$, and $k_{int} = -0.4896$, m.d. Å^{-1}. The subscripts s, ϕ, w, and int. refer respectively to the O-H stretch, the H-O-H bend, the O-H wag and the OH----OH interaction. The calculated frequencies for T_2O and T_3O^+ are given in Table V together with those for H_2O and H_3O^+ and D_2O and D_3O^+. The librational frequency shifts were evaluated for T_2O and T_3O^+ from the inverse square roots of the average moments of inertia calculated according to the formulae given by Moelwyn-Hughes (189) and are shown in Table VI. The bond lengths and valency angle for H_2O and T_2O were taken as 0.96 Å and 105° (189), respectively. The bond lengths and valency angle for H_3O^+ were taken as 1.05° Å (174) and 107° (185). Hence the average librational frequencies for T_2O and T_3O^+ are given, respectively, by

$$(\nu_{11b})_{T_2O} = (\nu_{11b})_{H_2O}/1.637$$

$$(\nu_{11b})_{T_3O^+} = (\nu_{11b})_{H_3O^+}/1.637$$

The ratio $f_{T_3O^+}/f_{H_3O^+}$ is calculated from an equation analogous

Table V

Frequency Assignments for Water and Lyonium Ions

At 20°C* in the Liquid Phase

Molecule	Frequency, ν cm.$^{-1}$ H-species	D-species	T-species	Degeneracy	Mode
H_2O	3440	2500	2196	1	ν_1
	1645	1208	901	1	ν_2
	3440	2500	2190	1	ν_3
	667	483	408	3	ν_{11b}
H_3O^+	3235	2445	1717	1	ν_1
	1150	868	829	1	ν_2
	2590	2000	1635	2	ν_3
	1700	1255	1025	2	ν_4
	643	486	385	3	ν_{11b}
OH^-	3615	2556	2206	1	ν_1
	477	345	291	2	ν_{11b}

* The internal frequencies for H_3O^+ and D_3O^+ are the values reported by Ferriso and Hornig (188).

Table VI

Moments of Inertia of H and T Species

Molecule	Moment of Inertia x 10^{40} gm. $cm.^2$ A	B	C	Average
H_2O	1.080	1.79	2.987	1.955
T_2O	2.823	4.786	8.103	5.237
H_3O^+	3.609	3.609	5.931	3.954
T_3O^+	9.021	9.021	15.117	11.053

to [213] but written for tritium as

$$\frac{f_{T_3O^+}}{f_{H_3O^+}} = \left(\frac{M_{T_3O^+}}{M_{H_3O^+}}\right)^{3/2} \left(\frac{\sinh h c \nu_{lib,H}/2}{\sinh h c \nu_{lib,T}/2}\right)^3 \prod^{6} \frac{\sinh u_H/2}{\sinh u_T/2}$$

and it is found that

$$f_{T_2O}/f_{H_2O} = 3.056 \times 10^4 \qquad (a)$$

$$f_{HTO}/f_{H_2O} = 349.6 \qquad (b) \qquad [221]$$

$$f_{T_3O^+}/f_{H_3O^+} = 2.805 \times 10^6 \qquad (c)$$

and from equation [205]

$$f_{H_2TO^+}/f_{H_3O^+} = 423.12 \qquad (a)$$

$$f_{HT_2O^+}/f_{H_2TO^+} = 141.04 \qquad (b) \qquad [222]$$

$$f_{T_3O^+}/f_{HT_2O^+} = 47.01 \qquad (c)$$

In order to calculate the partition function ratio f_{OT^-}/f_{OH^-}, the method of Swain and Bader is again used and it is found that (see Table V)

$$\frac{f_{OT^-}}{f_{OH^-}} = \left(\frac{M_{OT}}{M_{OH}}\right)^{3/2} \left(\frac{\sinh u_{H,lib}/2}{\sinh u_{T,lib}/2}\right)^2 \frac{\sinh u_{H,str}/2}{\sinh u_{T,str}/2}$$

i.e.

$$\frac{f_{OT^-}}{f_{OH^-}} = 286.49 \qquad [223]$$

C. Calculation of Lyonium Ion Concentrations

(1) Lyonium Ion Concentrationsin Mixed H/D Solutions

In order to calculate the concentrations of the lyonium ions H_3O^+, H_2DO^+, HD_2O^+ and D_3O^+ in a mixed solution of H and D, the following two equilibrium constants are needed in addition to K_{21} and L:

$$H_2O + D_3O^+ \rightleftharpoons HDO + HD_2O^+ \quad K_{224} = 8.478 \qquad [224]$$

and

$$H_2O + D_2O \rightleftharpoons 2HDO \quad K_{225} = 3.96 \qquad [225]$$

K_{225} is calculated using the rule of the geometric mean and K_{225} is close to the statistical value of 4 as found by Urey (190). The above relationships enable the ratios

$$\frac{[H_3O^+]}{[D_3O^+]} = \frac{[H_2O]}{[D_2O]}^{3/2} L^{1/2} = \frac{1}{\lambda_1},$$

$$\frac{[H_3O^+]}{[H_2DO^+]} = \frac{[H_2O]}{[HDO]} \frac{1}{K_{214}} = \frac{1}{\lambda_2}$$

and

$$\frac{[HD_2O^+]}{[D_3O^+]} = \frac{[H_2O]}{[HDO]} K_{224} = \lambda_3/\lambda_1$$

to be calculated. Denoting the total lyonium concentration by $[L_3O^+]$, then

$$[L_3O^+] = (1 + \lambda_1 + \lambda_2 + \lambda_3)[H_3O^+] = \lambda[H_3O^+] \qquad [226]$$

$$\lambda = 1 + \frac{[D_2O]^{3/2}}{[H_2O]^{3/2}L^{1/2}} + \frac{[HDO]}{[H_2O]} K_{214} + \frac{K_{224}[D_2O]^{3/2}}{[HDO][H_2O]^{1/2}L^{1/2}} \qquad [227]$$

The units of concentration are moles in a fixed number of moles (e.g. 55.34) of solvent. The ratios of the lyonium ion concentrations are fixed by the above equilibrium constants and are independent of any other processes occurring in solution. The D/H ratio used in the present work was 0.111.....(i.e. 10% D_2O by volume in H_2O), and by carrying out the calculations indicated by equations [226] and [227] for $[L_3O^+] = [H_3O^+] + [H_2DO^+] + [HD_2O^+] + [D_3O^+] = 1$, the individual lyonium ion concentrations can be obtained and are shown in Table VII.

(11) Lyonium Ion Concentrations in Mixed D/T Solutions

The relevant equilibrium constants required for calculation of the various lyonium ion concentrations are obtained from the rule of the geometric mean employing equations [221] and

Table VII

Lyonium Ion Concentrations in 1N Acid Solutions at 25°C

Ion	$c_D/c_H = 0.111$ Concentration (mole litre^{-1})	Ion	$c_T/c_H = 1.807 \times 10^{-7}$ Concentration (mole litre^{-1})
H_3O^+	0.7982	H_3O^+	0.9999...
H_2DO^+	0.1865	H_2TO^+	4.374×10^{-7}
HD_2O^+	0.0150	HT_2O^+	$\sim 10^{-10}$
D_3O^+	0.0004	T_3O^+	$\ll 10^{-10}$
$\frac{[H_2O]}{[HDO]}$ (neutral solution)	4.544	$\frac{[H_2O]}{[HTO]}$ (neutral solution)	2.76×10^{-7}

[222]. Hence

$$H_2O + T_2O \rightleftharpoons 2HTO \qquad K = 4.0 \quad (a)$$

$$H_2O + H_2TO^+ \rightleftharpoons HTO + H_3O^+ \qquad K = 0.8262 \quad (b)$$

$$H_2O + T_3O^+ \rightleftharpoons HTO + HT_2O^+ \qquad K = 7.437 \quad (c) \qquad [228]$$

$$2T_3O^+ + 3H_2O \rightleftharpoons 3T_2O + 2H_3O^+ \qquad I_T = 3.627 \quad (d)$$

A typical experiment for S_T determinations would involve about 10^{-5} mole T_2O so that the ratio $(c_T/c_H)_{soln} = (10^{-5}/55.344) = 1.807 \times 10^{-7}$. By a similar mass balance treatment which led to equations [226] and [227], the following relations can be obtained:

$$[L_3O^+] = (1 + \lambda_1 + \lambda_2 + \lambda_3)[H_3O^+] = \lambda[H_3O^+] \qquad [229]$$

$$\lambda = 1 + \frac{[T_2O]^{3/2}}{[H_2O]^{3/2}L_T^{1/2}} + \frac{[HTO]}{[H_2O]}\frac{1}{K_{228b}} + \frac{[T_2O]^{3/2}K_{228b}}{[HTO][H_2O]^{1/2}L_T^{1/2}} \qquad [230]$$

A material balance calculation for $[L_3O^+] = 1$ is given in Table VII.

D. The Separation Factors S_D and S_T

(1) The Discharge Mechanism

From equations [148], [217] and Table VII, the separation factor S_D in acid solution, based on the slow discharge

mechanism is

$$S_D = 38.08 \frac{f_{\neq,H}}{f_{\neq,D}} \qquad [231]$$

where the $f_{\neq}$ quantities have been defined previously. Similarly, S_T for the discharge step in acid solutions is obtained from equations [149], [221], [222] and Table VII, as

$$S_T = 174.75 \frac{f_{\neq,H}}{f_{\neq,T}} \qquad [232]$$

In neutral or alkaline solution, discharge occurs from a water molecule* so that the separation factors S_D and S_T are given by equations [149] and [150], respectively. Substituting the appropriate values for concentrations and partition functions into these two equations gives

$$S_D = 38.275 \frac{f_{\neq,H}}{f_{\neq,D}} \qquad [233]$$

and

$$S_T = 174.812 \frac{f_{\neq,H}}{f_{\neq,T}} \qquad [234]$$

It is seen that there is very little difference** between the

---

* Except at Hg where the cation metal amalgam is formed and the rate limiting step is the decomposition of the amalgam.

** Theoretically these "pre-$f_{\neq}$" factors should be identical for acid and alkaline solutions. The small differences between the values in equations [231] and [232] and between those in equations [233] and [234] arise because different types and sources of numerical data are used in the partition function and concentration calculations for the species in acid and alkaline solutions.

values of the numerical factors in the equations for S_D and S_T) in acid solution (equations [231] and [232]) and those for S_D (and S_T) in alkaline or neutral solutions (equations [233] and [234]). The ratio of partition functions for the activated states are, however, different as shown below.

(ii) The Atom + Ion Recombination Mechanism

From equations [154], [155], [216], [217] and Table VII, the separation factors S_D for acid and neutral solutions based on the atom + ion mechanism will, respectively, be given by

$$S_D = 76.16 \left(\frac{f_{\neq,HD}}{f_{\neq,H_2}} + \frac{f_{\neq,DH}}{f_{\neq,H_2}} \right)^{-1} \qquad [235]$$

and

$$S_D = 76.55 \left(\frac{f_{\neq,HD}}{f_{\neq,H_2}} + \frac{f_{\neq,DH}}{f_{\neq,H_2}} \right)^{-1} \qquad [236]$$

Similarly for the separation factors S_T in acid and neutral solutions, respectively, the following two relations are obtained:

$$S_T = 349.50 \left(\frac{f_{\neq,HT}}{f_{\neq,H_2}} + \frac{f_{\neq,TH}}{f_{\neq,H_2}} \right)^{-1} \qquad [237]$$

and

$$S_T = 349.62 \left(\frac{f_{\neq,HT}}{f_{\neq,H_2}} + \frac{f_{\neq,TH}}{f_{\neq,H_2}} \right)^{-1} \qquad [238]$$

(iii) Atom + Atom Recombination Mechanism

The separation factors, S_D, for acid and neutral

solutions, respectively, are obtained by combining equations [160] and [161] with [217] and [216] and using the data in Table VII; i.e.

$$S_D = 76.16 \frac{f_{\neq,H_2}}{f_{\neq,HD}} \qquad [239]$$

for acid solutions and

$$S_D = 76.55 \frac{f_{\neq,H_2}}{f_{\neq,HD}} \qquad [240]$$

for neutral on alkaline solutions. Similarly, from equations [162], [222] and [221], and the data in Table VII,

$$S_T = 349.50 \frac{f_{\neq,H_2}}{f_{\neq,HT}} \qquad [241]$$

in acid solutions and

$$S_T = 349.62 \frac{f_{\neq,H_2}}{f_{\neq,HT}} \qquad [242]$$

in neutral or alkaline solutions.

In equations [231] to [242], the terms in $f_{\neq}$ all include a symmetry number, $\sigma_{\neq}$, for the activated complex. The terms in f for the initial state quantities have already been corrected for σ (see equation [204]. Distinction need not, in the above cases, be made between the symmetry number σ and the number of reaction paths, l. It has been claimed (59) that the symmetry numbers automatically account for the various reaction paths available. This statement is not necessarily true for all reactions. Consider, for example, the formation of an Hg-H-C

activated complex/by the two reactions

$$v_{H,1} = k(1-\theta)\,[H_2DO^+]\,\frac{f^{\neq}_{H,1}}{f^{\neq}_{H,2}}\,e^{-\beta\phi/RT}$$

and

$$v_{H,2} = k(1-\theta)\,[HD_2O^+]\,\frac{f^{\neq}_{H,2}}{f_{HD_2O^+}f_M}$$

The ratio of rates is

$$\frac{v_{H,1}}{v_{H,2}} = \frac{[H_2DO^+]}{[HD_2O]}\,\frac{f_{HD_2O^+}}{f_{H_2DO^+}}\,\frac{f^{\neq}_{H,1}}{f^{\neq}_{H,2}}$$

It is obvious that there are two ways of discharging a proton from H_2DO^+ compared to only one way for discharge from HD_2O^+. However the symmetry number σ for either species is unity and an apparent anomaly arises. This apparent anomaly has recently been discussed by Laidler and Bishop (162) where a factor of 2 is shown to originate in $f^{\neq}_{H,1}/f^{\neq}_{H,2}$ by consideration of the geometry of the activated complex.

B. The Ratio of Exchange Current Densities, R

(1) The Discharge Mechanism

From equation [152]

$$R = \frac{f_{D_3O^+}}{f_{H_3O^+}}\,\frac{f'^{\neq}_{H}}{f'^{\neq}_{D}}\,\exp\beta(\phi^o_{r,D}-\phi^o_{r,H})F/RT \qquad [152]$$

it is seen that in addition to the partition function ratio $f_{D_3O^+}/f_{H_3O^+}$, the term in $\phi^\circ_{r,D}-\phi^\circ_{r,H}$ is required to evaluate E_o. Although the absolute standard single potential ϕ°_r is inaccessible, the difference $\phi^\circ_{r,D}-\phi^\circ_{r,H}$ can be calculated as a function of temperature by reference to the cell

$$Pt,\ D_2 \ \Big|\ D_2O^+, D_2O \ \Big\|\ H_3O^+, H_2O \ \Big|\ H_2, Pt \qquad [243]$$

The reaction corresponding to the above cell is

$$2\,H_3O^+ + 2D_2O + D_2 \rightleftharpoons 2\,D_3O^+ + 2H_2O + H_2 \qquad [244]$$

and the equilibrium constant is

$$K_{244} = \left(\frac{f_{D_3O^+}}{f_{H_3O^+}}\right)^2 \cdot \left(\frac{f_{H_2O}}{f_{D_2O}}\right)^2 \frac{f_{H_2}}{f_{D_2}} \qquad [245]$$

Since $\Delta G^\circ = -RT \ln K = -zF\,\Delta\phi^\circ$ it follows that

$$\Delta\phi^\circ = \phi^\circ_{r,D}-\phi^\circ_{r,H} = \frac{2.3\,RT}{zF} \log K_{244} \qquad [246]$$

We can immediately calculate $\Delta\phi^\circ$ from the above principles since K_{244} at 25° is easily available, but it is also advantageous to know $\Delta\phi^\circ$ as a function of temperature which can indeed be estimated as shown below.

The partition functions in equation [245] are obtained by the following methods:

(1) f_{H_2}/f_{D_2} is calculated from

$$\frac{f_{H_2}}{f_{D_2}} = \left(\frac{M_{H_2}}{M_{D_2}}\right)^{3/2} \left(\frac{\mu_{H_2}}{\mu_{D_2}}\right) \frac{\sinh h c \nu_D / 2kT}{\sinh h c \nu_H / 2kT} = 0.03953 \frac{\sinh u_D/2}{\sinh u_H/2} \quad [247]$$

where μ terms are the reduced masses. The internal frequencies ν_H and ν_D are 4395 $cm.^{-1}$ and 3118 $cm.^{-1}$ (109) and are taken to be independent of temperature.

(2) f_{D_2O}/f_{H_2O} is calculated from

$$\frac{f_{D_2O}}{f_{H_2O}} = \left(\frac{M_{D_2O}}{M_{H_2O}}\right)^{3/2} \left(\frac{\sinh u_H/2}{\sinh u_D/2}\right)^{3}_{11b} \left(\frac{\sinh u_H/2}{\sinh u_D/2}\right)_{bend} \prod^{2} \frac{\sinh u_H/2}{\sinh u_D/2} \quad [248]$$

In equation [248], the librational frequencies are temperature dependent below room temperature and were obtained from the data of Giguère and Harvey (191). The bending frequency is observed to be independent of temperature (172) and the stretching frequency increases linearly by 0.5 cm^{-1}, $^{o}C^{-1}$ as the temperature increases (171,172). The frequencies used for making the temperature corrections to the stretching mode are given in Table VIII.

(3) $f_{D_3O^+}/f_{H_3O^+}$ is calculated from

$$\frac{f_{D_3O^+}}{f_{H_3O^+}} = \left(\frac{f_{D_2O}}{f_{H_2O}}\right)^{3/2} \cdot \frac{1}{L^{1/2}} \quad [207]$$

Table VIII

Frequencies and Partition Function Ratios as a Function of Temperature

Temperature °C	Water Molecule Frequencies, $cm.^{-1}$						Partition Function Ratios			$\phi^{o} - E^{o}$
	$\nu_{Str,H}$	$\nu_{Str,D}$	$\nu_{b,H}$	$\nu_{b,D}$	$\nu_{lib,H}$	$\nu_{lib,D}$	f_{H_2}/f_{D_2} x 10^3	$\frac{f_{D_2O}}{f_{H_2O}}$	$\frac{f_{D_3O^+}}{f_{H_3O^+}}$	[illegible] mv.
0	3453	2509	1645	1208	750	543	1.372	3072	54381	- 9.9
25	3440	2500	1645	1208	667	494	1.815	1434	19023	-1[illegible]
50	3428	2491	1645	1208	667	494	2.301	853.6	9296	-1[illegible]
80	3413	2480	1645	1208	667	494	2.929	507.0	4582	-21.[illegible]

Notes on Table: (a) Bending and stretching frequencies for H_2O and D_2O at 25°C were taken from ref. 177.

(b) Effect of temperature on the stretching frequency was taken from the data of Weston (172) and Cross *et al.* (171).

(c) Libr tional frequencies (columns 6 and 7) at v rious temperatures were taken from ref. 191.

where f_{D_2O}/f_{H_2O} is obtained from equation [248] above and L from the data of Heinzinger and Weston (183). The results of the calculations for $\phi^\circ_{r,D}-\phi^\circ_{r,H}$ are shown in Table VIII. The error involved in this calculation can be estimated as follows: from equations [245], [246] and [208], it follows that $\Delta\phi^\circ_r$ is given by

$$\Delta\phi^\circ_r = \frac{2.3\,RT}{2F}\,\log_{10}\left(\frac{1}{L}\,\frac{f_{D_2O}}{f_{H_2O}}\,\frac{f_{H_2}}{f_{D_2}}\right)$$

Taking the maximum error in the experimental determination of the zero-point energy difference between H_2O and D_2O as equivalents to 50 $cm.^{-1}$ (183) and the experimental limits for L as 3.0-3.4 (183), the $\Delta\phi^\circ_r$ term in the above equation is -16.8 mV at 25°C. This differs from the value given in Table VIII by 2 mV and is considered to be a maximum probable error at this temperature. The magnitude of the error in $\Delta\phi^\circ_r$ at low temperatures is more difficult to estimate, and a maximum error of about 20% is estimated.

The relation between $\Delta\phi^\circ_r$ and temperature is shown in Figure 39. From the slope a temperature coefficient, $d\Delta\phi^\circ_r/dT$, of 0.148 mV deg^{-1} for cell [243] is obtained. The entropy change for reaction [244] is therefore 6.8 e.u.

From equations [152] and [217], R for acid solutions is

Figure 39.

The reversible potential difference $\phi^{\circ}_{r,D} - \phi^{\circ}_{r,H}$ as a function of temperature in aqueous acid solution.

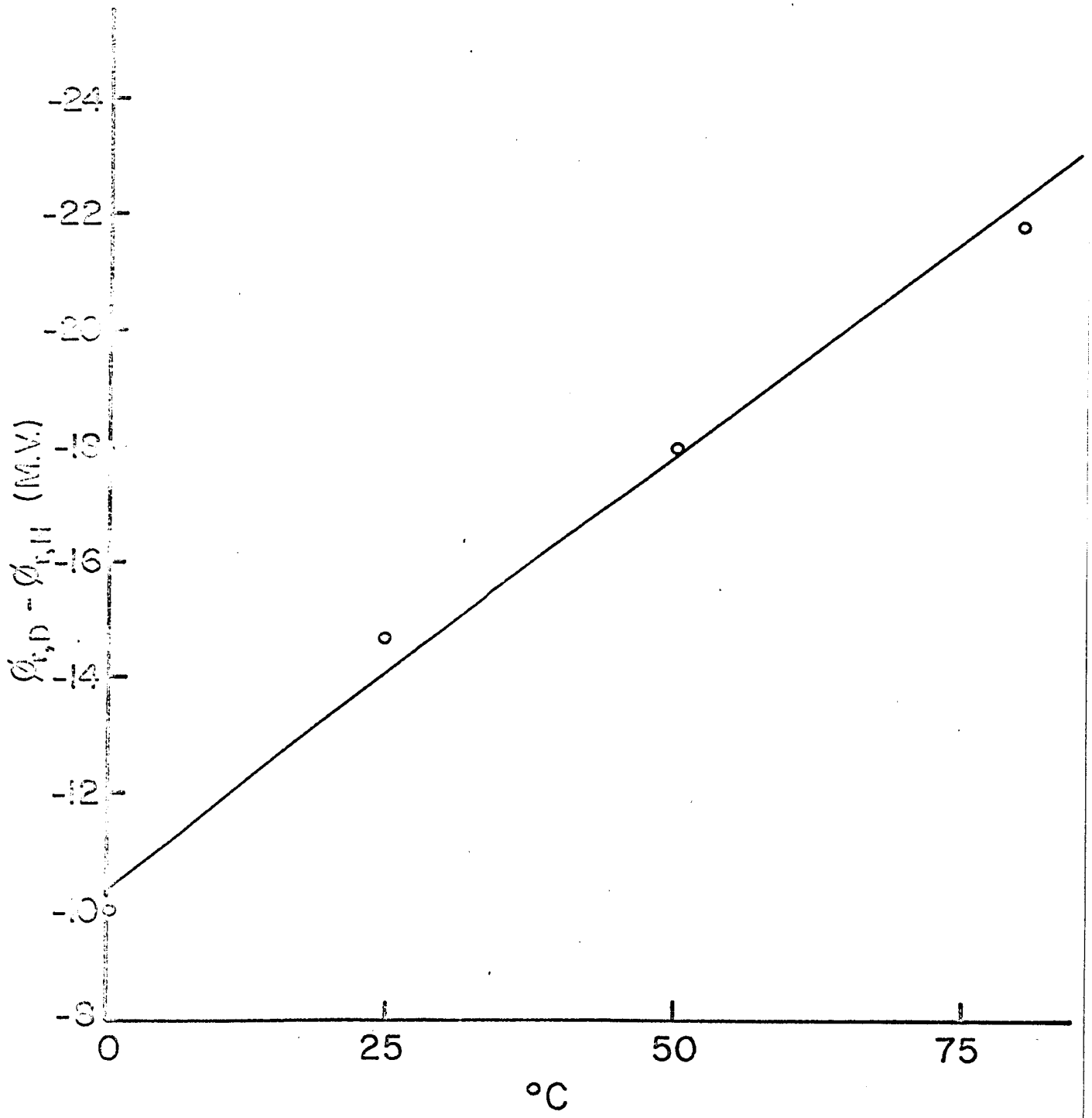
-24
-22
-20
-18
-16
-14
-12
-10
-8
$\phi_{s,D} - \phi_{s,H}$ (M.V.)
0
25
50
75
°C

given by

$$R = 19023 \frac{f'_{\neq,H}}{f'_{\neq,D}} \exp \beta(\phi^{\circ}_{r,D} - \phi^{\circ}_{r,H})F/RT$$

From Table VIII, $\phi^{\circ}_{r,D} - \phi^{\circ}_{r,H} = -14.8$ mV at 25° in acid solutions and taking $\beta = 1/2$, the above equation becomes

$$R = 14260 \frac{f'_{\neq,H_2}}{f'_{\neq,D_2}}$$

The term $f'_{\neq,H}/f'_{\neq,D}$ in the above equation contains contributions from two unreacting O-H and O-D bonds. The usual assumption is made that these bonds do not suffer any changes in frequency as the reacting entity passes from the initial to the activated state (e.g. see references, 51,59,81). In the present case, this assumption was justified in the previous discussion (see page 85) in which it was pointed out that the H_3O^+ molecule ion would be expected to retain its full charge in the electrochemical activated state.* This assumption was made on the grounds that both β and the force constants would vary if retention of charge were not the case. Hence the partition function contributions associated with the unreacting O-H and O-D groups

---

* If charge were lost, an increase in the OH and OD bond frequencies (150) would arise (cf. page 85).

can be removed from $f'_{\neq,H}/f'_{\neq,D}$ by multiplication by $(f_{H_3O^+}/f_{D_3O^+})^{3/2}$ which gives

$$R = 20.00 \frac{f_{\neq,H_2}}{f_{\neq,D_2}} \qquad [249]$$

In neutral or alkaline solutions, the term $\phi^o_{r,D}-\phi^o_{r,H}$ is -26.7 mV at 25°C and the relation for R is, from equations [152a] and [216],

$$R = \frac{f_{D_2O}}{f_{H_2O}} \cdot \frac{f'_{\neq,H_2}}{f'_{\neq,D_2}} \exp \beta(\phi_{r,D}-\phi_{r,H})F/RT$$

i.e.

$$R = 853.98 \frac{f'_{\neq,H_2}}{f'_{\neq D_2}}$$

The ratio $f'_{\neq,D_2}/f'_{\neq,D_2}$ contains contributions from the single unreacting O-H and O-D bonds in H_2O and D_2O. These contributions are removed (cf. the discussion above for H_3O^+ and D_3O^+) from $f'_{\neq,H_2}/f'_{\neq,D_2}$ by multiplying the above equation by $(f_{H_2O}/f_{D_2O})^{1/2}$ which yields

$$R = 22.53 \frac{f_{\neq H_2}}{f_{\neq D_2}} \qquad [250]$$

(ii) The Atom + Ion Mechanism

From equations [158] and [216] and [217], the ratio of exchange current densities in acid solutions is

$$R = \left(\frac{1-\theta_H}{1-\theta_D}\right)\left(\frac{f_{D_3O^+}}{f_{H_3O^+}}\right)^2 \cdot \frac{f_{H_2O}}{f_{D_2O}} \cdot \frac{f'_{\neq,H_2}}{f'_{\neq,D_2}} \exp\,(1+\beta)(\phi^\circ_{r,D}-\phi^\circ_{r,H})F/RT$$

i.e.

$$R = \left(\frac{1-\theta_H}{1-\theta_D}\right) 2.5183 \times 10^5 \frac{f'_{\neq,H_2}}{f'_{\neq,D_2}} \exp\,(1+\beta)(\phi^\circ_{r,D}-\phi^\circ_{r,H})F/RT \qquad [251]$$

where the θ_H and the θ_D terms are the steady state coverages by H and D, respectively (see equation 158). These θ factors do not enter into the determination of R for the discharge step (see p. 15). Taking $\beta = 1/2$ and $\phi^\circ_{r,D}-\phi^\circ_{r,H} = -14.8$ mV, the relation for R in acid solutions is

$$R = 1.0608 \times 10^5 \frac{f'_{\neq,H_2}}{f'_{\neq,D_2}} \left(\frac{1-\theta_H}{1-\theta_D}\right)$$

Since the $f'_{\neq,H_2}/f'_{\neq,D_2}$ ratio contains contributions from two unreacting O-H and O-D bonds in H_3O^+ and D_3O^+, respectively, the above equation is multiplied by $(f_{H_3O^+}/f_{D_3O^+})^{2/3}$ yielding

$$R = 148.9 \frac{f_{\neq,H_2}}{f_{\neq,D_2}} \left(\frac{1-\theta_H}{1-\theta_D}\right) \qquad [252]$$

For neutral or alkaline solutions, $\phi^\circ_{r,D}-\phi^\circ_{r,H} = -26.7$ mV and the relation for R is, from equations [159], [216] and [219]

$$R = \left(\frac{1-\theta_H}{1-\theta_D}\right)\left(\frac{f_{D_2O}}{f_{H_2O}}\right)^2 \cdot \frac{f_{OH^-}}{f_{OD^-}} \cdot \frac{f'_{\neq,H_2}}{f'_{\neq,D_2}} \exp\,(1+\beta)(\phi^o_{r,D}-\phi^o_{r,H})F/RT$$

i.e.

$$R = \left(\frac{1-\theta_H}{1-\theta_D}\right) 3.0390 \times 10^4 \frac{f'_{\neq,H_2}}{f'_{\neq,D_2}} \exp -\tfrac{3}{2}(0.02672)F/RT$$

with $\beta = 0.5$, so that

$$R = 6379.9 \frac{f'_{\neq,H_2}}{f'_{\neq,D_2}} \left(\frac{1-\theta_H}{1-\theta_D}\right)$$

Then correcting the above equation for the contributions from the unreacting O-H and O-D bonds in the activated state by multiplication by $(f_{H_2O}/f_{D_2O})^{1/2}$ (cf. equation 250), the final relation for R is

$$R = 160.29 \frac{f_{\neq,H_2}}{f_{\neq,D_2}} \left(\frac{1-\theta_H}{1-\theta_D}\right) \qquad [253]$$

Coverage factors will be discussed below.

(iii) <u>The Atom + Atom Recombination Mechanism</u>

In acid solutions, the ratio of exchange current densities for the isotopic reactions [3] is, from equations [164], [216] and [217]

$$R = \left(\frac{1-\theta_H}{1-\theta_D}\right)^2 \left(\frac{f_{D_3O^+}}{f_{H_3O^+}}\right)^2 \left(\frac{f_{H_2O}}{f_{D_2O}}\right)^2 \cdot \frac{f_{\neq,H_2}}{f_{\neq,D_2}} \exp\,2(\phi_{r,D}-\phi_{r,H})F/RT$$

which gives

$$R = 55.33 \frac{f_{\neq,H_2}}{f_{\neq,D_2}} \left(\frac{1-\theta_H}{1-\theta_D}\right)^2 \qquad [254]$$

In neutral or alkaline solutions, from equations [165], [216] and [219]

$$R = \left(\frac{1-\theta_H}{1-\theta_D}\right)^2 \left(\frac{f_{D_2O}}{f_{H_2O}}\right)^2 \left(\frac{f_{OH^-}}{f_{OD^-}}\right)^2 \frac{f_{\neq,H_2}}{f_{\neq,D_2}} \exp 2(\phi_{r,D}-\phi_{r,H})F/RT$$

which gives

$$R = 55.82 \frac{f_{\neq,H_2}}{f_{\neq,D_2}} \left(\frac{1-\theta_H}{1-\theta_D}\right)^2 \qquad [255]$$

F. Partition Functions for Activated Complexes in Proton Discharge

(1) Introduction

In this section, the methods used to calculate partition function ratios $f_{\neq,H}/f_{\neq,D}$ and $f_{\neq,H}/f_{\neq,T}$ for two models of the activated complex for the proton discharge step are presented. The first corresponds to the linear three-center transition state and the second model is that for a four-center planar XY_2 molecule. The latter corresponds to the "complex site model" where the adsorption of hydrogen is regarded as occurring at a dual site in the surface of the metal (see Chapter V).

(11) The Linear Three-Center Activated Complex

The H and D transition states in the proton discharge from H_3O^+, H_2DO^+, and D_3O^+ are regarded as linear pseudo-triatomic structures (e.g. for similar assumptions see refs. 59, 70,193) of the form

$$M \text{——} H^{\ddagger} \text{——} OH_2$$

$$M \text{——} D^{\ddagger} \text{——} OH_2$$

$$M \text{——} D^{\ddagger} \text{——} OD_2$$

The partition function ratio for these activated states is

$$\frac{f^{\ddagger}_{s,H}}{f^{\ddagger}_{s,D}} \frac{\sigma_D^{\ddagger}}{\sigma_H^{\ddagger}} \prod^{2} \frac{f^{\ddagger}_{t,H}}{f^{\ddagger}_{t,D}} \prod^{2} \frac{f^{\ddagger}_{r,H}}{f^{\ddagger}_{r,D}} \prod^{3} \frac{\sinh u^{\ddagger}_{i,D}/2}{\sinh u^{\ddagger}_{i,H}/2} \qquad [256]$$

where $f^{\ddagger}_t$ and $f^{\ddagger}_r$ are the translational and rotational partition functions, respectively, and $u_i = h\nu_i/kT$ (ν has the units of $cm.^{-1}$). Both $f^{\ddagger}_t$ and $f^{\ddagger}_r$ can be calculated from the known atomic masses and assumed geometry of the activated complexes. The ratio of symmetry factors $\sigma^{\ddagger}$ is unity for the activated complexes in the discharge mechanism and the remaining terms in $u^{\ddagger}_i$ are obtained from a vibrational analysis for the above model.

The vibrational analysis for a linear three-center activated complex has been reviewed by several authors (60,61, 70,71) and is also presented briefly here. We consider the linear complex

$$M \ldots \overset{1}{\ldots} H \ldots \overset{2}{\ldots} X$$

$$x_M \qquad x_H \qquad x_X$$

where x_M, x_H and x_X are the displacements of the atoms from their equilibrium positions. Let the M-H stretching force constant be k_1 and the X-H stretching force constant be k_2. Coupled motions can also be accounted for by introducing a coupling or interaction force constant k_{12}. The total potential energy of this three-center complex is

$$V = \tfrac{1}{2} k_1(x_H-x_M)^2 + \tfrac{1}{2} k_2(x_X-x_H)^2 + k_{12}(x_H-x_M)(x_X-x_H) \qquad [257]$$

with respect to the potential energy of the system at zero displacement of its constitutent atoms. The forces F on M, H, and X can be calculated as the negative partial derivatives of the potential energy with respect to the displacements along the various coordinates, i.e.

$$\left(\frac{\partial V}{\partial x_M}\right)_{XH} = -F_M = -k_1(x_H-x_M) - k_{12}x_X + k_{12}x_H \qquad [258]$$

$$\left(\frac{\partial V}{\partial x_H}\right)_{MX} = -F_H = k_1(x_H-x_M) - k_2(x_X-x_H) + k_{12}x_X - 2k_{12}x_H + k_{12}x_M \qquad [259]$$

$$\left(\frac{\partial V}{\partial x_X}\right)_{MH} = -F_X = k_2(x_X-x_H) + k_{12}x_H - k_{12}x_M \qquad [260]$$

From one of Newton's laws of motion, the force F is given by the product of the mass and acceleration a, i.e.

$$F = ma = m\frac{d^2x}{dt^2} \qquad [261]$$

In order to find the acceleration, the particles are assumed to execute simple harmonic motions so that

$$x = L \sin(2\pi\nu t + \delta) \qquad [262]$$

where L and δ are constants and ν is the unknown frequency (now in $sec.^{-1}$). Differentiating twice with respect to time gives

$$\ddot{x} = d^2x/dt^2 = -4\pi^2 \nu^2 L \sin(2\pi\nu t + \delta) = -\lambda x \qquad [263]$$

where

$$\lambda = 4\pi^2\nu^2 \qquad [264]$$

Combination of equations [258], [259] and [260] with [261] and [263] leads to

$$(m_A\lambda - k_1)x_M + (k_1 - k_{12})x_H + k_{12}x_X = 0, \qquad [265]$$

$$(k_1 - k_{12})x_M + (m_H\lambda - k_1 - k_2 + 2k_{12})x_H + (k_2 - k_{12})x_X = 0 \qquad [266]$$

and

$$k_{12}x_M + (k_2 - k_{12})x_H + (m_X\lambda - k_2)x_X = 0 \qquad [267]$$

Equations [265], [266] and [267] constitute three homogeneous linear equations in x_M, x_H and x_X. Equation [262] arose from the assumption of simple harmonic motion, and from [265], [266] and [267] it is seen that this assumption is valid only for such values of λ as satisfy the determinantal equation

$$\begin{vmatrix} m_M\lambda - k_1 & k_1 - k_{12} & k_{12} \\ k_1 - k_{12} & m_H\lambda - k_{12} - k_2 + 2k_{12} & k_2 - k_{12} \\ k_{12} & k_2 - k_{12} & m_X\lambda - k_2 \end{vmatrix} = 0 \qquad [268]$$

The determinant gives the polynomial

$$m_M m_H m_X \lambda^3 - (m_M m_H k_2 + m_M m_X k_1 + m_M m_X k_2 + m_H m_X k_1 - 2m_A m_X k_{12})\lambda^2$$

$$+ (m_M + m_H + m_X)(k_1 k_2 - k_{12})^2 \lambda = 0 \qquad [269]$$

There are two solutions to equation [269] which yield

$$\lambda_1 + \lambda_2 = \frac{k_1}{m_M} + \frac{k_2}{m_X} + \frac{k_1 + k_2 - 2k_{12}}{m_H} \qquad [270]$$

and

$$\lambda_1 \lambda_2 = \frac{k_1 k_2 - k_{12}^2}{m_M m_H + m_H m_X + m_H m_X} \qquad [271]$$

where λ_1 and λ_2 refer to the symmetric and asymmetric stretching modes, respectively. For the bending mode, λ_ϕ is given (71) by

$$\lambda_\phi = \left[\frac{r_1^2}{m_H} + \frac{(r_1+r_2)^2}{m_H} + \frac{r_2^2}{m_X}\right] \frac{k_\phi}{r_1 r_2} \qquad [272]$$

Equation [269] contains no constant term so that one of its solutions is $\lambda = 0$. Since the structure is an activated complex, absolute rate theory requires that another vibration be zero or imaginary, i.e. the vibration becomes a translation. This is the asymmetric stretching mode, λ_2, which corresponds to

the reaction coordinate. For simplicity (see also below) λ_2 is set equal to zero (70,193) by equating the numerator $k_1k_2 - k_{12}^2$ in equation [271] to zero, i.e. the condition that the molecule H....H....X be an activated complex is

$$k_1k_2 - k_{12}^2 = 0 \qquad [273]$$

In more sophisticated treatments (51) of isotope effects, it is assumed that $k_1k_2 - k_{12}^2$ is negative, therefore giving the imaginary frequency $\nu_L^{\neq}$. If $\lambda_2 = 0$, equation [270] reduces to

$$\lambda_1 = \frac{k_1}{m_H} + \frac{k_2}{m_X} + \frac{k_1 + k_2 - 2k_{12}}{m_H} \qquad [274]$$

From equation [274], it is seen by reference to equation [173] that if the groups M and X are identical, the term $k_1 + k_2 - 2k_{12}$ is zero so that the symmetric vibration frequency would be independent of isotopic substitution with H, D, or T. For the case of proton discharge onto a mercury cathode, the three-center linear activated complex would have the form $Hg....H....OH_2$ so that for this case the symmetric vibration frequency would be expected to show significant dependence on isotopic mass.

At the present time there is no adequate theoretical method of evaluating the force constants for an activated complex. The semi-empirical method of Eyring (51,66) breaks down badly as discussed by Johnston (81) in the critically important region of the saddlepoint. Sato's (65) method is but a formal extension of Eyring's method which still employs simple London theory to

correlate empirical Morse functions. Instead of using the semi-emperical method, in this thesis a strictly empirical method (81) is used where the parameters are fixed from considerations of molecular structure and molecular spectroscopy. It is claimed by Johnston (81) that by this more empirical approach the required parameters can be fixed, in fact, with increased accuracy. Thus, if reasonable values for the force constants can be estimated by reference to the force constants of molecules of similar structure, such values can be used in the partition function calculations for the activated complex to evaluate the isotope effects S_D, S_T and R.

(iii) Normal Coordinates of the Planar XYZ_2 Molecule (71-73)

There is considerable evidence which was examined in a previous section, that hydrogen atom adsorption can occur at dual or trigonal sites. The activated complex for proton discharge at a dual metal site would then be represented by the planar structure

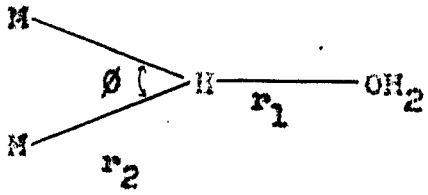

[275]

If the OH_2 group is regarded as a single mass point, then the complex can be treated, for the purpose of vibrational analysis, as analogous to the planar XYZ_2 structure discussed by Herzberg (71).

For this idealized local structure in the metal surface, there are six normal modes which are described by the six equations

$$\lambda_1 + \lambda_2 + \lambda_3 = k_1 \left(\frac{1}{m_{OH_2}} + \frac{1}{m_H} + k_2 \quad \frac{1}{m_H} + \frac{2}{m_H} \cos^2\phi \right)$$

$$+ \frac{2k_\phi + k_{\phi'}}{r_2^2} \left(\frac{1}{m_M} + \frac{2}{m_H} \sin^2\phi \right) \qquad [276]$$

$$\lambda_1 \lambda_2 + \lambda_2 \lambda_3 + \lambda_1 \lambda_3 = k_1 k_2 \left(\frac{1}{m_{OH_2} m_M} + \frac{1}{m_H m_M} + \frac{2}{m_H m_{OH_2}} \cos^2\phi \right)$$

$$+ k_2 \frac{2k_\phi + k_{\phi'}}{r_2^2} \left(\frac{1}{m_M^2} + \frac{2}{m_H m_M} \right)$$

$$+ k_1 \frac{2k_\phi + k_{\phi'}}{r_2^2} \left(\frac{1}{m_{OH_2} m_M} + \frac{1}{m_H m_M} + \frac{2}{m_{OH_2} m_H} \sin^2\phi \right) \qquad [277]$$

$$\lambda_1 \lambda_2 \lambda_3 = k_1 k_2 \frac{2k_\phi + k_{\phi'}}{r_2^2} \left(\frac{1}{m_{OH_2} m_M^2} + \frac{1}{m_H m_M^2} + \frac{2}{m_H m_{OH_2} m_M} \right) \qquad [278]$$

$$\lambda_4 + \lambda_5 = k_2 \left(\frac{1}{m_M} + \frac{2}{m_H} \sin^2\phi \right) + \frac{k_{\phi'}}{r_1^2 r_2^2} \left(\frac{2r_2^2}{m_{OH_2}} + \frac{2(r_2 + r_1 \cos\phi)^2}{m_H} \right) \qquad [279]$$

$$\lambda_4 \lambda_5 = k_2 \frac{k_{\phi'}}{r_1^2 r_2^2} \left(\frac{2r_2^2}{m_{OH_2} m_M} + \frac{r_1^2}{m_M^2} + \frac{2(r_1^2 + r_2^2}{m_H m_M} + \frac{4r_1 r_2 \cos\phi}{m_H m_M} \right.$$

$$\left. + \frac{4r_2^2}{m_{OH_2}^2} \sin^2\phi \right) \qquad [280]$$

$$\lambda_6 = \frac{k_\Delta}{r_1^2 r_2^2 \cos^2\phi}\left[\frac{r_1^2}{2m_M} + \frac{r_2^2\cos^2\phi}{m_{OH_2}} + \frac{(r_1+r_2\cos\phi)^2}{m_H}\right] \qquad [281]$$

The force constants k_1 and k_2 are those of the O-H and M-H stretching modes, respectively; k_ϕ is the M-H-M bending force constant and $k_{\phi'}$ is that for the O-H bend in H_3O^+; k_Δ refers to the force constant associated with a change of the angle between the H-O bond and the plane of

and is very low (e.g. Lechner (73) takes $\lambda_6 = 0$). The six normal modes are shown in Figure 40 (after Herzberg (71), page 65) and it is evident that the mode λ_2 represents the reaction coordinate. The condition that this model represent the activated complex is hence met by taking the vibrational mode λ_2 as being equal to zero, which requires k_1, the stretching force constant for the reacting OH bonds, to be taken as zero (cf. equation [278]); then equations [276] and [277] reduce, respectively, to

$$\lambda_1 + \lambda_3 = k_2\left(\frac{1}{m_M} + \frac{2}{m_H}\cos^2\phi\right) + \frac{2k_\phi + k_{\phi'}}{r_2^2}\left(\frac{1}{m_M} + \frac{2}{m_H}\sin^2\phi\right) \qquad [282]$$

and

$$\lambda_1\lambda_3 = k_2\,\frac{2k_\phi + k_{\phi'}}{r_2^2}\left(\frac{1}{m_M^2} + \frac{1}{m_H m_M}\right) \qquad [283]$$

Figure 40

Normal modes of vibration of planar XYZ_2 molecules (after Herzberg; reference 71, page 65).

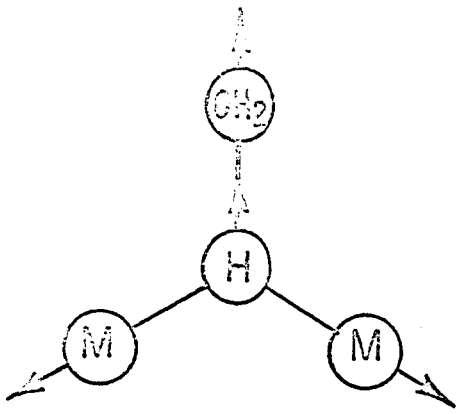

ν_1

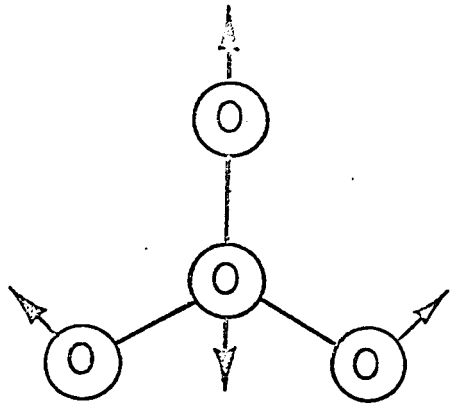

ν_2

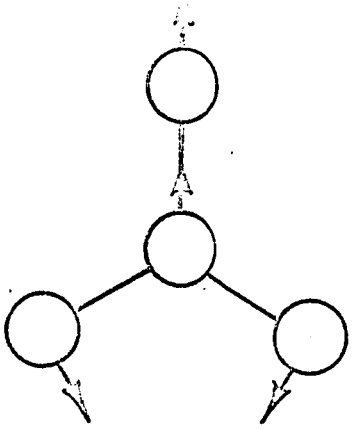

ν_3

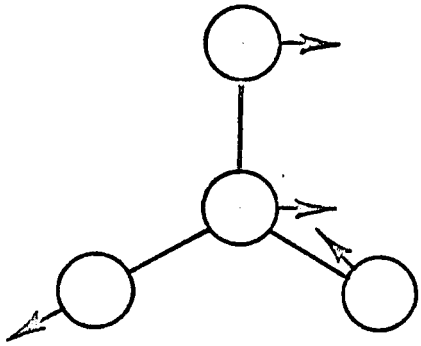

ν_4

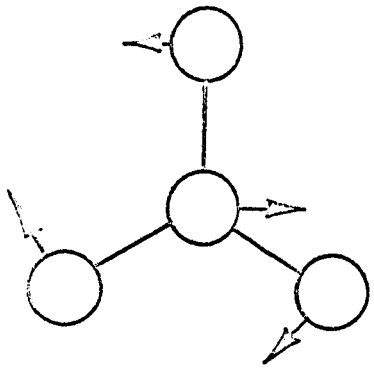

ν_5

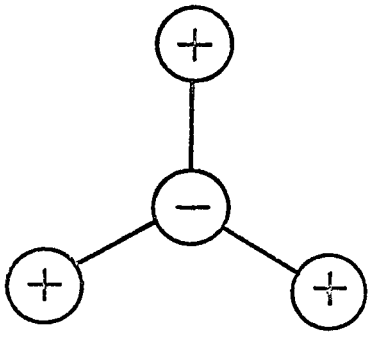

ν_6

From the above treatment, the vibrational frequencies for the planar XYZ_2 activated complex are obtained and substituted into the partition function ratio

$$\frac{f^{\neq}_{H_2}}{f^{\neq}_{HD}} = \frac{\sigma_D^{\neq}}{\sigma_H^{\neq}} \prod^{2} \frac{f^{\neq}_{t,H}}{f^{\neq}_{t,D}} \prod^{2} \frac{f^{\neq}_{r,H}}{f^{\neq}_{r,D}} \prod^{5} \frac{\sinh u^{\neq}_{HD}/2}{\sinh u^{\neq}_{H_2}/2} \qquad [284]$$

(iv) General Considerations

It must be emphasised that the empirical method used here to estimate force constants is to be regarded as an approximate one and is used in an exploratory fashion to examine the values of S_D, S_T and R which can be obtained for the models suggested and for ranges of values of the relevant force constants. It cannot be regarded as absolute in the sense that exact agreement between theory and experiment is expected. In the theory presented above, several points which are considered in more sophisticated treatments have been neglected. As discussed above, however, it would also be extremely naive to expect the more sophisticated treatment to predict any exact agreement between theory and experiment. The simpler treatment presented here provides a basis for indicating the principles involved and the expected magnitudes of the isotope effects which can arise for different models and mechanisms.

G. Results of the Calculations

(1) Rate-controlling Proton Discharge at Mercury Cathodes

(a) The Separation Factors S_D and S_T, and the Exchange Current Density Ratio R at Mercury Cathodes - The Linear Pseudo-Three Atom Model

In order to evaluate equation [256] for the linear complex

$$Hg \overset{1}{\text{———}} H \overset{2}{\text{———}} OH_2$$

values for r_1, r_2, k_1, k_2, and k_β must be assigned. The distances involved in the activated complex were calculated as follows: the position of the reacting H, D, or T entity is assumed to be half way between its position in the initial and final states (this corresponds, approximately, to taking β as 0.5 which is close to the experimentally observed value); the metallic radius for Hg is 1.50 Å (194); the O-H distance in the initial state of H_3O^+ is taken as 1.05 Å (74,195); the Hg-H distance in the final state is taken as 1.74 Å (163); finally, the thickness of the double-layer has been previously taken as 1.79 Å (110), i.e. the distance between the center of the oxygen atom and the surface of the electrode. This gives a total distance of 0.5 Å through which the proton is transferred from the initial to the final state as in the previous potential energy profile calculations (100,110).

For the linear pseudo-three-atom model, there are four frequencies associated with the activated complex. The asymmetric stretch corresponds to decomposition; $\nu_1^{\neq}$ is the symmetric stretching frequency and $\nu_\phi^{\neq}$ is the bending frequency which is doubly degenerate; $\nu_1^{\neq}$ and $\nu_\phi^{\neq}$ are calculated by taking $k_1k_2 - k_{12} = 0$ as discussed previously. Since the coupling constant k_{12} can be significant for activated complexes (70), k_1 or k_2 is not necessarily taken as zero. The condition that $k_1 > k_2$ is taken for the following reasons: the activated complex has the form Hg-H-O in which the initial bond between H and O (corresponding to k_2) is being broken while the new bond between Hg and H (corresponding to k_1) is being formed. The condition that the system Hg-H-O be an activated complex is that one of its frequencies is low and becomes a translation (51). This condition is met by taking the frequency (and hence the force constant) for the asymmetric stretch in the dissociating bond as equal to, or close to zero. This assumption is contrary to the usual assumption that the activated complex is invariant as th the direction from which it is formed; i.e. the above assumption results in two <u>different</u> activated complexes depending whether the reduction of H^+ ions is occurring (reaction [1] or whether the oxidation of adsorbed hydrogen is occurring (the reverse of reaction [1]). This situation is not considered to be unrealistic since the formation of the activated complex is associated with a momentum in the <u>direction</u> of the reaction and its structure may therefore be regarded as being "polarized"

in this direction. The problem centers around the nature (and characterization) of the activated complex and the overall reaction mechanism. One cannot distinguish between the possibility of electron tunneling to the activated complex and the possibility of an electron transfer to the proton after it has physically reached the electrode surface. Hence any treatment of the activated complex is open to question and in this thesis, we have sought to calculate maximum (and minimum) isotope effects for all possible types of models. In calculating S and R for this assumption, three calculations have been made where k_1, k_2, and k_ϕ are varied to test the sensitivity of the calculated quantities on the choice of force constants. The data for these calculations are given in Table IX. In addition to these three calculations, a fourth calculation was made which corresponds to the conventional concept that the activated complex is invariant as to the direction from which it is formed. This is shown as calculation number 4 in Table IX. The values of k_1 and k_2 were chosen to be one-half their normal value (81,60). The results of the vibrational analysis are shown in Tables X and XI. S_D, S_T and R are calculated from [231], [232] and [249], respectively, and the results are given in Table XII.

The importance of the above calculations is to test the sensitivity of S and R quantities by reference to any possible structure of the activated complex in order to obtain maximum (and minimum) values. It is seen in Table XII that the S and R values are, of course, significantly dependent on the choice of force constants, but in no case does S_D approach

Table IX

Numerical Data Used for Vibrational Analysis of the Linear Hg-H-O Complex

Calculation Number	Interactomic Distances (Å)		Force Constant (m.d. Å^{-1})			Force Constants for the Isolated Molecule (m.d. Å^{-1})*	
	r_1	r_2	k_1	k_2	k_ϕ	k_1'	k_2'
1	1.99	1.30	1.15	0.414	0.077-0.035	1.159(HgH); 4.9 (H_3O^+)	
2	1.99	1.30	1.159	0.1	0.077-0.035		
3	1.99	1.30	1.159	0	0.077-0.035		
4	1.99	1.30	0.53	2.46	0.077-0.035		

* Force constants for Hg-H, H_3O^+, and H_2O were obtained from references 163, 107, and 61, respectively.

Table X

Bending Frequencies ($\nu_{\phi}^{\neq}$) for the Hg-H-O Complex as a Function of the Force constant k_{ϕ} (25°C)

Frequency	$k_{\phi} \times 10^{11}$ erg/rad^2 0.1	0.15	0.20
$\nu_{\phi,H_2}^{\neq}$ (cm^{-1})	845	1035	1196
$\nu_{\phi,HD}^{\neq}$	601	736	850
$\nu_{\phi,HT}^{\neq}$	493	604	697
$\nu_{\phi,D_2}^{\neq}$	600	735	849
$\frac{\sinh u^{\neq}_{HD}/2}{\sinh u^{\neq}_{H_2}/2}$	0.5335	0.4755	0.4276
$\frac{\sinh u^{\neq}_{HT}/2}{\sinh u^{\neq}_{H_2}/2}$	0.3950	0.3366	0.2902
$\frac{\sinh u^{\neq}_{D_2}/2}{\sinh u^{\neq}_{H_2}/2}$	0.5325	0.4740	0.4268

Table XI

Stretching Frequencies ($\nu_1^{\neq}$) and Moments of Inertia (I) for the Linear Three-Atom Complex Hg-H-O. (25°C)

	Calculation Number			
	1	2	3	4
$\nu_1^{\neq}{}_{,H_2}$ (cm^{-1})	994	1000	1405	1200
$\nu_1^{\neq}{}_{,HD}$	710	714	996	915
$\nu_1^{\neq}{}_{,HT}$	585	588	709	798
$\nu_1^{\neq}{}_{,D_2}$	709	712	995	914
$\left(\frac{\sinh u^{\neq}_{HD}/2}{\sinh u^{\neq}_{H_2}/2}\right)_1$	0.4918	0.4895	0.3701	0.4986
$\left(\frac{\sinh u^{\neq}_{HT}/2}{\sinh u^{\neq}_{H_2}/2}\right)_1$	0.3539	0.3512	0.1807	0.3722
$\left(\frac{\sinh u^{\neq}_{D_2}/2}{\sinh u^{\neq}_{H_2}/2}\right)_1$	0.4907	0.4895	0.3700	0.4983
Moments of Inertia				
I_{H_2} (x 10^{38} gm.cm.^{2})		3.509		
I_{HD}		3.568		
I_{HT}		3.628		
I_{D_2}		3.952		

Table XII

Calculated Values of S_D, S_T and R for the Linear Hg-H-O Complex at 25°C

Quantity	Bending Force Constant, $k_\phi \times 10^{11}$ erg/rad^2			Calculation Number
	0.1	0.15	0.20	
S_D	5.22	4.14	3.35	1
S_T	9.24	6.71	4.99	
R	2.78	2.21	1.79	
S_D	5.19	4.13	3.34	2
S_T	9.17	6.66	4.95	
R	2.77	2.20	1.78	
S_D	3.92	3.12	2.52	3
S_T	4.72	3.43	2.55	
R	2.10	1.66	1.35	
S_D	5.29	4.20	3.40	4
S_T	9.71	7.06	5.25	
R	2.82	2.24	1.82	

the value of 13 claimed as limiting by Keil and Kodera (168).

Hence acceptable S and R values can be predicted by varying k_1 from its normal value of 1.159 md. Å^{-1} in the isolated Hg-H molecule (163) to one-half this value. Bending force constants are assigned by comparison with approximately similar stable molecules. For bending about X-H-X half bonds, the force constant derived from hydrogen-bonded systems was assigned (196) the value of 0.16×10^{-11} erg/rad^2. By the fitting of force constants to the kinetic data for the reaction $H_2 + Cl = H + HCl$, the bending force constant of H-H-Cl was assigned (197) the value of 0.05×10^{-11} erg/rad^2. For activated complexes in which bending occurs about a central H atom, the force constants k_β assigned are reduced and are taken to be around one-half the value of the force constant in the analogous stable molecule (81,200). For the Hg-H-C activated complex, Keil and Kodera (168) have calculated a value of 0.15 m.d. Å^{-1} for k_β (i.e. 0.39×10^{-11} erg/rad^2). This value appears to be rather too high and in order to test Keil and Kodera's method of evaluating k_β, Conway and Salomon (198) have made a similar calculation of the bending force constant of the $F\text{-}H\text{-}F^-$ ion (using the molecular parameters for the HF molecule) as a model for the transition state in proton transfer (cf. 18). A bending frequency of 1225 cm^{-1} is calculated which is in satisfactory agreement with the observed (199) value of

1240 cm^{-1}. The very good agreement between the observed and calculated frequency is surprising and may in part result from the neglect of repulsion forces which would tend to cancel with the delocalization forces as they do in H-bonds in ice (201,202). The calculation made by Keii and Kodera employs the $H-H_2$ repulsive energy function of Amdur (161) for estimating the $H-OH_2$ repulsion and the possible errors involved in this calculation has been discussed in Chapter III. The Keii and Kodera value (166) of $0.39.10^{-11}$ erg/rad^2 would give somewhat lower values of S and R when the present method of calculation is used (their own method, neglecting the symmetrical stretching mode gives too high values for S_D).

(b) The Planar XYZ_2 Configuration

The partition function ratio for this kind of activated complex is given by equation [284] and the following approximations are made: both the rotational and translational partition function ratios are taken as unity on account of the nature of the surface Mg_2-H-O complex. Thus the main isotope effect arises from the differences of vibrational frequencies and the ratio $f_{\neq,H_2}/f_{\neq,HD}$ is given by

$$\frac{f_{\neq,H_2}}{f_{\neq,HD}} = \prod^{5} \frac{\sinh u^{\neq}_{HD}/2}{\sinh u^{\neq}_{H_2}/2} \qquad [285]$$

The vibrational analysis is made using equations [279]-[283]. The distances r_1 and r_2 and the angle ϕ are calculated according to the geometry of the problem using the data previously applied to the three-center model. The data used to carry out the vibrational analysis are shown in Table XIII. The choice of force constants is here more arbitrary and values could be changed significantly from those given in Table XIII and still predict acceptable values for S and R. For the most part, force constants were chosen by reference to accepted values for analogous stable molecules; i.e. k_2 has as its analogue the B-H ring stretching force constant given as 1.43 m.d. Å^{-1} by Bell and Longuet-Higgins (154) for diborane. The force constant k_ϕ, used here corresponds to Bell and Longuet-Higgins's d_1 which was given the value 0.12×10^{-11} erg/rad^2 (.059 m.d. Å^{-1}) and the value used here is 0.16×10^{-11} erg/rad^2. Bell and Longuet-Higgins's force constant d_3 (taken by them as zero) corresponds to k_ϕ which has been assigned the value of 0.25×10^{-11} erg/rad^2 (222) in the present calculation. The activated complex considered here does not have any satisfactory stable molecule analogue. There are no planar XYZ_2 molecules in which a hydrogen constitutes the central (Y) atom. In view of this situation, it becomes necessary to test the sensitivity of the calculated values of S and R to the choice of force constants. This has been done and the results are shown in Table XVI. It

Table XIII

Parameters Used for S and R Calculations at H_2 for the Dual Site Model

Calculation Number	Angle ø	Interatomic Distances (Å)		Force Constants (m.d.Å^{-1})				
		r_1	r_2	k_1	k_2	k_ϕ	k_ϕ'	k_Δ
1	104°5'	1.325	1.894	0.0	0.6	0.10	0.064	0.08- .02
2	"	"	"	0.0	0.8	0.10	0.064	0.08-0.02
3	"	"	"	0.0	1.0	0.10	0.064	0.08-0.02

is seen that the values of S and R, although significantly different, cannot be "adjusted" by any reasonable choice of force constants, to give values of S_D higher than ca. 5. The importance of this calculation therefore lies in the fact that reasonable values of S and R can be predicted for the dual site model on the basis of discharge step. In the calculation of Keii and Kodera (168), a minimum value of 13 was claimed to arise for S_D on the basis of a rate-limiting discharge step. In the present calculations, values of $S_D = 13$ cannot be approached even if an appreciable degree of freedom is allowed in the choice of force constants.

For the dual site model, there are five vibrations in the activated complex as indicated by equation [285]. Upon carrying out the vibrational analysis, the vibrational mode terms λ_3 and λ_5 turn out to be independent of isotopic substitution, i.e. $\nu^{\neq}_{3,H} = \nu^{\neq}_{3,D}$ and $\nu^{\neq}_{5,H} = \nu^{\neq}_{5,D}$. The results of the vibrational analysis are given in Tables XIV and XV, and the calculations for S and R are given in Table XVI.

(c) Comparison of Calculated and Experimental S and R Values

It must be emphasized again that the main purpose of the comparisons to be made in this section is not to demonstrate any exact agreement between experimental results and the theoretically calculated values of S which would be presumptuous for calculations

Table XIV

Frequency $\nu_6^{\neq}$ for the Planar Hg_2-H-O Type Complex as a Function of the Force Constant k_Δ

Quantity	$k_\Delta \times 10^{11}$ erg/rad^2 0.05	0.10	0.15	0.20
$\nu_{6,H}^{\neq}$ ($cm.^{-1}$)	385	545	667	771
$\nu_{6,D}^{\neq}$ "	275	390	477	551
$\nu_{6,T}^{\neq}$ "	222	315	385	445
$\left(\frac{\sinh u_D^{\neq}/2}{\sinh u_H^{\neq}/2}\right)_6$	0.6681	0.6286	0.5930	0.5610
$\left(\frac{\sinh u_T^{\neq}/2}{\sinh u_H^{\neq}/2}\right)_6$	0.5260	0.4834	0.4454	0.4124

Table XV

Frequencies $\nu_1^{\neq}$ and $\nu_4^{\neq}$ for the Planar Mg_2-H-O Type Complex

Quantity	Calculation Number* 1	2	3
$\nu_{1,H}^{\neq}$ ($cm.^{-1}$)	849	875	900
$\nu_{1,D}^{\neq}$ "	601	620	638
$\nu_{1,T}^{\neq}$ "	490	505	520
$\nu_{4,H}^{\neq}$ "	1408	1618	1804
$\nu_{4,D}^{\neq}$ "	1000	1149	1280
$\nu_{4,T}^{\neq}$ "	813	934	1042
$\left(\frac{\sinh u_D^{\neq}/2}{\sinh u_H^{\neq}/2}\right)_1$	0.5279	0.5211	0.5132
$\left(\frac{\sinh u_T^{\neq}/2}{\sinh u_H^{\neq}/2}\right)_1$	0.3871	0.3796	0.3721
$\left(\frac{\sinh u_D^{\neq}/2}{\sinh u_H^{\neq}/2}\right)_4$	0.3841	0.3213	0.2811
$\left(\frac{\sinh u_T^{\neq}/2}{\sinh u_H^{\neq}/2}\right)_4$	0.2418	0.1900	0.1580

* The calculation number refers to the corresponding data and calculations in Table XII; it also refers to the different values of k_2 used.

Table XVI

Calculated Values of S and R at 25° for Discharge at Hg Based on the Dual Site Model

	$k_\Delta \times 10^{11}$ erg/rad^2				
	0.05	0.10	0.15	0.20	Calculation Number
S_D	5.16	4.85	4.58	4.33	
S_T	8.60	7.81	7.29	6.75	1 (k_2= 0.6 m.d. A^{o-1})
R	2.71	2.55	2.40	2.28	
S_D	4.26	4.01	3.78	3.56	
S_T	6.63	6.09	5.61	5.20	2 (k_2= 0.8 m.d. A^{o-1})
R	2.24	2.11	1.99	1.88	
S_D	3.67	3.46	3.26	3.08	
S_T	5.40	4.46	4.57	4.24	3 (k_2= 1.0 m.d. A^{o-1})
R	1.93	1.61	1.71	1.62	

Experimental values at 25°C for S_D, S_T and R are given in Table XVIII.

of isotope effects. The main purpose is rather to show that: (α) the value of $S_T = 13$ deduced by Keii and Kodera (168) and $S_T = 37$ deduced by Kodera and Saito (170) can be brought down to values comparable with the observed ones by the appropriate inclusion of a symmetrical stretching mode in the activated complex and (β) the radical deduction from the previous calculations of S_D and S_T (168,169,170) that the slow discharge mechanism is <u>not</u> operative at mercury electrodes, is hence, in fact, unnecessary, and finally (γ) a model for dual site chemisorption of hydrogen atoms can satisfactorily explain the observed isotope effects. We cannot, however, expect to differentiate between the applicability of the dual site and single site models on the basis of quantitative agreement with experiment. The importance of the calculation lies more in the fact that with a physically more realistic model for H-atom adsorption (as discussed above), the same magnitudes of S_D, S_T and R can be calculated for either model, and are still well below those claimed as <u>limiting minimum</u> values by Kodera <u>et al.</u> (168,169,170) and Horiuti (11). Experimental values of S_D, S_T, and R for mercury reported in several papers, including the present work, are summarized in Table XVII. By comparison of the predicted and experimental values of S and R, there is no doubt that the observed kinetic isotope effects can be reasonably explained on the basis of a rate-limiting H^+ ion

Table XVII

Experimental S_D, S_T and R Values at Mercury at 25°C

	Experimental Value (25°)	Reference
S_D	2.5-4 (aqueous)	present work (cf. also 113,115,116,117)
	4.00 (non aqueous)	present work
S_T	5.8 (average value)*	114
	3.8, 5.1**	117
R	2.0 (aqueous)	111,112
	3.3 (non aqueous)	present work.

* Average value without consideration of potential dependence.

** Two values of S_T are reported for a current density of 100 mA. cm^{-2}.

discharge step. Although there have been other attempts to calculate S on the basis of the discharge mechanism (see Chapter III), no other workers have either justified the isotope effects in terms of the slow discharge step or offered a satisfatory explanation of the decrease in S as η increases. In addition, there has not been any attempt to calculate R values from first principles or to relate them to corresponding S values, and only in recent work from this Laboratory have R values in fact been available (150).

In the previous discussion (Chapter V), the decrease in S at mercury as η increases was attributed to a compression of the double-layer which could result in either (or both) the increase of the bending or stretching force constants. The dependence of S_D and S_T on values of the relevant force constants is shown in Figure 41 where S_D and S_T values for the linear model for several values of k_2 (Hg-H force constant) are plotted against k_ϕ (the bending force constant). No calculations have been made to relate S to R in terms of a slow discharge mechanism at mercury in alkaline solution since the discharge step has been shown not to be rate-determining under these conditions (see discussion in Chapter II).

Figure 41

S_D and S_T at mercury cathodes as a function of bending (k_β) and stretching (k_2) force constants based on a linear three-center activated complex.

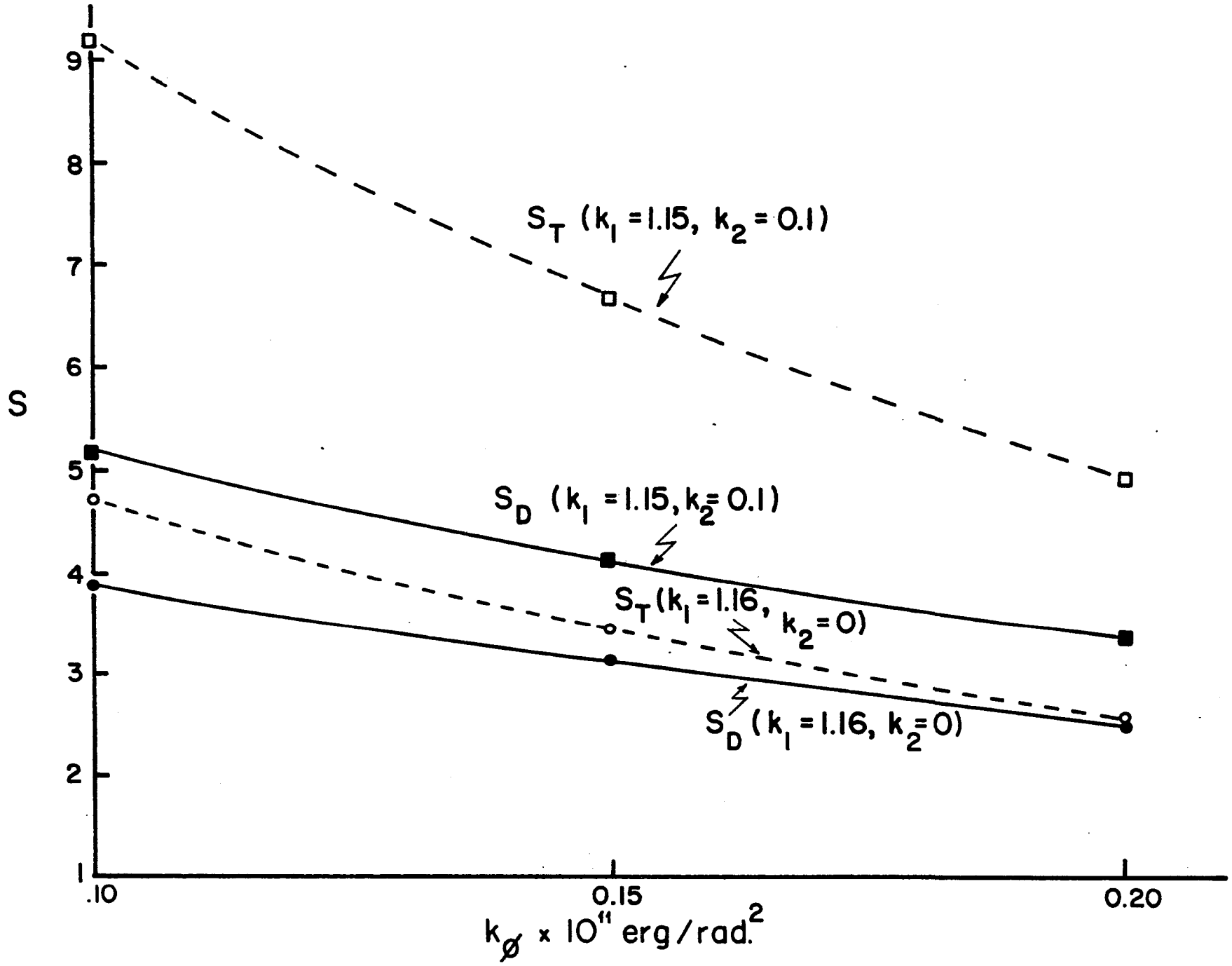
S
1
9
8
7
6
5
4
3
2
1
S_T (k_1 = 1.15, k_2 = 0.1)
S_D (k_1 = 1.15, k_2 = 0.1)
S_T (k_1 = 1.16, k_2 = 0)
S_D (k_1 = 1.16, k_2 = 0)
.10
0.15
0.20
k_ϕ x 10^{11} erg/rad.^{2}

(ii) Values of S_D, S_T and R at Ni, Fe and W Electrodes Based on the Slow Discharge Mechanism

(a) General Discussion of Mechanisms

At nickel electrodes a Tafel slope of 90-110 mV. in acid solutions(203-207) indicates either slow discharge or slow atom-ion desorption at appreciable H-coverage. Owing to the tendency for dissolution of Ni and Fe in acid solutions, studies at low overpotentials are difficult and do not yield significant information. In alkaline solutions a Tafel slope of 90-110 mV. is also observed (203,205,211). There is sufficient evidence, however, (203,207) from electrode-kinetic behaviour that the discharge step is rate-controlling at nickel in alkaline solution.

For tungsten electrodes in acid solutions, two Tafel slopes are observed (45,93,114), the initial slope having a value of 60-80 mV and being followed by a slope of 105-116 mV. The mechanism(s) operative are unclear in that any one of mechanisms [1]-[3] can be ascribed to the various slopes (see Table I). Thus Bockris et al. (45,93,114) are in favour of a slow electrochemical mechanism as an explanation for the higher slope (110mV) and a slow surface migration of H atoms for the initial 60 mV region (93). It is clear (see Table I) that this value could also arise with steps [2] or [3] under activated adsorption conditions. In alkaline solutions, a slow discharge mechanism

is indicated (114,203) for the 110 mV. region.

At iron electrodes in acid solutions, a Tafel slope of 133 mV. is found (45) which is attributed to a slow discharge step. It appears that for these cases the assignment of mechanism can possibly be aided by a study of isotope effects.

(b) Calculation of Isotope Effects

By a method identical with that used to calculate S and R at mercury for the linear three-center activated complex, the corresponding values for Ni, Fe, and W electrodes have also been estimated. The numerical data used for the vibrational analysis are given in Table XVIII and the results of the calculations are given in Table XIX. The R and S values based on discharge at a dual nickel site have been calculated and the results are given in Table XX. In Table XXI, the experimental S and R values are given for Ni, W, and Fe cathodes for comparison. For nickel no R values in alkaline solutions are available. S_D and S_T values are available but the values of S_T found by Vielstich et al. (117) differ from those of Bockris et al (114). The latter value is probably the better one since in the former, Raney-nickel was used and the presence of traces of aluminium would almost certainly affect S_T. The value of 4.1 for S_T in alkaline solutions is in accord with the possible values calculated in Tables XIX and XX for the discharge mechanism. The value of 18 for S_T in acid solutions on nickel cannot be accounted for

Table XVIII

Numerical Data Used for Vibrational Analysis of Linear Ni, W, and Fe Activated Complexes in the Discharge Mechanism

Metal	Interatomic Distances (Å) r_1	r_2	Proton Source	Force constants (m.d.Å^{-1}) k_1	k_2	k_ϕ	Force Constants* for the Isolated Molecules (m.d.Å^{-1}) k_1	k_2	Calculation Number
	1.732	1.308	H_3O^+	2.062	0.246	0.09-0.04	2.11	4.9	1
Ni	1.720	1.240	H_2O	2.062	0.390	0.09-0.04		7.8	
	1.732	1.308	H_3O^+	1.95	0.49	"	"	"	2
Ni	1.720	1.240	H_2O	1.95	0.78				
	1.732	1.308	H_3O^+	1.15	0.10	"	"	"	3
Ni	1.720	1.240	H_2O	1.15	0.159				
	1.880	1.295	H_3O^+	2.11	0.49	0.08-0.04	2.35(212)	"	1
W	1.875	1.230	H_2O	2.11	0.78	"			

(Continued next page)

Table XVIII - continued

W	1.880 1.875	1.295 1.230	H_3O^+ H_2O	1.15 1.15	0.10 0.159	0.08-0.04	2.35	4.9 7.8	2
Fe	1.732 1.720	1.308 1.240	H_3O^+ H_2O	1.10 1.10	0.10 0.159	0.09-0.04 "	2.2(212)	"	1

* These force constants k_1 and k_2 refer to the metal-H interaction and the OH stretch in H_3O^+ or H_2O, respectively.

Table XIX

Calculated Isotope Effects (25°C) for Proton Discharge at Several Metals (Linear 3-centre Complexes)

Source of H / Metal		H_3O^+ $k_\phi \times 10^{11}$ erg/rad^2 0.1	0.15	0.2	H_2O $k_\phi \times 10^{11}$ erg/rad^2 0.1	0.15	0.2	Calculation Number*
Ni	S_D	3.20	2.55	2.01	5.32	4.31	3.55	1
	S_T	4.71	3.44	2.55	9.68	7.19	5.49	
	R	1.68	1.34	1.06	3.13	2.54	2.09	
Ni	S_D	5.60	4.46	3.53	7.30	5.92	4.87	2
	S_T	11.53	8.43	6.24	15.38	11.43	8.73	
	R	3.09	2.46	1.94	4.23	3.43	2.83	
Ni	S_D	5.45	4.34	3.43	6.77	5.49	4.52	3
	S_T	10.08	7.33	5.46	11.97	8.89	6.79	
	R	2.86	2.28	1.80	3.98	3.23	2.66	
W	S_D	5.57	4.39	3.59	6.64	5.26	4.28	1
	S_T	9.69	5.67	5.18	13.48	9.55	7.31	
	R	2.88	2.28	1.86	3.90	3.09	2.51	

(Continued next page)

Table XIX - Continued

	S_D	5.43	4.28	3.50	6.00	4.76	3.87	
W	S_T	9.22	5.39	4.93	11.14	7.90	6.04	2
	R	2.85	2.225	1.84	3.53	2.80	2.28	
	S_D	5.59	4.42	3.64	5.96	4.85	3.85	
Fe	S_T	10.49	7.69	5.78	11.74	8.78	6.40	1
	R	2.93	2.32	1.91	3.51	2.85	2.27	

For other force constants used see corresponding calculation numbers in Table XX.

Table XX

Calculated Isotope Effects (25°) at Ni for Discharge at a Dual Site

	H_3O^+ $k_\Delta \times 10^{11}$ erg/rad^2			H_2O $k_\Delta \times 10^{11}$ erg/rad^2			Distances (Å) and Angle of the Ni-H-Ni Link						Force Constants*			
							H_3O^+			H_2O						
	0.1	0.15	0.2	0.1	0.15	0.20	r_1	r_2	Ni⁄H⁀Ni angle	r_1	r_2	Ni⁄H⁀Ni angle	k_1	k_2	k_ϕ	k_ϕ'
S_D	2.41	2.03	1.73	3.40	3.08	2.72	1.286	1.621	99° 48'	1.251	1.652	98° 24'	0	0.6	0.25	0.16
S_T	3.99	3.07	2.47	5.2	4.2	3.6		"			"					
R	1.27	1.06	0.91	2.00	1.32	1.61		"			"					

* k_1 in units of m.d. Å^{-1}

k_ϕ and k_ϕ' in units of 10^{-11} erg/rad^2.

Table XXI

Observed S and R Values at Ni, W, and Fe Cathodes at 20-25° C

Metal	Proton Source	H_3O^+	(Reference)	H_2O	(Reference)
Ni	S_D	7.0 6.7	113 9,68	4.5-6.5	116-117
	S_T	18.0(average value)	114	24.5(Raney-Nickel) 4.1(Average value)	117 114
	R	3.0	125	-	-
Fe	S_D	-	-	7(max. value)	116,213
	S_T	-	-	12.0(max. value)	117
	R	3.0	45	-	-
W	S_D	-	-	-	-
	S_T	6.0** (Average value)	114	4.4** (Average value)	114
	R	3.4* 6.3**	45	-	-

* Value for initial (low) Tafel slope region.

** Value for second (high) Tafel slope region.

in terms of a slow discharge mechanism by any reasonable adjustment of force constants. The reported average value of $S_p = 4.1$ (114) is, however, misleading since it does not explain (or even infer) a possible potential dependence of S_p. That S_p would be potential dependent at Ni is indicated from the work of Vielstich et al. (116). These authors find that as η increases, S_p increases from ca. 3.8 to a maximum of ca. 6.5 and then decreases to ca. 5. This result more clearly shows the facts than the reported average values and can be qualitatively explained in terms the slow discharge step as follows:

At nickel, it appears that the discharge step is rate-determining in alkaline solutions (203,208) with desorption by the atomic recombination mechanism (208). Under these conditions, θ_H can be increased with increasing cathodic potential or current density (208). The increase of S with potential may hence arise through the effects of increasing coverage of the electrode by H. If the energy of adsorption of H falls with increasing coverage, as is the case at most metals (174), it may be expected that the frequency and associated force constant also decrease with coverage; for example, Conway (125) has indicated / that for a series of metals, the M-H bond frequency in diatomic hydrides decreases linearly with the M-H bond energy (Figure 42). Thus, in the case of Ni, it appears reasonable to suppose that decreasing M-H adsorption energy with increasing θ_H can lead to increasing S values owing

Figure 42

Fundamental frequencies and dissociation energies for certain diatomic hydrides (after Conway, reference 125).

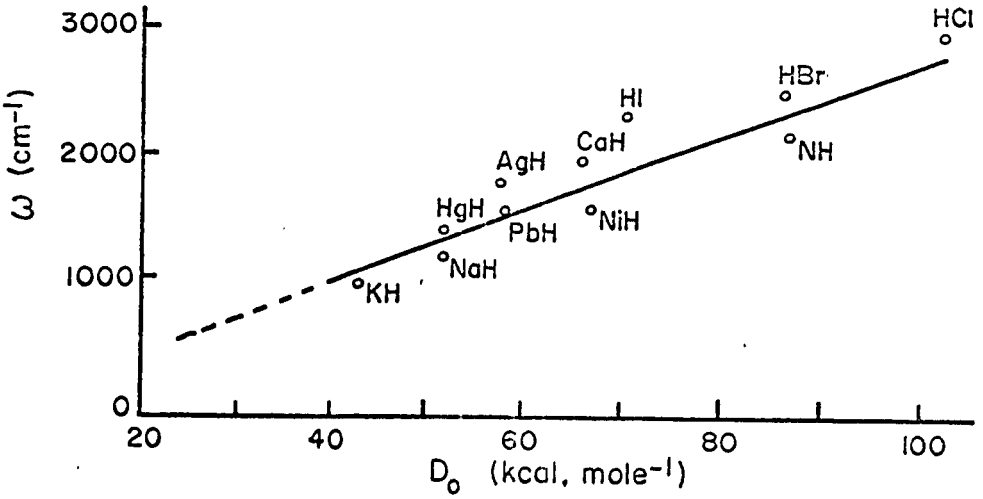
3000
2000
1000
0
ω (cm⁻¹)
HCl
HBr
HI
CaH
AgH
NH
HgH
NiH
PbH
NaH
KH
20
40
60
80
100
D₀ (kcal. mole⁻¹)

to the decrease in the M-H force constant. This is qualitatively shown in Figure 43 for the linear three-center activated complex. For a given value of k_β and k_2 (the Ni-H-O bend and O-H force constants, respectively), the separation factor is evaluated in neutral or alkaline solutions for variation of Ni-H force constant k_1. The values of k_1 were chosen such that they corresponded to a decrease in the heat of adsorption of about 16 kcal mole^{-1} from the initial value of -67 kcal mole^{-1} at zero coverage (e.g. see reference 125). To explain the final decrease in S_D at high values of η, the effect of compression of the double-layer is suggested (see p. 163-166). The effect can be seen in Figure 43 where the three curves are significantly dependent on k_β. Hence the calculated and observed values of the isotope effects at nickel electrodes can be qualitatively explained in terms of slow atom-ion recombination in acid solution and slow discharge in alkaline solution.

The assignment of mechanism for W electrodes is more ambiguous than that for Ni. The published experimental data are incomplete and only qualitative assignments can be made. On the basis of $S_T = 4.4$ for alkaline solutions, slow proton discharge is inferred as the rate-controlling mechanism since the value for S_T was obtained in the Tafel region where the slope is 110 mV. However, since the value for S_T is an average value (114), the nature and magnitude of any possible maxima or changes with

Figure 43

S_D at nickel electrodes as a function of k_1 and k_ϕ for discharge from a water molecule.

1. $k_2 = 0.1$ md. Å^{-1}; $k_\phi = 0.1 \times 10^{-11}$ erg/rad^2
2. $k_2 = 0.1$ md. Å^{-1}; $k_\phi = 0.15 \times 10^{-11}$ erg/rad^2
3. $k_2 = 0.1$ md. Å^{-1}; $k_\phi = 0.20 \times 10^{-11}$ erg/rad^2.

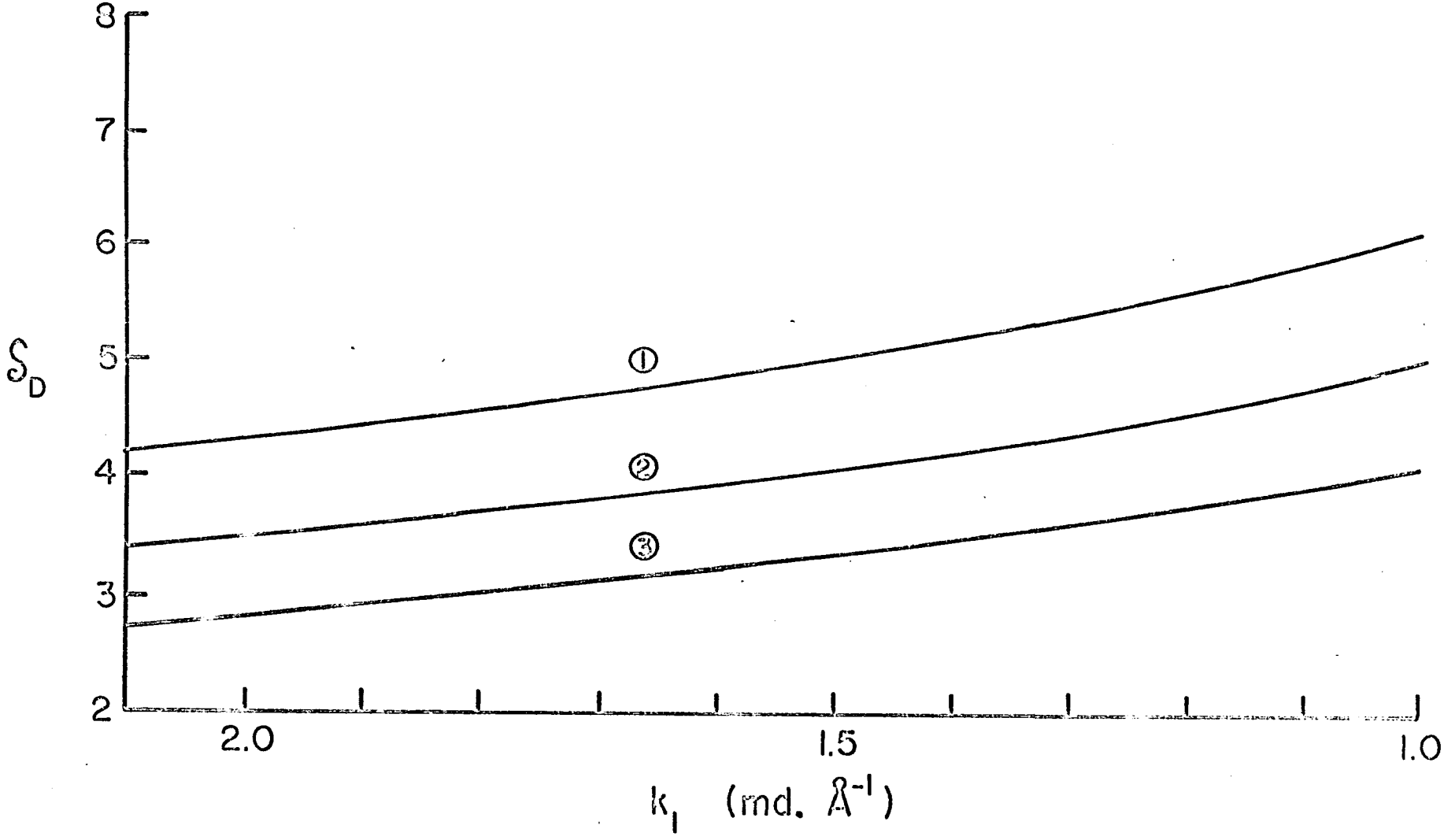
8
7
6
5
4
3
2
S_D
①
②
③
2.0
1.5
1.0
k_1 (md. Å^{-1})

potential are unknown. Similarly in acid solutions, the atom-ion recombination is a fair assignment for the high Tafel slope region.

Assignment of mechanism to the process at Fe cathodes also involves some speculation. On the basis of the Tafel slopes and isotope effects, it is difficult to distinguish between a slow discharge or a slow atom-ion desorption.

(iii) The Recombination Steps [2] and [3]: Mechanism of the H.E.R. on Platinum Electrodes

(a) General Discussion

In a previous discussion, the rate-determining mechanisms operative at platinum electrodes were stated to be the atom-atom recombination at low η and the atom-ion recombination at high η. This assignment was seen to be compatible with behavior at various pH's, the Tafel slopes, anion effects on S_p, and the proposal of a multiple site adsorption mechanism. Multiple site adsorption is indicated by adequate evidence as shown previously, and the fact that the isotope effects based on a discharge mechanism can be shown to be not inconsistent with the dual adsorption site model is regarded as some confirmation of this model. Once it is conceded that dual site adsorption is possible, adsorption at sites of higher multiplicity (i.e. 3 and 4 centre sites) becomes a possibility. The vibrational analysis for the atom-atom recombination step for this model is extremely complex and the most efficient method of

analysis would be by machine computation. Schachtschneider (214) has written a programme for the I.B.M. 7090 which enables such an analysis to be carried out. Since the programme is not available at the present, the vibrational analysis for the atom-atom recombination step is not given here. In the case of atom-ion desorption, additional problems concerning geometry of the activated complex arise. In the previous discussion (Chapter III; equations 235-238, Chapter VI), a linear activated complex was assumed in which case differentiation must be made between the two complexes M-H-D-O and M-D-H-O. However, if a non-linear complex exists, such as that considered by Horiuti (10,11), there is the possibility that the D-activated complex is indistinguishable whether the initial state is M-H + H_2DO^+ or M-D + H_3O^+. Such an activated complex may be visualized as a resonating structure of the following type

[286]

Complexities of this type do not arise in either the discharge step or the atom-atom recombination mechanism. As a consequence of this possibility for atom-ion desorption, the equations for S reduce, however, to a simpler form. If the activated complex is of the form given in the relation / [286] above, then from equations [235] and [236] it is seen that $f_{\neq,HD} = f_{\neq,DH}$ and the equations become

$$S_D = 38.08 \frac{f_{\neq,H_2}}{f_{\neq,HD}} \qquad [287]$$

and

$$S_D = 38.78 \frac{f_{\neq,H_2}}{f_{\neq,HD}}, \qquad [288]$$

respectively, for acid and alkaline solutions. Under these conditions, the relations for S_T in acid and alkaline solution, equations [248] and [249]) respectively, become

$$S_T = 174.7 \frac{f_{\neq,H_2}}{f_{\neq,HD}} \qquad [289]$$

and

$$S_T = 174.8 \frac{f_{\neq,H_2}}{f_{\neq,HD}} \qquad [290]$$

Frumkin (29) has discussed possible evidence for the existence of the (adsorbed) H_2^+ ion as an intermediate in the atom-ion desorption step.* In the discussion which follows, the activated complex for this mechanism will be treated as the resonating structure given as [286].

(b) Approximate Calculation of Isotope Effects at Pt

In Table XXII, the observed values of S and R for

---

* The suggestion here that the H_2^+ molecule-ion is involved as an intermediate in the atom-ion desorption step is different from Horiuti's suggestion that the neutralization of the H_2^+ species is rate-determining. In the atom-ion mechanism, the formation of H_2^+ would be regarded as the rate-controlling step and its neutralization is fast (29).

Table XXII

Observed Isotope Effects at Pt Cathodes at Room Temperature

	Acid Solutions			Alkaline Solutions		
	Value	Reference	Comments	Value	Reference	Comments
S_D	5.3	113 213,215	15°C in HCl H_2SO_4	7-7.8-5.8	117	KOH
	3.6-6.8-6.2	12	H_2SO_4			
	4.2-9.8-7	present work	HCl			
	4.4-2.8-4	present work	$HClO_4$			
	8.3	117	maximum value in H_2SO_4			
S_T	9.6	114	average value	15.3	114	average value in KOH
	21.5	117	maximum value in H_2SO_4	15.3	117	value at η =300 mV in KOH
				17.5	117	maximum value (η=?) in KOH
				14	216	
R	2.0	45	R value corresponds to 30 mV Tafel slope region in HCl/DCl.			
	1.5	125	R value for Pt-black in HCl/DCl for 30 mV Tafel slope region			
	1.9-2.5	142	Tafel region? H_2SO_4-HCl mixture.			

for platinum electrodes are given for various experimental conditions. There are several striking features of the experimental results shown in Table XXIV. First the S_D values for Pt vary appreciably in acid solution and values significantly below 5 are observed. Secondly there are no data for R values in alkaline solutions and there is only one reliable value reported for S_D at Pt in alkaline solution. Also, S_T values reported for acid solutions differ significantly between two authors (114,117). This difference is irreconcilable and requires further investigation. Values of S_T for alkaline solutions show good agreement between the three reported values (114,117,216). The potential dependence of S_T is indicated but not discussed by one group of authors (117) and neglected by others (114,216) and requires further experimental investigation.

By means of an approximate calculation of R, it will be shown that the mechanism occurring at platinum in the 30 mV Tafel slope region cannot correspond to the atom-ion desorption step (as also indicated by this value of the Tafel slope- see Chapter II). If we assume atom-ion desorption to be rate-determining for the region where $S_D \doteq 6$, then from equation [207], it is seen that

$$\frac{f_{\neq,H_2}}{f_{\neq,RD}} \doteq \frac{6.0}{30.08} = 0.1576$$

From the rule of the geometric mean,

$$\left(\frac{f_{\neq,H_2}}{f_{\neq,D_2}}\right)^{1/2} = \frac{2f_{\neq,H_2}}{f_{\neq,HD}} \qquad [291]$$

the following value of $f_{\neq,H_2}/f_{\neq,D_2}$ may be calculated;

$$\frac{f_{\neq,H_2}}{f_{\neq,D_2}} = 0.09929$$

Inserting this value into equation [252], leads to the result

$$R = 14.78 \frac{(1-\theta_H)}{(1-\theta_D)}$$

For Pt electrodes, coverages of <u>ca.</u> 0.5 are indicated (142,144,155) and using the experimental relation (142) $\theta_H \doteq 0.85\ (\theta_D)$, the above equation, becomes, upon taking $\theta_D \doteq 0.5$

$$R = 17$$

This value for R is quite irreconcilable with the experimental value of around 2 even allowing for uncertainties in the approximate calculation. (see Table XXIV).

If the atom-atom desorption step is assumed to be operative, then from equation [239] the ratio $f_{\neq,H_2}/f_{\neq,HD}$ is

$$\frac{f_{\neq,H_2}}{f_{\neq,HD}} = \frac{6.0}{76.16} = 0.07878$$

From the rule of the geometric mean given by equation [291], it is found that

$$\frac{f_{\neq,H_2}}{f_{\neq,HD}} = 0.02483$$

Inserting this value into equation [254], it is found that

$$R = 1.374 \frac{(1-\theta_H)^2}{(1-\theta_D)^2}$$

Taking again $\theta_D \doteq 0.5$ and from $\theta_H = 0.85\ \theta_D$, the final value for R is

$$R = 1.3$$

which is in satisfactory agreement with the observed value. It is interesting to note that by repeating this procedure for $S_D = 4$ (i.e. corresponding to the S_D values found in the present work for $HClO_4$ solutions), R values of 0.8 to 1.0 are calculated. The significance of this result is that in the absence of specific anion adsorption, the bonding in the activated complex may be "tight" enough to cause small or even inverse isotope effects in R. Inverse isotope effects have been observed for some proton transfer reactions (124) and the possibility that this effect might occur at platinum electrodes is of great interest. The apparent fact that the bonding in the activated complex increases or becomes "tighter" as specific anion adsorption decreases,

supports the view presented in this thesis that the $S_D - \eta$ relation can be explained partially in terms of the multiple site model for proton discharge (e.g. an increase in S_D can correspond to a change from multiple to single site adsorption).

In view of the above remarks, it is apparent that values of S_D for either type of recombination mechanism can be significantly less than 6-7. In addition, S_D values based on a discharge mechanism can be significantly greater than 3 (see discussion on nickel electrodes in alkaline solution, page 258). The view that the values of S_D can be generally separated into two groups (i.e. $S_D \doteq 6\text{-}7$ for the catalytic metals Pt, Ni, Rh, etc., and $S_D \doteq 3$ for the non-catalytic metals Hg, Sn, and Pb) can hence no longer be maintained. On the basis of the findings presented in this thesis, experimental values of S and R can be given significant meaning only when a complete study is made to relate these quantities to overpotential (i.e. to the Tafel relation), to the effect of the anion present in solution, and to other kinetic criteria of mechanism, e.g. reaction order as discussed in Chapter II.

3. New Contributions in the Study of Low Temperature Kinetics

A. Mercury: Apparent and True Frequency Factor Ratios

In this section, the role of proton tunneling will be examined, and in view of the present experimental results, will

be shown to be negligible. Christov (24,25) has offered the data of Post and Hiskey (111,112) as proof of significant tunneling of protons in the discharge reaction at mercury electrodes in aqueous solution. A major part of his evidence in support of tunneling is based on the experimental fact that the apparent frequency factor ratio A_H^*/A_D^* is significantly less than unity. It was suggested in Chapter V that the true frequency factor ratio is actually close to unity and therefore the conclusion based on $A_H^*/A_D^* = 0.5$ that tunneling is significant is unnecessary. It was also stated that several important factors which have not been previously discussed by other authors, enter into the evaluation of the true difference in activation energies and the true ratio of frequency factors. These factors are; (1) that the apparent* heats of activation $\Delta H^{\neq}$ (and their isotopic differences) cannot be used directly (139) to obtain true, chemically significant frequency factors from a given observed rate since the $\Delta H^{\neq}$ values include a heat content change for the single electrode reaction (134)

$$H_3O^+ + e \rightleftharpoons \tfrac{1}{2} H_2 + H_2O \qquad [292]$$

Similarly, isotopic ratios of frequency factors must be evaluated with proper consideration for isotopic differences of the entropy

---

* The apparent heat of activation, $\Delta H^{\neq}$ discussed here does not include any corrections due to tunneling. Hence the symbol $\Delta H^{\neq}$ has been used to distinguish it from the apparent energy of activation E^* used when tunneling corrections are considered.

changes for reaction [292] and its D analogue;

(iii) differences of the metal-solution potential differences at the reversible potential for the h.e.r. and the d.e.r. must be considered in the evaluation of the frequency factor ratios. Taking these factors into consideration, we may make estimates of isotope effects in the frequency factor ratio as follows.

In terms of absolute rate theory (51), the rate of discharge of H (from H_3O^+) or D (from D_3O^+) is

$$i_o = \tau zF \frac{kT}{h} \exp(\Delta S^{o\neq}/R).a_+ \exp \Delta E^{\neq}/RT \exp -\beta\phi_r F/RT \qquad [293]$$

where $\Delta E^{\neq}$ is the <u>true</u> activation energy at zero absolute metal-solution potential difference (134). ϕ_r, the reversible potential of a single electrode, is an underterminable quantity (140) and the measured energy of activation will therefore be an apparent one ($\Delta H^{\neq}$) due to contributions from ϕ_r. Since ϕ_r is the single electrode potential difference corresponding to the single electrode reaction [292], we can write

$$-\frac{\phi_r F}{RT} = \frac{\Delta G}{RT} = \frac{\Delta H}{RT} - \frac{\Delta S}{R} \qquad [294]$$

where ΔH and ΔS are the heat content change and entropy change, respectively, for the half-cell reaction [292]. Substituting for ϕ_r from [294] into equation [293] gives

$$i_o = \tau zF \frac{kT}{h} \exp(\Delta S^{o\neq}/R) \exp(-\beta\Delta S/R). a_+(1-\vartheta) \exp-(\Delta E^{\neq} - \beta\Delta H)/RT \qquad [295]$$

or

$$i_o = \gamma zF \frac{kT}{h} \exp(\Delta S^*/R) \cdot a_+ (1-\theta) \exp -\Delta H^{\neq}/RT \qquad [295a]$$

where

$$\Delta S^* = \Delta S^{o\neq} - \beta \Delta S \qquad [296]$$

$$\Delta H^{\neq} = \Delta E^{\neq} - \beta \Delta H \qquad [297]$$

It is seen from equations [295]-[297] that the measured quantities $\Delta H^{\neq}$ and A^* are not the kinetically significant ones. As a result, the measured frequency factor will be an <u>apparent</u> value due to the term in $\beta\Delta S$, and $\Delta H^{\neq}$ (the measured quantity) will differ from $\Delta E^{\neq}$ by $\beta\Delta H$. This was not considered in Christov's estimate of A_H/A_D (25) and the value of $A_H^*/A_D^* = 0.5$ cited by Christov and other authors (29) is therefore incorrect.

The specific rate constants for the h.e.r. and d.e.r. may be defined for i_o in terms of the Arrhenius relation

$$k = A \exp -\Delta E^{\neq}/RT \cdot \exp -\beta \phi_r F/RT$$

Then, for the isotopically analogous reactions, the ratio of rate constants k_H/k_D is given in logarithmic form by*

$$\log k_H/k_D = \log A_H/A_D + (\Delta E_D^{\neq} - \Delta E_H^{\neq})/RT + \beta(\phi_{r,D} - \phi_{r,H})F/RT \qquad [298]$$

---

* In equation [298], as in previous ratios of isotopic quantities, the ratios of activity coefficients for H, D, and T species has been taken as unity. The justification for this assumption is that the rule of the geometric mean which has been experimentally verified for H_2O-D_2O mixtures (176), implies that H_2O and D_2O form ideal solutions. This assumption, also made by others (177, 178), therefore appears to be quite satisfactory.

where A_H/A_D is now the ratio of true frequency factors. The quantities A_H/A_D and $\Delta E_D^{\neq}-\Delta E_H^{\neq}$ can be evaluated if $\phi_{r,D}-\phi_{r,H}$ is known as a function of temperature. The temperature dependence of $\phi_{r,D}-\phi_{r,H}$ in aqueous acid solutions has been calculated in a previous section (see Table VIII and Figure 39). By rewriting equation [298] as

$$\log \frac{k_H}{k_D} - \frac{\beta(\phi_{r,D}-\phi_{r,H})F}{RT} = \log \frac{A_H}{A_D} + \frac{\Delta E_D^{\neq}-\Delta E_H^{\neq}}{RT} \qquad [299]$$

it is seen that a plot of $\log k_H/k_D - \beta(\phi_{r,D}-\phi_{r,H})F/RT$ against $1/T$ enables the evaluation of the desired quantities A_H/A_D and $d\Delta E^{\neq}$ to be made. Taking the data of Post and Hiskey (111,112), the necessary corrections are made (see Table XXIII) and an Arrhenius plot is constructed as seen in Figure 44. Analysis of the data in this plot gives $A_H/A_D = 1.20$ and $\Delta E_D^{\neq}-\Delta E_H^{\neq} = 0.45$ kcal mole^{-1}. By an identical procedure, the data for the methanol work (see Table XXIII) can be plotted in Arrhenius form (Figure 45) and is found that $A_H/A_D = 1.27$ and $\Delta E_D^{\neq}-\Delta E_H^{\neq} = 0.77$ kcal mole^{-1}. In this Arrhenius type plot for the methanol data, it is assumed that the potential difference $\phi_{r,D}-\phi_{r,H}$ is the same in methanol solutions as it is in aqueous solution. This assumption is probably valid for the most part, since the term $\phi_{r,D}-\phi_{r,H}$ in various solvents will depend largely upon the difference in heats of solvation of H^+ and D^+. This can be seen by reference

Table XXIII

Data for Arrhenius Type Plots

System	°C.	$\log \frac{i_{o,H_2}}{i_{o,D_2}} = \log \frac{k_H}{k_D}$	$\phi_{r,D}-\phi_{r,H}$ mV.	β	$\log \frac{k_H}{k_D} - \frac{\beta(\phi_{r,D}-\phi_{r,H})F}{RT}$
Aqueous HCl/DCl (111,112)	0	0.349	- 9.92	0.49	0.440
	30	0.283	-14.41	0.49	0.402
	60	0.232	-19.87	0.49	0.372
	70	0.216	-20.75	0.49	0.365
Non-aqueous HCl/DCl (present work)	-125	1.338	+ 7.44	0.36(7)	1.25
	-106.7	1.171	+ 4.74	0.37(5)	1.12
	- 73	0.937	- 0.24	0.41(1)	0.961
	- 25	0.702	- 7.32	0.45(9)	0.770
	+ 60	0.468	-19.87	0.52(8)	0.627

Figure 44

Corrected Arrhenius plots for the h.e.r and d.e.r. on mercury cathodes in aqueous acid solution.

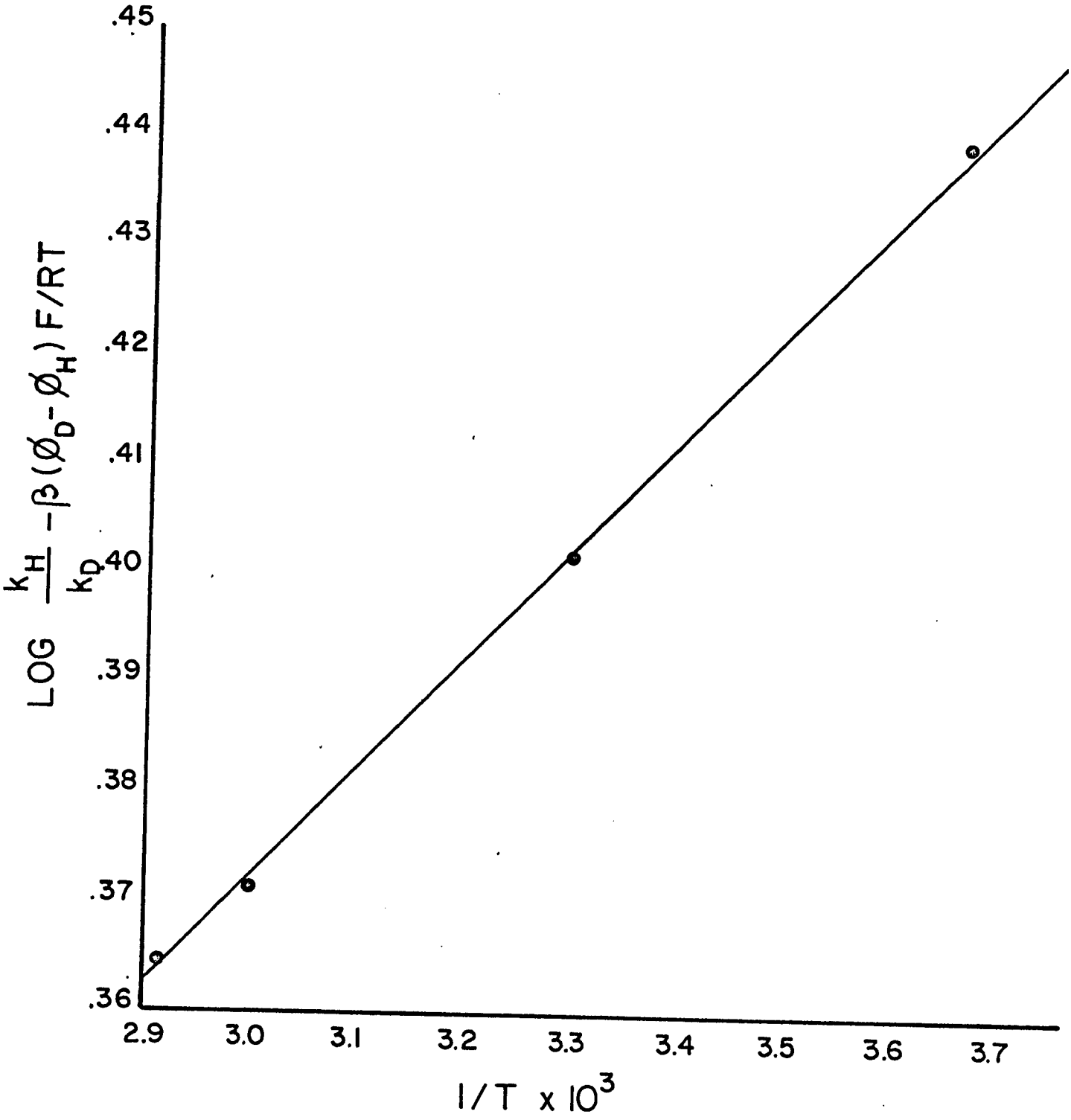
.45
.44
.43
.42
.41
.40
.39
.38
.37
.36
LOG $\frac{k_H}{k_D} - \beta(\phi_D - \phi_H) F/RT$
2.9
3.0
3.1
3.2
3.3
3.4
3.5
3.6
3.7
$1/T \times 10^3$

Figure 45

Corrected Arrhenius plots for the h.e.r and d.e.r. on mercury cathodes in methanolic acid solutions.

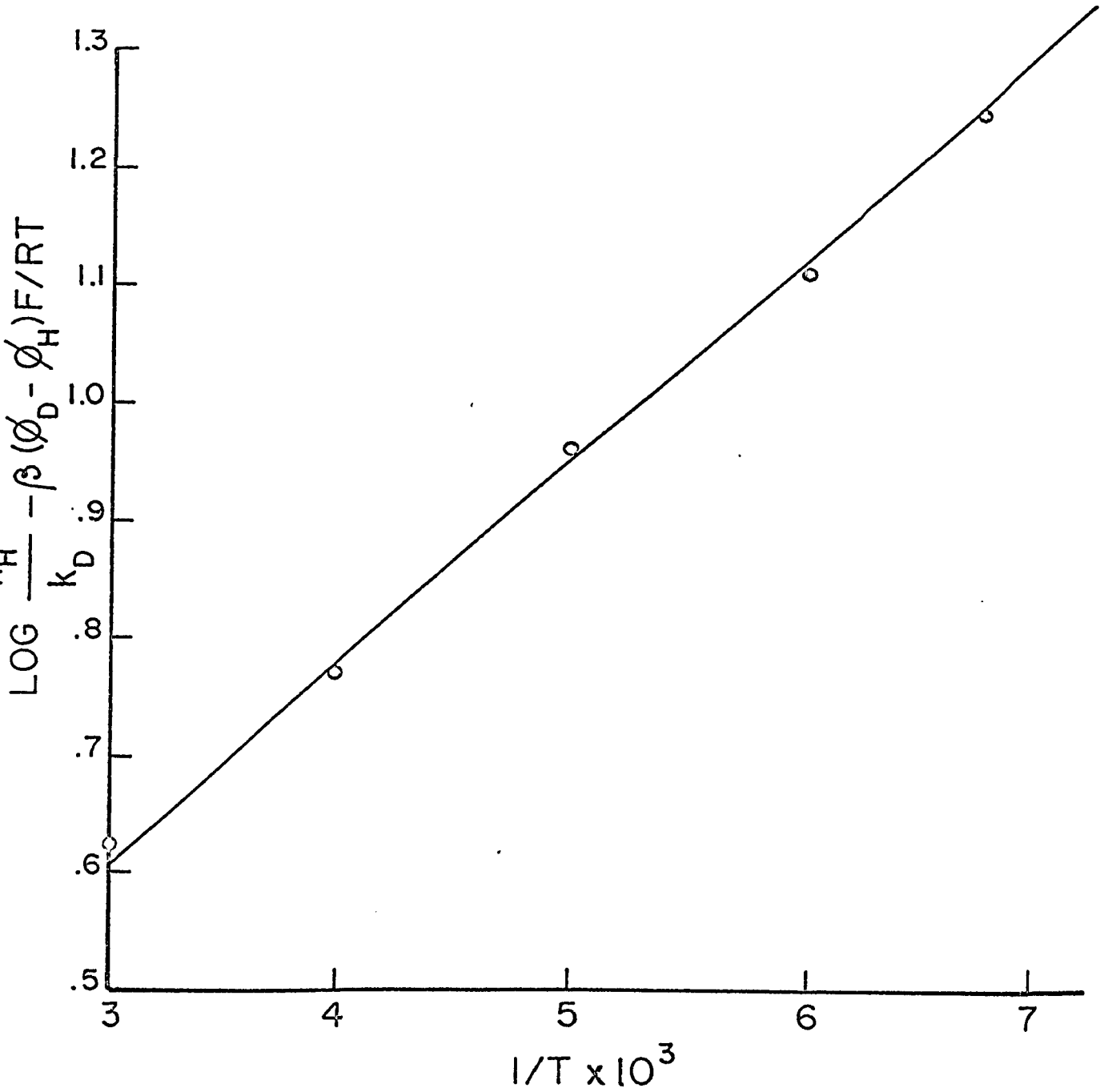
1.3
1.2
1.1
1.0
.9
.8
.7
.6
.5
3
4
5
6
7
LOG $\frac{k_H}{k_D} - \beta(\phi_D - \phi_H)F/RT$
$1/T \times 10^3$

to the following thermodynamic cycle

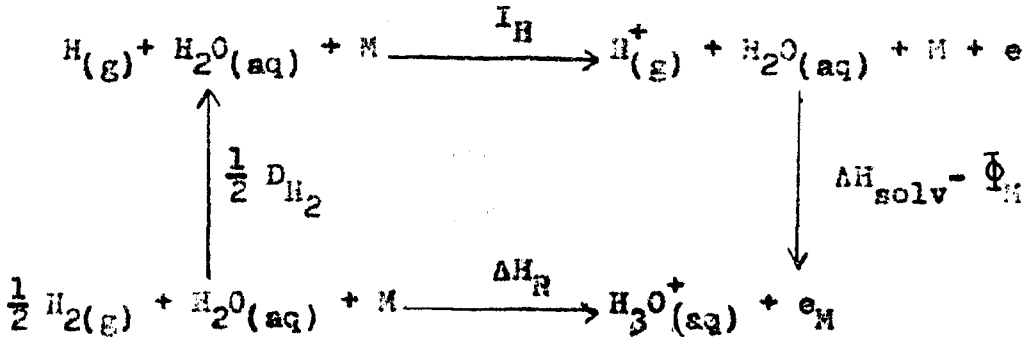

It is seen that upon changing the solvent, the dissociation energy, D and ionization energy, I, remain constant. Minor change in Φ_M is probable due to dipole orientation and interactions at the surface, but the main effect upon changing solvent arises from the term in solvation energy, $\Delta H_{solv.}$ Since the mean probable heat of proton solvation in aqueous solution (263 kcal mole^{-1}) is very similar (see reference 74) to that for methanol ($\doteq$ 261 kcal mole^{-1}), the assumption that $(\phi_{r,D}-\phi_{r,H})_{aq} = (\phi_{r,D}-\phi_{r,H})_{alc.}$ is, approximately, a valid one only since the calculation involves isotopic differences of this solvation energy. The fact that $\Delta E_D^{\neq}-\Delta E_H^{\neq}$ is independent of temperature down to -125°C and that A_H/A_D is close to unity are considered to constitute sufficient evidence in favor of a classical mechanism.

B. Platinum

On the basis of the experimental work presented in this thesis, it is concluded that proton tunneling participates

negligibly in the h.e.r. at Pt electrodes. In the previous discussion (Chapter V), the mechanism assigned to the h.e.r. at Pt in ethanolic HCl solution was atom-ion recombination. This mechanism bears some resemblance to that of the discharge step in that it involves a type of proton discharge and therefore can be qualitatively compared with the simple discharge step. As proof against a tunneling mechanism, the temperature independence of $\Delta E_H^{\neq}$ down to -150°C is offered, a result which cannot be explained in terms of any significant contribution from tunneling. Although no isotopic studies have been made for the Pt-ethanol system, this conclusion is supported by the analogy to the isotopic results obtained for the Hg-methanol system in which proton tunneling contributions were found to be negligible.

C. Discussion

The problem of estimating proton tunneling contributions in the measured total rates of reactions is of great importance. The probability of a significant role of proton tunneling was recognized for many years but since Bell's initial interest in this problem in the 1930's, only two or three reactions have been found which might indicate or suggest such contributions (217,218). Bell et al. (217) investigated the base catalysed bromination of 2-carbethoxy-cyclopentanone in D_2O and found that $A_H^*/A_D^* = 0.44$ for the D_2O catalysis, and $A_H^*/A_D^* = 0.042$ for

catalysis by fluoride ions. Shiner and Smith (218) investigated the rates of reaction of 1-bromo-2-phenyl propane and the 2-deuterio analogue with sodium ethoxide and found A_H^*/A_D^* to be 0.37. One or two other reactions which indicate possible tunneling contributions are referred to briefly by Bell (reference 18, page 213), but the fact remains that, excepting the above examples, tunneling is not observed to any appreciable extent in most proton transfer reactions. The problem then, is to explain this marked absence of proton tunneling when theoretical investigations (15-19,23-26,60,76,80-83) predict its significant participation. At the present, only qualitative reasons can be given to explain this apparent contradiction. Such reasons are:

(a) The treatment of the reaction coordinate in terms of a single dimension has been questioned (60,80,81). Johnston (81) has pointed out that the kinetic isotope effect at low temperatures shows large degrees of tunneling for methyl radical abstraction reactions, but still substantially less than is predicted from treatments based on a one-dimensional reaction coordinate. The question of hydrogen atom abstraction by a tunneling mechanism is not raised in this thesis (but see reference 79 by the present author) but the important factor here is that the attempt to retain the one-dimensional representation of the reaction

coordinate leads to predictions of larger degrees of tunneling than those for a multidimensional surface (80-83).

(b) In the calculation of the permeability G_w (see equations [81] and [85]), the assumption that the effective mass, m_c, is equal to the mass of a proton (or deuteron) may not be correct. The use of an effective mass different from that simply for H, for the complex such as Hg-H-OH_2 would require a detailed knowledge of the potential energy surface since m_c would vary as a function of r_1 and r_2;

(c) In the special cases of hydrogen ion discharge at Hg and Pt electrodes, a questionable quantity often used to evaluate equations [78] or [88] (22-26) is the apparent activation energy $\Delta E^{\neq}$ defined by equation [297]. If ΔH, the heat of reaction [292], is negative then $\Delta E^{\neq}$ will be less than the experimentally observed quantity. Since ΔH is an undeterminable quantity, the magnitude of the height of the real barrier is unknown;

(d) Apparent deviation from classical behaviour for reactions occurring in solution can be sometimes be ascribed to phenomena other than quantum-mechanical tunneling (219). Such phenomena include (1) a change in mechanism, (2) a change of solvation in the activated complex, and (3) a change of solvent structure with temperature.

CLAIMS TO ORIGINAL RESEARCH

1. The dual effects of potential and co-anion on the separation factor S_D are reported for the first time for Pt and Hg cathodes. The results are discussed both qualitatively and quantitatively in terms of reaction mechanism and the physical model for hydrogen atom adsorption.

2. Anion effects are suggested as being one of the possible causes for the discrepancies between the values of S reported by various workers. The dependence of S and R on the anion of the electrolyte has been discussed in terms of effects the anions may have on the adsorption of H at single and multiple sites at the electrode surface.

3. The justification for the multiple site model has been discussed both qualitatively and quantitatively. Although the concept itself is not new, its application to electrode kinetics is. Calculations have been presented for mercury and nickel cathodes and the multiple site model is shown to lead to the prediction of reasonable S and R values.

4. Qualitative explanations are offered for the potential dependence of S at Pt and Hg in terms of the multiple site model for H-atom adsorption, and in terms of double-layer effects. Previous discussions as to the nature of the S-relation, have either been incorrect (e.g. with regard to the role of catalytic exchange according to reaction [169]:

$H_{2(g)} + HOD_{(aq)} \rightleftharpoons H_2O_{(aq)} + HD_{(g)}$) or the possible effects of potential have been neglected.

5. The effect of variation of electrode surface coverage by H with potential has been considered by reference to the possible dependence of the MH stretching force constant on coverage when the heat of adsorption of H varies with coverage.

6. By the empirical method of assigning force constants by reference to analogous stable molecules, the observed isotope effects S_D, S_T and R have been shown to be theoretically consistent with a slow discharge mechanism for mercury in acid solutions and for nickel in alkaline solutions. This theoretical justification for the slow discharge step with regard to S values clarifies criticisms that have been raised against its applicability for some 30 years.

7. A detailed analysis of reaction order applied to the electrochemical kinetics of the h.e.r. has been given which supports the conclusions deduced from the isotope effects. Original calculations of reaction order for the h.e.r. at platinum and mercury electrodes are presented. It is shown that such considerations confirm the existence of a rate-determining atom-atom recombination at platinum which is followed by atom-ion discharge. Similarly, the

discharge step is confirmed for mercury. Previous formulations of pH effects (8) assumed that both the atom-ion mechanism [2] and the Horiuti mechanism [4] gave identical results. This is shown to be incorrect and that the mechanisms [1], [2], [3] and [4] lead to distinguishable pH effects.

8. The hydrogen and deuterium evolution reactions have been studied for the first time below 0°C down to very low temperatures. Although the h.e.r. on mercury in methanolic HCl solutions has been studied previously (133), the range of temperatures studied here has been extended to much lower values and the analogous deuterium reaction was also examined. At platinum, the experimental study of proton transfer down to -150°C involves the lowest reported temperature used to study proton transfer in any reaction.

9. The role of proton tunneling in electrochemical discharge reactions is shown to be negligible. This conclusion is based on: (a) the independence of Tafel slope on the H and D content of the solutions, (b) the temperature independence of the <u>true</u> activation energy difference $\Delta E_D^{\neq} - \Delta E_H^{\neq}$, and (c) the deduction of a value of approximately unity for the <u>true</u> frequency factor ratio A_H/A_D.

10. A method has been presented which permits the calculation of the true activation energy difference, $\Delta E_D^{\neq} - \Delta E_H^{\neq}$ and the true frequency factor ratio, A_H/A_D. The method is based upon calculation of the standard reversible potential difference $\phi^{\circ}_{r,D} - \phi^{\circ}_{r,H}$, and its temperature dependence together with allowance for isotope effects in the heat change for the single overall h.e.r. which determines the difference between apparent and true heats of activation. These factors are required in the consideration of the role of tunneling.

11. The decrease of values of β with decreasing temperature has been discussed. The effect is most probably due to a decrease in double-layer thickness as temperature decreases. The values of β for the h.e.r. at platinum were found to <u>increase</u> as temperature decreased. This effect has been attributed to varying surface coverage by adsorbed H or anions. There is a negligible isotope effect in the Tafel slope b.

REFERENCES

1. J. Tafel, Z. Physik Chem., 50, 641 (1905).
2. T. Erdey-Gruz and M. Volmer, ibid., A150, 203 (1930).
3. A.N. Frumkin, ibid., A160, 116 (1932).
4. M. Volmer and H. Wick, ibid., A172, 429 (1935).
5. A. Slygin and A.N. Frumkin, Acta Physicochim. U.R.S.S., 3, 791 (1935); A. Slygin and B.V. Ershler, ibid., 11, 45 (1939).
6. J.O.'M. Bockris, Modern Aspects of Electrochemistry, ed. Conway and Bockris, Vol. I, Butterworths (1954), Chapter 4.
7. A.N. Frumkin, Disc. Faraday Soc., 1, 64 (1947).
8. R. Parsons, Trans. Faraday Soc., 47, 1332 (1951).
9. J. Horiuti and G. Okamoto, Sci. Pap. Inst. Phys. Chem. Res. (Tokyo), 28, 231 (1936).
10. J. Horiuti, T. Keii and K. Hirota, J. Res. Inst.Cat., 2, 1 (1951).
11. J. Horiuti, Proc. Symp. Electrode Processes Philadelphia, 1959 ed. E. Yeager, John Wiley, (1961) P. 17.
12. M. Fukuda and J. Horiuti, J. Res. Inst. Cat., 10, 43 (1962).
13. C.E.H. Bawn and G. Ogden, Trans. Faraday Soc., 30, 432 (1934).
14. M.P. Appelby and G. Ogden, J. Chem. Soc., 163 (1936).
15. R.P. Bell, Proc. Roy. Soc., London, A139, 466 (1933).
16. R.P. Bell, ibid., A148, 241 (1935).

17. R.P. Bell, Acid-Base Catalysis, Oxford, (1941).

18. R.P. Bell, The Proton in Chemistry, Cornell, (1959).

19. R.P. Bell, Trans. Faraday Soc., 55, 1 (1959).

20. R.W. Gurney, Proc. Roy. Soc., A134, 137 (1931).

21. R.W. Gurney, ibid., A136, 378 (1932).

22. M.I. Temkin, Proc. 3rd Conf. Electrochem. Moscow, Acad. Sci. Moscow, p. 181 (1953).

23. Von St. Christov, Z. Elektrochem., 62, 567 (1958).

24. B.E. Conway, Symposium on Charge Transfer Processes (Chem. Inst. Can.) paper No. 7 (1958); see also Can. J. Chem., 37, 178 (1959).

25. Von St. Christov, Electrochimica, Acta, 4, 194 (1961).

26. Von St. Christov, ibid., 4, 306 (1961).

27. D.C. Grahame, Chem. Rev., 41, 441 (1947).

28. R. Parsons, Modern Aspects of Electrochemistry, I. eds. J.O'M. Bockris and B.E. Conway, Butterworths, 1954, Chapter 3.

29. A.N. Frumkin, Advances in Electrochemistry, I, ed. P. Delahay, Wiley 1961, Chapter 2.

30. R. Parsons, Advances in Electrochemistry, III, ed. P. Delahay, Wiley, 1963, Chapter 2.

31. E. Lange, Wien-Harms Hand. Exp. Phys. -12, 2, 267 (1933); Z. Elektrochem., 55, 76 (1951).

32. A.N. Frumkin, Zhur, Fiz. Khim., 24, 244 (1950).

33. A.N. Frumkin, z. Physik. Chem., 164, 121 (1933).

34. A.N. Frumkin, V.S. Bagotskii, S. Iofa and B.N. Kabanov, Kinetics of Electrode Processes, Moscow Acad. Press. (1952).

35. M. Breiter, M. Kleinerman, and P. Delahay, J. Am. Chem. Soc., 80, 5111 (1955).

36. J.G.N. Thomas, Trans. Faraday Soc., 57, 1603 (1961).

37. B.E. Conway and E. Gileadi, Ibid., 58, 2493 (1962).

38. E. Gileadi, Ph.D. Thesis, Ottawa, 1963.

39. M.I. Temkin, Zhur. Fiz. Khim., 15, 296 (1941).

40. K.J. Vetter, Z. physik. Chem., 194, 284 (1950); see also Trans. Symposium on Electrode Processes, Philadelphia 1959, ed. E. Yeager, Wiley, (1961), p. 47.

41. R. Parsons, Ibid., p. 61

42. O. Stern, Zeit. fur Elektrochem., 30, 508 (1924).

43. J.O'M. Bockris and E.C. Potter, J. Electrochem. Soc., 99, 169 (1952).

44. J.O'M. Bockris, J. Chem. Phys., 24, 817 (1956).

45. J.O'M. Bockris, and D.F.A. Koch, J. Phys. Chem., 65, 1941 (1961).

46. S. Levina and V. Sarinsky, Acta Physicochim., U.R.S.S., 1, 485 (1937).

47. V. Bagotski, Dokl. Akad. Nauk, U.S.S.R., 58, 1387 (1947).

48. V. Bagotski and I. Jablokova, Zhur. Fiz. Kim., 23, 413 (1949).

49. E. Gileadi and B.E. Conway, Modern Aspects of Electrochemistry, Vol. III, Ed. J.O'M. Bockris and B.E. Conway, in press.

50. H.C. Urey, and D. Rittenberg, J. Chem. Phys., 1, 137 (1933).

51. S. Glasstone, K.J. Laidler, and H. Eyring, Theory of Rate Processes, McGraw-Hill, 1941.

52. J.O. Hirschfelder and E. Wigner, J. Chem. Phys., 7, 616 (1939).

53. L. Melander, Isotope Effects on Reaction Rates, Ronald Press, 1960.

54. J. Biegeleisen, J. Chem. Phys., 17, 675 (1949).

55. O. Redlich, Z. physik. Chem., B28, 371 (1935).

56. J. Bigeleisen and M. Wolfsberg, J. Chem. Phys., 21, 1972 (1953); 22, 1204 (1954).

57. J. Bigeleisen and M. Wolfsberg, Advan. Chem. Phys., 1, 15 (1958).

58. H. Eyring and F.W. Cagle, J. Phys. Chem., 56, 889 (1952).

59. H.S. Johnston and K.S. Pitzer, A.I.Ch. E. Journal, 5, 277 (1959).

60. H.S. Johnston, Notes on Lectures on Reaction Rate Theory, Brussels, 1961.

61. E.B. Wilson, J.C. Decius and P.C. Cross, Molecular Vibrations, McGraw-Hill, 1955.

62. W. Heitler, and F. London, Z. Physik., 31, 765 (1925).

63. Y. Sugiura, Ibid., 45, 484 (1927).

64. P.M. Morse, Phys. Rev., 34, 57 (1929).

65. S. Sato, J. Chem. Phys., 23, 592, 2465 (1955).

66. H. Eyring and M. Polanyi, Z. physik. Chem., B12, 279 (1931).

67. F. London, Problem der Modernen Physik, Sommerfeld Festschrift, p. 104, Hirzel, Leipsig (1928).

68. J. Horiuti, G. Okamoto and K. Hirota, Sci. Pap. Inst. Phys. Chem. Res. Tokyo, 29, 223 (1936).

69. R.E. Weston, J. Chem. Phys., 31, 892 (1952).

70. F.H. Westheimer, Chem. Revs., 61, 265 (1961).

71. G. Herzberg, Infrared and Raman Spectra, Van Nostrand, 1945.

72. K.W.F. Kohlrausch, Der Smekal-Raman Effect, Springer, Berlin, 1938.

73. F. Lechner, Wien. Ber., 141, 633 (1932).

74. B.E. Conway, Modern Aspects of Electrochemistry, Vol. III. Chap. 3, in press.

75. L. de Broglie, Thesis, Paris, 1924; Ann. de phys., (10)3, 22 (1925).

76. R.P. Bell, Proc. Roy. Soc., A158, 128 (1930).

77. C. Eckart, Phys. Rev., 35, 1303 (1930).

78. E. Wigner, Z. physik. Chem., B19, 203 (1932).

79. M. Salomon, Can. J. Chem., 42, 610 (1964).

80. H.S. Johnston and D. Rapp, J. Am. Chem. Soc., 83, 1 (1961).

81. H.S. Johnston, Advances in Chemical Physics, Vol. 3, Chap. 4, ed. I. Prigogine, Interscience, 1961.

82. H.S. Johnston and J. Heicklen, J. Phys. Chem., 66, 532 (1962).

83. H. Shin, J. Chem. Phys., 39, 2934 (1963).

84. B.E. Conway and M. Salomon, Electrochimica Acta, in press, 1964.

85. A.N. Frumkin, Sci, Pap. Inst. Phys. Chem. Res. Tokyo, 37, 473 (1940).

86. A.N. Frumkin, Acta Physicochim. U.R.S.S., 13, 23 (1943).

87. I.A. Ammar and M. Hassanein, J. Phys. Chem., 62, 805 (1958).

88. S. Jofa and A.N. Frumkin, Acta Physicochim., 18, 183 (1943).

89. A. Mituya, J. Res. Inst. Cat. Hokkaido Univ., 4, 228 (1956-7).

90. F.P. Bowden and K.E.W. Crew, Disc. Faraday Soc., 1, 86 (1947).

91 J.O'M. Bockris, and R.G.H. Watson, J. Chim. Phys., 49, 670 (1952).

92. J.O'M. Bockris, J. Res. Inst. Cat., Hokkaido Univ., 2, 105 (1953).

93. J.O'M. Bockris, I.A. Ammar and A.K. Huq, J. Phys. Chem., 61, 879 (1957).

94. J. Horiuti, Proc. First Autralian Conference on Electrochemistry, in press, Pergamon, 1964.

95. B.E. Conway and E. Gileadi, Can. J. Chem., 42, 90 (1964); J. Chem. Phys., 39, 3420 (1963).

96. B.E. Conway, E. Gileadi and M. Dzieciuch, Electrochim. Acta, 8, 143 (1963).

97. A.N. Frumkin, Trans. Symposium on Electrode Processes, Philadelphia 1959, ed. E. Yeager, Wiley (1961), p. 41.

98. J.O'M. Bockris, M.A.V. Devanathan and K. Müller, Proc. Roy. Soc., A274, 55 (1963).

99. B.E. Conway, J.O'M. Bockris and I.A. Ammar, Trans. Faraday Soc., 47, 756 (1951).

100. A. Mutsuda, J. Res. Inst. Cat. Hokkaido Univ., 8, 426 (1954).

101. S. Schuldiner, J. Electrochem. Soc., 101, 426 (1954).

102. D.D. Eley, Disc. Faraday Soc., 1, 128; 137 (1947).

103. F. Boeld and M. Breiter, Z. Elektrochem., 64, 897 (1960).

104. P.V. Popat and N. Hackerman, J. Phys. Chem., 62, 1198 (1956).

105. J.O'M. Bockris and A.M. Azzam, Trans. Faraday Soc., 48, 145 (1952).

106. G. Czapski, J. Jortner and G. Stein, J. Phys. Chem., 63, 1769 (1959).

107. T.W. Davis, S. Gordon and E.J. Hart, J. Am. Chem. Soc., 80, 4487 (1958).

108. G. Stein, Disc. Faraday, 29, 235 (1960).

109. E.A. Moelwyn-Hughes, Physical Chemistry, Pergamon, 1961.

110. R. Parsons and J.O'M. Bockris, Trans. Faraday Soc., 47, 914 (1951).

111. B. Post and C.F. Hiskey, J. Am. Chem. Soc., 72, 4203 (1950).

112. B. Post and C.F. Hiskey, ibid., 73, 161 (1951).

113. H.F. Walton and J.H. Wolfenden, Trans. Faraday Soc., 34, 436 (1938).

114. J.O'M. Bockris and S. Srinivasan, Electrochimica Acta, 9, 31 (1964).

115. M. Rome and C.F. Hiskey, J. Am. Chem. Soc., 76, 5207 (1954).

116. W. Vielstich, T.H. Schuchard and M. von Stacklberg, Ber. Bunsenges, 67, 645 (1963).

117. H.V. Butler, W. Viesltich and H. Barth, ibid., 67, 650 (1963).

118. G.N. Lewis and P. Ruetschi, J. Phys. Chem., 66, 1487 (1962).

119. B.E. Conway and M. Salomon, J. Phys. Chem., in press, July, 1964.

120. a) E.W. Washburn and H.C. Urey, Proc. Natl. Acad. Sci., 18, 496 (1932).

b) G.N. Lewis and R.T. MacDonald, J. Chem. Phys., 1, 823 (1933).

121. J.F. Black and H.S. Taylor, J. Chem. Phys., 11, 395 (1943).

122. J. Kirschenbaum, Physical Properties and Analysis of Heavy Water, National Nuclear Energy, Ser. III-4a, (1951).

123. M. Enyo, M. Hoshi and H. Kita, J. Res. Inst. Catalysis Hokkaido, 10, 153 (1962).

124. C.G. Swain, R.F.W. Bader, R.M. Esteve, and R.N. Griffin, J. Am. Chem. Soc., 83, 1951 (1961).

125. B.E. Conway, Proc. Roy. Soc., A256, 128 (1960).

126. J.O'M. Bockris and B.E. Conway, J. Sci. Inst., 25, 8 (1948).

127. H.C. Urey, F.G. Brickwedde, and G.M. Murphy, Phys. Rev., 40, 1 (1932).

128. A.M. Azzam, J.O'M. Bockris, B.E. Conway and H. Rosenberg, Trans. Faraday Soc., 46, 918 (1950).

129. J.O'M. Bockris and R. Parsons, Trans. Faraday Soc., 45, 916 (1949).

130. A. Murray and D.C. Williams, Organic Synthesis with Isotopes II, Interscience (1958).

131. A.N. Frumkin, Advances in Electrochemistry, Vol. III. Chap. 5, ed. P. Delahay, Wiley, 1963.

132. J.O'M. Bockris and B.E. Conway, Trans. Faraday Soc., 45, 989 (1949).

133. J.O'M. Bockris, R. Parsons and H. Rosenberg, ibid., 47, 766 (1951).

134. M.I. Temkin, Zh. Fiz. Khim., 22, 1081 (1948).

135. J.R. MacDonald and C.A. Barlow, J. Chem. Phys., 36 3062 (1962).

136. B.E. Conway and M. Dzieciuch, Can. J. Chem., 41, 38 (1963).

137. S. Jofa, B.N. Kabanov, A.T. Chistyakov and B.H. Kuchinski, Acta Physicochim., 10, 317 (1939).

138. S. Minc and J. Sobkowski, Bull. Acad. Polon. Sci., 8, 29 (1959).

139. B.E. Conway, Trans. Roy. Soc. Can., 54, (III), 19 (1960).

140. E.A. Guggenheim, J. Phys. Chem., 33, 842 (1929); 34, 1540 (1930).

141. R. Parsons, J. Chim. Phys., 49, 682 (1952).

142. K.I. Rozenthal, P.I. Dolin and B.V. Erschler, Acta Physicochim., 21, 213 (1946).

143. H. Dietz and H. Gohr, Electrochimica Acta, 8, 343 (1963).

144. D.A. Dowden, Chemisorption, ed Garner, Butterworths, 1957, Chap. 1.1.

145. P.H. Emmet, J. Phys. Chem., 63, 449 (1959).

146. F.C. Tompkins and A.S. Porter, Proc. Roy. Soc., A217, 529, 544 (1953).

147. L. Pauling, Phys. Rev., 54, 899 (1938); Proc. Roy. Soc., A196, 343 (1949).

148. J.C.P. Mignolet, Disc. Faraday Soc., 8, 105 (1950).

149. R.V. Culver and F.C. Tompkins, Advances in Catalysis, XI, Academic Press, 1959.

150. J.H. de Boer, Chemisorption, ed. Garner, Butterworths, 1957, Chap. 1.3.

151. O. Beeck, Advances in Catalysis, Vol. II, Academic Press, 1960, page 153.

152. T.B. Grimley, Advances in Catalysis, Academic Press, 1960, page 13.

153. R.P. Eischens and A. Pliskin, Am. Chem. Soc. Meeting, Boston, 1959; z. Phys. Chem., N.F. 24, 11 (1960).

154. R.P. Bell and H.C. Longuet-Higgins, Proc. Roy. Soc., A183, 357 (1945).

155. M. Breiter, L. Kandler, B. Kennel and M. Feigl, Tech. Rept. No. AF. 61 (052)-305, 31 Oct. 1960; see also reference 103 and M. Breiter and B. Kennel, Z. Elektrochem., 64, 1180 (1960).

156. R. Parsons, Trans. Faraday Soc., 54, 1053 (1955).

157. W.J. Youden, Statistical Methods for Chemists, Wiley, N.Y., 1951; see also Y. Beers, Theory of Error, Addison-Wesley, Mass., 1953.

158. B.E. Conway, Proc. Roy. Soc., A247, 400 (1958).

159. J. Horiuti and M. Polanyi, Acta Physicochim. U.R.S.S., 2, 505 (1935).

160. J.A.V. Butler, Proc. Roy. Soc., A157, 423 (1936).

161. I. Amdur, J. Chem. Phys., 17, 844 (1949).

162. K.J. Laidler and D.M. Bishop, J. Chem. Phys., in press.

163. G. Herzberg, Diatomic Molecules, Van Nostrand, 1950.

164. J. Horiuti and T. Nakamura, J. Res. Inst. Cat., Hokkaido, 2, 73 (1951).

165. M. Ikusima and S. Azakami, J. Chem. Soc., Japan, 59, 40 (1938).

166. O. Sepall and S.G. Mason, Can. J. Chem., 38, 2024 (1960).

167. F.G. Wall, Extended abstract No. 199, Electrochemical Society Meeting, Toronto, May 1964.

168. T. Keii and T. Kodera, J. Res. Inst. Cat., Hokkaido, 5, 105 (1957).

169. T. Kodera, ibid., 8, 161 (1959).

170. T. Kodera and T. Saito, ibid., 8, 5 (1959).

171. P.C. Cross, J. Burnham, and P.A. Leighton, J. Am. Chem. Soc., 59, 1134 (1937).

172. R.E. Weston, Spectrochim. Acta, 18, 1257 (1957).

173. J.T. Vanderslice, J. Chem. Phys., 32, 515 (1960).

174. M. Boudart, J. Am. Chem. Soc., 72, 3556 (1952).

175. G.N. Lewis and R.E. Cornish, J. Am. Chem. Soc., 55, 2616 (1933); B. Topley and H. Eyring, J. Chem. Phys., 2, 217 (1934); J. Bigeleisen, ibid., 23, 2264 (1955).

176. L. Merlivat, R. Botter and E. Nief, J. Chim. Phys., 60, 56 (1963).

177. C.G. Swain and R.F.W. Bader, Tetrahedron, 10, 182 (1960); C.G. Swain and R.F.W. Bader, and E.R. Thornton, ibid., 10, 200 (1960).

178. E.L. Purlee, J. Am. Chem. Soc., 81, 263 (1959).

179. J.C.P. Mignolet, J. Chim. Phys., 54, 19 (1957).

180. R. Suhrmann, G. Wedler and H. Gentsch, Z. Physik. Chem., N.F.17, 350 (1958).

181. W.M.H. Sachtler and G.J.H. Dorgelo, ibid., NF25, 69 (1960).

182. F.D. Rossini, J.W. Knowlton and H.L. Johnston, J. Res. Nat. Bur. Stand., 24, 369 (1940).

183. K. Heinzinger and R.E. Weston, Paper presented at the Vienna meeting on isotopes, December 1963: see also J. Phys. Chem., 68, 744 (1964).

184. R.F.W. Bader, Ph.D. Thesis, M.I.T., 1959.

185. E.R. Thornton, J. Am. Chem. Soc., 84, 2474 (1962).

186. Reference 71, pages 187, 188.

187. M. Wolfsberg, private communication.

188. C.C. Ferriso and D.F. Hornig, J. Chem. Phys., 23, 1464 (1955).

189. Reference 109, pages 455-456 and 502-503.

190. H.C. Urey, J. Chem. Soc., 569 (1947).

191. P.A. Giguere and K.B. Harvey, Can. J. Chem., 34, 798 (1956).

192. F.R. Bowden and S. O'Connor, Proc. Roy. Soc., A128, 317 (1930).

193. S.I. Miller, J. Phys. Chem., 66, 978 (1962).

194. L. Pauling, Nature of the Chemical Bond, Cornell Univ. Press, Ithaca, 1948.

195. B.E. Conway, J.O'M. Bockris and H. Linton, J. Chem. Phys., 24, 834 (1956).

196. D.J. Wilson and H.S. Johnston, J. Am. Chem. Soc., 79, 29 (1957).

197. K.S. Fitzer, J. Am. Chem. Soc., 79, 1804 (1957).

198. B.E. Conway and M. Salomon, Extended abstracts of the Electrochemical Society Meeting, Toronto, May 1964, paper 196.

199. G.L. Cote and H.W. Thompson, Proc. Roy. Soc., A210, 206 (1952).

200. T.E. Sharp and H.S. Johnston, J. Chem. Phys., 37, 1541 (1962).

201. C.A. Coulson, Research, 10, 149 (1957).

202. C.A. Coulson, Hydrogen Bonding, ed. D. Hadzi, Pergamon 1959, page 350.

203. J.O'M. Bockris and E.C. Potter, J. Chem. Phys., 20, 614 (1952).

204. P. Lukovsev, S. Levina and A.N. Frumkin, J. Phys. Chem., (U.S.S.R.), 13, 916 (1936).

205. B.E. Conway, E.M. Beatty and P.A. DeMaine, Electrochim. Acta, 7, 39 (1962).

206. F. Bowden and E. Rideal, Proc. Roy. Soc., A120, 86 (1928).

207. R. Jefferys, E. Yeager and F. Hovorka, Electrochemical Society Meeting, San Francisco, 1956, paper 129.

208. M.A.V. Devanathan and M. Selvaratnam, Trans. Faraday Soc., 56, 1820 (1960).

209. A.C. Mackrides, J. Electrochem. Soc., 109, 977 (1962).

210 A. Matuda and T. Ohmori, J. Res. Inst. Cat., Hokkaido Univ., 10, 203, 215 (1962).

211. H. Kita and T. Yamazaki, Ibid., 11, 10 (1963).

212. B.E. Conway and J.O'M. Bockirs, J. Chem. Phys., 26, 532 (1957).

213. B. Topley and H. Eyring, J. Am. Chem. Soc., 55, 5058 (1933); (see also reference 175).

214. J.H. Schachtschneider, Shell Development Company, Tech. Rep. No. 263-62 (1962).

215. A. Eucken and K. Bratzler, Z. Phys. Chem., 174A, 273 (1935).

216. M.L. Eidenhoff, J. Am. Chem. Soc., 69, 2507 (1949).

217. R.P. Bell, J.A. Pendley and J.R. Hulett, Proc. Roy. Soc., A235, 453 (1956).

218. V.J. Shiner and M.L. Smith, J. Am. Chem. Soc., 83, 593 (1961).

219. E.F. Caldin, Fast Reactions in Solution, Blackwell, 1964.

220. M.J. Dignam, Can. J. Chem., 42, 1155 (1964).

221. E.C. Noonan and V.K. La Mer, J. Phys. Chem., 43, 247 (1939).

222. N.V. Sidgwick, Chemical Elements and their Compounds, Vol. I, page 343, Oxford, 1950.